UNCLASSIFIED

AD 410263

DEFENSE DOCUMENTATION CENTER

FOR

SCIENTIFIC AND TECHNICAL INFORMATION

CAMERON STATION, ALEXANDRIA, VIRGINIA

UNCLASSIFIED

NOTICE: When government or other drawings, specifications or other data are used for any purpose other than in connection with a definitely related government procurement operation, the U. S. Government thereby incurs no responsibility, nor any obligation whatsoever; and the fact that the Government may have formulated, furnished, or in any way supplied the said drawings, specifications, or other data is not to be regarded by implication or otherwise as in any manner licensing the holder or any other person or corporation, or conveying any rights or permission to manufacture, use or sell any patented invention that may in any way be related thereto.

AD No. 410263
DDC FILE COPY
410263

(5) 161400

INVESTIGATION OF ENERGY AND MASS TRANSFERS NEAR THE GROUND INCLUDING THE INFLUENCES OF THE SOIL-PLANT-ATMOSPHERE SYSTEM

FINAL REPORT

JUNE 1963

University of California
Davis

Department of Agricultural Engineering
and
Department of Irrigation

Task 3A99-27-005-08
Under Contract Number DA-36-039-SC-80334
Meteorology Department
U.S. Army Electronic Proving Ground, Fort Huachuca, Ariz

$18.50

DDC
JUL 18 1968

ATI - tgt Ord Nov. 14 - Emma -

FILM REPLACEMENT

CORRECTIONS

New Target	New Document	Replaces	Reel No. ----------
ATI -	11003 -	conf - group	- 4 -

INVESTIGATION OF ENERGY AND MASS TRANSFERS NEAR THE GROUND INCLUDING THE INFLUENCES OF THE SOIL-PLANT-ATMOSPHERE SYSTEM

FINAL REPORT

Task 3A99-27-005-08

Prepared by:

F.A. Brooks, Project Leader

W.O. Pruitt

D.R. Nielsen

and others

Department of Agricultural Engineering and Department of Irrigation

UNIVERSITY OF CALIFORNIA, DAVIS, CALIFORNIA

Under Contract Number

DA-36-039-SC-80334

For

Meteorology Department

U.S. Army Electronic Proving Ground

Fort Huachuca, Arizona

June 1963

SUMMARY

This report includes the main findings and describes the research methods and data processing for the initial 3-year contract for basic research in the energy and mass transfers near the ground and in plants and soil. Fundamental measurements of diurnal cycles of energy and moisture flux rates are reported in Chapter I. These include preliminary measurements of air drag on a sod surface of 6-meter diameter which indicate that von Karman's constant varies from less than 0.4 to more than 0.5. Concurrent hourly profiles of airspeed, temperature and moisture are reported in Chapter II. These cover a range of Richardson No. from +0.5 to -2 and show curvatures in the stable case opposite to those reported by Best (1935) and by Deacon (1953) and reveal dissimilarities between velocity and temperature profiles which indicate that the eddy transfers processes are more complex than usually assumed. A square-root function of z/L is used to represent the curvature of semilog profiles ranging from strong thermal convection in the daytime to strong stable conditions at night.

Large diurnal variations in moisture transfer rates for the same gradients are reported in Chapter III. The applicability of various evaporation equations was checked in Chapter IV. An extension of eddy diffusivity as influenced by stability is given in Chapter V. A sinusoidal analysis for alternate warm and cold areas in Chapter VI provides analytical insight into local advection problems. Resistance interpretations of moisture transfer are described in Chapters X and XI. Investigations in the movement of water in plants and soil are reported in Chapters XII and XIII. The instrumentation is described and comments included on programming the IBM 1410 computer system (such as to evade 9 errors arising in the punched card input). The metric system is used throughout. Various tables are included in the appendices and a description given of the air sampling system for measuring moisture by an infrared spectrometer.

In general, the comprehensive program for simultaneous measurements of three flux rates and the corresponding profiles has yielded much basic data. Full operation is continuing to provide dependable data needed for full understanding and analytical description of the highly complex systems of energy and moisture transfers in nature.

Considerable support for instrumentation and personnel in this project has been received from the Water Resources Center of the University of California and the California Department of Water Resources.

TABLE OF CONTENTS

Chapter		Page No.
	Title Page	
	Summary	i
	Table of Contents	iii
	List of Figures	v
	List of Tables	xi
I	Outline of 3-Year UCD Research in Energy and Moisture Transfers Near the Earth's Surface F.A. Brooks, Project Leader	1
II	Physical Interpretations of Diurnal Variations of Eddy Transfers Near the Ground F.A. Brooks	27
III	Atmospheric and Surface Factors Affecting Evapotranspiration W.O. Pruitt and Mervyn J. Aston	69
IV	Application of Several Energy Balance and Aerodynamic Evaporation Equations Under A Wide Range of Stability W.O. Pruitt	107
V	Eddy Diffusivity As A Function of Stability Todd V. Crawford	125
VI	Boundary Layer Transport Under Conditions of Sinusoidal Down Wind Surface Fluxes H.F. Poppendiek	137
VII	Introductory Measurements of Shear-stress Across Rye Grass Sod W.B. Goddard	149
VIII	Automatic Data Recording System F. Lourence	159
IX	Data Processing and Computing Programming F.A. Brooks and F.V. Jones	169
X	Calculating Evaporation from Diffusive Resistances J.L. Monteith	177
XI	Resistance to Water Loss From Plants Mervyn J. Aston	191

TABLE OF CONTENTS (Continued)

Chapter		Page No.
XII	Movement and Distribution of THO in Tissue Water and Vapor Transpired by Shoots of Helianthus and Nicotiana Franklin Raney and Yoash Vaadia	203
XIII	The Measurement and Description of Water Infiltration into Uniform Soils D.R. Nielsen, J.M. Davidson and J.W. Biggar	227
	Appendix A List of Instruments, Dry Air Properties and Wet-Bulb Computation of Moisture Content	265
	Appendix B Radiometer Calibration	270
	Appendix C Anemometer Calibration and New Pulse Counter	272
	Appendix D Temperature Profile Masts	278
	Appendix E Humidity Sampling System (I.R. Hygrometer)	281
	Project Conclusions	284
	Project Recommendations	285
	Distribution List	
	Abstract Cards	

LIST OF FIGURES

Figure No.		Page No.
I-1	Plot diagram of site and nearby fields	2
I-2	4-component heat balance at the ground at Davis, California 15 May to 16 May 1961	6
I-3	_____ 31 August 1962	6
I-4	_____ composite day 28 July to 28 July 1961	7
I-5	_____ composite day 30 July to July 1962	7
I-6	_____ composite day 28 October to 29 October 1961	8
I-7	_____ 30 October 1962	8
I-8	_____ 13 December to 14 December 1962	9
I-9	Combined data for 1960 and 1961, Regular Eppley	10
I-10	Annual curves of average daily evapotranspiration and net radiation at Davis, California (W.O.P.)	11
I-11	Midday diagram of surface layer exchanges	17
II-1	Semi-log plot of velocity and eddy viscosity for a density current	33
II-2	Semi-log plot of Klebanoff's (1955) measurements of turbulent flow over a flat plate with calculation of eddy viscosity revealing a maximum at 1/3 the thickness of the boundary layer	35
II-3	Machined smoothed typical diurnal curves of 4 air temperatures of 20 minute means using 9-point least squares parabolic fitting	46
II-4	Hourly windspeed profiles 30-31 July 1962	47
II-5	Hourly profiles of temperature 30-31 July 1962	48
II-6	Humidity profiles 30-31 July 1962	49
II-7	Graphical determination of velocity profile coefficients	51
II-8	Graphical determination of temperature profile coefficients	51
II-9	Time transition between stable and unstable profiles 0630-0700 31 July 1962 interpreted by Poppendiek's system	53

LIST OF FIGURES (Continued)

Figure No.		Page No.
II-10	Tentative ratios of eddy diffusivities 30-31 July 1962	56
II-11	Preliminary asymptotic Karman coefficients 31 July 1962	56
III-1	Recorder record of millivolt output of the Infrared hygrometer during three different days.	71
III-2	Smoothed profiles of humidity, ρq in gms/meter^3 for several half-hour periods ending at time indicated	73
III-3	Ratio of $L(ET)/(R_n + G)$ during half-hour periods for 3 1/2 days in 1962.	74
III-4	Energy balance and surface and air temperature data. 31 August, 1962	75
III-5	_____ 30 October 1962	78
III-6	_____ 31 July 1962	80
III-7	_____ 12 March 1963	81
III-8	ET; saturation deficit of air at 100 cm level; vapor 8 gradients.....August 31, 1962	83
III-9	Evapotranspiration versus the vapor pressure gradient between 50 and 100 cm above the soil surface	84
III-10	Variation of a dimensionless form of K_D and K_H with the gradient Richardson Number, Ri_{75}cm.....	86
III-11	The variation of the ratio K_H/K_D with Ri_{75}	88
III-12	Evapotranspiration versus the vapor pressure gradient from leaf surface to air at 25-cm level.....	88
III-13	The variation of the ratio $ET/(e_s - e_{100})$ with wind speed at the 100-cm level.....	90
III-14	The ralationship of mean monthly evapotranspiration by ryegrass, ET to incoming solar radiation, R_c and net radiation, R_n	93
III-15	Mean monthly evapotranspiration for ryegrass and evaporation from USWB Class A pan and from a USDA-BPI pan	93

LIST OF FIGURES (Continued)

Figure No.		Page No.
IV-1	Measured evapotranspiration compared with calculated vapor flux using the Thornthwaite-Holzman Eq.	108
IV-2	Measured ET compared with calculated vapor flux E, using Pasquill's Eq.	111
IV-3	Measured ET compared with calculated vapor flux E_1 and E_2 using the Deacon-Swinbank Eq.	113
IV-4	Measured ET compared with calculated vapor flux (Eq. 4)	116
IV-5	_____ (Eq. 5)	118
IV-6	_____ (Eq. 6)	121
V-1	Nondimensional evaporative flux as a function of Richardson numbers	134
V-2	The temperature-profile shape characteristic as a function of negative Richardson numbers	134
VI-1	Dimensionless temperature contours	142
VI-2	Dimensionless vertical temperature gradient contours	143
VI-3	Dimensionless vertical heat flux contours	144
VI-4	Dimensionless temperature profiles as a function of $\overline{X}$	145
VI-5	Temperature profiles, 28 October 1961	146
VII-1	Shear-stress lysimeter design	150
VII-2	Introductory shear-stree transducer	151
VII-3	Field site reading of introductory shear-stress transducer	151
VII-4	Shear-stress transducer output record	153
VIII-1	Calibrated constant voltage input	160
VIII-2	Response to applied triangle waveform	164
VIII-3	Ability of the system to track on a changing signal	165
VIII-4	Digital voltmeter sensitivity control set at 75% of max.	166
VIII-5	_____ 90% of max.	166
IX-1	Scanning schedule for transducers to center in middle of each round trip, 13-14 December 1962.	174
X-1	Diurnal variation of stomatal resistance	180
X-2	Evaporation on 30 to 31 July 1962	180

LIST OF FIGURES (Continued)

Figure No.		Page No.
X-3	Seasonal variation of grass evaporation at Davis, 1960	183
X-4	Evaporation at Davis in 1960 as a function of surface roughness	184
XI-1, a-b	Daily fluctuations of evapotranspiration.....	197
XI-2, a-c	Daily fluctuations of plant resistance.....	198,199,200
XII-1	Absorption of THO from vapor by tissues.....	214
XII-2	Influx and efflux of THO in stem tissue of THO- and HHO- grown sunflower plants 30 days old	215
XII-3	_____ in veins _____	216
XII-4	_____ in mesophyll _____	217
XII-5	Influx of THO into root and stem tissue of HHO-grown sunflower plants 30 days old	218
XII-6	Gain of THO by mesophyll of HHO-grown sunflower plants 80 days old	219
XII-7	Distribution of THO in various tissues of THO-grown tobacco plants 80 days old	220
XII-8	Amount of THO in tissue water of leaf discs from THO-grown tobacco 80 days old	221
XII-9	Relation between transpiration rate and THO activity of transpired water vapor from sunflower plants....	222
XII-10	Trend of THO activity in water vapor transpired from leaves of THO-grown tobacco plants.....	223
XII-11	Absorption of THO (C) from vapor by shoot tissues of HHO-grown sunflower plants of increasing age	224
XII-12	Efflux of THO from leaves of THO-grown sunflowers into saturated vapor.....	225
XIII-1	Schematic diagram of apparatus used for horizontal and vertical soil water movement	242
XIII-2	Values of λ determined by visual distance to the wetting front divided by the square root of time for water infiltrating air-dry Columbia silt loam	243
XIII-3	_____ Hesperia sandy loam	244
XIII-4	Values of λ for Columbia soil determined from water content distribution measured for 3 time periods of infiltration with $\theta_o = 0.45\ cm^3/cm^3$	245

LIST OF FIGURES (Continued)

Figure No.		Page No.
XIII-5	_____ with θ_o = 0.325 cm^3/cm^3	246
XIII-6	Values of λ for Hesperia soil determined from water content distributions measured for 3 time periods of infiltration with θ_o = 0.385 cm^3/cm^3	247
XIII-7	_____ for 2 time periods of infiltration with θ_o - 0.30 cm^3/cm^3	248
XIII-8	Experimental values of capillary conductivity K and soil water diffusivity D for Columbia silt loam used to calculate vertical soil water movement	249
XIII-9	_____ for Hesperia sandy loam used to calculate vertical soil water movement	250
XIII-10	Distance to the wetting front of air-dry Columbia silt loam versus square root of time for horizontal and vertical movement	251
XIII-11	Distance to the wetting front of air-dry Hesperia sandy loam versus square root of time for horizontal and vertical movement	252
XIII-12	Columbia soil water content distributions for vertical profiles developed in air-dry soil with θ_o = 0.45 cm^3/cm^3	253
XIII-13	_____ with θ_o = 0.425 cm^3/cm^3	254
XIII-14	_____ with θ_o = 0.325 cm^3/cm^3	255
XIII-15	Hesperia soil water content distributions for vertical profiles developed in air-dry soil with θ_o = 0.385 cm^3/cm^3	256
XIII-16	_____ with θ_o = 0.30 cm^3/cm^3	257
XIII-17	Calculated values of λ, χ, and ψ defined in equation (7) for Columbia silt loam	258
XIII-18	_____ for Hesperia sandy loam	259
XIII-19	Calculated and measured soil water profiles for air-dry Columbia soil allowed to wet at θ_o = 0.45 cm^3/cm^3	260
XIII-20	_____ Hesperia soil allowed to wet at θ_o = 0.385 cm^3/cm^3	261
A-1	Log law for saturation vapor pressure	268

LIST OF FIGURES (Continued)

Figure No.		Page No.
C-1	Two methods of calibration for two Thornthwaite anemometers	275
C-2	Whirling-arm correction for circulating air	276
C-3	Pulse sensing circuit	277
D-1	Temperature, humidity and wind direction mast	280
E-1	Infrared hygrometer sampling system	283

LIST OF TABLES

Table No.		Page No.
I-1	Meteorological conditions at Davis, Calif. May and July 1961	13
I-2	Meteorological conditions at Davis, Calif. October 1961	14
I-3	Meteorological conditions at Davis, Calif. July and December 1962	15
I-4	Radiation exchange components, Davis, Calif. 28 October 1961	20
II-1	Nikuradse characterization of flow regimes	39
II-2	Parallel array of formulas for eddy transfers of momentum, heat and moisture	54a
II-3	Preliminary evaluation of curved log-law coefficients of profiles of velocity, temperature and moisture, 30-31 July 1962	61
II-4	Nomenclature for Chapters I and II	66
III-1	Humidity of air; temperature of soil, leaf surface, and air; and wind velocity at various levels, 30-31 July 1962	96
III-2	Humidity of air; temperature of soil, leaf surface, and air; and wind velocity at various levels, 31 August 1962	98
III-3	Humidity of air; temperature of soil, leaf surface, air; and wind velocity at various levels, 30 October 1962	99
III-4	Humidity of air; temperature of soil, leaf surface, air; and wind velocity at various levels, 12 March 1963	100
III-5	The energy balance	101
III-6	Eddy diffusivity for water vapor	103
VII-1	Summary of introductory shear-stress measurements for 13-14 December 1962	155
VII-2	Summary of introductory shear-stress measurements for 13-14 December 1962; also von Karman constant	156

LIST OF TABLES (Continued)

Table No.		Page No.
VIII-1	Shorted input channels - 20-minute means, microvolts	162
VIII-2	Variances for fixed voltage channels, microvolts	162
X-1	Mean hourly resistances, surface humidity, and evaporation rates, 30-31 July 1962	187
X-2	Stomatal resistance and relevant data on selected days	188
XIII-1	Measured values of capillary conductivity of Columbia silt loam by two methods	238
A-1	Instrument list for research in heat and moisture transfers	265
A-2	Dry air density and kinematic viscosity	266
B-1	Repeatability in field calibrations of radiometers	271
C-1	Parameter allowable deviation with normal operation	273

CHAPTER I

OUTLINE OF 3-YEAR UCD RESEARCH IN ENERGY AND MOISTURE TRANSFERS NEAR THE EARTH'S SURFACE

F. A. Brooks, Project Leader

1. Primary Objective: Simple description of the physics of the environment conforming with the basic exchanges of heat and moisture. A broad question is: Can the hourly micrometeorological environment be forecast to a satisfactory degree knowing the ground-cover, soil temperature and the meteorological conditions of the atmosphere? The answer involves the interdependence of many factors and their diurnal and annual variations. Both the magnitude of "a satisfactory degree" and the soundness of a method used for making forecasts depend on multiple, simultaneous observations particularly of natural flux rates of five forms of energy and the potential gradients. To lay a firm physical foundation for this highly complex problem, the simple cases, clear sky and flat uniform ground cover, are studied first.
2. Test Site: The original 12 1/2-acre plot of rye grass, mowed frequently to 10 cm height, was doubled in 1962 by adding an alfalfa planting to the south and southwest as shown in Figure I-1 so that the usual S.S.W. wind has a clear fetch over irrigated cropland of more than 400 meters. This does not alter our capability in late summer for advection measurements in a dry north wind impinging suddenly on the irrigated plot 200 meters upwind of the lysimeters. Poppendiek in Chapter VI gives a sinusoidal solution for alternating strips of moist and of dry ground. In Chapter II, Figure II-9 provides an interpretation of the temperature field based on the Poppendiek formulas.
3. Measurements of Flux Rates: An array of 8 radiometers is used to determine 5 parts of radiation exchange as discussed later. For flux rate of moisture the 6-m diameter lysimeter provides positive measurement of daily evapotranspiration and also gives a meaningful measure of fluctuation in periods as short as 20 minutes throughout the diurnal cycle. This reliable determination of moisture flux rate can be used to analyze eddy transfer of moisture independently of the heat balance. With continuous recording of evapotranspiration under various conditions, significant diurnal and annual hysteresis in the

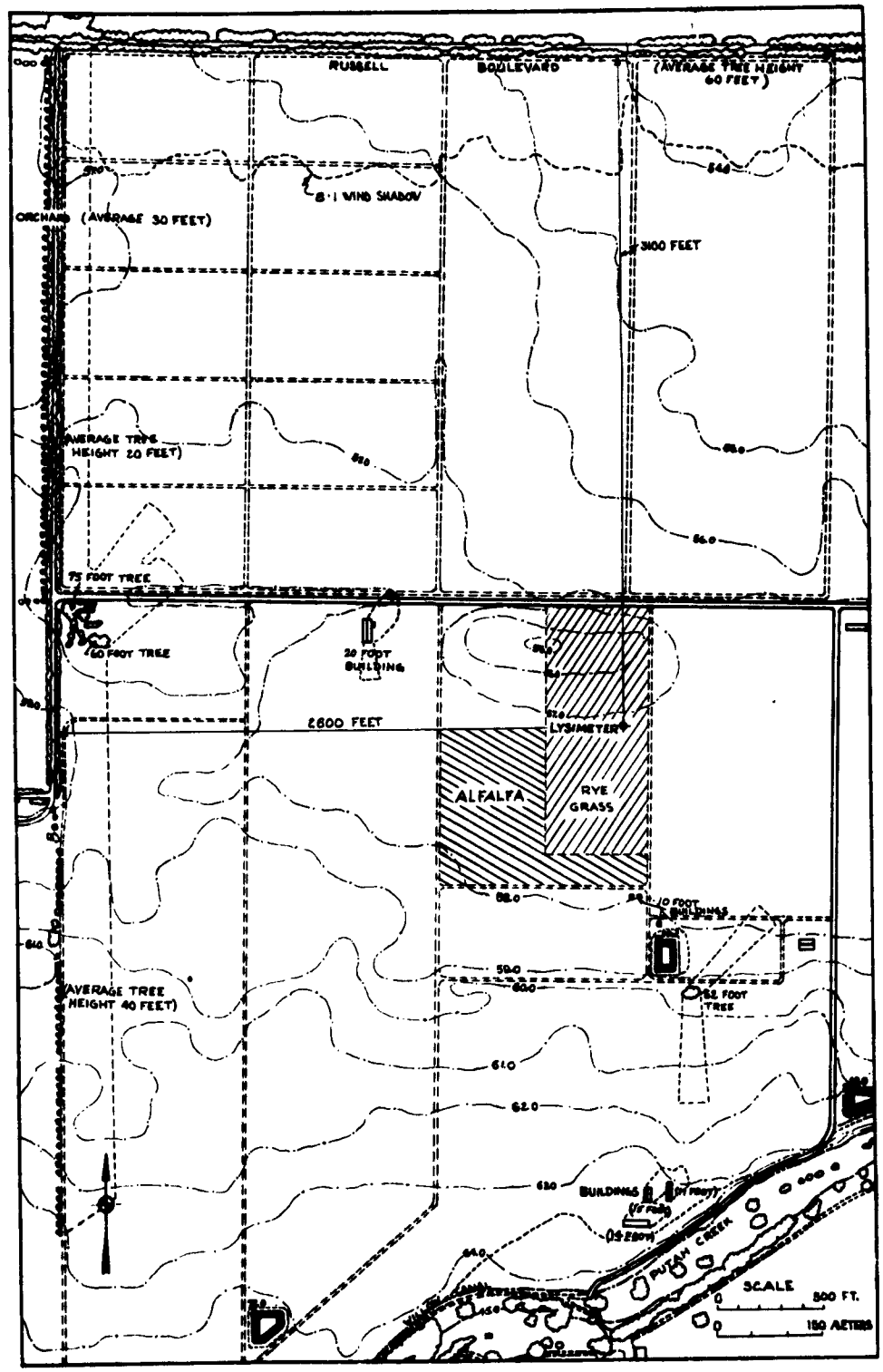

Figure I-1. Plot diagram of site and nearby fields (before tract levelling).

evapotranspiration rates have been demonstrated by Pruitt and Aston, Chapters III, IV. This includes special investigations of leaf temperatures and in the resistance to moisture flow from leaf stomata to turf air. Laboratory studies of water movement in soils and plants have been made with tritiated water and reported by Vaadia, Chapter XII and Nielsen, Chapter XIII.

For the conduction heat flux we measure the soil heat flow near the surface. This is also used in determining convective heat flux as residual from net radiation absorbed by the surface and the latent heat involved in evapotranspiration. In 1961 direct measurements of eddy heat transfer rates were made by Dr. Dyer (1962) with the Australian C.S.I.R.O. evapotron. The fifth energy flux, for metabolism, was found by Monteith to be negligible because the mowed rye grass has slow growth.

The unique capability of the new 6-m diameter floating lysimeter is its use as a shear-stress meter for measuring momentum flux. Initial tests by Goddard show a diurnal range in air shear stress of from 0.3 to 1.1. dynes/sq. cm in light wind. These give a drag coefficient about twice that measured on a smooth desert dry lake.

4. Measurements of Air Profiles of Potentials for Eddy Transfers: Because aerodynamic interpretation is the only way to relate directly our outdoor eddy transfers to well-established wind-tunnel results, 4 masts with thermocouples at 9 levels up to 6-meter height are in use registering temperatures with standard deviations of less than 0.1°C. For moisture the use of the recording spectrographic hygrometer furnishes dependable profiles which have already been related to the lysimeter water loss rates by Dr. Monteith for the 35-hour run 30-31 July 1962. Crawford extends eddy diffusivity determination in Chapter V. Measurements of wind profiles in the December 36-hour run were made at 8 levels using Thornthwaite and Casella-Sheppard cup anemometers on two masts.

5. Automatic Computer Analyses: The overall objective in the research procedure is to measure simultaneously all the flux rates and profiles of micrometeorological factors with a digital electronic system described by Lourence, Chapter VIII. Processing the data by automatic computers

is described in Chapter IX. The conventional electrical transducers using the electronic digital millivoltmeter system give an overall sensitivity of about 4 microvolts (0.1°C). About 180 items every 2 minutes are recorded automatically by the IBM 526 punch. The various transducers used are listed in Appendix A.

Computer programs are now handling cards via magnetic tape and evading 9 kinds of errors in the original card data. The time required on the IBM 1410 for means and variances of 167 scan points is now about 1/5 of real time. The z_o parameters and the slopes for logarithmic interpretation of vertical profiles can be determined by computer including a tentative square-root curvature function for diabatic conditions. This permits comparisons of respective eddy diffusivities for momentum, heat and moisture transfers and their individual Karman coefficients.

The first step in automatic analyses is to program the computer to find twenty-minute or half-hourly mean magnitudes and variances* (or standard deviations) for each transducer. The means are then arranged for hand verification by comparison with measurements by instruments of different character or with calculations of different components of fluxes. Where comparable readings exist for the full diurnal cycle, Fourier harmonic smoothing is desirable before such comparison ratios are determined. When the daily cycle is distorted or incomplete, a 5- or 9-point automatic parabolic smoothing of the 20- or 30- minute time means provides a consistent smoothing free of personal bias. All the parameters need to be smoothed by the same method to establish close time relationships as between the diurnal cycles of fluxes and gradients.

6. Annual Cycles of Heat Fluxes over Perennial Rye Grass: The year-round variation in heat and moisture fluxes can now be judged from field tests selected throughout the whole 3-year contract period. Although the various days of major tests differed in windiness, humidity and in previous ground condition, the tests reported in the following curves are almost all for cloudless sky and thus together show consistent annual

* When using constant half-hour means, the variances will be greater than if calculated for a sloped mean natural to the diurnal cycles. A proper sloped mean, however, should be determined by Fourier harmonic smoothing which seems an unnecessary complication at this stage of data interpretation.

cycles. Special purpose runs of a few hours each have been made in all months as reported in Chapter XI. Of the 14 day-long field runs 7 have been put in energy balance form, Figures I-2 to I-8. Three of these continued through the night and all the next day.

Figure I-9 gives the annual curve of cloudless noon maximum solar radiation (direct plus diffuse). This supplements the diurnal net radiation curves which are influenced by ground conditions. The corresponding diurnal curves of shortwave insolation are almost perfect half sine waves from sunrise to sunset.

Also available for annual cycles are Pruitt's continuous averages of evapotranspiration and net radiation, Figure I-10. These are for day by day weather and therefore lower than the cloudless sky rates shown in Figures I-2 to I-8. Only a few extreme days of very strong dry wind were omitted from these averages because the evapotranspiration flux curves on these days differed considerably from the typical and would not be appropriate for comparison with average monthly weather reports.

7. Meteorological Conditions.* To describe gross conditions covering the test periods for which heat balance curves have been presented, the 12-hour U.S. Daily Weather maps and local observations were used as shown in Tables I-1, 2, and 3. The weather types listed are based on Brooks's 1960 table. Briefly Type #1 is for Polar continental air mass; #2, Tropical continental, and #3, Polar maritime. Cloudless sky can exist in all three, but the net radiation rates would differ.

For the major test in October 1961 various facsimile maps were furnished by the Sacramento office of the U.S. Weather Bureau, of which the following give significant meteorological data.

1. Surface barometric pressure, U.S. Daily Wea.; scale 3.4''/(30-40°Lat), 4 mb intervals, 24 hours.
   Surface temperature by station.
2. 1000 mb isentropic height, ASXIV 58, polar map; 1.25''/(30-40°L), 20 x 10 ft. intervals.
3. 850 mb isentropic height, AUNA 8 84, N. Amer; 2.6''/(30-40°L), 100 ft. intervals.
4. 12-hour pressure change, every 6 hours corrected for diurnal cycle; 1.7''/(30-40°L), 4 mb interval.

* Interpreted by H.B. Schultz

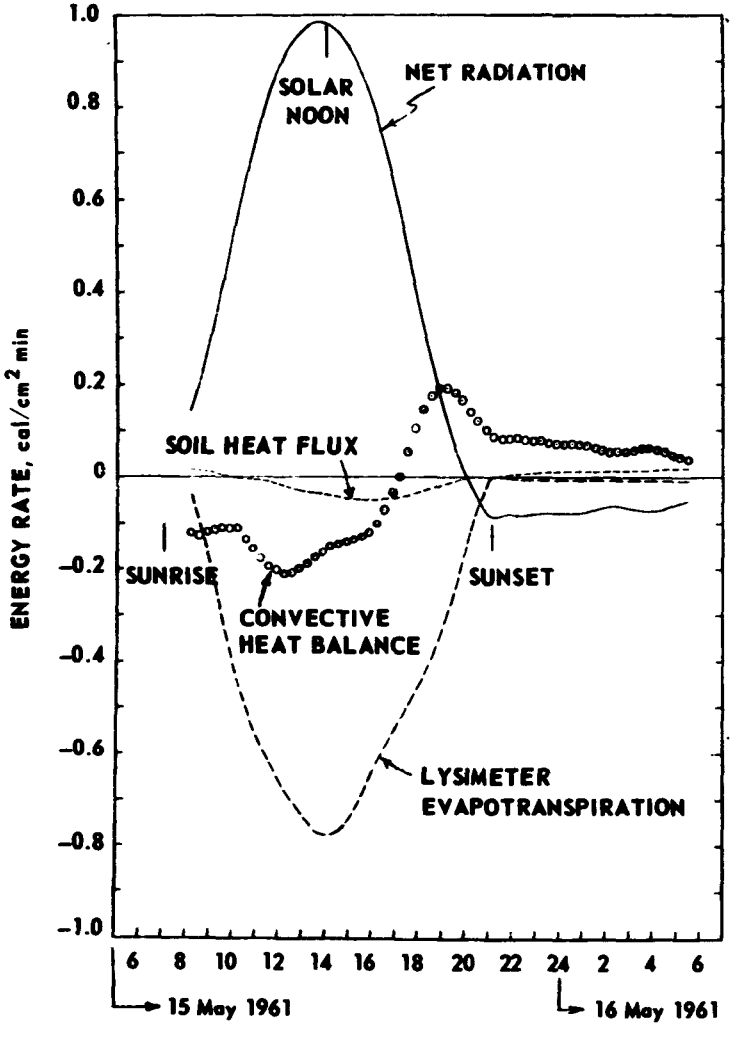

Figure I-2. Four-component heat balance at the ground at Davis, California 15 May to 16 May 1961.

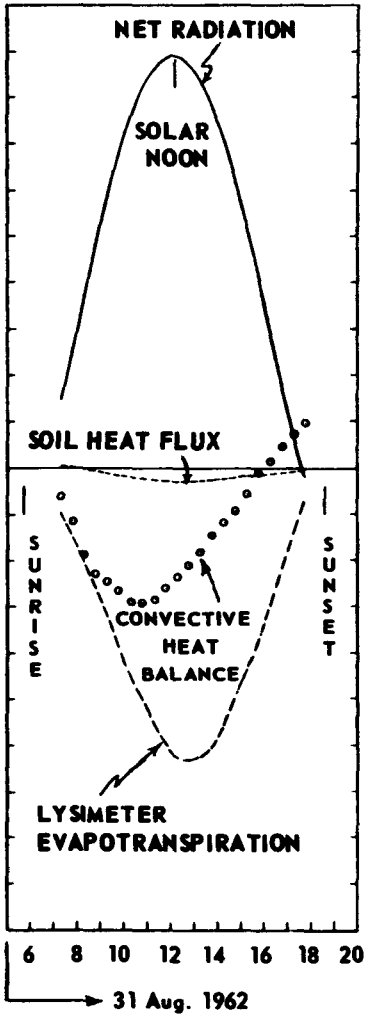

Figure I-3. Four-component heat balance at the ground at Davis, California 31 August 1962.

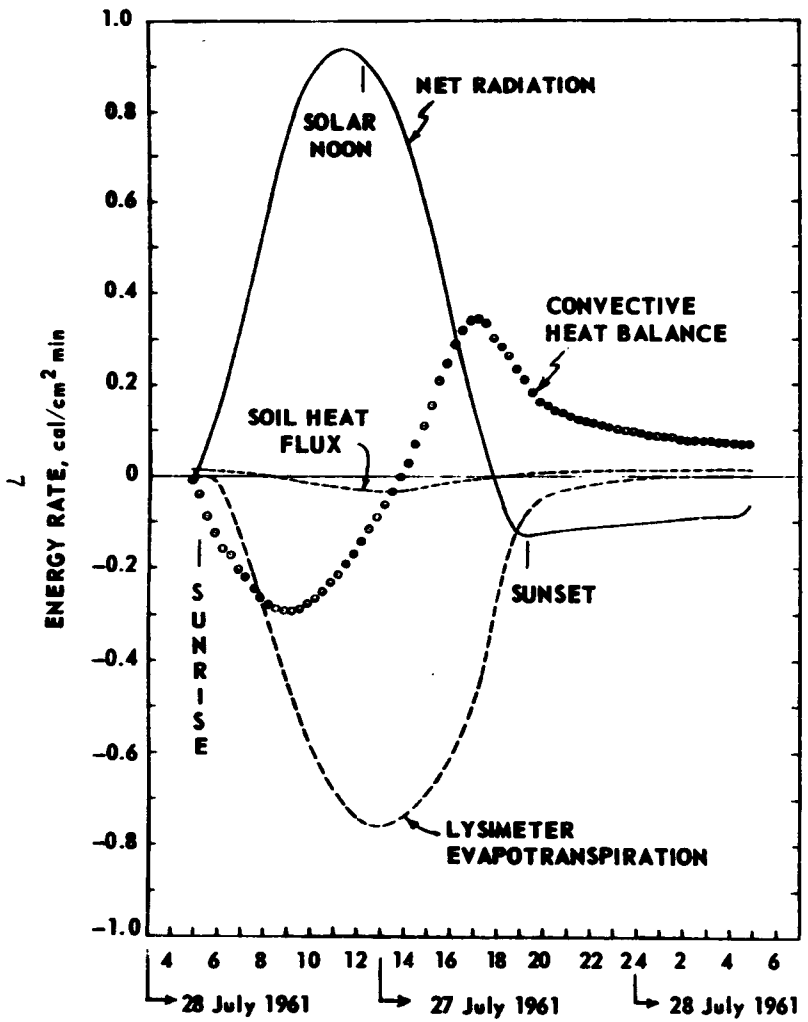

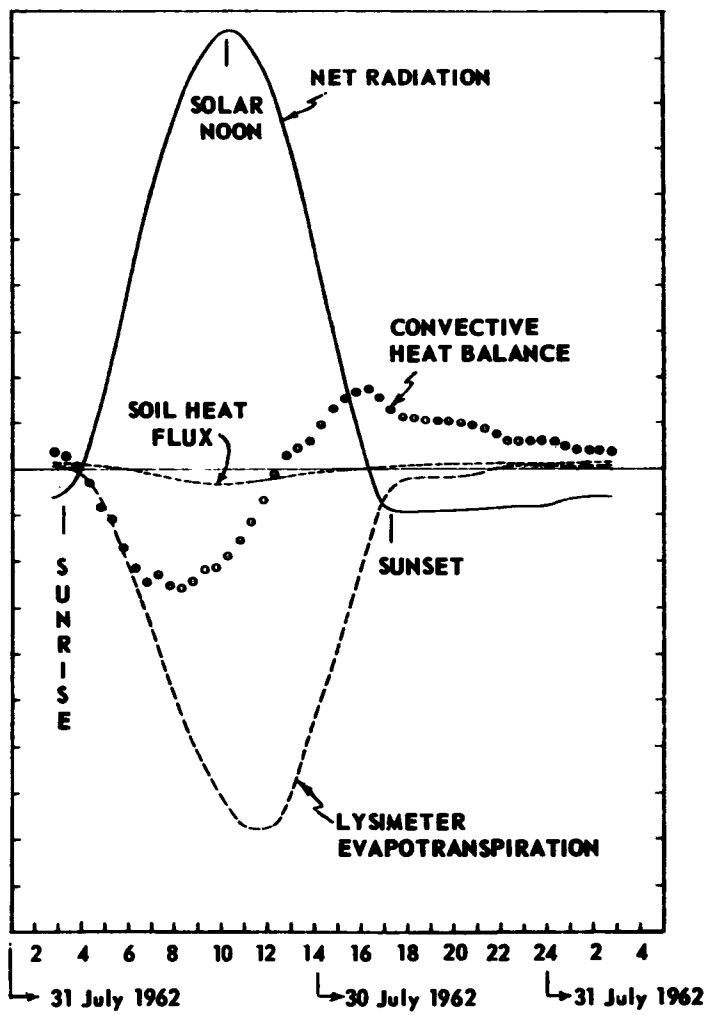

TIME, HOURS, P.S.T.

Figure I-4. Four-component heat balance at the ground at Davis, California com-

Figure I-5. Four-component heat balance at the ground at Davis, California com-

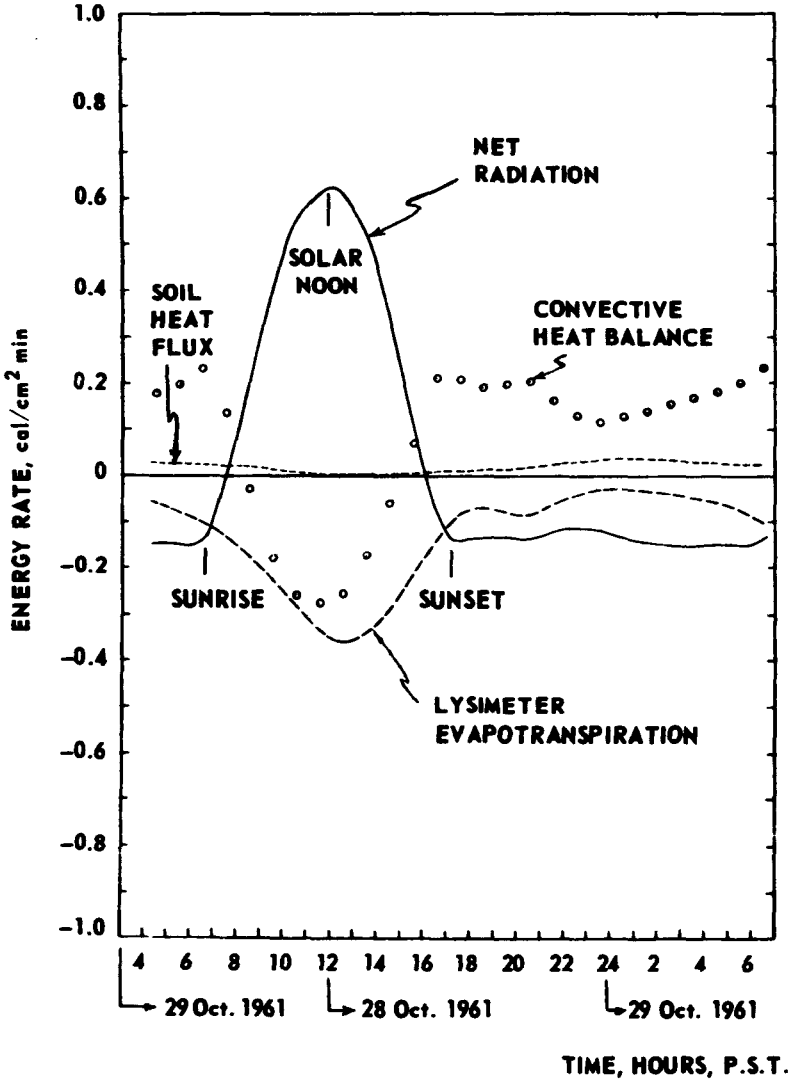

Figure I-6. Four-component heat balance at the ground at Davis, California composite day 28 October to 29 October 1961.

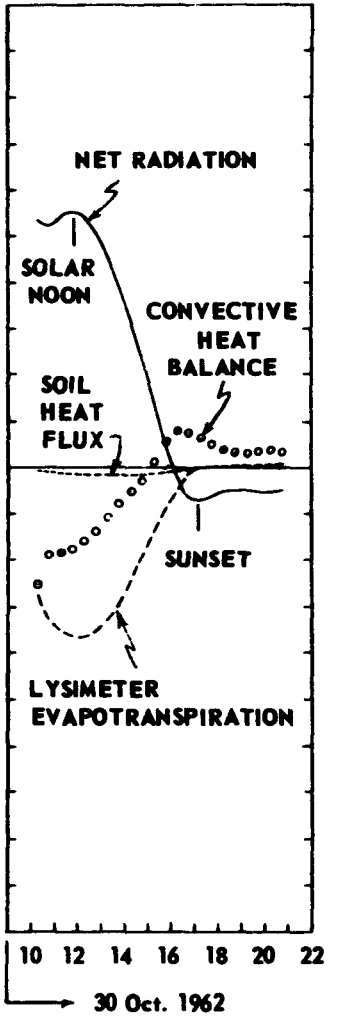

Figure I-7. Four-component heat balance at ground at Davis, California 30 October 1962.

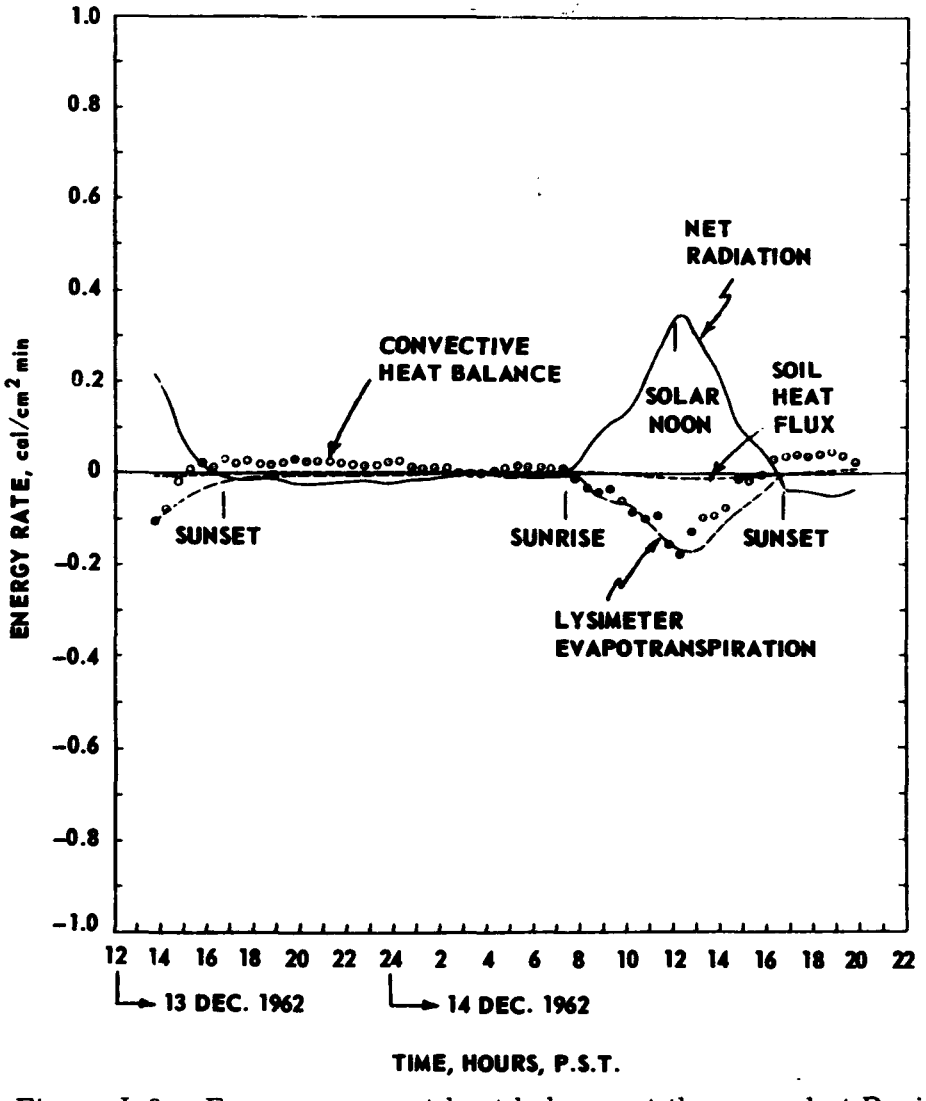

Figure I-8. Four-component heat balance at the ground at Davis, California 13 December to 14 December 1962

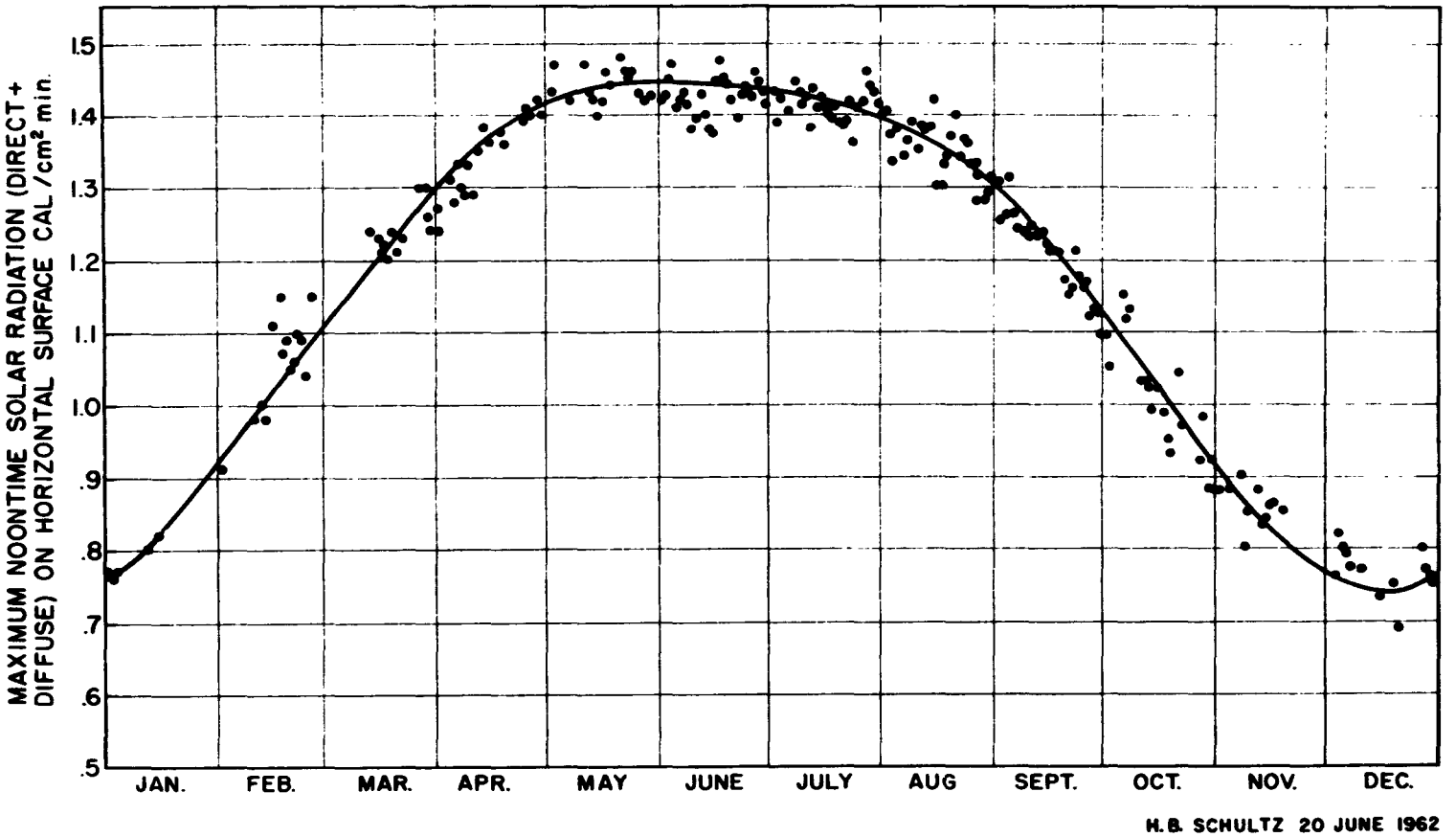

Figure I-9. Combined data for 1960 and 1961. Regular Eppley, clear middays only.

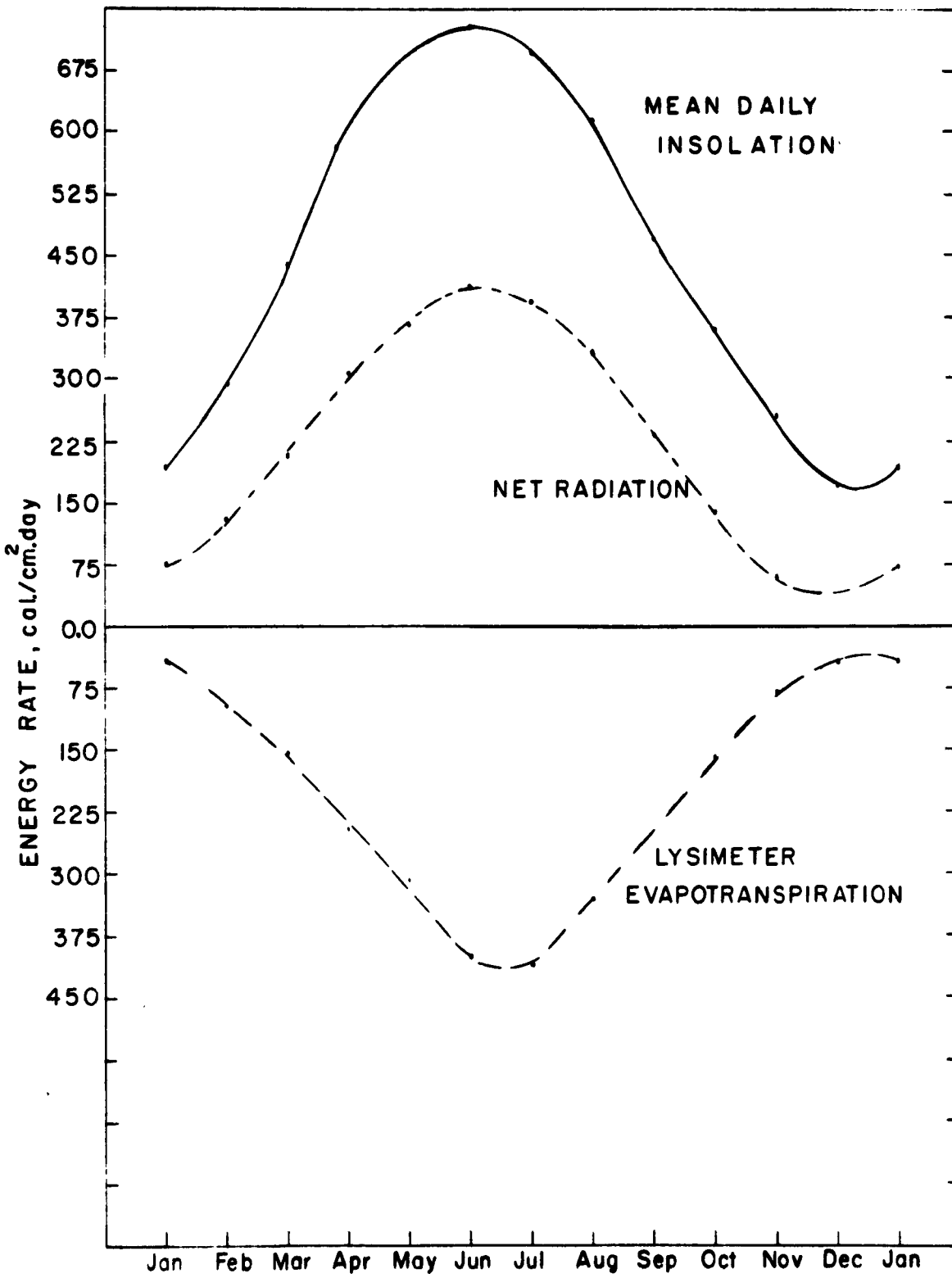

Figure I-10. Annual curves of average daily evapotranspiration and net radiation at Davis, California.

5. Precipitable water, inches, U.S. map 2.6''/(30-40°L), station (denominator to 0.01'', contours 0.25''.)
6. 1000 - 500 mb thickness, 1/2 N. Hemis., 1.7''/(30-40°L), dotted contour lines, 2 x 100 ft. intervals, (to indicate density gradient).

Interpolating these maps for Davis, California, Table I-2 gives the essential meteorological data covering the major test period 0800, 28 October to 1600, 30 October 1961. It is to be noted that test period fell in the wake of a cold front that was followed by rapid pressure rise to the northwest causing influx of polar continental air. There were some remnants of the front shown by some cloudiness in the east on the morning of 28 October, but the sky was cloudless from noon to noon 29 October.

The 4-mb isobar spacings on weather maps of 2.4 Latitude-degrees gives only a rough indication of the strong wind during most of the test period. The cross-isobar flow cannot be determined well from such size maps, and the pi-bal and radiosonde wind directions show change in direction with height. The speeds of overhead wind observed at the Sacramento airport above 500 feet apply well to Davis (15 miles west). These pi-bal readings taken every 6 hours show consistent strength and only slight turning at the 2000-foot level from 350° at 04 hour 28 October 1961 to 10° at 04 hour 29 October and to 30° at 22 hour.

The tests of 30/31 July 1962 were carried out under the typical summer conditions in which the Arizona Low develops an extention into Northern California. This extension even establishes a low pressure core of its own in the upper Sacramento Valley during the afternoon on many days. In the data compilation containing sea level pressures for Davis and Red Bluff, it can be seen that this was the case during the test period. This barometric phenomenon produces a distinct daily wind cycle at Davis. According to a diagram for average direction frequencies by H.B. Schultz (1961), southerly winds prevail most of the day. They, however, decrease and often are reversed in the morning hours as the Northern California low pressure core disappears. The test days of July 1962 experienced this regime in a more pronounced form. The influx of the marine air was somewhat stronger than usual in the daytime and could not be reversed to a northerly flow in the morning. The southerly directions lasted 21 hours, the remaining 3 hours

TABLE I-1. METEOROLOGICAL CONDITIONS AT DAVIS, CALIF. INDICATED BY U.S. DAILY WEATHER MAPS

		May 14		May 15		May 16		May 17
	P.S.T.		2200	1000	2200	1000	2200	1000
	Greenwich		0600	1800	0600	1800	0600	1800
Sea level	Pressure mb		1014	1014	1011	1012	1012	1014
	Isobar direc. from Az°		325	360	305	340	287	340
	4-mb spacing Lat. deg.		2.0	1.7	1.6	2.0	1.7	3.0
	Temperature at 5' °F		57	72	57	71	52	57
	Relative humidity at 5' o/o		72	37	75	51	85	75
	Wind MPH		SW 4	N 10	SW 8	SW 6	SW 9	N 5
	Sky		clear	clear		clear		Coastal fog lasted till 10:50 am
	Weather type		type 2	type 2		type 3 (marine air)		type 3

		July 25		July 26		July 27		July 28		July 29	
	P.S.T.	1000	2200	1000	2200	1000	2200	1000	2200	1000	2200
	Greenwich	1800	0600	1800	0600	1800	0600	1800	0600	1800	0600
Sea level	Pressure mb	1012	1012	1016	1015	1017	1011	1014	1011	1011	1011
	Isobar direc. from Az°	330	265	345	340	347	270	355	270	330	270
	4-mb spacing Lat. deg.	3.0	1.4	4.9	2.4	2.6	1.5	4.3	1.7	1.7	1.6
	Temperature at 5' °F	76	62	77	63	73	64	79	66	72	56
	Relative humidity at 5' o/o	49	67	46	63	49	59	45	47	51	80
	Wind MPH	S 2	W11	var 2*	SW 8	N 3	S 5	N 3	S 6	SW7	WSW-12
	Sky	clear		clear		clear moist-warm		clear		clear	
	Weather type	type 3		type 3		type 3-2					

* Transition from NW to SW lasted 2 hours

TABLE I-2. METEOROLOGICAL CONDITIONS AT DAVIS, CALIF. INDICATED BY U.S. DAILY WEATHER MAPS

Map No.		Oct. 27		Oct. 28				Oct. 29				Oct. 30
	P.S.T.	1600	2200	0400	1000	1600	2200	0400	1000	1600	2200	0400
	Greenwich	0000Z	0600	1200	1800	0000Z	0600	1200	1800	0000Z	0600Z	1200
1	Sea level, U.S. daily											
	(pressure, mb		1017		1020		1018		1017		1016	
	(isobar direc. from, Az°		349		026		057		064		68	
	4-mb spacing, Lat. deg.		2.2		2.3		2.0		2.4		3.0	
	temperature °F		51		55		47		58		49	
	Relative humidity at 5' o/o		56		48		37		40		37	
	Wind MPH		NNW 3		N 13		NNW 4		N 23		N 7	
	Sky		clear		clear		clear		clear		p. cloudy	
	Weather type		type 7		type 1		type 1		type 1		type 1	
2	1000 mb, polar (height, feet	420				450				330		
	(iso. direc. from, o	358				043				090		
	(40 mb spacing, Lat. deg.	6.4				6.8				9.6		
3	850 mb, N. Amer.											
	(height, feet	4800		4900		4900		4800		4800		4800
	(iso. direc. from, o	317		013		040		063		090		112
	(200 ft. spacing, Lat. deg.	3.7		5.2		3.1		1.9		2.7		3.5
4	Surf. press. 12-hr change, mb	-3.	0	1.	2.	1	-1	-3	-5	0	0	0
5	Precipitable moisture, inches	.32		.29		.31		.15		.23		
6	Thickness, 1000-500 mb, feet			17900		17900		17800		18000		
	gradient direc. o			040		058		090		115		
	" 200 ft. spacing, Lat. deg.			1.5		1.6		1.8		1.5		

TABLE I-3. METEOROLOGICAL CONDITIONS AT DAVIS, CALIF. INDICATED BY U.S. DAILY WEATHER MAPS

		29 July 1962		30 July				31 July			
P.S.T.		1600	2200	0400	1000	1600	2200	0400	1000	1600	2200
Greenwich		0000	0600	1200	1800	0000	0600	1200	1800	0000	0600
Sea Level Pressure Davis	mb	1012	1013	1014	1016	1015	1016	1016	1018	1016	1015
" " " Red Bluff	mb	1010	1012	1014	1016	1013	1015	1016	1017	1014	1014
Thickness 1000-500 mb	feet	19,000				18,900				19,000	
Wind direction (6')		SSW	S	SW	SW	SSW	S	S	SW	S	SSW
Wind velocity (6')	mph	14	7	2	3	11	8	2	3	11	10
Temperature (5')	°F	86	60	53	75	85	60	53	72	86	61
Relative Humidity (5')	o/o	37	72	93	55	32	75	94	58	35	71
Sky and Weather		clear	clear	clear	clear	clear	clear	clear	clear	clear	clear
Weather Type (see text)		3	3	3	3	3	3	3	3	3	3

	Dec. 12, 1962				Dec. 13				Dec. 14			
P.S.T.	0400	1000	1600	2200	0400	1000	1600	2200	0400	1000	1600	2200
Greenwich	1200	1800	0000	0600	1200	1800	0000	0600	1200	1800	0000	0600
Sea Level Pressure mb	1021	1023	1023	1024	1024	1026	1024	1024	1023	1023	1019	1019
Thickness 1000-500 mb feet			18,250		18,300		18,300		18,300		18,300	
Wind Direction (6')	S	S	N	NNW	S	variable	N	N	N	NNE	S	W
Wind Velocity (6') mph	2	3	1	3	1	1	4	3	3	2	2	2
Temperature (5') °F	43	43	46	45	44	49	55	52	52	56	60	51
Relative Humidity (5') o/o	100	100	100	100	100	92	78	93	98	92	75	91
Sky and Weather	fog	fog	fog	overcast			overcast				partly cloudy	rain
Weather Type	5	5	5	5	5	5	5	5	5	5	3	6

(from 6 to 9 A.M.) being calm or lightly variable.

The weather conditions at Davis during the test of December 13/14 were typical for a transition period from a high pressure regime to a cyclonic circulation. During the previous 8 days, a high had been centered over the Plateau States so that Northern California was at its western edge most of the time. The resultant winds had northerly directions, however with weak velocities. Clear skies with extended periods of heavy ground fog had been the prevailing character of the weather, the formation of which was favored by a high pressure ridge aloft.

A storm in the Eastern Pacific gradually intensifying brought an occluded front to the California coast on December 13. This front was halted by the high pressure ridge just west of the Davis area, producing rain only on the west side of the Sacramento Valley (Woodland, Williams) but not in the Central part (Marysville, Chico). The effect of this situation for Davis was a "low overcast" and a temporary change of wind direction. But with the dissipation of the front, the weak north wind regime became re-established from 1600 PST on 13 December for a 24-hour period. In the late afternoon of 14 December, the Davis area was affected by a stronger front, resulting in rain the following night.

8. Procedures for Hourly Determination of Energy Flux Rates: The schematic diagram Figure I-11 shows the many interdependent flux variables involved in transfers of momentum, heat and moisture near the surface of the ground. The sign convention for these figures is that heat flow toward the air/ground interface is positive and those away from it negative. This is the convention used in the basic five-part expression for conservation of energy.

(I-1) $$R_n + G + H + E_v + M_e = 0, \qquad \text{cal cm}^{-2}\text{min}^{-1},$$

where

R_n = Net whole-spectrum radiation exchange at a horizontal surface above the vegetation

G = Conductive heat flux in the ground

H = Convective heat flux in the air

E_v = Latent heat flux in the mass flow rate of water vapor in the air (= $h_{fg} \times Q_w$)

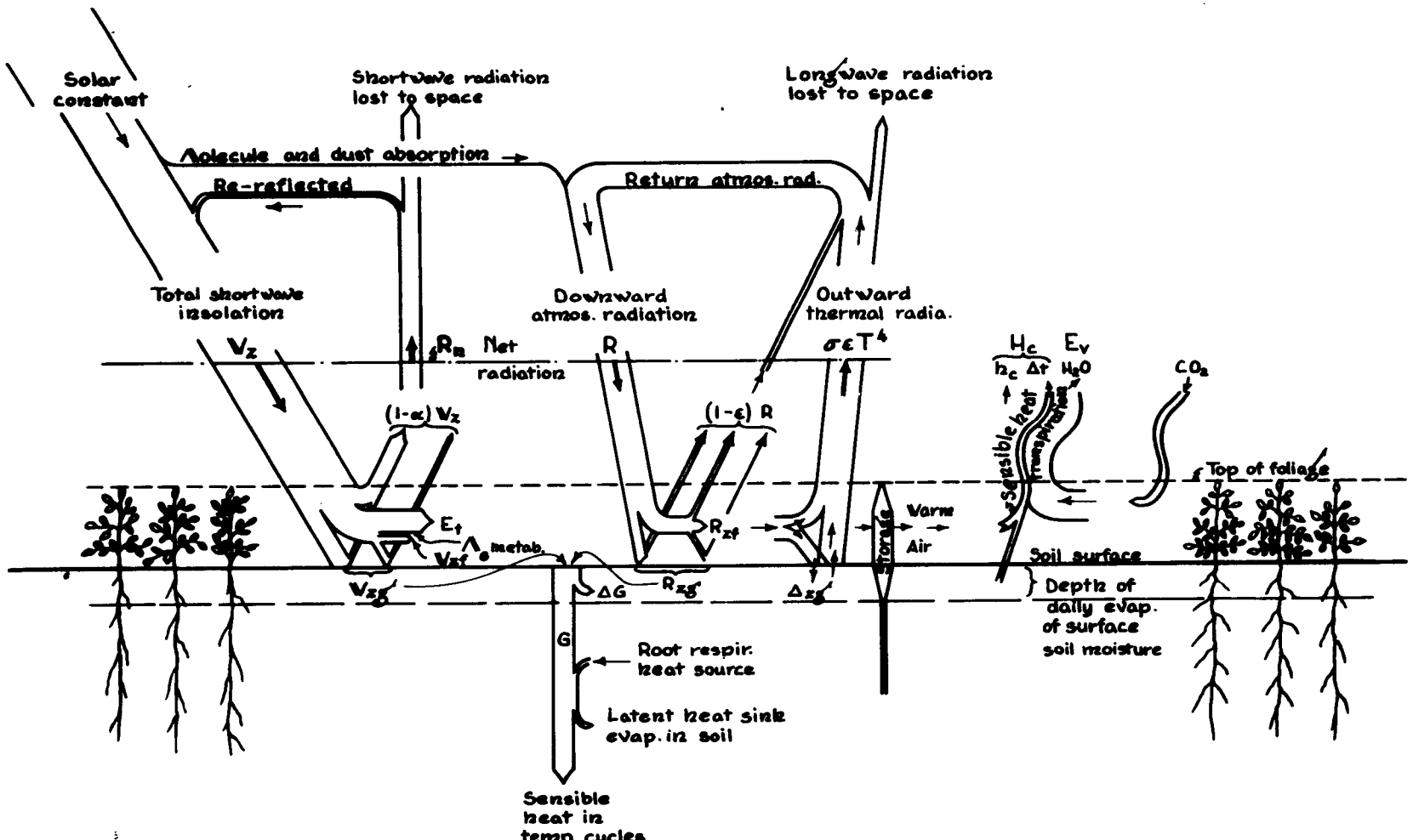

Figure I-11. Midday diagram of surface layer exchanges.

M_e = Net metabolic heat flux above soil surface used in photosynthesis with respiration.

This convention of signs means that at midday incoming solar energy is positive, heat flow into the ground is negative (under usual conditions), convective heat flux upward in the air is negative, the latent heat used in evapotranspiration is negative and net metabolic heat used in photosynthesis is negative. The last is negligible for rye grass turf frequently mowed but could be the same order of magnitude as soil heat conduction for a well developed crop growing vigorously.

Determination of Net Radiation Exchange. R_n. --If there were no radiometer errors such as due to unequal convective heat transfers from the upper and lower sides of plate receivers and no differences in blackness for shortwave (solar) radiation compared with that for longwave (thermal and atmospheric) radiation, the one radiometer required for energy balance would be either:

(2a)* Uncovered, aspirated, whole-spectrum, net exchange radiometer patterned after the original Gier & Dunkle (1950) radiometer, or

(2b) Black plate heat flux transducer enclosed with thin polyethylene covers on both upper and lower sides, such as the Funk (1960) C.S.I.R.O. Radiometer.

The direct emf response of each of these radiometers indicates the basic net radiation flux rate, R_n, if the grass turf underneath is a proper sample of the whole test site. This net radiation, however, is made of 5 parts each of which is of interest. An array of 8 radiometers, therefore, is used for a complete radiation study as follows:

I. Direct-beam sunshine intensity is now measured by:

(1a) The new model Eppley "normal-incidence" radiometer, temperature compensated and provided with clock-driven mounting geared to track the sun. This radiometer is glass-covered and can be provided with filters.

This instrument is our best means of calibration.

All shortwave radiation on a horizontal surface involving direct-beam radiation should be checked by observed normal-incidence

* Instrument numbers are listed in Table A-1.

intensity: I, multiplied by the sine of the sun's altitude. Namely, the error is indicated by (1b) - [(1d) + (1a) sin α].

II. (1d) The standard Eppley pyrheliometer used for diffuse, shortwave sky radiation is the same model as (1b) but is provided with motor-driven shade.

With cloudless sky (1d) ÷ (1b) should be less than 1/7 at noon.

III. (1c) A standard Eppley pyrheliometer (1c) is used inverted to measure upward reflection of total incoming shortwave diffuse sky radiation (1d) and direct beam (1a) reflected nearly diffusely.

This upward shortwave (1c) divided by (1b) standard insolation is the albedo of the surface. It varies with altitude angle of the sun and at low angles is less toward the sun (looking into shadows of surface roughness). At noon over grass turf it should be a little less than 25%. The net shortwave radiation exchange is (1b) - (1c).

IV. (2d) The present whole-spectrum single-hemisphere radiometer is the B & W "total" radiometer* having a bottom shield. The emf response of this instrument measures the difference between whole-spectrum incoming radiation and the outgoing emissive power of the plate depending on plate temperature.

The bottom shield causes errors in a wind because of unequal air velocities top and bottom (see Portman and Dias, 1959). Considerable reduction of error can be obtained by orienting the radiometer with the wind and possibly by shading it from direct-beam sunshine. The downward longwave radiation is (2d) - (1b) after allowing for outgoing emissive power of the black plate. This is the incoming atmospheric radiation mainly from water vapor and carbon dioxide. The simplest calculation is by FAB's syllabus formula 2-28. When radiosonde profiles are available (and extrapolated to local standard shelter air temperature and vapor pressure) fairly reliable calculation can be made by FAB's (1941) M.I.T. procedure. The measured incoming atmospheric radiation (longwave) when shaded is (2d) - (1d) after allowing for outgoing emissive power of the receiver surface.

---

* The B & W shielded radiometer will be replaced by the new California single-hemisphere radiometer which is to be used shaded from direct-beam sunshine.

TABLE I-4. RADIATION EXCHANGE COMPONENTS

Davis Lysimeter Site, 28 October 1961

1300 - 1340 Example		
Normal incidence direct-beam intensity	=	1.235 cal/cm^{2}min
Sun's altitude = 34°00', m = 1.8, sin = 0.560		
∴ vert. comp.	=	0.742 "
Incoming shortwave (regular Eppley)	=	0.894 "
Diffuse sky shortwave (through glass) =0.894-0.742	=	0.152 "
Upward shortwave (inverted Eppley)	=	-0.166 "
Net shortwave	=	0.728
Albedo	=	0.186 non-dim.
Incoming atmospheric longwave, calculated from 1500 radiosonde = 25.197 cal/cm^{2}hr	=	0.420 cal/cm^{2}min
Outgoing longwave radiation (σT^4 for 18.4°C = 35.472 cal/cm^{2}hr, black, to include reflected atmos. radiation)	=	-0.591 "
Net longwave radiation exchange	=	-0.171 "
Measured net whole-spectrum	=	+0.543 "
Calc. net shortwave (measured 0.728)	=	+0.714 "
Atmospheric transparency for longwave = $\frac{420}{591}$	=	71%
Whole-spectrum net diffuse, sky hemisphere + 0.152 - .171	=	-0.019 cal/cm^{2}min

V. (2c) Upward longwave is measured now by a shaded, whole-spectrum Gier & Dunkle net radiometer in conjunction with known grass surface temperature.

The longwave net radiation exchange is found by subtraction from net shortwave (1b) - (1c). Then the upward longwave is found after subtracting the downcoming atmospheric IV. This should be within a few percent of calculated emissive power of the grass turf based on 5 cm temperature. Table I-4 shows the radiation components determined for noon, 28 October 1961.

It is to be noted that although for energy balance we use net radiation, downcoming minus upgoing, this is not the total radiation load on man or foliage above the ground. Even total downcoming plus upgoing is not the whole spherical effect although the two-hemisphere sum explains fairly well the skier's sunburn over a snow surface. The best simple geometrical shape of receiver for total irradiation is a sphere, namely: black-globe thermometer interpreted as Mean Radiant Temperature by correcting for heat transfer in wind, (see Bond and Kelly 1955 or Syllabus chart 2-20, p.70). Its best verification is normal-incidence pyrheliometer in full (1a) plus shaded Eppley (1d) plus inverted Eppley (1c) plus incoming and outgoing longwave radiation IV + V, with some allowance for strong horizontal longwave radiation.

Determination of Heat Conduction in the Soil. Soil heat flux G can almost be read directly from heat-flow meters buried near the soil surface. Also by determining the thermal properties of the soil, it is possible to calculate the bulk heat flow using observed diurnal temperature cycles as in FAB's syllabus eq. 3-6, p. 82 and allowing for non-homogeneity.

Some of the transfer of sensible heat from soil to air occurs at a slight depth below the soil surface and thus the hourly temperature change in the top centimeter might reasonably be excluded from calculations of diurnal heat flux in the soil as a whole. This points to direct use of the heat-flow meters installed at 1 cm depth, except that these may not properly represent the heat flux at this "surface" level because of non-uniform root distribution. It is necessary, therefore, to consider as most reliable the heat-flow meters installed at 10 cm depth. These are at three locations within the 20-foot lysimeter and at two locations outside the lysimeter. Temperatures at all locations are measured at 1, 10, 50, and 83 cm depths,

but numerical analysis to treat variation of thermal properties with depth needs the 25 cm temperature which is measured at 2 places, one inside and one outside the lysimeter.

Under the rye-grass turf the soil heat flux is small relative to net radiation and evapotranspiration so probably it is not worthwhile to go further than the 10-cm deep heat-flow meters adding the calculated hourly change in heat content of the 10 (or 9) cm of soil above them. The change in temperature with time in this layer is measured by 3 strings of resistance thermometers both inside and outside the lysimeter.

Determination of Sensible Heat Flux in Air. Convective heat transfer rate, H, above the vegetation tops has been measured only by eddy correlation devices such as used at 4-meter height by A.J. Dyer here in 1961, and by the MIT group at 16-meter height. A sonic anemometer developed by Kaimal and Businger (1963) which also measures temperature should be tried at various heights from close to the ground up to 4 meters when we make the next advection test. In the absence of such eddy correlation sensors, the flux rate of sensible heat is necessarily found as the make-up term in equation (1), three of the other terms, R_n, G and E_v being known, and the net metabolic heat flux M_e being negligible as shown later.

Determination of Evaporative Heat Flux. Pruitt's 6-meter diameter lysimeter on scales gives a positive measurement of weight loss which is converted to energy term, E_v, by applying a standard latent heat of vaporization of 590 cal/gram. This figure is correct for 10°C and varies only 0.53 cal/gram °C in the ordinary temperature range. For the actual area of the lysimeter, the conversion from pounds weight loss are 0.015367 x pounds loss equals mm depth of water loss. And this times 59.0 gives cal/cm^2.

Ordinarily the weight is printed automatically every 4 minutes. There is some scatter especially in a wind and this is worse when the cover to the tunnel is open, but this does not alter the cumulative weight loss. The flux rate is the change in weight per unit time, namely the 1st derivative of the weight vs. time curve. The smoothed weight curve as used in the 1962 annual report, therefore, must not have high harmonics because these aggravate irregularities in the derivative curve.

This very reliable measurement of water loss can be used directly for comparison with eddy flux of water vapor as measured by Dyer without relating

to energy balance.

Determination of Energy Flux Rate for Net Metabolism. The hourly net metabolic energy use M_e is so small in comparison with the other energy flux rates it can be neglected in the energy balance. The following is the estimate, however, of this small term by J.L. Monteith (August 1962).

The formation of carbohydrate by photosynthesis and the converse process of respiration can be represented by

$$\text{(I-2)} \qquad n\,CO_2 + n\,H_2O \rightleftharpoons (CH_2O)_n + nO_2$$

where the heat of formation of 1 g of carbohydrate is about 3.6 kg cal. From the ratio of molecular weights, the assimilation of 1 g CO_2 requires the absorption of 2.4 kg cal in the form of solar energy in the wavelength range 0.4 - 0.7 μ.

For many common agricultural crops, the maximum rate of net CO_2 assimilation measured in terms of land area is about 3 mg $cm^{-2}day^{-1}$, equivalent to about 7 cal $cm^{-2}day^{-1}$ and representing a balance between daytime photosynthesis and respiration proceeding day and night. As a guide to the complete CO_2 balance of a vigorously growing crop the following figures are typical of summer measurements at Rothamsted:

	mg CO_2 $cm^{-2}day^{-1}$	cal $cm^{-2}day^{-1}$
Gross photosynthesis	+ 4.2	- 10.0
Respiration tops	- 0.7	+ 1.7
roots	- 0.5	+ 1.2
(micro-organisma	- 0.3	+ 0.7)
Net photosynthesis	+ 3.0	- 7.2

Respiration of roots and tops is temperature dependent, probably increasing by a factor of about 2 for an increase of 10°C. Respiration rates will, therefore, be somewhat higher during the day than at night, and during summer may be twice as great at Davis as at Rothamsted for two crops with the same total dry weight. Maximum gross rates of photosynthesis will also be higher at Davis because of higher mean daily radiation, perhaps by 20-40%, leaving roughly similar values for maximum net photosynthesis at the two stations.

On the lysimeter field, however, the rate of dry matter production appears an order of magnitude less than the maximum rate given above. In June and July, 1962, the mean yield was only 15 lb $acre^{-1}day^{-1}$ and allowing for root development, this may represent a net CO_2 uptake of about 0.18 mg

$cm^{-2}day^{-1}$. The depression of yield may be attributable to one or more of these factors: cutting before the sward reaches its maximum growth rate; high surface temperature well beyond the optimum for rye-grass; possible nutrient shortage although 30 to 40 pounds of nitrogen per acre are applied every 4 to 6 weeks. Assuming equal length of day and night, the energy absorbed by photosynthesis during daylight will be about 0.1 cal $cm^{-2}hr^{-1}$. At times the yield went up to 60 pounds per acre, but even so, the hourly daytime rate would be only about 0.4 cal/cm^2hr. Allowing for the relatively small amount of foliage allowed to develop between cuts, about the same heat flux would be released by respiration during the night. These figures should be regarded as guides to orders of magnitude, but they show how trivial the heat fluxes are.

Conclusions. Present results have firmly established the typical diurnal curves of 4 energy fluxes for the rye grass plot. Also momentum flux basic to all eddy transfers can now be measured by the new, floating shear-stress lysimeter. With the established physical relationships and the extra precision in measurement and with proved automatic computing for multiple observations, the next objective to determine horizontal differences (advection effects) can now be undertaken with confidence.

REFERENCES FOR CHAPTER I

Bond, T.E. and C.F. Kelly, 1955. "The Globe Thermometer in Agricultural Research", Agric. Eng., Vol. 36, No. 4, pp. 251-255, 260, April.

Brooks, F.A., 1941. "Observations of Atmospheric Radiation", Papers in Physical Oceanography and Meteorology, Vol. 8(2):1-23 (6 fig., 4 tables). Mass. Inst. of Technology and Woods Hole Oceanographic Inst., Oct.

Brooks, F.A., 1959. "An Introduction to Physical Microclimatology". Syllabus, University of California, Davis (reprinted 1960).

Brunt, David, 1939. "Physical and Dynamical Meteorology", Cambridge University Press.

Funk, J.P., 1960. "Measured Radiative Flux Divergence Near the Ground at Night". Quart. Jour. Royal Met. Soc., Vol. 86:382-389.

Kaimal, J.C. and J.A. Businger, 1963. "A Continuous Wave Sonic Anemometer-Thermometer", Jour. of Applied Meteoro, Vol. 2, pp. 156-164, February.

Portman, D.J. and F. Dias, 1959. "Influence of Wind and Angle of Incident Radiation on the Performance of a Beckman and Whitley Total Hemispherical Radiometer", Univ. Mich. Res. Inst., Project No. 2715-1-F-April.

Schultz, H.B., N.B. Akesson, and W.E. Yates, 1961. "The Delayed Sea Breezes in the Sacramento Valley and the Resulting Favorable Conditions for Application of Pesticides." Bull. A.M.S. 42, pp. 679-687.

CHAPTER II

PHYSICAL INTERPRETATIONS OF DIURNAL VARIATIONS OF EDDY TRANSFERS NEAR THE GROUND

F. A. Brooks

The main objective of this 3-year micrometeorological research project on eddy transfers in providing reliable data in simultaneous profiles and flux rates has revealed much more variability in basic constants for momentum, heat and moisture transfer and their ratios than was expected. It is pertinent, therefore, to examine first the implications of original limitations to steady shear flow under near-neutral conditions which have been far exceeded in diabatic conditions especially in cloudless summer weather. These limitations explain some of the wide diurnal variations found in coefficients applicable through the full height of measured profiles governed by friction velocity and other vertical fluxes. A method using the asymptotes of curved profiles has been developed from modified Monin-Obukhov formulas to evaluate related Karman coefficients for eddy transfers of heat and moisture. All 3 coefficients evidently have strong diurnal variation. Also the log-law intercept z_o ordinarily thought of as a fixed surface roughness parameter is found to have considerable diurnal variation. Hence, in progressing toward quantitative relationships between eddy transfer rates throughout the daily cycle and associated profiles, primary emphasis is placed on simple analytical expression of measured profiles and on systematic relations with observed flux rates. To prepare for later theoretical deductions, the basic physical concepts are kept in mind and attention is directed to the minimal adaptations in conventional analytical treatments to represent properly the outdoor diurnal variations in eddy transfers. In general the wide range of observations reported here requires some modification but not rejection of well known formulas.

Reconsidering the whole complex system of eddy transfers, the actual outdoor air flow is almost sure not to conform exactly with aerodynamic and conduit-flow theories in five respects:

1. If we try to use neutral stability (the natural isothermal condition for wind-tunnel research), we find suitable outdoor profiles of constant virtual temperature only momentarily, twice a day and imperfectly. The usual adaptation by micrometeorologists is to

work in steady winds or overcast weather or close to the ground. The latter results can be erratic because of nearby irregularity in surface roughness. To minimize very local temperature differences, we are using the averages of four profile masts spaced 35 x 50 meters. More important, however, in treating curved semi-log or log-log profiles is the consistent use of some general mathematical form (making least-squares fits by automatic computer described more fully in Chapter IX). The use of these formulas then yields the same vertical transfer rates at all levels (within the limits of applicability) in a given hour during steady conditions. Of the two coefficients used later to describe diabatic profiles, the β coefficient suits the usual concept of log linear profile for near-the-ground eddy transfer or for small departures from neutral stability.

2. If we use mean magnitudes of temperature and velocity outdoors, these must include effects of large convective circulations of cumulus cloud spacing. Low level organized thermal updrafts are difficult to find, but occasional downward gusts at the ground surface can be easily identified particularly in continuous recording of air drag. It is not practical, however, at present to filter large-scale perturbations out of all transducer responses. Our best procedure for averaging, therefore, is to use a long enough time period (20 or 30 minutes) to reduce many single gusts to statistical mean effects. For profiles, this is helped greatly by spacing the masts far apart yet related to the lysimeters and to the two directions of predominant winds. The Davis test site is surrounded by miles of very flat ground of substantially the same total roughness. Tests can be scheduled, therefore, for desirable wind direction. Thus for tests needing uniform evapotranspiration conditions, measurements are made in a S. or S.W. wind, and the 12 1/2-acre irrigated site has now been doubled to provide a fetch of over 400 meters. A north wind is used for advection tests; the moist-surface fetch in that direction being 200 meters.

3. If we try to use boundary-layer theory, three basic concepts do not hold:

i. There is no steady "free stream velocity" close above the earth's surface.

ii. There is no specific depth of the boundary layer.

iii. There is no length from a leading edge to use in a Reynolds number (except in field-edge contrasts in a dry north wind).

Nevertheless, there is striking similarity in mean profiles outdoors with traditional boundary layer profiles, so some methods of relating boundary layer findings will be discussed later.

4. If we try to use the "Law of the Wall" (log-law velocity profile), there are several difficulties:

   i. The surface of the grass turf is neither smooth nor rigidly rough.

   ii. The equivalent level of zero velocity (distant d above the soil surface) is not a solid plane but can be penetrated by eddies.

   iii. The law is not expected to hold near a level of velocity maximum and is useless above such a level.

   iv. In strong natural convections, mean profiles are only statistically representative of thermal updrafts, and the basic assumption that mixing length is small compared with height above the surface is not valid.

   There is little to be done about these difficulties. Practically they pose the question: Is the log law still useful or would the power law be more useful? At present it seems that stability-modified forms of aerodynamic relations via the log law are more useful.

5. If we try to use the concept of fully rough flow, we do not have:

   i. an overhead solid surface generating cross eddies, nor

   ii. fixed heights of roughness, k_s, as to top of sand grains, nor

   iii. a diameter of the flow section useable as a length element in a Reynolds number to characterize the flow regime into laminar, laminar-turbulent, and turbulent. Furthermore,

   iv. shear stress outdoors does not vary with height in the same manner as in conduit flow or channel flow, and

v. outdoor air flow is not the result of pressure drop along the direction of flow.

In spite of the above five limitations, the analytical forms used to describe aerodynamic and pipe flow are firmly established and should be very useful as a framework or starting base for analyzing the more complex outdoor eddy transfers. Some aerodynamic experts even say that if we could furnish an accurate enough velocity profile, they could specify the flow regime.

Excluding discussions on turbulence theory which need more basic data, the most prevalent doubt about mathematical formulation of vertical profiles of velocity concerns the choice between the logarithmic "law of the wall" and the power law (log-log plotting). The former is considered more theoretical and is firmly based on similarity concepts. The latter is usually found in analyses of diffusion and is closer to dimensional analysis. Neither form fits the data exactly for constant flux rates in non-neutral stability conditions; both, however, fit observations for limited heights within the usual precision of observations; and the two forms are related in ordinary shear flow. Thus the choice between these two mathematical forms depends more on familiarity and convenience in automatic computing programming than in possibly spurious results as the limits of applicability are approached. In reporting this initial phase of investigation of eddy transfers, we are using the log law concept modified by a low order two-term function to nearly fit the curvature seen in semi-log plotting of the data. Rather than expand to second order correction to improve the Monin-Obukhov (1954) approach, a function in $(z/L)^{1/2}$ is used on this year's profiles. This affects the magnitude of z_o and increases skepticism of its use as a "roughness parameter". Mathematically it is merely an integration constant. This is discussed in more detail under interpretation of profiles. More serious problems of mathematical form, however, can come above the layer of strong frictional shear especially near zero gradients. For instance, we need to know the finite magnitudes of eddy diffusivities where they are revealed only by turbulence intensity or by the transport of other fluxes whose gradients are not zero.

Finite Eddy Transfer Coefficients through Planes of Zero Net Momentum Flux.

Although eddy diffusivities do not describe a whole system well because they increase with height, one of the insidious deductions from steady

shear flow near a solid surface is that eddy viscosity itself varies with velocity gradient. This concept is a false carryover from its proper definition as the ratio of momentum flux rate to velocity gradient.

Since air flow outdoors is inherently more complex than steady-state fluid flow which forms the background of all conventional formulations for eddy transfers, the simplifying assumptions need to be examined with care. In view of the continuity in bulk flow, but frequently with irregular profiles of velocity and temperature, any concept that goes to infinity within the gross boundary layer must be considered not by itself but only in combination with another factor so that the two together are always of finite magnitude. Furthermore, no eddy transfer coefficient should be considered zero just because there happens to be zero gradient. Probably the best analogy for this is the known simultaneous evaporation and condensation at a water/air interface even when there is zero change in total quantity of liquid.# Similarly for net eddy transfers, it is erroneous to define eddy viscosity in terms of velocity gradient ignoring the concurrent shear stress that is an essential part of the basic defining equation: $\tau/\rho = K_M \, \delta\bar{u}/\delta z$.

The outstanding example of erroneous evaluation of K_M is that of Nikuradse (1932) still reported in authoritative texts in fluid mechanics. Berggren (1963) shows that this error comes from Nikuradse's using a semi-cubic equation to smooth his velocity profile (not publishing his original observations). Since eddy transports of sand grains and of heat transversely across conduit center are well proven, it is obvious that eddying occurs across the plane of zero shear and thus there must be a finite eddy viscosity at $\delta\bar{u}/\delta y = 0.0$ possibly of full magnitude as is true of viscosity in laminary flow. The essential mathematical requirement for indicating finite eddy viscosity here is simply that the velocity gradient and the shear stress both approach zero at proportional rates. This is substantially true for the parabola deduced for laminar flow and is also satisfied sufficiently by the error function (Brooks & Berggren 1944). The latter yielding a wide shallow dip at velocity maximum has since been found to explain satisfactorily the cross-midstream distribution of fine

A glass of tritiated water standing uncovered in a laboratory (where the dew point is near the water temperature) will lose its tracer quality in a week without change in water level.

sediment in turbulent flow.

Outdoors at the level of a velocity maximum in a bulge in the velocity profile, the change of sign is clear enough in passing through zero but not the real magnitude of eddy viscosity. Nevertheless there are natural outdoor air flows for which the actual change in shear stress can be estimated reasonably well. These are in density currents particularly of chilled air flowing downhill on clear calm nights such as shown in Fig. II-1. Below this level of zero net momentum exchange, the integrated body force of the chilled air in steady flow downhill is balanced by the surface friction drag force. Above the level of zero shear, the integrated body force in steady flow is balanced by the fluid friction in the air current underrunning the stationary overhead air. If the overhead air moves against the density current, the integrated body force above zero shear level can balance the greater overhead air friction by (i) increasing the shear in the current above zero shear level, or (ii) by decreasing the maximum velocity. For the laminar case the modification of Prandtl's (1952) solution (Brooks & Schultz, 1958) by N. H. Brooks shows that the maximum velocity decreases if a counter force is applied overhead, and the real velocity gradient increases above the level of zero shear. The greater gradient (with constant viscosity) balances the extra overhead drag. The corresponding extreme flow systems investigated in laboratories are of natural convection near a heated vertical plate. The laminar case reported by Schmidt & Beckmann (1930) includes a numerical solution by Pohlhausen well summarized by Jakob (1949). An alternative solution has been extended to natural turbulent convection near a longer heated, vertical wall by Eckert & Jackson (1950).

The physical likelihood of a strong eddy viscosity continuing across the plane of zero shear can be visualized readily in the substantial rms concept of gustiness. Developing Sutton's (1953) physical interpretation of eddy viscosity based on turbulence intensity instead of velocity gradient, eddy viscosity for vertical transport is defined:

$$\text{(II-1a)} \qquad K = \ell\,(\overline{w'^2})^{1/2} \qquad , \ \mathrm{cm}^2/\mathrm{sec},$$

which suits the flux equation for shear stress $\tau/\rho = K_M \frac{\delta \bar{u}}{\delta z}$.

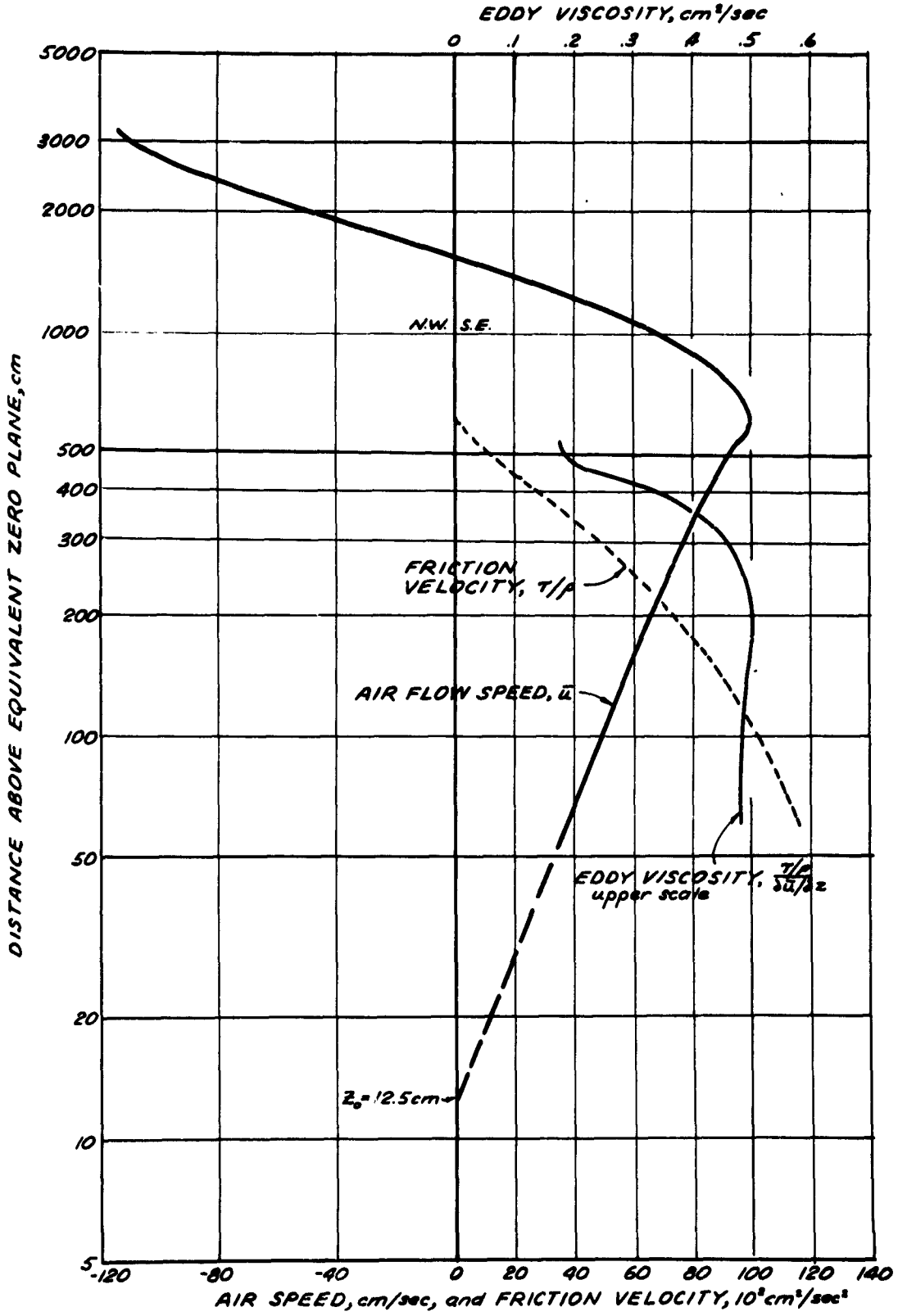

Figure II-1. Semi-log plot of velocity and eddy viscosity for a density current.

The root mean square vertical velocity is the essence of vertical gustiness

$G_z = (\overline{w^2})^{1/2}/\bar{u}$ and is evaluated by hot-wire anemometers or the conventional Taylor bivane. Measurements of diffusion can also be used. Thus eddy viscosity can be expressed:

(II-1b) $K_M = l\, G_z\, \bar{u}$, $cm^2 sec.$

This well shows the finite physical nature of eddy viscosity and that it is unlikely to change suddenly with height above ground since all three factors on the right hand side are smoothly continuous with distance above the ground.

Gustiness in the direction of mean wind $G_x = (\overline{u'^2})^{1/2}/\bar{u}$ is substantially the definition of turbulence intensity. For the carefully built wind tunnel at the University of California at Berkeley, which was used for anemometer calibration, this turbulence level varied from 1 to 4.5×10^{-4} for velocities ranging from 21 to 75 feet per second. For vertical eddy diffusion, measurements by Taylor bivane at 2-meter height over trampled dry grass near Davis, California (see Brooks, 1959, p. 108) show $G_z = 0.02$, 0.04, and 0.10 approximately for strongly stable, moderately stable and normal unstable conditions respectively. These are for very flat ground with no trees for more than a mile and windspeed less than 3 m/sec. Scrase (1930) reports $G_z = 0.15$ and 0.21 over grass in a mean wind speed of 10 m/s.

Single Surface Turbulent Flow

The primary difference between air flow outdoors and in a wind tunnel is, of course, the absence of a solid overhead surface generating cross eddies as previously mentioned in dissimilarity No. 5. Boundary-layer investigations are reported almost without reference to the surrounding surfaces, but are interpreted by using a horizontal length concept for organizing flow results by Reynolds Number. This is not applicable for continuous ground outdoors as outlined in dissimilarity No. 3. Some laboratory investigations in fluid flow, however, study the near-surface conditions in great detail and these give some insight into the problems of outdoor shear flow.

Before tackling the great difficulties with buoyancy-stratified fluid flows, the effect of a single rough, bounding surface (the ground and foliage)

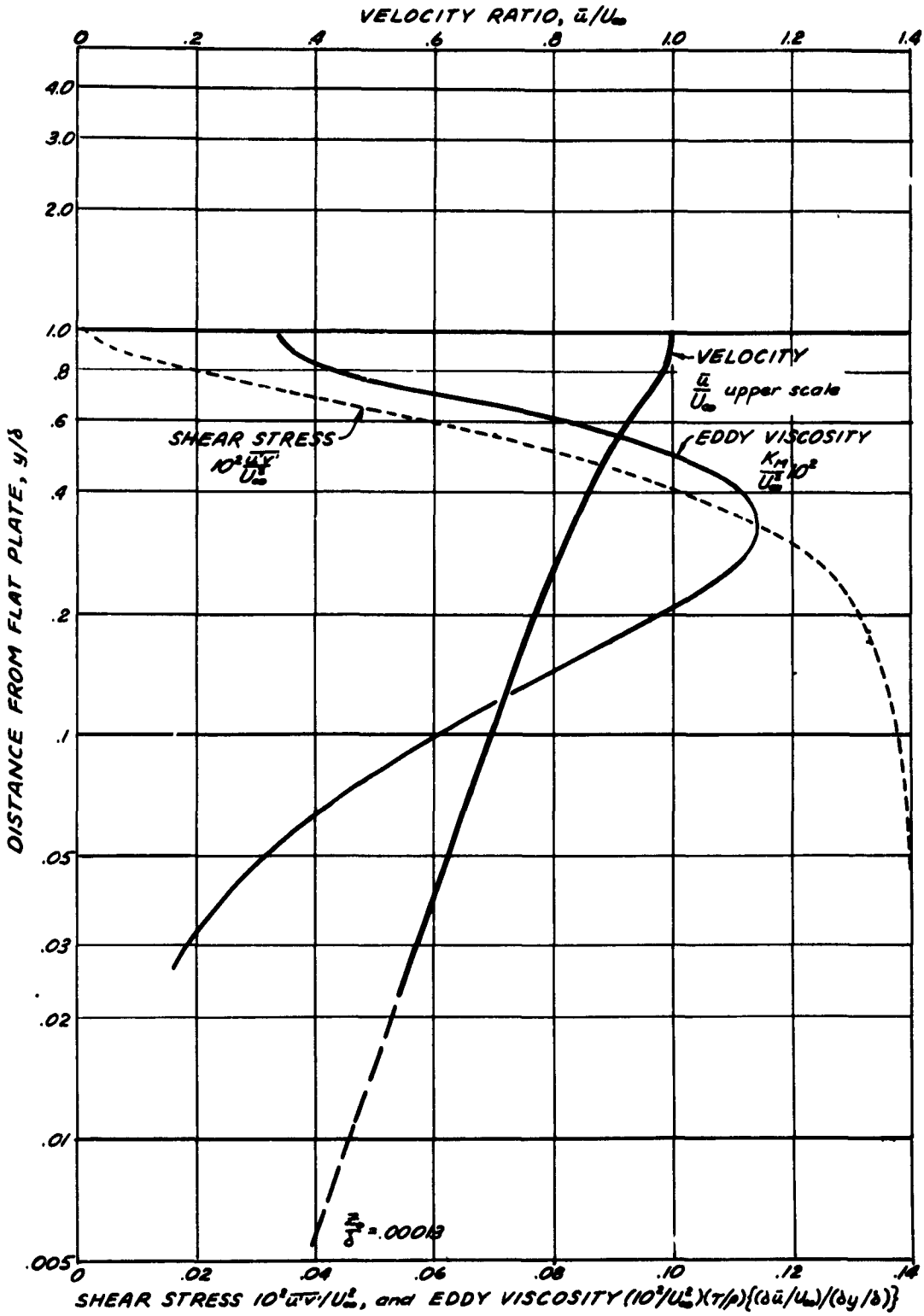

Figure II-2. Semi-log plot of Klebanoff's (1955) measurements of turbulent flow over a flat plate with calculation of eddy viscosity revealing a maximum at 1/3 the thickness of the boundary layer.

needs to be compared as well as possible with conduit flow between walls of known, regular roughness. First is the difference in single-sided generation of frictional eddies. Within the laminar layer the development of turbulent spots (Meyer and Kline 1961) is influenced by the upstream turbulence intensity which will be less when no turbulence eddies are arriving by migration from an opposite wall. Schultz-Grunow (1940) demonstrated that the velocity profile over a flat plate deviated from the pipe-flow formula at distances above about 1/10 the thickness of the boundary layer. Most of the experiments with rough surfaces, however, were made in conduits. It is essential, therefore, to find an acceptable method for adapting tunnel findings to infinite flat single surfaces.

Going directly to flat plate experiments by Klebanoff (1955), Figure II-2 gives the eddy viscosity factor calculated from his measurements of velocities and of Reynolds stresses at 20 successive distances from the wall extending to 4/3 boundary layer thickness. This shows clearly a maximum at $y/\delta = 1/3$ and a residual magnitude of about 30 per cent of maximum near the top of the boundary layer where it becomes indeterminate as velocity gradient and shear stress approach zero together. Presumably the intensity of turbulence here is the free stream turbulence which is always available for eddy transfers whenever a gradient occurs. Although the shape of eddy-viscosity profile shown in Fig. II-2 is highly significant, it leaves unsettled the question of how far is peak intensity from a surface of infinite length. Possibly this question could be answered by evaluating a natural downstream decay rate somewhat as in a wake or a jet in free air.

A surface drag interpretation independent both of distance from a leading edge and of conduit size needs to be made for interpreting open-sided flow over the ground. Ordinarily this is calculated from velocity gradient determined either by power-law log-log plotting of wind speeds at a series of heights, or by log-law plotting on semi-log graph paper.

Interpretation of Profiles by von Karman's Law-of-the-Wall

Micrometeorologists usually prefer the log-law concept of velocity distribution and consider the extrapolated intercept z_o at $u = 0.0$ as a roughness parameter. Although z_o varies with friction, it is merely the integration constant appearing from the assumed differential equation. Its physical significance is most apparent as the straight line intercept in steady wind at times of neutral stability. It seems more useful to investigate the von

Karman (1930) constant which is the basic factor for eddy transfers. The primary shear flow equation is:

$$\text{(II-2)} \qquad u_* = k_u \, z \, \frac{\partial \bar{u}}{\partial z} \qquad , \text{ cm/sec.}$$

The integrated form expressing velocity profile (including a height correction d) is:

$$\text{(II-3a)} \qquad \frac{\bar{u}_z}{u_*} = \frac{1}{k_u} \ln \frac{z-d}{z_o}$$

Converting this to 10-base logarithms and introducing u_*/ν in numerator and denominator of the log term, the common formula for velocity profile is:

$$\text{(II-3b)} \qquad \frac{\bar{u}_z}{u_*} = \frac{2.3026}{k_u} \log_{10} \frac{z-d}{z_o} = \frac{2.3026}{k_u} \left[\lg \frac{u_*(z-d)}{\nu} - \lg \frac{u_* z_o}{\nu} \right]$$

The first form of Eq. II-3b is used for graphical determination of z_o and for determining the displacement, d, of the equivalent zero plane.

The second form is used by Nikuradse to interpret his velocity profiles for water flow in rough-wall pipes as a function of lg $\frac{u_* k_s}{\nu}$ directly comparable with the conventional micrometeorological expression given in the first part of formula (II-3b) namely:

$$\text{(II-3c)} \qquad \frac{\bar{u}}{u_*} = 5.75 \lg \frac{z}{z_o} = 5.75 \lg \frac{z}{k_s} + A$$

His five expressions for A are given in Table II-1 ranging from smooth to fully rough flow. These expressions are for pipe walls coated one layer deep with sand particles of height k_s. In the table an example calculation for z_o assuming an equivalent k_s of 35 cm shows that z_o is not a constant "roughness" parameter because even for fixed sand roughness it varies with type of flow as expressed for the 5 regimes. All these are without effects of thermal stratification which also are important as shown by Sheppard (1947).

Sutton (1953, p.233) shows that the fully rough flow regime holds in most meteorological conditions. For low wind speed, however, it is evident that z_o may depend on both friction velocity and viscosity. To interpret flow regimes over various forms of roughness elements a very significant conversion

has been established by Schlichting (1960, p. 527) relating various widely-spaced obstructions to equivalent sand roughness k_s. Thus an equivalent surface Reynolds number $\frac{u_* k_s}{\nu}$ can be determined from surface drag given in terms of roughness height.

Plan of Interpretations of Eddy-Transfer Profiles

The main weakness in investigations of eddy transfers outdoors is the necessity for assuming the magnitudes of some of the basic coefficients, usually von Karman's coefficient. In this chapter, therefore, particular care has been taken to express the whole diurnal exchange system in coefficients directly measurable from observed profiles of windspeed, temperature and humidity, and simultaneous known flux rates directly measured as for evapotranspiration with Pruitt's weighing lysimeter (Chapter III) and by energy balance for convective heat flux (Chapter I). Working with the usual log-law concept for mathematical interpretation of profiles, two coefficients can be determined directly. The first is the slope of the profile (with logarithmic ordinate) which is labeled β and a second coefficient γ to describe the curvature of the profile as plotted on semilog paper. Graphical examples are given in Figures II-7 and 8. Both of these profile coefficients apply to the whole height (considered as having constant vertical flux rates) and are readily determined by automatic computer in the curved logarithmic regression line of least squares fit (see Chapter IX). An appropriate magnitude for z_o, however, needs to be specified because the downward extrapolation under diabatic conditions is highly sensitive to the scatter in observations at low levels.

Another difficulty in interpreting diabatic profiles is the lack of a stability criterion for the profile as a whole. Richardson Number is important but it varies nearly directly with height. The use of z_o/L has been suggested as a scale for stability but at this time a simpler stability index $t'_* = H/\rho c_p \beta_1$ seems adequate. This depends only on heat flux rate and the slope of the velocity profile. Hourly values for July are given in Table II-3 which describes conditions for the whole vertical spread of observations. This dimensional index, in ^oC, includes velocity gradient (in the β_1) to the first power instead of squared as in the Richardson Number. One advantage of the t'_* stability scale is the relatively uniform spread near neutral conditions.

TABLE II-1. NIKURADSE CHARACTERIZATION OF FLOW REGIMES

Flow Regime	$A = \frac{\bar{u}}{u_*} - 5.75 \log \frac{z}{k_s}$	$\text{Log } z_o = \log k_s - \frac{A}{5.75}$	Necessary values if $k_s = 35.4$ cm, $\nu = .142\ cm^2/sec$	
			u_* cm/sec	z_o cm
SMOOTH				
$0 \leq \log \frac{u_* k_s}{\nu} \leq 0.55$	$5.5 + 5.75 \log \frac{u_* k_s}{\nu}$	$\log k_s - .956 - \log \frac{u_* k_s}{\nu}$	.007	2.11
REGIME I				
$0.55 \leq \log \frac{u_* k_s}{\nu} \leq 0.85$	$6.59 + 3.5 \log \frac{u_* k_s}{\nu}$	$\log k_s - 1.146 - .609 \log \frac{u_* k_s}{\nu}$	.020	.956
REGIME II				
$0.85 \leq \log \frac{u_* k_s}{\nu} \leq 1.15$	9.58	$\log k_s - 1.667$	.040	.768
REGIME III				
$1.15 \leq \log \frac{u_* k_s}{\nu} \leq 1.83$	$11.5 + 1.62 \log \frac{u_* k_s}{\nu}$	$\log k_s - 2.000 + .282 \log \frac{u_* k_s}{\nu}$	.124	.932
FULLY ROUGH				
$\log \frac{u_* k_s}{\nu} > 1.83$	8.48	$\log k_s - 1.475$	observed 43.50	observed 1.22

Eddy transfers of momentum, heat and moisture all depend on air turbulence generated by shear flow above a smooth surface, by dynamic eddies around elements of a rough surface and by shear between two fluid streams. Wind tunnel research has developed transfer theories mainly based on the Prandtl mixing length concept and von Karman's similarity hypothesis which result in the log-law concept of velocity profiles above a solid surface. In the extension of this concept to eddy transfers of heat and moisture when gradients of temperature and moisture exist, all three transfers naturally depend on turbulence above a surface of given characteristics. As shown later the friction velocity, u_*, is taken as basic to all 3 eddy transfers so particular attention must be paid to its determination. Direct measurement of shear stress is, of course, the best method, and this is now possible here with the new floating lysimeter.

Two surface characteristics to be evaluated from velocity profiles should be determined at times of neutral stability to suit theory developed from isothermal wind-tunnel tests. For dry air, neutral stability is represented by temperature profiles nearly isothermal with height, namely by the small dry-adiabatic gradient of $-1^{\circ}C/100m$. When there is a vertical flux of water vapor, there is a further correction for air density near the ground because of the 18 molecular weight for water vapor compared with 29 for dry air. Instead of separately calculating the density influence of water vapor, the common practice is to use virtual temperature, namely a dry air temperature having the same density as that of the mixture of dry air and water vapor. Then the definition of neutral stability is when the gradient of virtual temperature equals the dry adiabatic rate (Brunt, 1939, p.44). In the usual diurnal cycle passing from unstable to stable in mid afternoon the extra upward flux of water vapor from strong evapotranspiration delays the time of neutral stability slightly.

Determination of Friction Velocity u_* from Measurement of Air Drag

With the new floating lysimeter of 6m diameter, determinations of u_* can now be made from calibrated observations of air drag on the $28.5m^2$ surface. This furnishes direct measurements of τ_o, and thus of the friction velocity $u_* = \sqrt{\tau_o/\rho}$. Under conditions of neutral stability# the measurement

Since perfectly neutral stability rarely exists even over moderate height, u_* should be considered as a function of height. Then possible departure at upper and bottom anemometer levels can be ascribed to advection effects or unavoidable temperature gradients.

of u_* compared with its expression by the corresponding velocity profile determines the Karman constant k_u shown in Table VII-2 and analogous profile indicators of friction.

The first need is to determine the height, d, of the equivalent zero plane (approximately 0.8 x height of close-planted, rounded vegetation). This is considered constant day and night and is best determined at the two times of neutral stability as the vertical shift in the z ordinate needed to make the semilog velocity profile straight. For the July 1962 run, the velocity profiles are somewhat unreliable because of occasional counter trouble and possibility of misreading. However, around the two neutral times of 0630 and 1500 a displacement height of d = 10 cm seems most suitable. The second characteristic, the z_o intercept, apparently is not constant throughout the 24 hours being about 1.1 cm in the morning and 1.9 cm in mid afternoon. This change shows a variation in flow regime rather than change in surface roughness. Although the observed outdoor velocities seem too high to get down to Nikuradse's regime III or II in Table II-1, the calculated z_o's agree. It seems likely, therefore, that stability modification of turbulence can act as if increasing kinematic viscosity thus increasing u_* to compare with observed outdoor magnitudes of velocity.

To calculate friction velocity for the two neutral times using a best fit of a vertical series of observations by machine computation, the expression II-3a is used. In the graphical determination of displacement heights, d, the neutral friction velocity u_{*N} is k_u times the slope, β of the ultimate straight line evaluated over one natural log cycle of the height scale. In common logarithms this coefficient is expressed:

$$\text{(II-4a)} \qquad \left(\beta_1\right)_N = \left(\frac{u_*}{k_u}\right)_N = \frac{\bar{u}_{z'} - \bar{u}_{0.1\,z'}}{2.3026(\lg z' - \lg 0.1\,z')} = 0.4343\,(\bar{u}_{z'} - \bar{u}_{0.1\,z'}) \text{ ,cm sec}^{-1}$$

where z' is used for the corrected height z-d above the zero plane. The intercept z_o determined simultaneously is highly sensitive to the choice of d, therefore keeping the indicated value of z_o reasonable is part of the process of determining d. As already mentioned, a diurnal fluctuation in z_o of possibly $\pm$ 40 per cent can be expected, so a preferred value or reasonable diurnal cycle needs to be specified for the intervening diabatic profiles as indicated by the bottom of the profiles in Figure II-4.

To evaluate friction velocity for diabatic conditions in the absence of measured air drag, the usual formulas indicate that besides the Karman constant, the temperature profile is involved in addition to the velocity profile. However, the curvature in the velocity profile is due to thermal effects, and this is only a departure from the main slope which reflects main shear. Thus, the asymptote of the curved shape of the velocity profile determines u_*/k_u which can be used in the formula for u_* in non-neutral conditions without evaluating temperature gradients. When the integral form of differences of two levels is used in order to avoid z_o, the common expression for non-neutral conditions is:

$$\text{(II-4b)} \qquad \frac{u_*}{k_u} = \frac{\bar{u}_2 - \bar{u}_1}{\ln z'_2 - \ln z'_1 + (\alpha_1/L)(z_2 - z_1)} \quad , \text{cm sec}^{-1},$$

it being assumed that both points lie on the same analytical curve and have the same z_o (not evaluated). The curvature of this semi-log graph is expressed by the last term in the denominator. Although the whole curvature is due to a constant heat flux represented by the Monin-Obukhov characteristic length L, the dimensional factor (α_1/L), for heights well below L, can be evaluated directly regardless of the magnitude of L. This is significant because the definition of L itself includes u_*^3:

$$\text{(II-5)} \qquad \frac{1}{L} = \frac{k_u\, g}{u_*^3\, T} \left| \frac{H}{\rho c_p} \right| = \frac{k_u}{u_*^2} \frac{g}{T} \left| t_* \right| \quad , \text{cm}^{-1},$$

To represent a full sweep of observations at 4 and more levels repeating every one or two minutes, the profile formula II-4b with u_1 = zero and $z'_1 = z_o$ is more useful and the automatic computer can solve this equation for u_*/k_u, α/L, and z_o simultaneously unless z' approaches L. The computer program thus yields calculated velocity for each observation level and also the curvelinear velocity gradient needed for determination of eddy viscosity and of Richardson number both of which increase with height. Automatic least squares determination of the deviation of the observed values then indicates the accuracy of interpretation by the log-law concept. If there is random scatter, this calculation of variance might be considered as indicating the combined three-fold inaccuracy of the observations, the statistical procedures of determining mean values, and the

application of the log-law profile concept. If, however, consistent deviation appears at the extremes of the profile, this may indicate that either the first-order stability function ϕ (z/L) is inadequate, or that the upper part should be excluded from the profile determination as being above the level properly dominated by the controlled area of the test site. Strong departures at the bottom indicate excessive influence by the local ground cover.

During high flux rates of convective heat it is found here that the two-term expression

$\left[\ln \frac{z-d}{z_o} + \alpha \frac{(z-d)}{L}\right]$ is inadequate. Rather than use 3 or more terms of the power series it seems better to use another mathematical form. The power law is the usual alternative to the log law and has proved very useful especially for profiles under stable conditions. Even this, however, often yields a curved line on log-log paper, so it seems better to stay closer to the log law and start with a differential expression having a fractional power correction for curvature, $\phi \left(\frac{z}{L}\right)^n$. When more precise data are available, the exponent n can be solved for or an entirely new function found more compatible with turbulence theory. Present data are fitted fairly well using simply $n = \frac{1}{2}$ for profiles. With this modification, the basic differential expression is:

$$\text{(II-8u)} \qquad \frac{\partial \bar{u}}{\partial z'} = \frac{u_*}{k_u z'} \phi \left(\frac{z'}{L}\right)^{1/2} = \frac{\beta_1}{z'} (1 + \gamma\sqrt{z'}), \qquad \text{sec}^{-1}$$

where $\gamma = \gamma'/L^{1/2}$. The gradients, however, are not as good as found by graphical smoothing above about half the z_γ height for indicated zero gradient (see Table II-3) unless the flux rate is known to approach zero at a low height. Upon integration this leads to the profile formula:

$$\text{(II-4u)} \qquad \bar{u}_{z'} = \frac{u_*}{k_u} \left[\ln \frac{z'}{z_o} + {}^2\gamma' 1 \left(\frac{z'}{L}\right)^{1/2}\right] = \beta_1 \left[\ln \frac{z'}{z_o} + {}^2\gamma 1 \sqrt{z'}\right], \quad \text{cm sec}^{-1}$$

where z' is used for convenience in place of z-d, z_o is on the z' scale, and $2\gamma\sqrt{z'_o}$ is negligible. Formulas for eddy transfers of momentum, heat and moisture are given in parallel in Table II-2 using this modified form which provides more gradual curvature than n = 1 as used by Monin-Obukhov.

In general, the prime objective in choosing the modified log law to fit all the observed profile data with smooth curves yielding the least algebraic

deviation, is to describe the vertical distributions of windspeed, temperature and humidity so consistently that time variations in flux rates measured at the surface can be followed logically in the time variations in eddy transfers above the ground. An important advantage in consistent smoothing procedures is the uniform time constant essential to evaluation of time lags known to exist between fluctuations in net radiation and responses in air profiles.

Profile Curvature Coefficients Related to α from the Function $(1 + \alpha (z/L))$

Considerable interest has been focussed heretofore on the numerical magnitude of the Monin-Obukhov α which they gave as $-0.6 \pm 10\%$. Taylor (1960) found a value 10 times greater and in theoretical analysis Neumann (1962) recommends 6. Our profiles are not well fitted by the original Monin-Obukhov function because often the heat length L is less than the height of our 6-meter masts. However, in the related function $\left[1+2\gamma'(z'/L)^{1/2}\right]$ fitting our profiles better, the numerical magnitude of $2\gamma'$ is of interest in the same sense that α is a significant constant. The calculations for 30-31 July 1962 are listed in Table II-3. The scatter in these hourly determinations is due largely to variable wind velocity which has an inverse effect on the degree of instability and also on slopes of the temperature and humidity profiles.

Although the Monin-Obukhov heat length L appears in the profile expression*, the analytical curve can be determined before the magnitude of 1/L is known simply by finding the $\gamma\sqrt{z'}$ that gives the best fit for the observed curvature in the profile. Then the γ' (which is like the Monin-Obukhov α) can be determined from $\gamma' = \gamma\sqrt{L}$. It is obvious that calculations during the collapse of the daytime heating are unrealistic for several hours. Part of the difficulty can be ascribed to differing time lags in the various components and the consequent involvement of heat storage not included in the simplified expressions used. Nevertheless, for 11 consecutive hours during stable conditions from 1800 to 0500, the non-dimensional curvature coefficient $2\gamma_1'$ has an average of 1.1 with standard deviation of only 0.14. In unstable, daytime conditions the average from 0700 to 1300 is -1.24 with standard deviation 0.50. With these values and a known velocity coefficient

* Only the absolute magnitudes of 1/L are used in order to avoid negative z/L when heat flux reverses. The proper sign for the temperature profile automatically appears in the determination of β_2.

β_1 one can construct curved semilog velocity profiles appropriate for a given heat flux rate for any time of day except during the afternoon period of transition from lapse to inversion condition.

The upper limit of applicability of the modified log-law expression for profiles under non-neutral conditions is no longer based on convergence requirements for a power series but depends simply on how well the two-term expression represents the observed data. However, under unstable conditions Eq. II-4c if extended upward will eventually reach a level indicating zero gradient, which is incompatible with the usual assumption of flux rates constant with height. Thus the extrapolated heights, z_γ, in Table II-3 are of some interest and become significant when the formulas represent profiles having maximums as expected with advection and shown in Poppendiek's sinusoidal treatment of horizontal differences.

Hourly Profiles

To show the daily sweep of temperature in midsummer Fig. II-3 gives the diurnal curves of air temperature at 25, 100, 200 and 600-cm levels smoothed by computer as described in Chapter IX. The observed 20-minute mean temperatures are also point plotted for the 25-cm level to show the advantage of the 9-point parabolic time smoothing which still retains hourly variations.

Figures II-4,5, and 6 give the hourly profiles of windspeed, temperature and humidity for 30-31 July 1962 in semi-log form - all influenced by the degree of atmospheric stability. These have since been computed by machine as logarithmic regression lines with square root modification for curvature as described in Chapter IX. Profiles of temperature are particularly significant for all eddy transfers outdoors because of the influence of temperature gradient on the degree of stability of atmospheric stratification near the ground. The temperature profile immediately shows stability or instability by the direction of its slope namely by whether β_2 is positive or negative. This depends, of course, on whether the convective heat flux, H_c, is toward or away from the interface. The characteristics of the temperature profile, however, can be described completely by the β_2 and γ_2 coefficients before knowing the magnitude of the heat flux.

So much depends on the shape of vertical profiles, a graphical description is presented in Figs. II-7 and 8. These are pairs of velocity and temperature profiles for 04 to 0500 and 11 to 1200, P.S.T. 31 July 1962 showing the

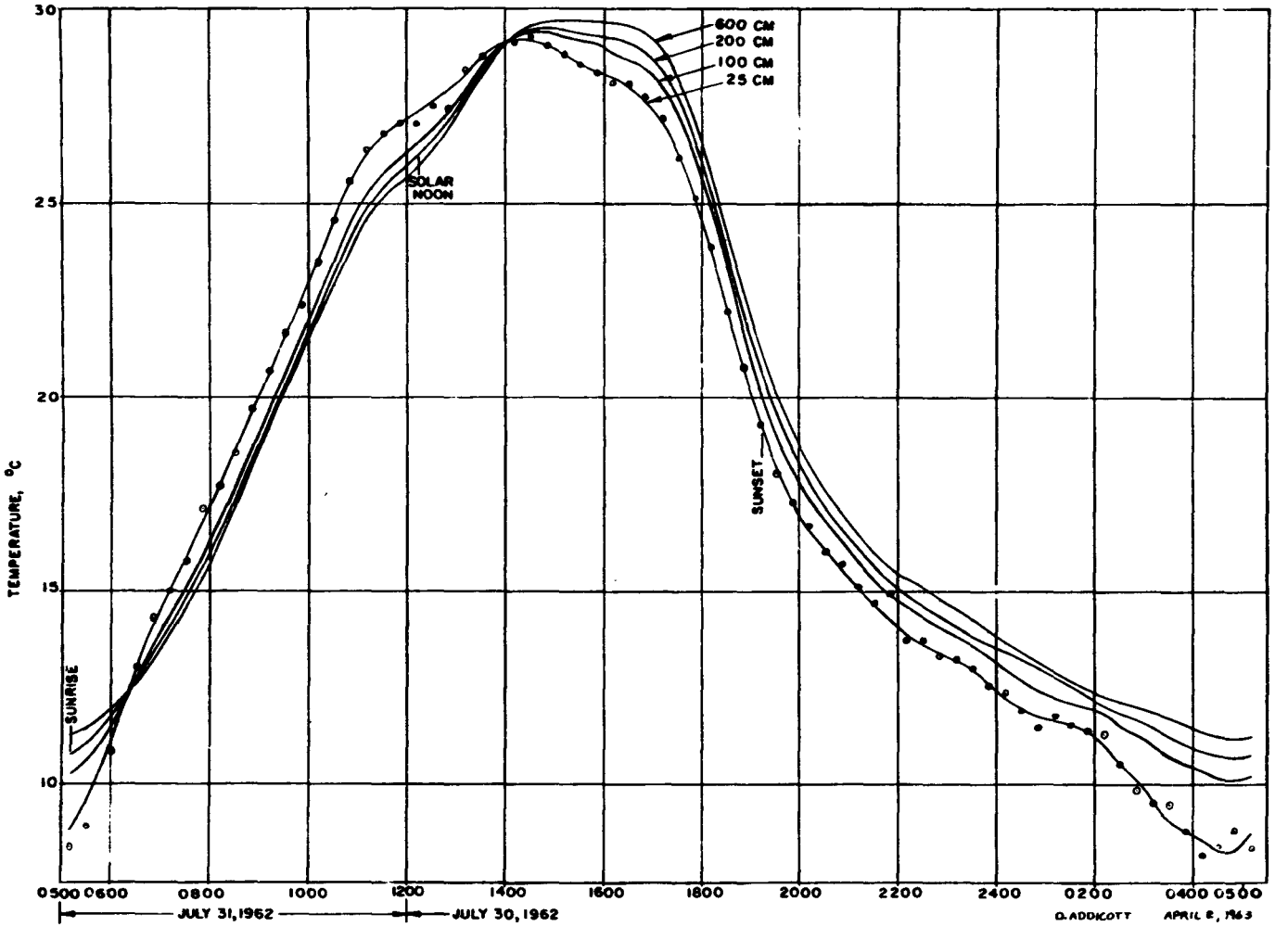

FIGURE II-3. Machined smoothed typical diurnal curves of 4 air temperatures of 20 minute means using 9-point least squared parabolic fitting.

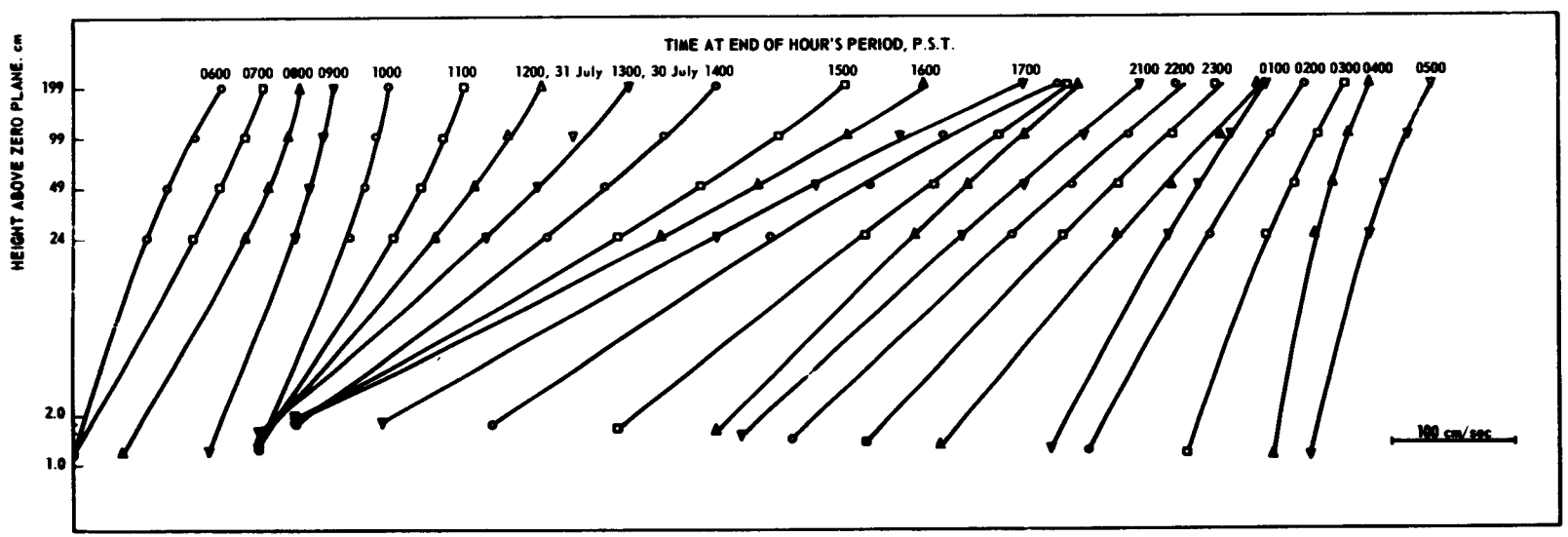

FIGURE II-4. Hourly windspeed profiles, 30-31 July, 1962

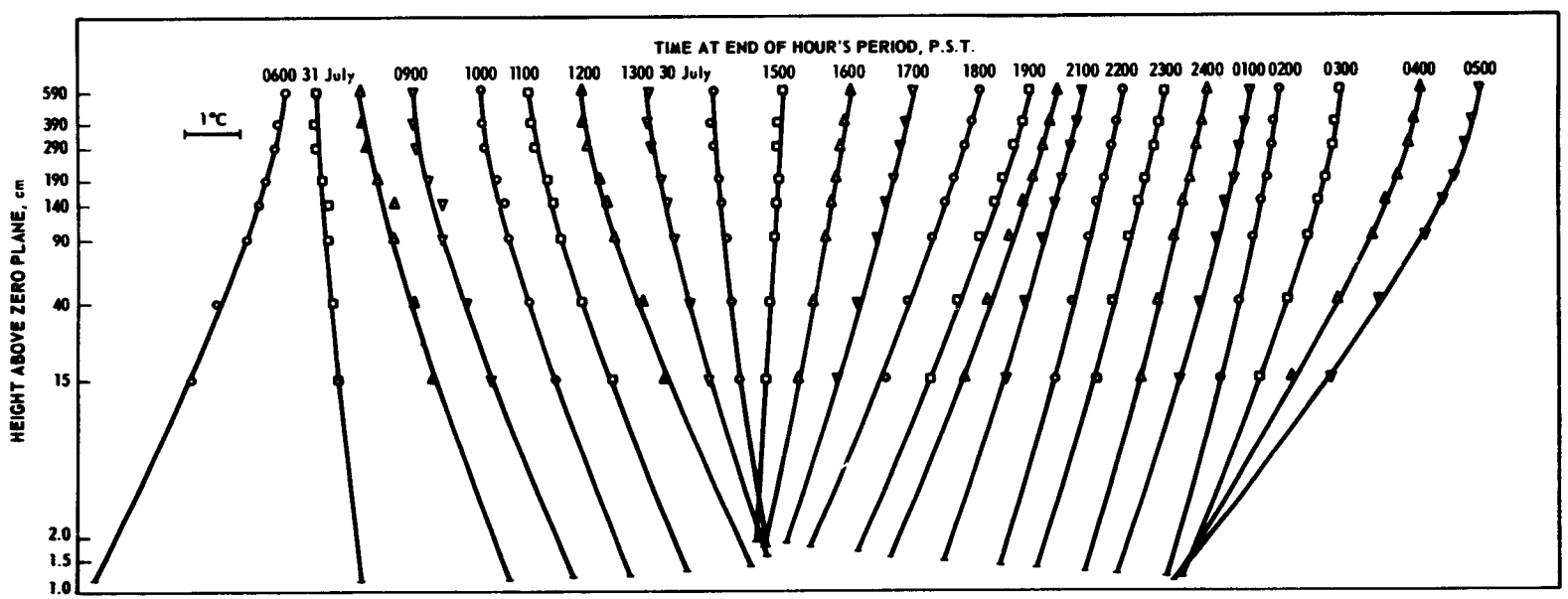

FIGURE II-5. Hourly profiles of temperature, 30-31 July 1962

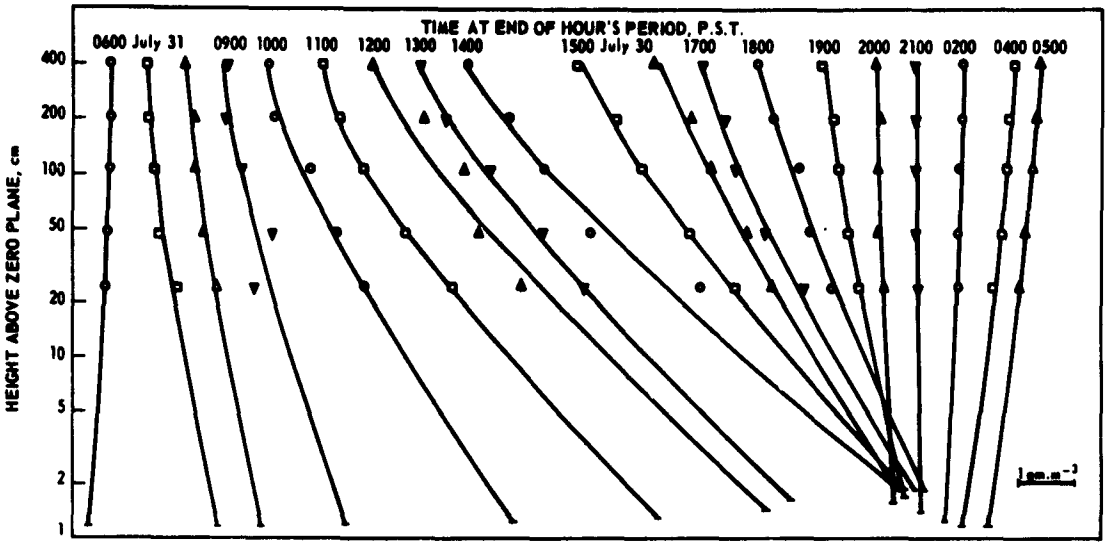

Figure II-6. Humidity profiles 30-31 July 1962.

natural slopes and curvatures for stable and unstable conditions respectively. These profiles are interpreted by Eqs. II-7 u,t. The asymptotic slopes β are obvious but for given profile data their magnitudes, except at times of neutral stability, change slightly with change of curvature function as from $1 + \alpha(z/L)$ to the $1 + \gamma'(z/L)^{1/2}$ used here. They also change with z_o, and, therefore, the hourly values of z_o are kept within the range determined at the two times of neutral stability and are used as virtual anchor points. The algebraic sign of the γ term is very significant. If negative, the curvature decreases the semilog magnitudes represented by the β slope. Furthermore, if a negatively curved profile is extrapolated upward, a limit of applicability is reached well below the level where analytically the gradient would be zero. The latter is indicated by z_γ in Table II-3.

The difficulty in machine determination of temperature and humidity profiles, because there is no level of zero temperature or humidity for a z_o intercept, is met by adopting the z_o used for velocity profiles and then finding a t_o or q_o suitable for the mathematical expression at that level. All the profiles are evaluated in terms of coefficients β and γ before L or t_* are determined. The heat flux rate is then used to organize the hourly variation in coefficients by a t'_* scale, previously described, which includes an observed β_1 instead of friction velocity. Measured rates of evapotranspiration show considerable eddy transfer of moisture during the afternoon neutral period. The humidity profile then has a large gradient as does the wind but not temperature.

The above profile interpretation would need to be modified if a low-level temperature maximum or minimum occurred as with density currents or near a significant horizontal change in ground conditions as anticipated by Poppendiek (Chapter VI) in advective flow. In a time sense, the equation can be applied to the rapid change of profile from low level neutral stability to a lapse of 1.2°C in 6 meters from 0630 to 0700, 31 July 1962 and might be interpreted by Poppendiek's system as shown by his profiles in Fig. VI-4. The modification from his figure VI-2 is that the median condition is not isothermal but has a lapse rate of 0.8°C in 6 meters linear in log-law plotting. This example is appropriate for natural heat flux regimes in two large areas, one in balance at a lower temperature than the other because of higher rate of latent heat conversion. The median lapse rate has been

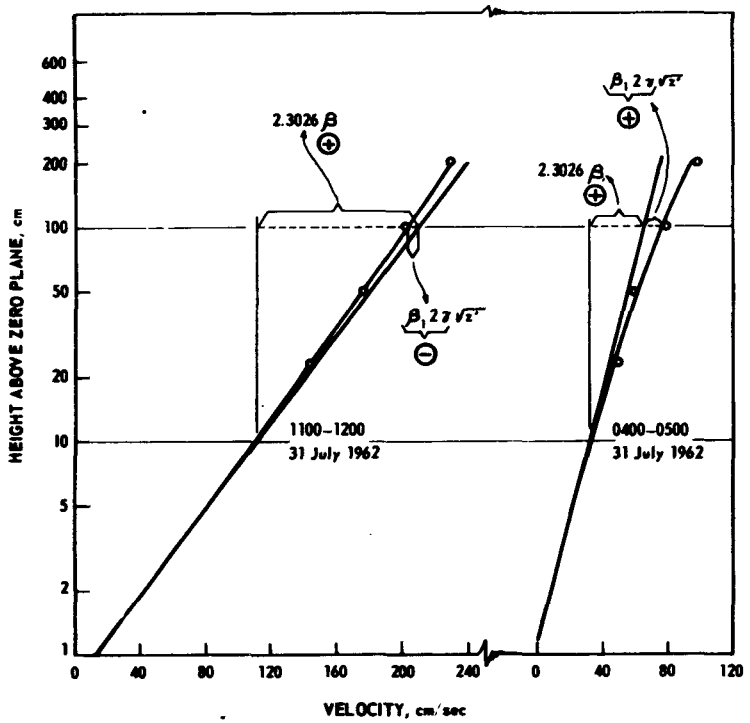

FIGURE II-7. Graphical determination of velocity profile coefficients.

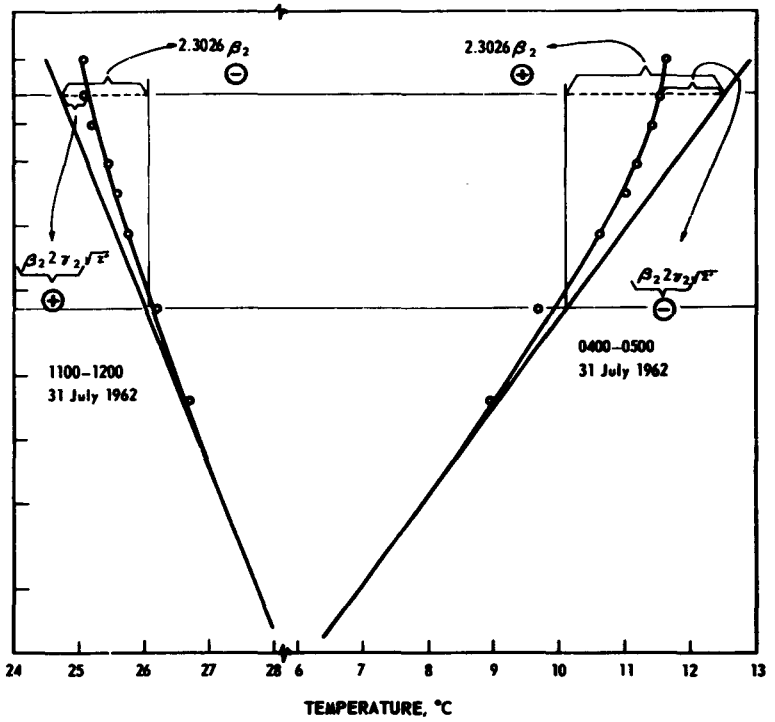

FIGURE II-8. Graphical determination of temperature profile coefficients.

crossplotted on his Fig. VI-4 profiles and the example profile temperatures spotted vertically, as if on 10 very tall masts at equal intervals for the whole length of z_o. Thus, Fig. II-9 shows a transition vertical temperature field. Above 6 meters the temperature waves look natural. In particular a temperature maximum is found in one of the profiles (above station 0.3) but not above stations 0.2, 0.3, and 0.4 as for the sinusoidal horizontal distribution of temperature, Fig. VI-4. This example shows positively that a temperature maximum can logically occur near the ground in which case the exponent n of the function $\phi\left(\frac{z}{L}\right)^n$ curvature correction for logarithmic profiles needs to be adjusted to bring the zero gradient at the observed height, or else some other mathematical form be used.

Determination of Eddy Diffusivities:

As mentioned previously, eddy diffusivities vary directly with height, and, therefore, they are not readily comparable except at chosen levels above the equivalent zero plane, namely at specified values of (z-d) and for specified Richardson number. The ratios of the 3 eddy diffusivities are more general and are commonly used for gross description of the relations between the three systems. The main objection to this is the unequal influence of Richardson number, which also varies with height but not at the same rate.

If there is any wind, all three eddy diffusivities depend on the turbulence structure of shear flow and each includes the friction velocity u_* because for given flux rates, profile gradients decrease with increase in wind speed. When all three flux rates: momentum τ_o, heat H_c, and moisture Q_w, are measured, the analyses of their corresponding profiles of windspeed, temperature and moisture are rather simple assuming a basic linear semilog near-neutral profile for each, with curvature for non-neutral conditionsdescribed by Eqs. 7u,t,q. All the neutral or linear near-neutral semilog profiles are the special cases of the general expressions when $\phi(z/L) = 1.0$ namely when $\gamma'(z'/L)^{1/2} = 0$. In diabatic conditions, equations 7u,t,q can still be used for determining the equivalent von Karman coefficients simply by resorting to the respective asymptotes as z' approaches z_o. The slopes β of these asymptotes depend on the shape of observed profile to its full height so it is not necessary to make all one's measurements within the first 50 cm as has been attempted to avoid diabatic curvature.#

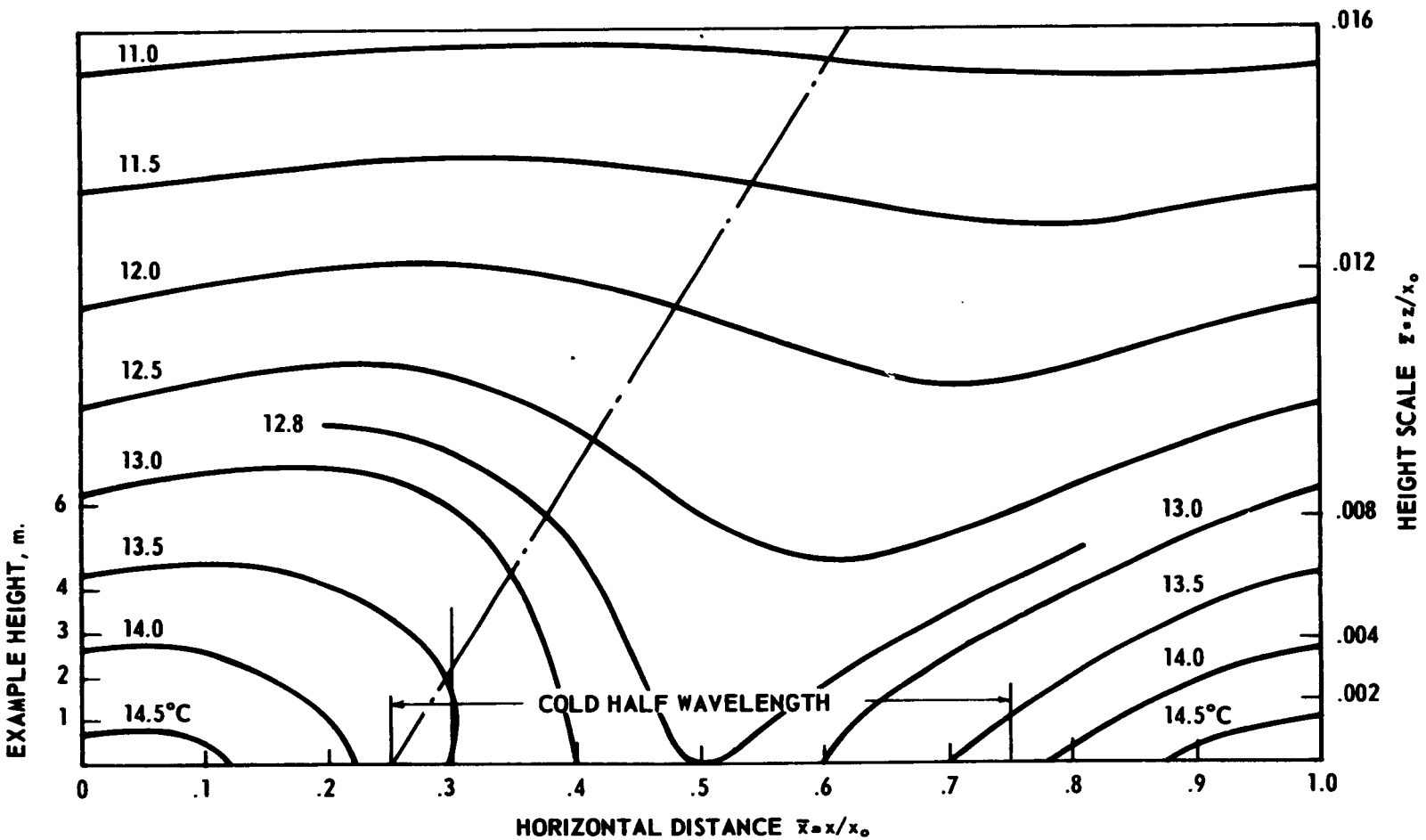

FIGURE II-9. Time transition between stable and unstable profiles 0630-0700 31 July 1962 interpreted by Poppendiek's system.

The usual assumption of similarity of temperature and velocity profiles shown by Best (1935) and by Deacon (1953) does not hold in stable conditions because curvatures observed here are opposite, γ_1' being positive while γ_2' is negative. For lapse conditions the profile shapes are more similar with γ_1' and γ_2' both negative, but the latter is within the whole temperature profile with β_2 negative.

Eddy Viscosity:

When actual shear stress and windspeed profiles are both measured, the eddy diffusivity for momentum, K_M, is known from the general defining equation:

(II-10u) $$\frac{\tau}{\rho} = K_M \frac{\delta \bar{u}}{\delta z^{\#}} \qquad , \quad cm^2 sec^{-2}.$$

This holds for all neutral and non-neutral stability conditions. The only limitation occurs when shear stress is measured only as air drag on the surface, τ_o. Then the equation applies only up to the height within which the vertical flux of horizontal momentum is constant. Once a velocity profile is expressed analytically the velocity is known as a function of corrected height z-d and evaluations can be made at any level by using β_1 and γ_1 parameters to express gradient. Thus:

(II-11u) $$K_M = \frac{z'(\tau/\rho)}{\beta_1(1+\gamma_1\sqrt{z'})} = \frac{k_u u_* z'}{1+\gamma_1\sqrt{z'}} \qquad , \quad cm^2 sec^{-1}.$$

This shows that for friction velocity constant with height eddy viscosity varies almost directly with height. The same will be true for eddy conductivity and eddy diffusivity but with different departures. Therefore, the ratios of eddy diffusivities may be more meaningful than each by itself.

Determination of Eddy Conductivity, K_H, and Eddy Diffusivity, K_D:

Since we are expressing temperature and moisture profiles in the same manner as the velocity profile, the formulas expressing eddy convection of heat and eddy diffusion of moisture are all similar as shown in Table II-2. Differences in magnitude of β and γ are to be expected and often a dissimilar sign for γ_2 as mentioned previously. These parallel expressions

That these β slopes do vary with stability can be seen by choosing a fixed profile value at some given level and then drawing through this two typically curved velocity profiles one for stable and one for unstable conditions. It is then seen that the β_1 asymptote shifts from one side of the point to the other.

TABLE II. 2 PARALLEL ARRAY OF FORMULAS FOR EDDY TRANSFERS OF MOMENTUM, HEAT AND MOISTURE USING $1+\gamma\sqrt{z'}$ FOR $\phi(z/L)$

Eq. No.	VELOCITY	TEMPERATURE	MOISTURE
6u,t,q,	$u_* \equiv \sqrt{(\tau/\rho)}$ cm sec^{-1}	$t_* \equiv H_c/\rho c_p u_*$; $t_*' \equiv H_c/\rho c_p \beta_1$, °C	$q_* = Q_w/u_*$ gm$_m$ cm^{-3}
	Log law profile integral expressions (in $z' = z-d$):		
7"	$\dfrac{\bar u_{z'}}{u_*/k_u} = \dfrac{\bar u_{z'}}{\beta_1} = \ln\dfrac{z'}{z_0} + 2\gamma_1\sqrt{z'}$, $\gamma_1 = \dfrac{\gamma_1'}{\sqrt{L}}$	$\dfrac{\bar t_{z'}-t_0}{t_*/k_t} = \dfrac{\bar t_{z'}-t_0}{\beta_2} = \ln\dfrac{z'}{z_0} + 2\gamma_2\sqrt{z'}$, $\gamma_2 = \dfrac{\gamma_2'}{\sqrt{L}}$	$\dfrac{\bar q_z - q_0}{q_*/k_q} = \dfrac{\bar q_{z'}-q_0}{\beta_3} = \ln\dfrac{z'}{z_0} + 2\gamma_3\sqrt{z'}$, —
8"	$\dfrac{\partial\bar u}{\partial z'} = \dfrac{u_*}{k_u z'}\left(1+\dfrac{\gamma_1'}{\sqrt{L}}\sqrt{z'}\right) = \dfrac{\beta_1}{z'}(1+\gamma_1\sqrt{z'})$, sec^{-1}	$\dfrac{\partial\bar\theta}{\partial z'} = \dfrac{\partial\bar t}{\partial z'} + \Gamma = \dfrac{t_*}{k_t z'}\left(1+\dfrac{\gamma_2'}{\sqrt{L}}\sqrt{z'}\right) + \Gamma = \dfrac{\beta_2}{z'}(1+\gamma_2\sqrt{z'}) + \Gamma$, °C cm^{-1}	$\dfrac{\partial\bar q}{\partial z'} = \dfrac{q_*}{k_q z'}\left(1+\dfrac{\gamma_3'}{\sqrt{L}}\sqrt{z'}\right) = \dfrac{\beta_3}{z'}(1+\gamma_3\sqrt{z'})$, gm$_w$ cm^{-4}
	Flux differential expressions from u_* & Eqs. 8.		
9"	$\dfrac{\tau}{\rho} = u_*^2 = \dfrac{k_u u_* z'}{1+\gamma_1\sqrt{z'}}\dfrac{\partial\bar u}{\partial z'}$, cm^2 sec^{-2}	$\dfrac{H}{\rho c_p} = u_* t_* = \dfrac{k_t u_* z'}{1+\gamma_2\sqrt{z'}}\left\{\dfrac{\partial\bar t}{\partial z'} + \Gamma\right\}$, °C cm sec^{-1}	$Q_w = u_* q_* = \dfrac{k_q u_* z'}{1+\gamma_3\sqrt{z'}}\dfrac{\partial q}{\partial z'}$ gm$_w$ cm^{-2} sec^{-1}
	Eddy diffusivity expressions:		
10"	$\tau/\rho \equiv K_M\,\partial\bar u/\partial z$, cm^2 sec^{-2}	$H/\rho c_p \equiv K_H\,\partial\theta/\partial z = K_H\left\{\dfrac{\partial\bar t}{\partial z} + \Gamma\right\}$, °C cm sec^{-1}	$Q_w \equiv K_D\,\partial q/\partial z$, gm$_w$ cm^{-2} sec^{-1}
	Eddy viscosity:	Eddy conductivity:	Eddy diffusivity:
11"	$K_M = \dfrac{z'(\tau/\rho)}{\beta_1(1+\gamma_1\sqrt{z'})} = \dfrac{k_u u_* z'}{1+\gamma_1\sqrt{z'}}$, cm^2 sec^{-1}	$K_H = \dfrac{z'(H/\rho c_p)}{\beta_2(1+\gamma_2\sqrt{z'})+\Gamma z'} = \dfrac{k_t u_* z'}{1+\gamma_2\sqrt{z'}+\Gamma z'/\beta_2}$, cm^2 sec^{-1}	$K_D = \dfrac{z' Q_w}{\beta_3(1+\gamma_3\sqrt{z'})} = \dfrac{k_q u_* z'}{1+\gamma_3\sqrt{z'}}$, cm^2 sec^{-1}
	Karman constant and analogous coefficients:		
12"	$k_u = \dfrac{u_*}{\beta_1} = \dfrac{\sqrt{(\tau/\rho)}}{\beta_1}$, —	$k_t = \dfrac{t_*}{\beta_2} = \dfrac{H_c/\rho c_p u_*}{\beta_2} = \dfrac{H_c/\rho c_p}{k_u\beta_1\beta_2}$, —	$k_q = \dfrac{q_*}{\beta_3} = \dfrac{Q_w/u_*}{\beta_3} = \dfrac{Q_w}{k_u\beta_1\beta_3}$, —
13"	$k_u \cong \sqrt{k_u k_q}$; $\dfrac{k_t}{k_u} = \dfrac{\beta_1 H/\rho c_p}{\beta_2 u_*^2}$, —	$k_u k_t = \dfrac{H/\rho c_p}{\beta_1\beta_2}$; $k_t \cong \sqrt{k_t^2 k_u/k_q}$, —	$k_u k_q = \dfrac{Q_w}{\beta_1\beta_3}$; $\dfrac{k_t}{k_q} = \dfrac{H_c/\rho c_p Q_w}{\beta_2\beta_3}$, —
	Ratios of eddy diffusivities:		
14"	$\dfrac{K_H}{K_M} = \dfrac{k_t}{k_u}\dfrac{1+\gamma_1\sqrt{z'}}{1+\gamma_2\sqrt{z'}+\Gamma z'/\beta_2}$, —	$\dfrac{K_H}{K_D} = \dfrac{k_t}{k_q}\dfrac{1+\gamma_3\sqrt{z'}}{1+\gamma_2\sqrt{z'}+\Gamma z'/\beta_2}$, —	$\dfrac{K_D}{K_M} = \dfrac{k_q}{k_u}\dfrac{1+\gamma_1\sqrt{z'}}{1+\gamma_3\sqrt{z'}}$, —
15"	Richardson No: $R_i \equiv \dfrac{g}{T}\dfrac{\partial\theta/\partial z'}{(\partial\bar u/\partial z')^2} = z'\dfrac{g}{T}\dfrac{\beta_2(1+\gamma_2\sqrt{z'})+\Gamma z'}{\beta_1^2(1+\gamma_1\sqrt{z'})^2} = \dfrac{z'/L}{1+\gamma_1\sqrt{z'}}\dfrac{K_M}{K_H}$;		Richardson flux number: $R_f = \dfrac{K_H}{K_M}R_i = \dfrac{z'/L}{(1+\gamma_1\sqrt{z'})}$.

FAB 7 May 63

permit easy generalization of eddy diffusivity ratios as shown in Eqs. II-14u,t,q. Ordinarily these are reported as functions of Richardson Number, Ri, because of strong variation with stability. It is not yet clear, however, that the eddy diffusivity ratios remain the same for Richardson Number changing with height or changing with heat flux and wind speed. The ratios shown in Fig. II-10 are for the few hours 31 July 1962 when strong enough gradients existed to indirectly calculate a reasonable magnitude of the Karman constant as plotted in Fig. II-11 using the asymptotic parameter t'_* for abscissa. This stability criterion used also in Fig. II-10 includes the observed slope β_1 of the logarithmic velocity profile in lieu of friction velocity u_* which was not measured until December 1962. The hourly ratios of eddy diffusivities plotted in Fig. II-10 show wide scatter primarily because, in addition to varying flux rates, these involve the ratios of differentials of diabatic profiles curved in semilog plotting as shown in Figs. II-4,5,6. Therefore each set for stable and unstable conditions should be considered as a whole by the group centroid shown. The weighting of each hourly point is by strengths of flux rates at each hour relative to the maximum for the day, $(\beta_1/\beta_{1\ max})$ $(\beta_2/\beta_{2\ max})$, etc. The centroids for K_H/K_D are the ratios of K_H/K_M and K_D/K_M because the simultaneous and significant hourly direct determinations are too few. The scatter in Karman coefficients Fig. II-11, calculated from the same machine-smoothed data, is less because the more basic asymptotic gradients are involved instead of first differentials of curved portions.

Evidence from the field measurements given in several chapters of this report shows that the usual simplifications such as assuming equal eddy diffusivities for momentum, heat and moisture are untenable for the whole diurnal range of conditions. Also the convenient assumption of one, universal Karman constant (= 0.41 $\pm$ .02) seems highly questionable. To pursue these differences, it is necessary to depart from Sheppard's very illuminating development of the 3 similar log-law profiles and keep separate the Karman constant and the analogous coefficients, $k_u k_t$, k_q, and for curvature to use modified ϕ functions of $(z'/L)^{1/2}$ namely the γ'_1, γ'_2, γ'_3 as curvature coefficients for profiles of wind, temperature and specific humidity respectively. This is done in parallel in Table II-2 using the sign convention described with Eq. I-1. The reciprocal of Monin-Obukhov's heat length is used to avoid the discontinuous jump from minus to plus infinity in going from unstable to

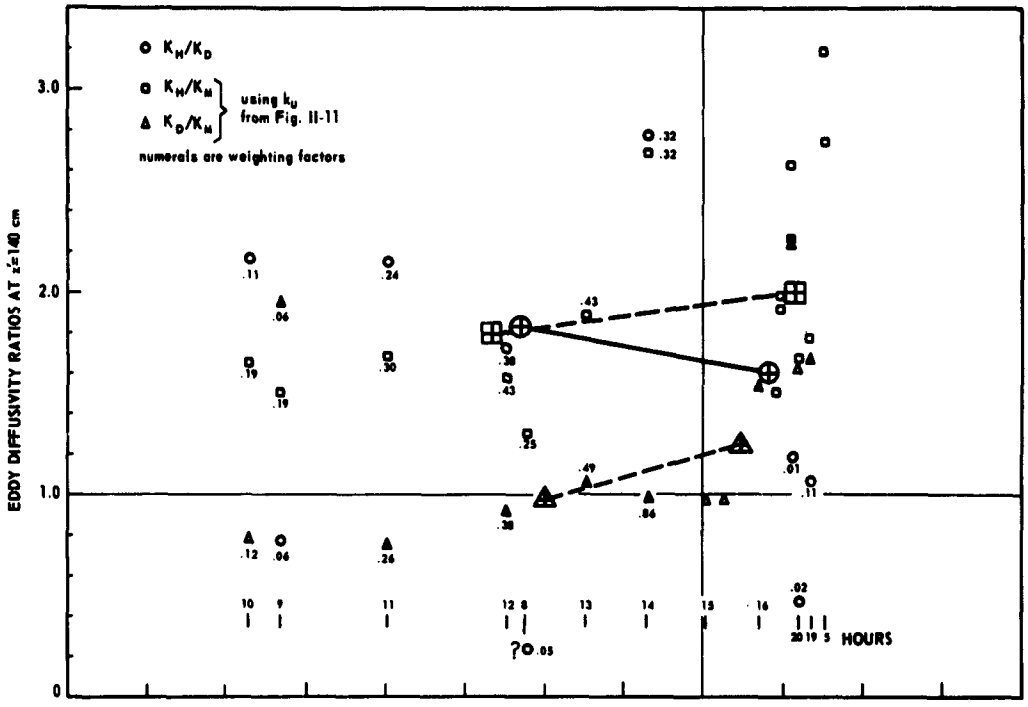

FIGURE II-10. Tentative ratios of eddy diffusivities 30-31 July 1962.

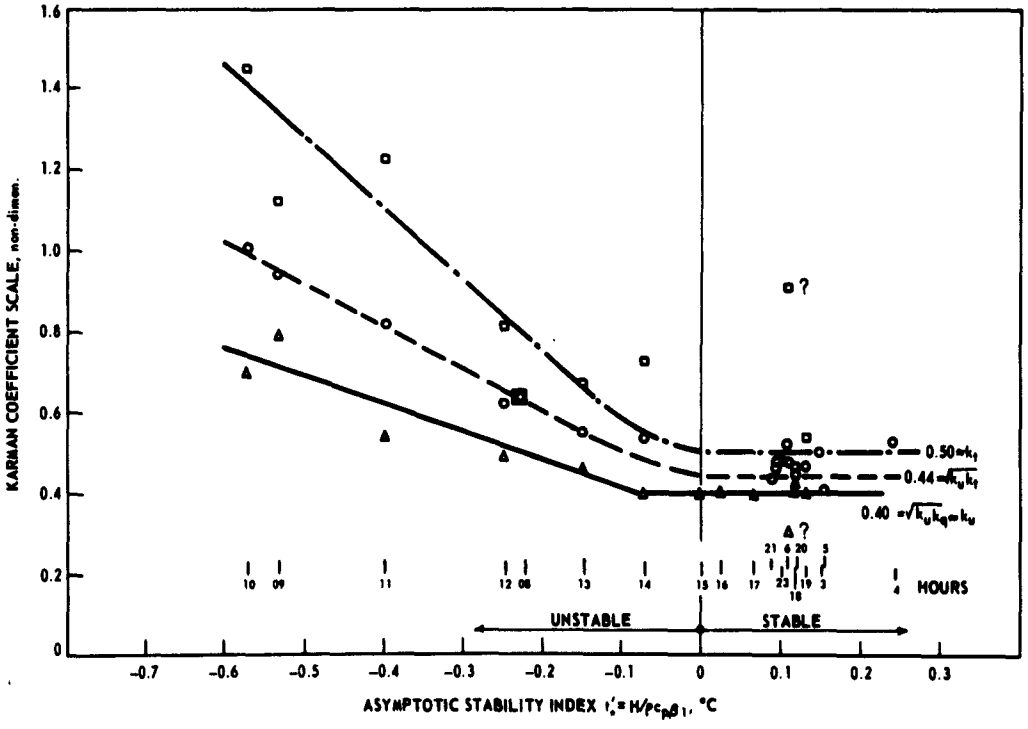

FIGURE II-11. Preliminary asymptotic Karman coefficients 31 July 1962.

stable conditions, with u_*, t_*, and q_* as defined in Eq. II-6u,t,q in Table II-2. The absolute value of heat flux rate is specified to avoid difficulties with fractional powers of L. The proper sign is specified with the profile slope β, and any averages need to be segregated accordingly.

Determination of Karman constants:

Von Karman (1930) originally described his turbulence coefficient as a universal constant relating the logarithmic velocity profile with shear stress. Its one magnitude 0.40 closely characterized the whole profile within the region of uniform shear stress while other characteristics such as mixing length and eddy diffusivity increased directly with distance from the wall. The large variations found under diabatic conditions, therefore, have caused considerable confusion. This indirectly has focussed more attention on turbulence spectrums and direct determination of Reynolds stresses by eddy correlations, but even these need full understanding of profile gradients. Now our first reports of multiple, simultaneous measurements of flux rates and profiles of windspeed, temperature, and humidity permit close examination of the Karman constant and analogous coefficients. Monin and Obukhov hint at two Karman constants in describing how to generalize their theory by replacing T with T/a, namely by including the ratio of eddy diffusivities $K_H/K_M = a$. A promising step, therefore, seems to be evaluation in three categories suiting the three expressions for profiles given by Monin-Obukhov but with u_*/k, t_*/k and q_*/k as modified by Sheppard (1958) and given here with a new curvature in $(z'/L)^{1/2}$. These are equations 7u,t,q, Table II-2.

To determine the Karman constant, k_u, in the general case of non-neutral stability, the non-dimensional curvature function $\phi\,(z'/L)$ is involved but only the asymptotic slope β_1 is needed namely the basic integral equation II-4c for the whole profile. Then, when shear stress is measured, all the variables are known directly and:

$$\text{(II-12u)} \qquad k_u = u_* / \beta_1 = (\tau_o/\rho)^{1/2} / \beta_1 \quad .$$

From the preliminary shear stress measurements with the floating lysimeter, Goddard has calculated k_u from observations under nearly neutral conditions with light wind as reported in Chapter VII. The magnitudes range from 0.3 to 0.6.

When shear stress is not measured, it is necessary to estimate a value for k_u (mainly to determine $u_* = k_u \beta_1$ after finding the profile slope coefficient). A neutral value of $k_u = 0.41$ is close to the usual values reported which range from 0.39 to 0.43. Large departures, however, have been reported for non-neutral conditions by Sheppard (1947, p.219), so for a single average value $k_u = 0.5$ may be more appropriate for a wide range of conditions. The analogous Karman coefficients for eddy transfers and moisture are expected to be nearly constant while friction velocity varies widely. At any given time, however, the friction velocity is the same for all eddy transfers, so some products and a ratio of Karman coefficients can be evaluated from observed profile shapes for velocity, temperature and moisture without knowing k_u. This offers another approach to an approximation of k_u as described later.

In all the formulas and discussions, the von Karman constant and related coefficients k with subscripts u,t,q apply to the profiles involving $(z/L)^{1/2}$ which may be slightly different from the k used in the first-power Monin-Obukhov function,

In the same way that shear stress determines the regular von Karman constant k_u, the convective heat flux rate H_c is the main parameter in determining a related Karman coefficient k_t for the temperature profile. When friction velocity u_* is known, then the similar $t_* = H/\rho c_p u_*$ is also known, and k_t is evaluated from the profile using equation II-7t:

$$\text{(II-12t)} \qquad k_t = t_*/\beta_2 = (H/\rho c_p u_*)/\beta_2 = \frac{H/\rho c_p}{k_u \beta_1 \beta_2}$$

If u_* is not known, a product of the two Karman constants can be evaluated from the two profiles:

$$\text{(II-13t)} \qquad k_u k_t = \frac{H/\rho c_p}{\beta_1 \beta_2}$$

Hourly values of these are plotted in Fig. II-11 for 30-31 July 1962 omitting indeterminate periods. Naturally, there is wide scatter during the mid-afternoon when there is rapid change and reversal of the direction of heat flux at the interface. In fact, eddy conduction and k_t are indeterminate twice daily at the times of neutral gradient. During the morning unstable conditions, there is, however, a definite increase in $k_u k_t$ with increasing

heat flux. Using the square root of this product to be in the same scale as the Karman constant, the rate of change can be expressed tentatively as $\Delta\sqrt{k_u k_t}/(-\Delta t'_*) \cong 0.5$, the 0.5 having dimension $^{\circ}C^{-1}$ to cancel the t'_* dimension.

Similarly the moisture flux rate Q_w is the main parameter in determining the Karman coefficient k_q for the moisture profile again using u_* previously evaluated. Before knowing k_u, however, the product $k_u k_q$ can be evaluated similarly to $k_u k_t$ by Eq. II-13q. Hourly values of these are plotted in Fig. II-11 for 30-31 July 1962. In contrast with $k_u k_t$ the mid-afternoon values of $k_u k_q$ are significant because evapotranspiration is still proceeding strongly, and there is also some wind. It is at night with nearly zero evaporation that $k_u k_q$ is indeterminate, and 10 hours have been skipped for lack of moisture gradient. To look into the possibility that k_q varied with moisture flux rate, a trial plot was made of $\sqrt{k_u k_q}$ vs q'_*, but no consistent pattern was found. More important is the question of the influence of atmospheric stability indicated in Fig. II-11 plotted with t'_* abscissa which represents heat flux divided by velocity gradient. As with $\sqrt{k_u k_t}$ a consistent relation can be suggested tentatively as $\Delta\sqrt{k_u k_q}/(-\Delta t'_*) \cong 0.35$ in unstable conditions.

Reconsidering the physical concepts of eddy transfers commonly assuming that eddy diffusivity for inert aerosols should be the same as for momentum, it is logical to assume that the small water-vapor content exerts only negligible influence on eddy-diffusivity in contrast to strong influence by heat transfer in its effect on buoyancy stability. The inference from the above is that k_u and k_q vary together. Then if equality is assumed as seems likely at least in stable conditions, the $k_u k_q$ product is virtually that for k_u^2. Thus, the diurnal variation of $\sqrt{k_u k_q}$ probably gives an indication of the variation of k_u without direct measurement of shear stress. For stable conditions this yields $k_u \cong 0.40$ as expected. For lapse conditions a rough linear approximation mentioned above might be interpreted as $\Delta k_u/(-\Delta t'_*) \cong 0.35$.

Another approach is possible toward a Karman coefficient for temperature when both heat and moisture flux rates and profiles are known. Then the ratio of k_t to k_q can be determined simply on the assumption that the same u_* is involved in both:

$$\text{(II-13tr)} \qquad \frac{k_t}{k_q} = \frac{\beta_3}{\beta_2}\,\frac{H/\rho c_p}{Q_w}$$

If the above common supposition is valid that k_u and k_q are substantially alike, then the definite determination of the ratio k_t/k_q, listed in Table II-3, can be used as a multiplier of the observed product $k_u k_t$ to obtain $k_t^2 k_u/k_q$ as a reasonable indication of the values of k_t^2 alone in relation to stability pending direct determination of the regular Karman coefficient, k_u, by measuring shear stress. The square root of this product to indicate k_t is also plotted in Fig. II-11 and a rough linear interpretation shows that $\Delta k_t/(-\Delta t'_*) \cong 0.9$.

Heretofore all the discussion on Karman coefficients has centered on their determination in the lower levels of the profiles dominated by frictional shear - specifically using only flux rates and asymptotic slopes β. Karman coefficients also exert their influence in the upper, curved portions of the profiles and can be studied in the determinations of eddy diffusivities which vary directly with height but which, nevertheless, can be definitely determined as the ratio of flux rate to profile gradient.

Since the diurnal variations of profile coefficients β and γ determined by computer for curved logarithmic regression lines are of interest, hourly values are given in Table II-3a for the composite day 30-31 July 1962 made from the 35-hour continuous test. These two coefficients describing the whole shape of the profiles can be used directly in the formulas for eddy diffusivities specifically to evaluate the curve gradient at any height. As discussed previously, the β coefficients represent transfer conditions close to the surface on the straight portion of the profiles before the effects of stability become apparent in the curvature of the logarithmic profiles (mathematically represented in this chapter by the γ terms). Nevertheless, the asymptotic gradients indicating the actual eddy flux rates are governed by the overlying stability and differ slightly depending on whether $1 + \alpha (z/L)$ or $1 + 2\gamma'(z'/L)^{1/2}$ is used for curvature correction. There is no surface Richardson number to use for a general whole-profile scale of stability so the t'_* parameter in Table II-3 is again used in Fig. II-11. No non-dimensional rationalizing is attempted pending further study on the suitability of using absolute temperature although this seems useable because of its control of air density.

TABLE II-3. PRELIMINARY EVALUATIONS OF CURVED LOG-LAW COEFFICIENTS OF PROFILES OF VELOCITY, TEMPERATURE AND MOISTURE, 30-31 JULY 1962
(composite day, 9-point parabolic smoothing of 20-min. means)

Col. No.	(1)	(2)	(3)	(4)	(5)	(6)	(7)	(8)	(9)	(10)	(11)	(12)	(13)	(14)	(15)	(16)	(17)
Description	Time	Heat Flux	Stability Index	Velocity Intercept	Profile Asymptotic Gradients			Curvature Coefficient			Karman Coefficients				Extrapolated Heights to Zero Gradient #		
Terms	P.S.T.	H_c	$t'_* = \frac{H_c}{\rho c_p \beta'}$	z_o	β_1	β_2	β_3	$z_{y'1}$	$z_{y'2}$	$z_{y'3}$	$\sqrt{k_u k_q}$	$\sqrt{k_u k_t}$	k_t/k_q	$\sqrt{k_t^2 k_u/k_q}$	z_{y1}	z_{y2}	z_{y3}
Dimension	31 July '62	$\frac{cal}{cm^2 sec}$	^oC	cm	$\frac{cm}{sec}$	^oC	$\frac{gm}{cm^3}$	--	--	--	$\sim k_u$	--	--	$\sim k_t$	cm	cm	cm
	05-0600	0.32×10^{-3}	0.059	1.15	18.2	1.63	$+0.11 \times 10^{-6}$	+2.21	-1.07	-2.52	--	--	--	--	--	--	--
	0700	-0.96"	-0.098	1.16	33.0	-0.39	-0.31"	-1.52	-2.35	-2.22	--	--	--	--	1500	--	--
	0800	-2.31"	-0.220	1.17	35.6	-1.26	-0.32"	-1.60	-1.03	-2.98	.635	.634	0.999	.634	700	1700	200
	0900	-3.83'	-0.531	1.19	24.8	-1.38	-0.51"	-0.71	-0.52	-1.04	.788	.942	1.426	1.125	720	1360	335
	1000	-3.99"	-0.570	1.22	26.1	-1.30	-0.99"	-0.71	-0.53	-0.54	.696	1.004	2.083	1.450	740	1330	1260
	1100	-4.19"	-0.396	1.28	39.5	-1.38	-1.38"	-1.07	-0.95	-1.06	.538	.813	2.283	1.228	1080	1360	1100
	30 July '62																
	1200	-3.62"	-0.246	1.40	52.1	-1.47	-1.54"	-1.24	-1.50	-1.37	.488	.620	1.686	.805	2260	1540	1860
	1300	-2.88"	-0.146	1.59	69.9	-1.10	-1.47"	-2.13	-2.96	-2.16	.453	.552	1.486	.672	2320	1200	2260
	1400	-1.56"	-0.068	1.81	81.2	-0.55	-1.73"	-3.26	-6.20	-3.32	.395	.535	1.832	.724	2860	790	2760
	1500	+0.11"	+0.004	1.90	107.7	+0.19	-1.27"	--	--	--	.394	--	--	--	2860	--	2800
	1600	0.87"	0.026	1.90	121.2	0.70	-0.91"	-6.94	-5.58	-6.28	.398	--	--	--	3740	--	4565
	1700	1.90"	0.067	1.86	101.2	1.09	-0.86"	+3.29	-2.89	-4.91	.392	--	--	--	--	--	1990
	1800	2.69"	0.117	1.78	81.2	1.42	-0.66"	3.07	-1.99	-2.38	.400	--	--	--	--	--	3120
	1900	2.76"	0.134	1.67	72.1	1.45	-0.33"	1.03	-1.80	-3.22	.396	.461	1.351	.535	--	3760	1180
	2000	1.99"	0.120	1.56	57.3	1.41	-0.09"	0.91	-1.59	-5.08	.424	.443	1.090	.463	--	3400	333
	2100	1.81"	0.092	1.47	67.8	1.14	-0.02"	0.98	-1.89	--	--	.432	--	--	--	4360	--
	2200	1.73"	0.098	1.39	60.4	1.02	--	1.27	-1.95	--	--	.470	--	--	--	3070	--
	2300	1.62"	0.102	1.33	53.8	1.07	--	1.24	-1.78	--	--	.470	--	--	--	2800	--
	2400	1.36"	0.096	1.28	47.8	1.04	--	1.34	-1.72	--	--	.462	--	--	--	2525	--
	31 July '62																
	0100	1.03"	0.111	1.24	31.3	1.13	--	1.07	-1.12	--	--	.476	--	--	--	2180	--
	0200	1.03"	0.112	1.21	31.3	0.94	+0.10"	0.95	-1.27	-3.37	.30 ?	.522	3.02 ?	.91 ?	--	1950	277
	0300	0.92"	0.152	1.19	20.4	1.40	--	1.17	-0.75	--	--	.500	--	--	--	1540	--
	0400	0.70"	0.245	1.17	9.6	2.05	+0.21"	1.04	--	--	--	.525	--	--	--	--	--
	04-0500	0.67"	0.156	1.15	14.3	2.18	$+0.22 \times 10^{-6}$	1.25	-0.62	-0.61	--	.406	--	--	--	1068	--

Gradients are not as good as found by graphical smoothing above about half z_y height unless the flux rate is known to approach zero at a low height.

Vertical Transition in Flow Regimes Above Ground in the Daytime

The interaction between buoyancy stability and shear stress is universally scaled by Richardson number, Ri. Priestley (1959) demonstrated clearly that the mechanism of upward eddy transport of heat changed with Ri starting as forced convection by friction eddies near the ground and developing into heat plumes of natural convection at higher levels. Since for usual steady daytime conditions Ri increases with height above ground, his H* diagram (like Crawford's Fig. 1) serves to describe the vertical transition in flow regimes. Starting at the extreme left and proceeding to larger Richardson numbers as if increasing in height above ground, the frictional flow is indicated by the sloped line of forced convection. Then at a height above ground where Ri is about -.03 the regime changes to natural convection in the unstable case (negative Ri) by a developing system of heat plumes.

What is not shown by the Richardson number is the progressive increase with height of the size of individual heat plumes. Ordinarily this is treated in terms of frequency spectrum. The physical process of growth of a reduced number of plumes each expanding by entrainment is yet to be formalized. From photographs of smoke screens at sea there seem to be favorable locations where plume growth is aided by suppression of surrounding plumes because of downward airflow around the main updraft technically described in Benard cells. Thus one can visualize the gradual organization of a field of little plumes into widely spaced updrafts typical for cumulus cloud development. Woodcock (1940) judging by the start of circle soaring of birds estimates the lowest level of organized updrafts as greater than 50 meters. This might be considered as the depth of the continuous boundary layer over the sea. These well-spaced updrafts also affect the eddy transfer of momentum in their strong vertical exchange of momentum. This is seen in the narrowing of the Ekman spiral angle with strong convection over the ocean. On land increased turbulence due to terrain roughness widens the spiral angle.

Conclusions

Only a few estimates of 3 Karman coefficients have been made in this project pending full tests with shear stress measured by the new floating lysimeter, but the simultaneous measurements of heat and moisture flux rates along with hourly profiles of windspeed, temperature and humidity have already demonstrated consistent variations in the Karman coefficients for

temperature and humidity profiles in unstable conditions. Ratios of eddy diffusivities show K_H at least 2 1/2 times K_M before noon on clear summer days. In the July 1962 35-hour run the curvature coefficient γ' (related to Monin-Obukhov's α but for $(z/L)^{1/2}$) averages roughly -1.1 and +1.2 for unstable and stable conditions respectively.

Except for meteorological size circulations above the frictional boundary layer, it is very convenient to use the well established aerodynamic concepts of boundary-layer flow based on repeatable profiles and flux rates.

Outdoors, consistent patterns of profile variability with distance are explainable, but for quantitative evaluation, comparable to wind-tunnel profiles, outdoor observations require an area distribution of profile transducer masts. The averaging of several masts, then, helps to reduce area variability toward the conventional concepts of horizontal uniformity. It is thus possible to adapt many of the analyses of wind-tunnel experiments to outdoor air flow. In spite of serious discrepancies between outdoor, single-surface conditions and wind-tunnel conditions, some of the methods already developed for characterizing tunnel-flow findings near the wall should prove useful in characterizing flow regimes in outdoor eddy transfer problems. Of particular significance is the concept of equivalent sand roughness which, in fact, converts a surface shear stress into a characteristic roughness length useable in the $\frac{u_* k_s}{\nu}$ surface Reynolds number and the z/k_s ratio for profiles. Much remains to be done in applying the detailed laboratory measurements of natural convective turbulent flows near heated vertical walls to the questions of eddy viscosity and eddy conductivity in density currents on outdoor slopes.

Further tests with replicated measurements of all 3 flux rates and measurements of velocity and humidity profiles by two distinct methods each will provide basic data suitable for very close analyses of the eddy transfer processes outdoors.

CURRENT LITERATURE REFERENCES FOR CHAPTER II

Berggren, W. P. (1963). "Influence of Mid-Stream Turbulent Velocity-Profile Representation on Predicted Variation of Eddy Diffusivity". Submitted for the L.M.K. Boelter Anniversary Volume, Amer. Soc. Mech. Engrs.

Best, A. C. (1935). "Transfer of Heat and Momentum in the Lowest Layers of the Atmosphere". Air Min., Geophys. Mem.#65. H.M. Sta. Ofc., London.

Brooks, F. A. and W. P. Berggren (1944). "Remarks on Turbulent Transfer across Planes of Zero Momentum Exchange". Trans. Amer. Geophys. U. Part VI, pp. 889-896.

Brooks, F. A. and H. B. Schultz (1958). "Observations and Interpretations of Nocturnal Density Currents". Climatology and Microclimatology, Proc. Canberra Symposium UNESCO, Arid Zone. pp. 272-279.

Brooks, F. A. (1959). "An Introduction to Physical Microclimatology". Syllabus, University of California, Davis (reprint 1960).

Brunt, D. (1939). "Physical and Dynamical Meteorology". Cambridge at the University Press.

Deacon, E. L. (1953). "Vertical Profiles of Mean Wind in the Surface Layers of the Atmosphere". Air Min., Geophys. Mem.#91. H.M. Sta. Ofc., London.

Eckert, E.R.G. and T. W. Jackson (1950). "Analysis of Turbulent Free-Convection Boundary Layer on Flat Plate". Nat'l. Advis. Com. Aeron. Report #1015.

Jakob, Max (1949). "Heat Transfer". John Wiley & Sons, Vol. I:444.

Karman, T. von (1930). "Nachr. Ges. Wiss. Göttingen". Math-physik. Klasse, p. 58 and a report given at the third International Congress on Applied Mechanics, Stockholm, 1930 (see the Proceedings of this Congress, v.1:85.

Klebanoff, P. S. (1955). "Characteristics of Turbulence in a Boundary Layer with Zero Pressure Gradient". NACA Report #1247.

Meyer, K. A. and S. J. Kline (1961). "A Visual Study of the Flow Model in the Later Stages of Laminar-Turbulent Transition on a Flat Plate". Thermosciences Div., Mech. Eng. Report #MD-7, Stanford University 43 pages + plates, Dec.

Monin, A. S. and A. M. Obukhov (1954). Transl. "Basic Regularity in Turbulent Mixing in the Surface Layer of the Atmosphere". U.S.S.R. Acad. of Sc., Works Geophys. Inst. No. 24(151).

Neumann, J. (1962). "Turbulent Transfer in the Lower Layers of a Stratified Atmosphere Overlaying and Infinite Plane". Mimeographed paper, Dept. of Meteorology, University of California, L. A.

Nikuradse, J. (1932). "Gesetzmaessigkeiten der Turbulenten Stroemung in glatten Rohren". V.D.I. Forschungshaft 356.

Prandtl, L. (1952). "Essentials of Fluid Mechanics". Hafner Pub. Co., N.Y.

Priestley, C.H.B. (1959). "Turbulent Transfer in the Lower Atmosphere". Univ. of Chicago Press, 130 pp.

Schlichting, H. (1960). "Boundary Layer Theory". McGraw-Hill Book Co.

Schmidt, E. and W. Beckmann (1930). Techn. Mech. u. Thermodynamik, v.1:341 and 391.

Schultz-Grunow, F. (1940). "Neues Widerstandsgesetz für glatte Platten", Luftfahrtforschung v. 17:239, also Natl. Advis. Com.Aeron., Tech. Mem. #986 (1941).

Scrase, F. J. (1930). "Some Characteristics of Eddy Motion of the Atmosphere" Air Ministry, Geophys. Mem. No. 52. H.M. Stationery Office, London.

Sheppard, P. A. (1947). "The Aerodynamic Drag of the Earth's Surface and the Value of von Karman's Constant in the Lower Atmosphere". Proc. Roy. Soc. London, v. A 188:208-222.

Sheppard, P. A. (1958). "Transfer Across the Earth's Surface and Through the Air Above". Quart. J. Roy. Meteoro. Soc., v. 84 (361):205-224.

Sutton, O. G. (1953). "Micrometeorology". McGraw-Hill Book Co., New York pp. 73, 233, 250.

Taylor, R. J. (1960). "Similarity Theory in the Relation between Fluxes and Gradients in the Lower Atmosphere", Quart. J. of Roy. Meteoro. Soc., v. 86:67-78.

Woodcock, Alfred H. (1940). "Convection and Soaring over the Open Ocean", J. Marine Res., v. 3(3):248-253.

TABLE II-4. NOMENCLATURE FOR CHAPTERS I AND II*

Symbol	Dimension	Description
C_D	non-dim.	Drag coefficient
E_t	cal/cm^2 min	Insolation used for latent heat in transpiration
E_v	cal/cm^2 min	Evaporative heat flux into the air
G	cal/cm^2 min	Heat flux into the ground by conduction, negative for heat flow into the soil
H_c	cal/cm^2 min	Convective heat flux into the air
H_e	mm/day	Unit evaporation rate for radiation (59 cal/cm^2 = 1mm)
I	cal/cm^2 min	Direct solar radiation rate on surface perpendicular to sun's rays
K_D	cm^2/sec	Eddy diffusivity (for matter)
K_H	cm^2/sec	Eddy conductivity (for heat)
K_M	cm^2/sec	Eddy viscosity (for momentum)
K_q	cm^2/hr	Thermal diffusivity ($=k/C_q$)
L	cm	Monin-Obukhov characteristic length for heat flux
M_e	cal/cm^2 min	Net metabolic heat flux above the soil surface
Q_w	gm_w/cm^2 sec	Water vapor flux rate above the soil surface
R	cal/cm^2 min	Down coming atmospheric radiation
R_n	cal/cm^2 min	Net radiation absorbed at the surface (positive in daytime)
R_{z_f}	cal/cm^2 min	Atmospheric radiation absorbed by foliage
R_{z_g}	cal/cm^2 min	Atmospheric radiation incident on bare ground
T	^oKelvin	Absolute temperature
W_z	cal/cm^2 min	Total solar radiation rate on a horizontal surface (=insolation)
W_{z_f}	cal/cm^2 min	Insolation warming the foliage
W_{z_g}	cal/cm^2 min	Solar energy incident on bare ground

*See Fig. I-11 and Table II-2 for relationship of fluxes and of eddy-transfers.

Symbol	Dimension	Description (Continued)
a_1	------	Ratio of eddy diffusivities K_H/K_M
c_p	cal/gram°C	Heat capacity (dry basis, constant pressure)
d	cm	Displacement height of equivalent zero plane
e	millibars	Vapor pressure of the atmosphere
g	cm/sec^2	Gravity constant (980.665)
h_{f_g}	cal/gm_m	Latent heat from fluid phase to gas
k	-----	Number of neighbors adjacent to point being smoothed
k_u	-----	Karman constant for universal velocity profile
k_s	cm	Height of sand roughness (Nikuradse)
n	-----	Stability factor exponent
p	millibars	Pressure of the atmosphere or gas
q	gm/cm^3	Water vapor concentration
q^*	gm/cm^3	Water vapor flux characteristic ($=Q_w/u_*$)
t	°C	Temperature
t_*	°C	Heat flux characteristic ($=H/\rho c_p u_*$)
t'_*	°C	Asymptotic stability index ($=H/\rho c_p \beta_1$)
$\bar{u}$	cm/sec	Average velocity in x-direction (in line)
u_*	cm/sec	Friction velocity ($= \sqrt{\tau_o/\rho}$)
v	cm/sec	Velocity component in y-direction (transverse)
w	cm/sec	Velocity component in z-direction (vertical)
x	cm	Length in direction of flow
z_o	cm	Integration constant for log-law velocity profile
z	cm	Depth or height
z'	cm	Height above equivalent zero plane (= z - d)
α	-----	Albedo
α	-----	Monin-Obukhov curvature coefficient
β_1	cm/sec	Logarithmic profile gradient for velocity

Symbol	Dimension	Description (Continued)
β_2	^{o}C	Logarithmic profile gradient for temperature
β_3	gm/cm^3	Logarithmic profile gradient for water-vapor
Γ	$^{o}C/cm$	Adiabatic lapse rate (=1.0 C/100 m = 0.0001 $^{o}C/cm$)
γ	$cm^{-1/2}$	Dimensional curvature coefficient
γ'	-----	Profile curvature coefficient
ϵ	-----	Longwave emittance
Θ	^{o}K	Potential temperature
ν	cm^2/sec	Kinematic viscosity
ρ	$grams/cm^3$	Density, mass
σ	$cal/cm^2 hr\, ^{o}K^4$	Stefan-Boltzmann black-body, hemispherical radiation constant (=0.4921)
τ	$dynes/cm^2$	Fluid shear stress
Φ	as needed	Potential function or other

CHAPTER III

ATMOSPHERIC AND SURFACE FACTORS AFFECTING EVAPOTRANSPIRATION

W. O. Pruitt and Mervyn J. Aston

INTRODUCTION

A high correlation of evapotranspiration (ET) and net radiation (R_n) under non-limiting moisture supply conditions has been indicated by a number of workers in the last several years. Much of the data collected has been for daily or longer periods. However, in some cases a close relationship between ET and R_n has been observed for hourly or shorter periods. Good examples of this have been given by Tanner and Pelton (1960) and by Pruitt (1962).

These and similar results seemed to confirm a generally accepted concept, among Agriculturalists at least, that with extensive moist surfaces almost all of the net radiation energy, less heat flux into the soil, is used in evaporation at the surface. Convective heat flux away from or to the surface has been considered to be almost negligible under such conditions and in the absence of advection.

Results at Davis, California, indicate that such a concept of the variation in the partitioning of energy at a cropped surface during daytime periods overlooks several important factors. Pruitt (1962) and Brooks, Pruitt, Pope and Schultz (1962) found that on calm days especially, the pattern of ET for a well-watered crop of perennial ryegrass was not closely in phase with the pattern of R_n less heat flux into the soil. The convective heat flux on calm days was shown to follow a typical pattern with heat transfer away from the surface reaching an appreciable peak near mid-morning; then dropping to zero by mid-afternoon, with considerable heat transfer to the surface thereafter. Even under fairly strong advection conditions Brooks et al (1962) found considerable heat transfer away from the grass surface during morning and mid-day periods with a peak value at about noon under maximum radiation. Pruitt (1962) has shown one example, however, where ET exceeded R_n during every hour of one record breaking 24-hour period when a total of 11.56 mm of water was used by ryegrass.

In the summer of 1962 during several major data-collection periods at Davis, profiles of temperature, wind, and humidity above the ground surface were measured along with R_n, ET, and soil heat flux, G. In addition, leaf temperature, air temperature, and humidity within the grass turf were measured. The results shed considerable light on the effect of surface and atmospheric factors on the partitioning of energy at the surface. With the conditions encountered during the runs it was possible to compare the transport of water vapor and of heat under a wide range of air stability and wind conditions.

Continuing long term studies of seasonal ET - radiation relationships have provided 2 1/2 years of such data. These results are summarized herein.

INSTRUMENTATION AND METHODS OF ANALYSIS

General descriptions of the instrumentation at Davis have been given in previous reports. Pruitt and Angus (1960) (1961) described in detail the 20-foot weighing lysimeter used to obtain evapotranspiration measurements.

A description of four 6-meter temperature masts constructed during the fall of 1962 is given in the appendix. Two temperature masts used during a July 30-31 run were earlier models but similar in construction. Temperature was measured at nine heights from 10 cm to 6 meters. During the test period on August 31, air temperatures were measured with aspirated thermocouples shielded from direct sunlight, at heights of 6, 12, 25, 50, 100, and 200 cm. During the July run, leaf temperatures were recorded using 6 thermocouples made from fine (40 gauge) copper and constantan wire. Two thermocouples were installed at each of the three depths within the ryegrass sward; near the blade tips, in the middle, and near the bottom of the grass blades. In the August and October runs, 6 thermocouples at each level were used. During the March 12, 1963 run two of the 6-meter masts described in the appendix were used. Only 6 leaf thermocouples were used.

Wind data were obtained using two 2-meter Thornthwaite anemometer masts.

Net radiation data reported herein were obtained with a forced-ventilation radiometer mounted 2 meters above the sod surface. A locally determined calibration constant obtained by the shading technique described in the Appendix was used and corrections for plate temperature were made.

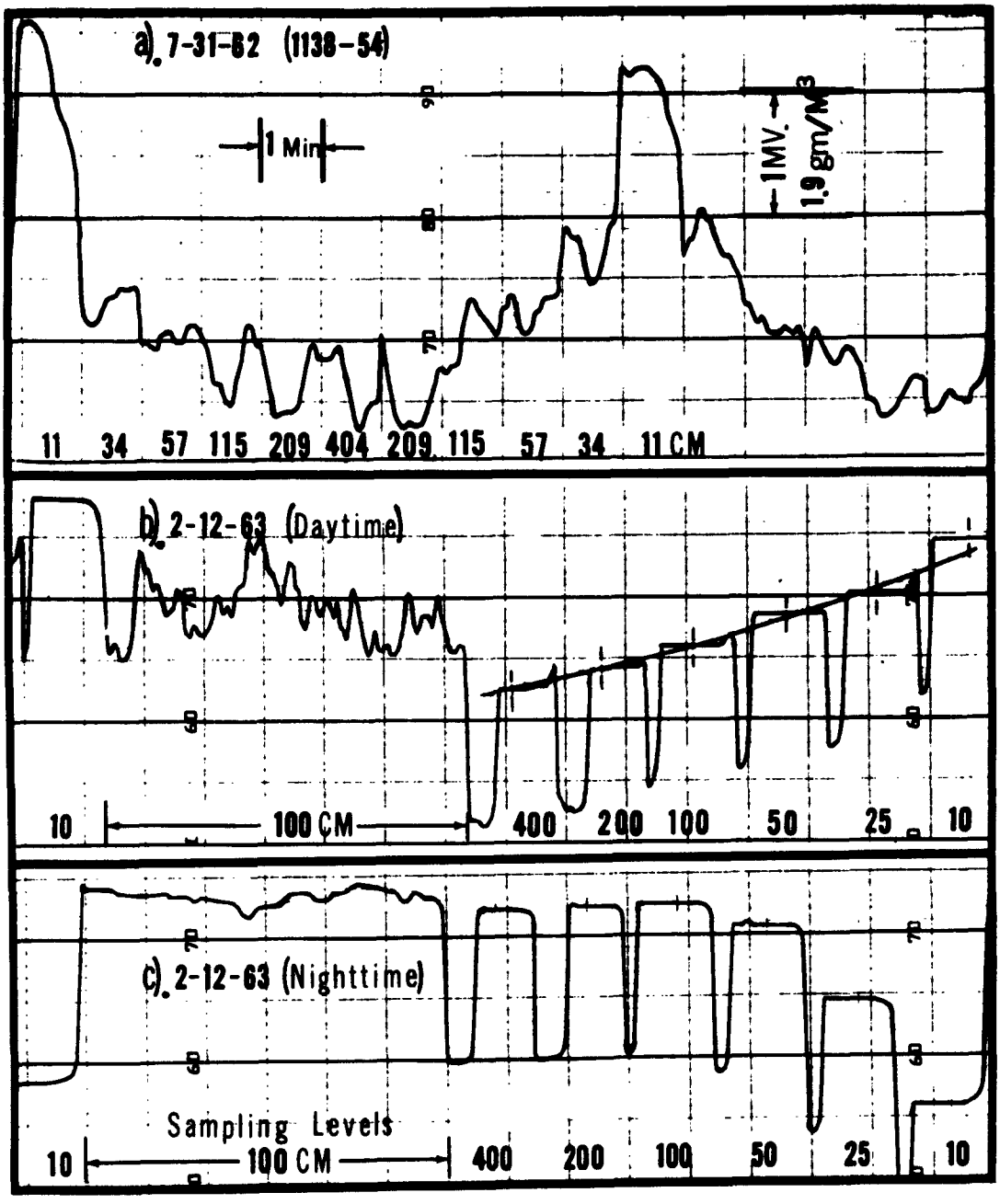

Figure III-1. Recorder record of millivolt output of the Infrared hygrometer during three different days. a): Sequential sampling, one minute at each level. b) and c): 15-minute samples collected in plastic bags plus a 6-minute record of humidity at 100 cm level. The sharp dips in the record following each plateau occurs when bags are empty and a partial vacuum reduces moisture in sampling chamber.

Soil heat flux was measured by 3 heat flux plates located at a 1-cm depth below the soil surface of the lysimeter. No corrections were made for changes in heat stored in the 1-cm layer above the plates nor were corrections made for plate temperature. Errors due to the latter are less than 1-2%.

Absolute humidity, ρq, in grams per meter^3 was determined by sequentially sampling at six heights between the surface and 4 meters in the July and August runs with a 1-minute sampling time for each level. The sensing element was the General Mills infrared hygrometer. The difficulty in analyzing results using this method is evident in Figure III-1$_a$ where a 16-minute record is shown. In the 6-minute portion of part b) of this figure where continuous sampling at 100 cm is indicated, wide fluctuations in daytime moisture concentration occur during periods of less than a minute. When the moisture concentration at any one level is changing as much in a few seconds as the gradient being measured, and a record at any given level is obtained for only 5 minutes out of every 30, it is obvious that the sampling technique used to obtain the upper record was not making full use of the capabilities and sensitivity of the hygrometer. The record shown in parts b) and c) of Figure III-1 were obtained with the collecting system described in the Appendix. Air from all six levels is pumped simultaneously into plastic bags over 15-minute periods where it is allowed to come to equilibrium for three minutes or longer before being drawn out of each bag and through the hygrometer. This technique, used after August 1962, is highly superior to the previous method used. By switching to an alternate set of six bags every other 15-minute period, an average humidity value from each level is obtained for every 15-minute period. The 6-minute record of the variation of humidity at 100 cm is recorded when air from the bags is not being sampled.

All of the data were averaged over half-hour periods. For temperature, humidity and wind speed, the data were plotted on semi-log paper. Eye-smoothed curves were drawn and, where available, relevant values were obtained from the curves at the 25, 50, 100, 200 and 400-cm levels. These data for the July, August, October and March test periods are given in Tables III-1, III-2, III-3 and III-4 at the end of the chapter.

In Figure III-2 moisture data collected under sequential sampling during August 31 indicate the general moisture profile shapes throughout

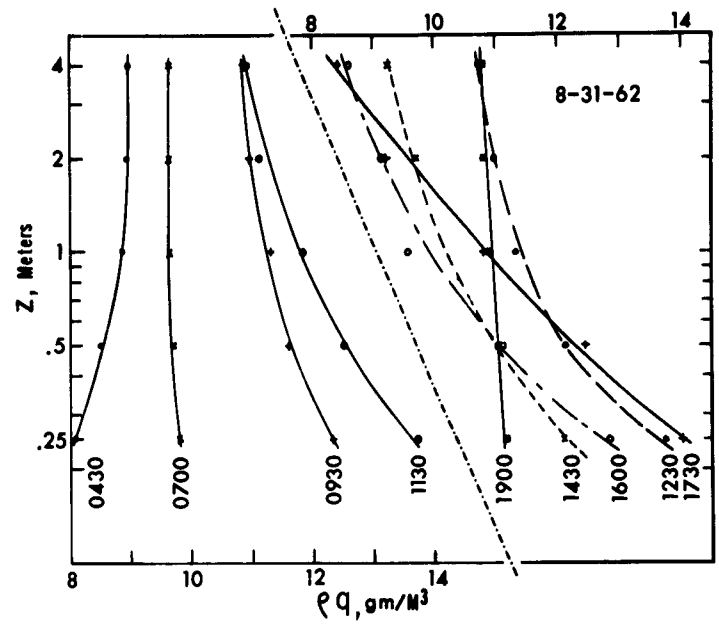

Figure III-2. Smoothed profiles of humidity, ρq in gms/meter^3 for several half-hour periods ending at time indicated.

the day. This figure also serves to illustrate the method of obtaining the smoothed data. Scatter of the data points was reduced considerably in the October and March run when the bag collection system was used.

RESULTS AND DISCUSSION

The Energy Balance and Temperatures of Surface and Air

As indicated earlier, it has been rather tacitly assumed that within an extensive moist area convective heat transfer tends to be almost negligible and that the diurnal patterns of ET and (R_n+G) should thus be closely in phase. Although the Davis site does not provide an extensive moist area, the lysimeter located near the middle of a 13-acre field of well-irrigated grass should be little affected by advective heating (or cooling) effects, particularly on calmer days.

In Figure III-3, data for 3 1/2 clear days in 1962 are given. On these relatively calm days it is clearly evident that the relationship between L(ET)

and (R_n+G) was far from constant. The form of the energy balance equation used is R_n + G + L(ET) + H = O, so that heat flux (evaporative or sensible) away from the surface is considered as negative. A steadily increasing proportion of (R_n+G) is used in evaporation as the day progresses. It is clear here (and in Figures III-4 to 8) that convective heat transfers can be far from negligible even over a well irrigated crop.

The 1962 results not only provided energy balance data, but with the measurement of grass surface temperature, and temperature and humidity of the air down in the sward, provide for a better understanding of factors which determine the partitioning of energy at the surface between L(ET) and H.

In Figure III-4 the energy balance data (except for R_n) are given for August 31 together with wind velocity and temperature data.

The amount of vapor transfer away from a surface at any time is a function of the difference in moisture concentration at the surface and in the air above as well as the turbulent transfer characteristics of the air mass.

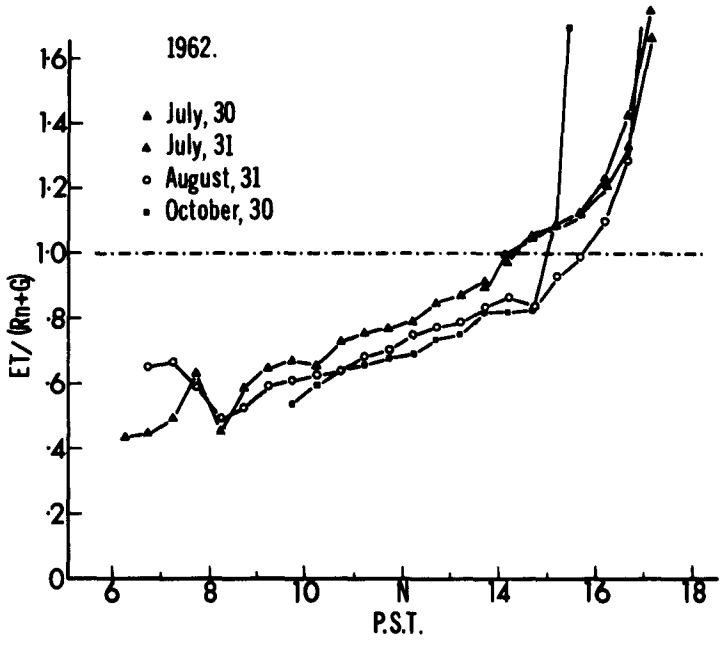

Figure III-3. Ratio of L(ET)/(R_n + G) during half-hour periods for 3 1/2 days in 1962.

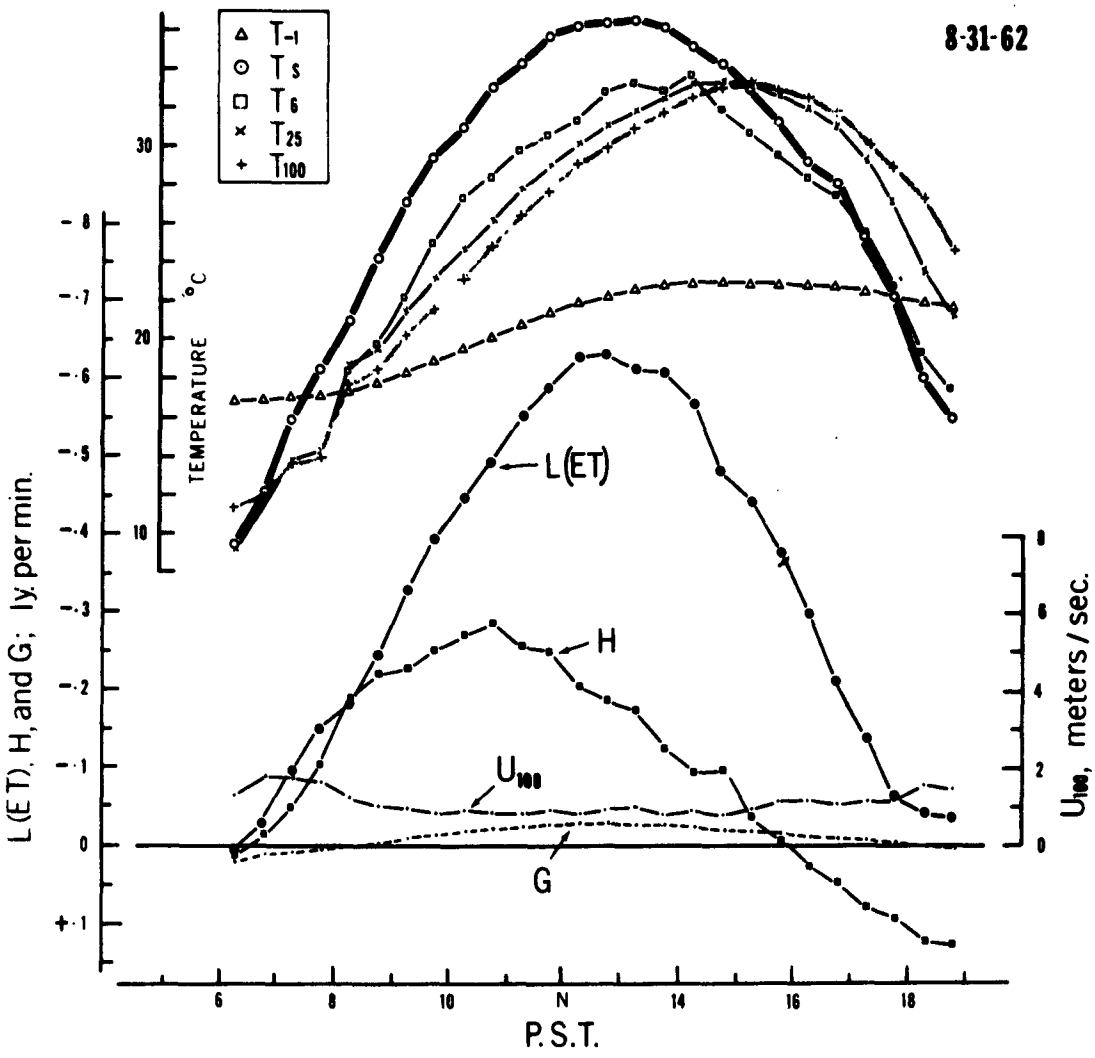

Figure III-4. Three of the energy balance components, L(ET), H and G; wind speed at 100 cm, u_{100}; and temperature of soil at 1 cm, T_{-1}, air in sward at 6 cm, T_6, air at 25 cm, T_{25}, air at 100 cm, T_{100}; and average temperature of grass leaves, T_s. August 31, 1962.

The temperature patterns for August 31 indicate that the dissipation of energy by evaporative cooling at the surface in the morning was more than overcome by the net heating effect of the radiation exchanges. Considerable radiation heating of the surface resulted. By 1030 the grass surface temperature T_s, exceeded air temperature at the 100-cm level by 8.3°C (15°F). Air within the sward T_6, was heated to a value 4°C warmer than T_{100} by 1030 resulting in an appreciable convective heat flux H, away from the surface. The difference in temperature between leaf and air had started decreasing rapidly by 1300 as T_s started dropping while T_{100} continued to climb. The curves crossed at about 1510 and a strong inversion developed by 1800 (T_{100}-T_s = 8.2°C).

The surface temperature on August 31 reached a maximum only slightly later than the time of peak evapotranspiration although both lagged somewhat behind net radiation, which, although not shown in Figure III-4, reached a maximum at true solar noon (T.S.N.=1207 P.S.T. on August 31). It is significant that both L(ET) and T_s were considerably higher at any specific time after T.S.N. than at a corresponding time before noon. For example, at 1507 T_s was 33.3°C compared to 26.6°C at 0907. Corresponding values of L(ET) were approximately .450 and .305 ly/min, or 47% higher 3 hours after than before T.S.N. The saturation vapor pressure over water at 33.3°C (T_s) is exactly 47% greater than the saturation vapor pressure over water at 26.6°C (T_s). For this day at least, the major cause of the lag in response of ET to R_n appears to be the out of phase relationship between R_n + G and surface vapor pressure.

The curves for T_{100} and T_{50} are considerably out of phase with both T_s and the ET curves. The temperature of air down in the sward, T_6, tended to be closer to air temperature above the sward than to T_s during morning hours but was much closer to T_s as radiation dropped to a low level. The fact that the soil was acting as a heat sink most of the day provides an explanation for T_6 becoming cooler than both T_s and T_{25} for a period in the afternoon. Grass height on this day averaged about 10-12 cm so the sampling level for 6-cm air was approximately half-way between the soil surface and the tips of the blades of grass.

The soil heat flux, G, at the 1-cm soil depth reached a maximum at the same time as T_s, reaching a value of 0.03 ly/min. This was only 3.5%

of R_n at the time. Since the change in heat storage in the 1-cm level above the flux plates was not taken into account, the actual sensible heat transfer into the surface would run slightly higher than indicated in morning hours and slightly lower than indicated in afternoon hours, but the total magnitude of the error would be small.

The fact that H does not reach zero until about 40 minutes after the inversion develops, perhaps gives some indication of the magnitude of combined errors in measurement of the other three components of the energy balance plus the failure to account for the net energy requirements of the plant (photosynthesis minus respiration). Changes in heat storage of the plants and air were also neglected.

The results presented in the previous figures appear to be typical for clear, relatively calm days at Davis. Additional energy balance data given in Chapter I show similar results with appreciable convective heat transfer away from the surface in morning hours with appreciable transfer of heat to the surface after an inversion develops between 1430-1600. On the calmer days particularly it seems unlikely that advective cooling was involved in the low ratios of $L(ET)/(R_n + G)$ during morning hours. In fact, on August 31, the incurrent air mass may represent a case of slight advective heating. Table III-2 indicates that T_{200} exceeded T_{100} during several periods before 1400 when there was a lapse rate from the 100-cm level on down. Up until this time the light breezes were occasionally from the NE where the road and a recently cut alfalfa field only 30-60 meters away probably had a higher surface temperature than that of the grass field.

After 1400 the gentle breeze was from the NNW where the air traveled over 185 meters of ryegrass before reaching the lysimeter. With this fetch of grass and with a wind speed of only 1-meter per sec it seems unlikely that advective heating was an appreciable factor in causing the late afternoon ratios of $L(ET)/(R_n+G)$ to be well over 1.0. The block of energy represented by the convective heat flux to the surface after the development of an inversion for all three of the days, is considerably less than that transferred into the air during the morning hours, no doubt due to the somewhat smaller gradients and the stable afternoon conditions.

In Figure III-5, comparable results are shown for October 30, another clear, relatively calm day. Similar patterns as those for August 31 are

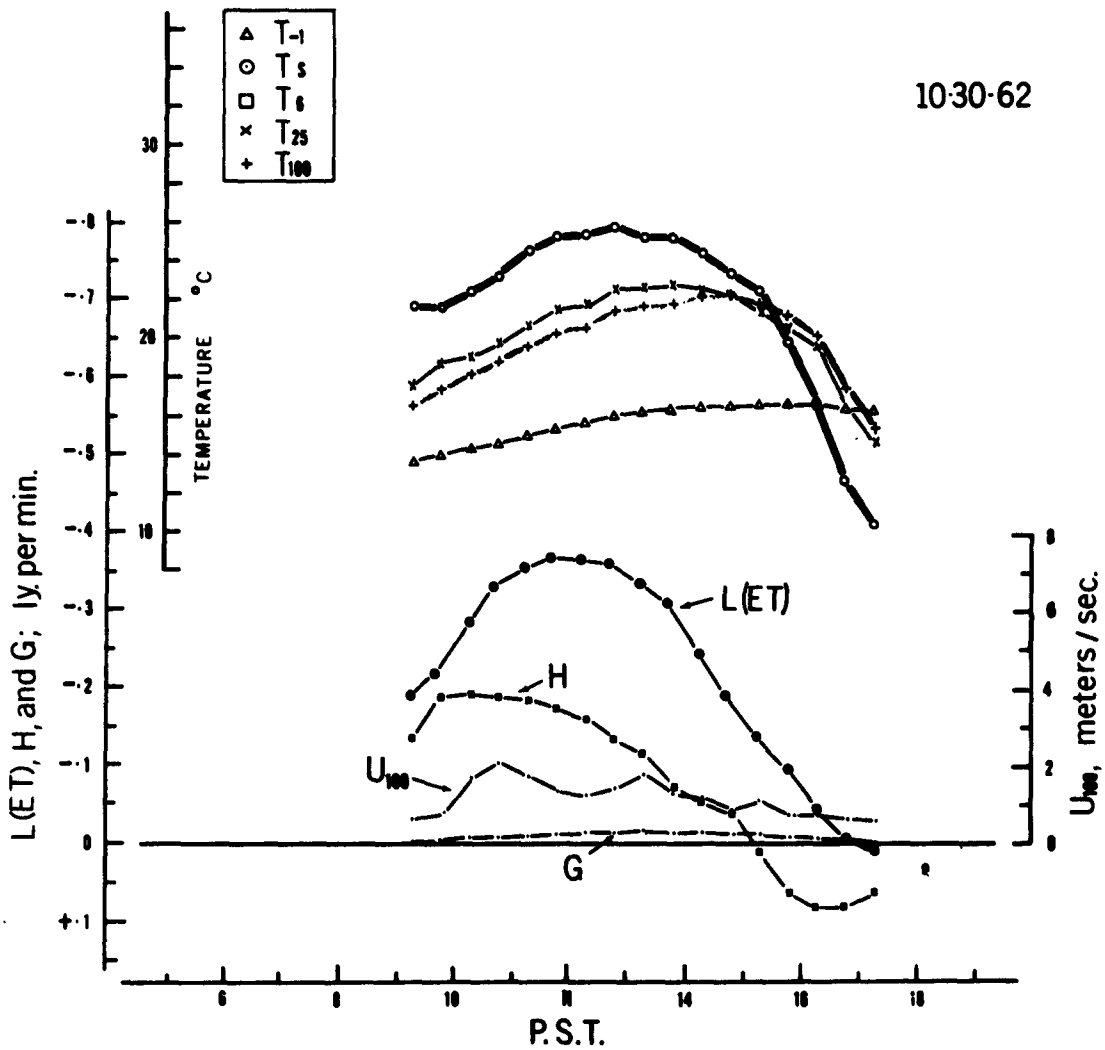

Figure III-5. Energy balance, wind speed, and leaf and air temperatures for October 30, 1962.

evident for the various parameters. However, with lower radiation, the temperatures along with the various components of the energy balance are lower.

In Figure III-6 results for July 31 are given. This was another clear day with similar wind velocity during early morning hours as that for the previously mentioned two days. However, on July 31 wind velocity increased after 1000, reaching a maximum value of approximately 4 meters per second by 1400. This increase in wind speed apparently produced greater evaporative cooling and prevented both surface and air temperatures from reaching as high a peak as on August 31. Except for a lateral displacement due to an earlier sunrise on July 31, the patterns of ET, H, and surface and air temperatures are similar for the two days up until 1000. With increasing winds thereafter, the patterns for the two days diverged considerably. In spite of 7 1/2% higher maximum radiation for July 31, T_s on July 31 reached a peak level almost 4°C lower than the peak level of the later date. T_{100} on July 31 reached a maximum level at 29.6°C compared to 33.4°C on August 31. In contrast, maximum ET on the July date exceeded the maximum ET on August 31 by 22%.

The maximum convective heat transfer away from the surface was similar for the two days although with increasing wind speed H dropped off to zero around 1430, almost 1 1/2 hours earlier on July 31 than on August 31.

Results for the clear, strong, north-wind day of March 12, 1963 are shown in Figure III-7. On this day the air mass moving down the valley was very dry having a dewpoint temperature of -2°C. On a number of similar days over the past 3 1/2 years, it has been observed that evapotranspiration on such days is considerably greater than on calm, clear days with equal radiation. In this case, however, ET was actually lower than on the previous calm, clear day of March 11. The temperature pattern indicates that the surface was warmed by radiation appreciably above the rather cool air mass overhead, and thus with the strong turbulence a high convective heat transfer resulted. It is believed, however, that considerable plant control was in effect most of this day. Otherwise, a higher ET would have occurred, and with subsequent increased evaporative cooling, the surface temperature would have stayed much cooler resulting in less convective heat transfer away from the surface.

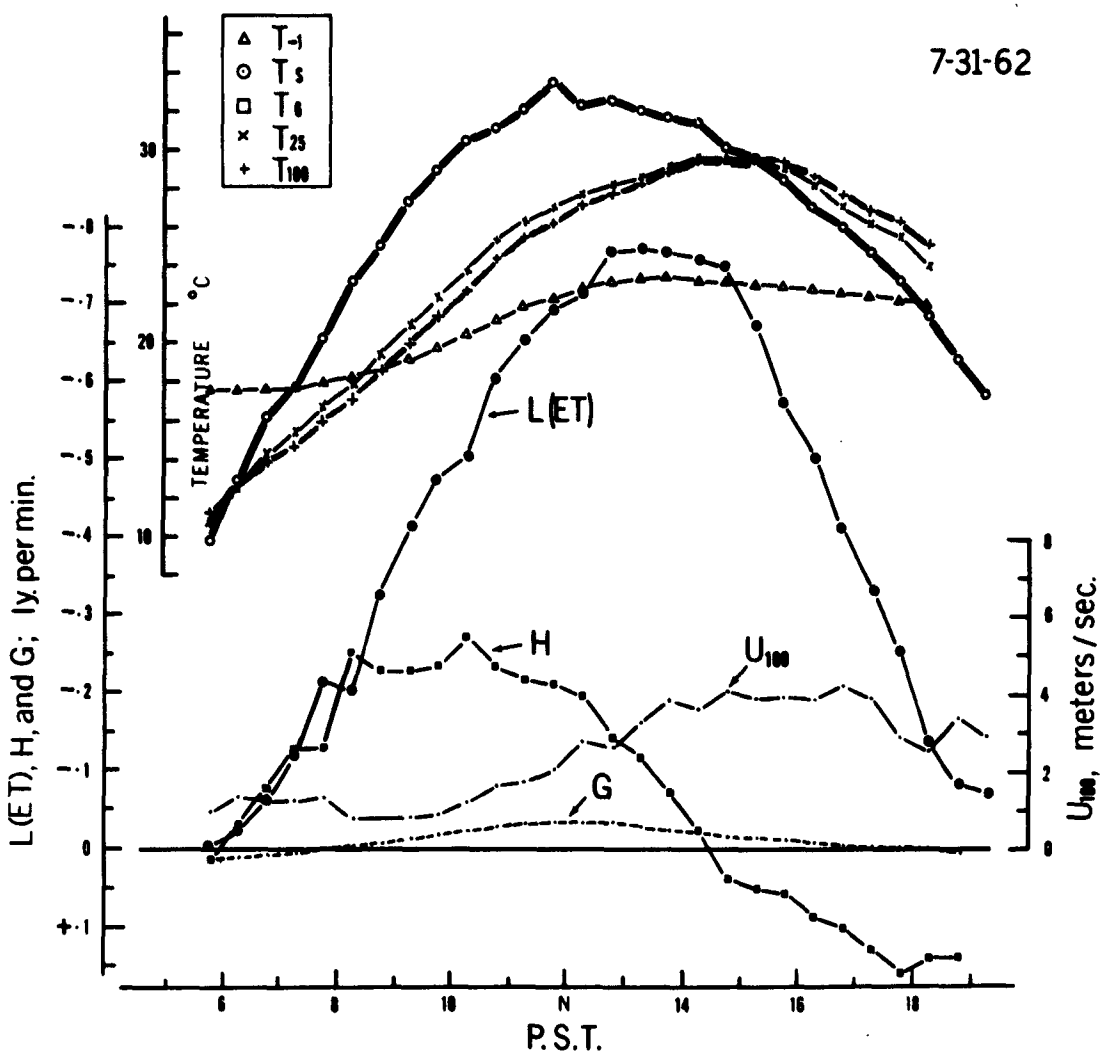

Figure III-6. Energy balance, wind speed, and leaf and air temperatures for July 31, 1962.

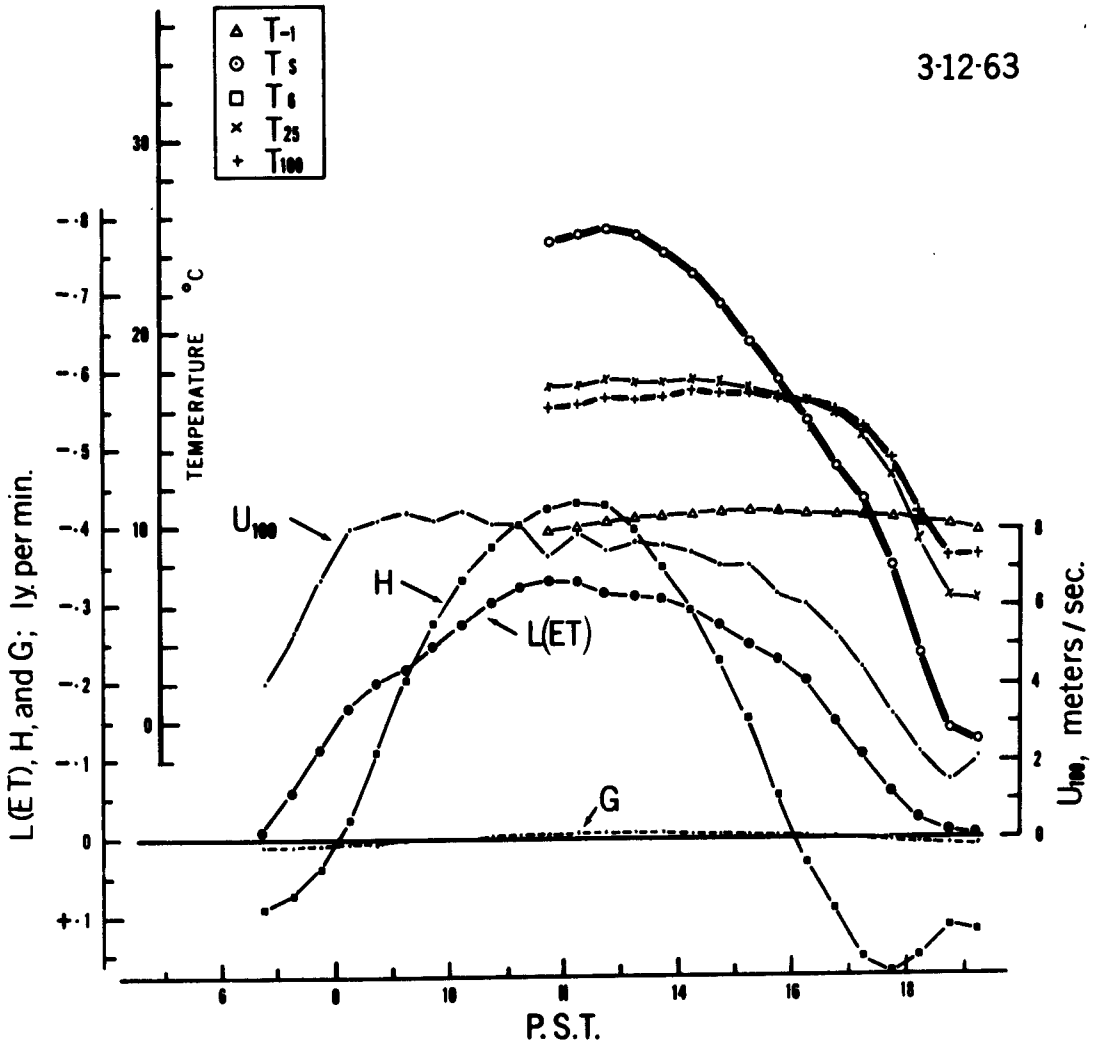

Figure III-7. Energy balance, wind speed, and leaf and air temperatures for March 12, 1963.

Flux-Gradient Relationships

With the strong morning and mid-day lapse conditions and the late afternoon inversions indicated in the Figures III-3 to 6, these results have provided an opportunity to study flux-gradient relationships under a gradual transformation from highly unstable to highly stable conditions. Data for the steadily calm day of August 31 have been especially valuable for such an evaluation.

In Figure III-8 the saturation deficit of the air at 100 cm $(e_a - e_{100})_{100}$ and the vapor pressure gradient between the surface and the 25-cm height $(e_s - e_{25})$ are compared with the ET curve. The value of e_s approximates the vapor pressure inside the sub-stomatal cavity of the leaves, assuming this to be a fully saturated atmosphere at leaf temperature.

Since the saturation deficit is so much a function of air temperature, and as ET is considerably out of phase with air temperature, a very poor relationship between ET and the saturation deficit should be expected. This is clearly the case in Figure III-8. On days when the surface temperature pattern is considerably different from the pattern of air temperature, the saturation deficit of the air above a surface is an extremely misleading index of the true driving potential for vapor flux away from the surface.

The curve for $(e_s - e_{25})$ is the only gradient curve which appears to be nearly in phase with the ET curve. During much of the afternoon the vapor gradient between air within the sward and air at the 25 cm height $(e_6 - e_{25})$ is in phase with the ET curve but this is not the case during a considerable portion of the morning.

The gradients of vapor in the air above the grass show a general increase during the day until 1730 as was earlier demonstrated by the profiles of absolute humidity shown in Figure III-2 where the strongest gradient shown was for the 1700-1730 period.

In Figure III-9, half-hour values of ET are plotted versus the vapor pressure gradients above the grass for August 31 and July 31. On the continually calm day in August a very pronounced loop effect in this comparison results with much greater gradients required in the stable afternoon conditions to give a comparable vapor transfer to that realized under the highly buoyant mid-morning conditions. The effects of stability on moisture transfer are particularly striking when the data for the unstable condition

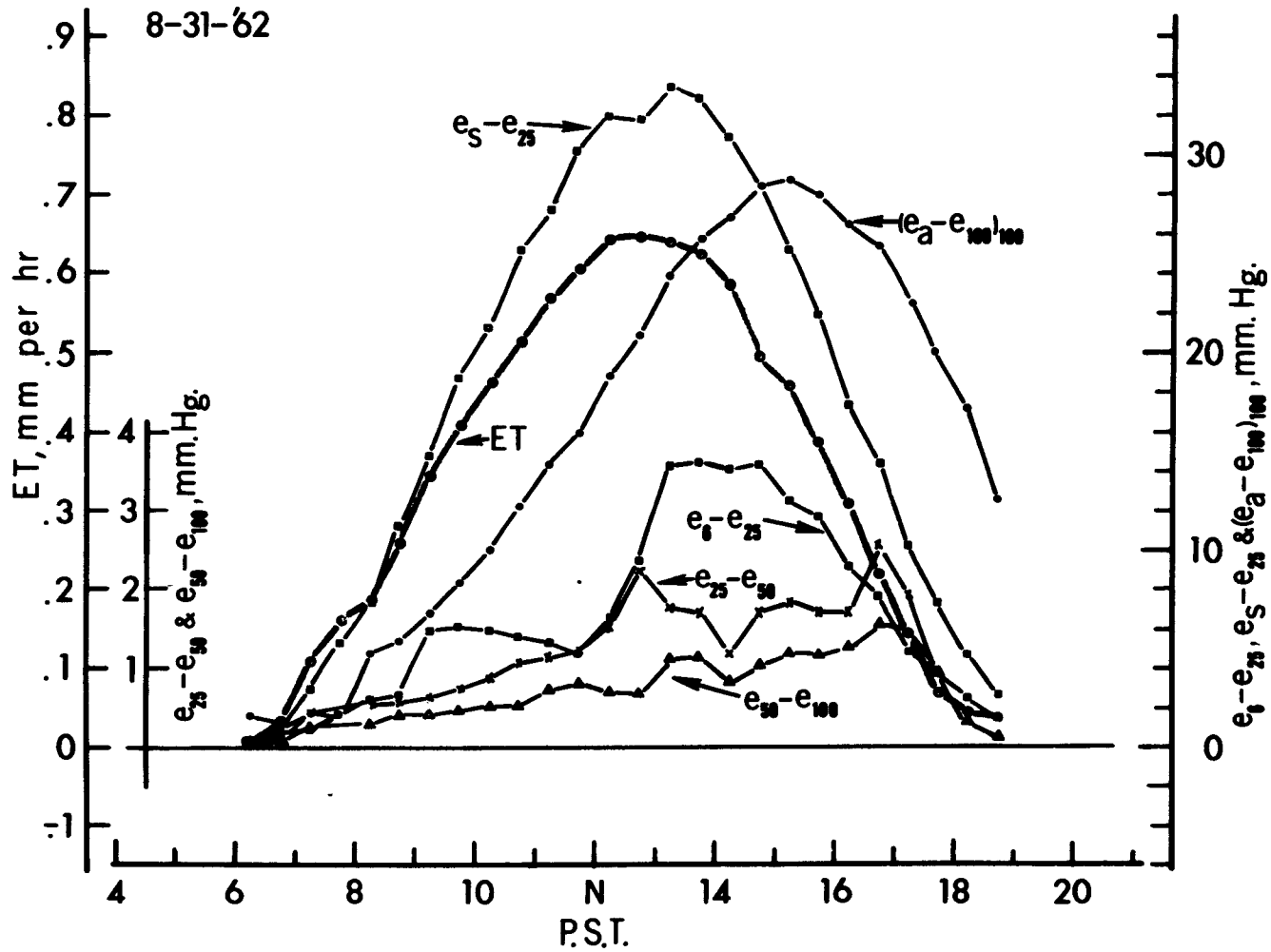

Figure III-8. Evapotranspiration, ET; saturation deficit of air at 100 cm level, $(e_a - e_{100})_{100}$; vapor gradient between various levels above the soil surface, $(e_6 - e_{25})$, $(e_{25} - e_{50})$ and $(e_{50} - e_{100})$; and vapor gradient from leaf surface to air at 25 cm level, $(e_s - e_{25})$ where e_s is the saturation vapor pressure at leaf temperature, T_s and not a meas-

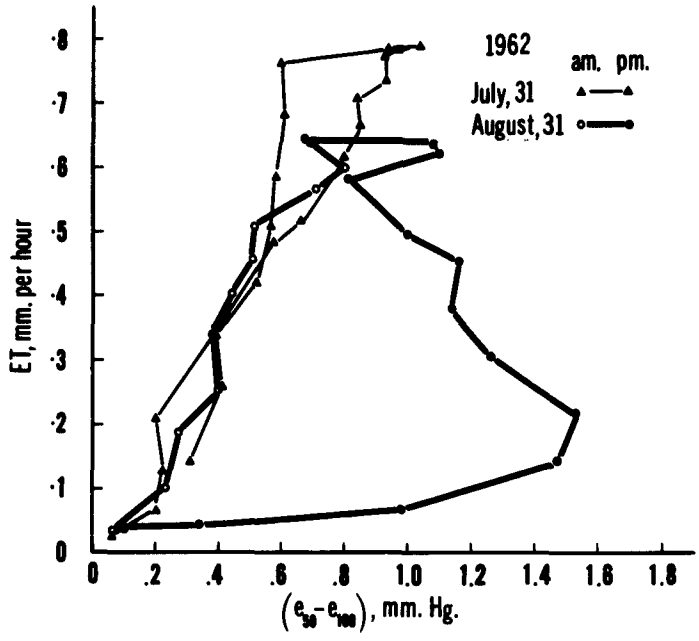

Figure III-9. Evapotranspiration versus the vapor pressure gradient between 50 and 100 cm above the soil surface, $(e_{50} - e_{100})$.

at 1100 - 1200 are compared with the highly stable period from 1730 - 1800. The vapor gradient is about 0.8 - 1.0 mm Hg for both periods but the transfer in the morning period is 8 times that of the afternoon period. Up until 1130 the relationship of ET to the vapor pressure gradient for both days is similar but with increasing turbulent transport as the wind increased on July 31 the results for the two days become quite different. Here is obviously a case of high moisture transfer with a given gradient during morning hours largely due to buoyancy, with a correspondingly high or even higher afternoon transfer under similar gradients but now due to greater turbulence as the result of higher wind speeds.

With the large variations in stability encountered during the 1962 runs it was deemed especially worth-while to compare the eddy diffusivity for water vapor (K_D), and the eddy conductivity for heat (K_H), since there have been few studies where an adequate measure of evaporative heat flux over

short periods was obtained. In this study considerably more confidence can be placed in the measurement of ET than in the calculated value of H. Nevertheless during many times of the day the H values calculated from the energy balance are probably within $\pm$ 5 to 10% of the actual value for H.

There is disagreement in the literature as to the expected relationship of K_D to K_H. Some workers indicate that the transfer mechanisms for water vapor and heat are similar [Bowen (1926) and Ellison (1957)]. Pasquill (1949) measuring evaporation from small pots of turfed soil in natural surroundings found the two were similar in stable conditions but under unstable conditions, K_H exceeded K_D appreciably.

In Table III-6 (at the end of this chapter) values of eddy diffusivity for water vapor K_D and eddy conductivity for heat K_H are given. K_D and K_H were calculated for a height, z of 75 cm from the expressions,

$$ET = \rho K_D \, \partial q/\partial z \quad \text{and} \quad H = \rho c_p K_H \, \partial T/\partial z$$

where ET is in gms/cm^2 sec, H is in cal/cm^2 sec, ρ is the density of air in gms/cm^3, c_p is the specific heat of air at constant pressure in cal/gm$^\circ$C, $\partial q/\partial z$ is the moisture gradient at 75 cm in gms per gm of air estimated from $q_{100} - q_{50}$, and $\partial T/\partial z$ is the temperature gradient estimated from $T_{100} - T_{50}$ in $^\circ$C. K_D and K_H are in cm^2/sec.

Also included in Table III-6 are values of one of the common stability parameters, the gradient form of the Richardson Number, Ri, where $Ri_{75} = \frac{g}{T} \frac{(\partial T/\partial z + \Gamma)}{(\partial u/\partial z)^2}$ where g is gravitational acceleration (980 cm/sec^2), T is the absolute temperature of the air $^\circ$K and Γ is the adiabatic lapse rate (neglected in these calculations because of its small effect over a 50 cm distance).

Pasquill (1949) in analyzing the results of his study of eddy transfers of water vapor and heat determined the variation of the dimensionless parameters $\frac{K_D}{z^2 \, \partial u/\partial z}$ and $\frac{K_H}{z^2 \, \partial u/\partial z}$ under different conditions of stability. These two terms will be designated here as K_D^* and K_H^* respectively. He plotted values of K_D^* and K_H^* against values of Ri_{75}, which under the conditions of his study ranged from -.25 to +.125. Under highly stable conditions the above two parameters were found to be nearly equal. At neutral conditions K_H^*/K_D^* was around 1.5 but as instability increased to a degree as

indicated by $Ri_{75} = -.15$, K_H^* was approaching 2 times the value of K_D^* indicating transfer mechanisms for water vapor and heat were not alike except under strong stability.

In Figure III-10, values of K_D^* and K_H^* are plotted as a function of Ri numbers. The top half of the figure is for the unstable conditions and the bottom half covers the periods of stability. The open circles are values of K_D^* and the triangles are values of K_H^*. All data contained in Table III-6 identified with a single or double asterisk were left out of Figure III-10 for reasons indicated at the bottom of the table.

It is obvious that with a given wind gradient $\partial u/\partial z$, the eddy diffusivity and the eddy conductivity increase rather drastically with greater negative Ri values beyond -0.1. Both K_D^* and K_H^* are nearly an order of magnitude greater at Ri = -2 than at an Ri of -0.02.

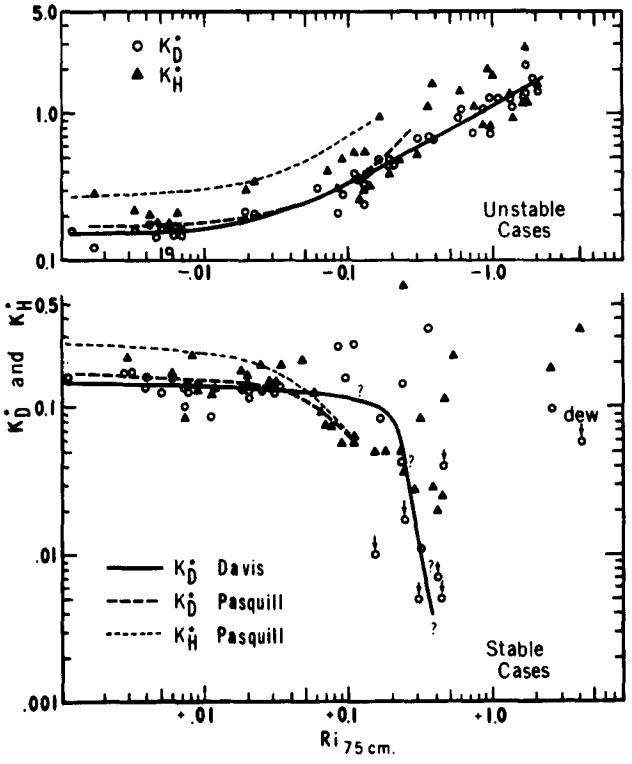

Figure III-10. Variation of a dimensionless form of K_D and K_H with the gradient Richardson Number, $Ri_{75\ cm}$ where $K_D^* = K_D/(z^2\ \partial u/\partial z)$ and $K_H^* = K_H/(z^2\ \partial u/\partial z)$. Pasquill's (1949) results were replotted for comparison with 1962-63 Davis data.

Under the stable conditions there is little effect of stability on either K* values until somewhere around an Ri of +0.1. Although the scatter is great the results provide some support for the occurrence of a rapid decay of turbulent transport beyond this point. This is discussed in more detail in Chapter V by Crawford (1963).

The solid line in Figure III-10 is an eye-fitted curve through the K_D^* values for Davis. The heavy dashed lines represent the relationship for K_D^* found by Pasquill for both the stable and unstable condition. The results are quite compatible except for the slopes of the lines near the end of the range of Pasquill's data for negative Ri. If extrapolated out in a straight line beyond the range of his measurements his results would indicate K_D^* values at Ri = -2 of almost twice those for the Davis data.

The Davis data for K_H^* versus Ri numbers are not in agreement with the average relationship reported by Pasquill (indicated by light dashed lines in Figure III-10). Almost all of the Davis data lie below the light dashed line except in the highly stable cases. There is little support here for a conclusion of any real difference between K_H^* and K_D^* in the highly unstable case.

A real disparity in trends between the Davis results and those of Pasquill, is more apparent in Figure III-11 where the ratios of K_H/K_D taken from Table III-6 are plotted versus the Ri numbers. In Pasquill's study, within the narrow range of stabilities realized, the ratio of K_H/K_D varied as indicated from near 1.0 at the highest stability encountered to near 2.0 at the greatest instability. Although the scatter is considerable, the Davis data indicate an opposite trend. The relationship of K_H/K_D is close to 1.0 in the highly unstable case, averages around 1.2 to 1.3 near an Ri of zero and if anything appears to average well over 1.0 under highly stable conditions. Most of the data with Ri > + 0.04 represent a transfer of water vapor to the surface rather than away from it. Under this condition of deposition of dew, the accuracy of determinations of the very low flux rates for 1/2-hour periods is highly questionable. However, the average flux over a 2-4 hour period is still fairly accurately determined. The gradients for both temperature and humidity were strong on the night of October 30 and were thus quite accurately determined. It is therefore suggested that in spite of the scatter of the data, the average condition of the dew deposition periods represents significant evidence of a $K_H/K_D \rightarrow$ 2 to 3. There is considerable

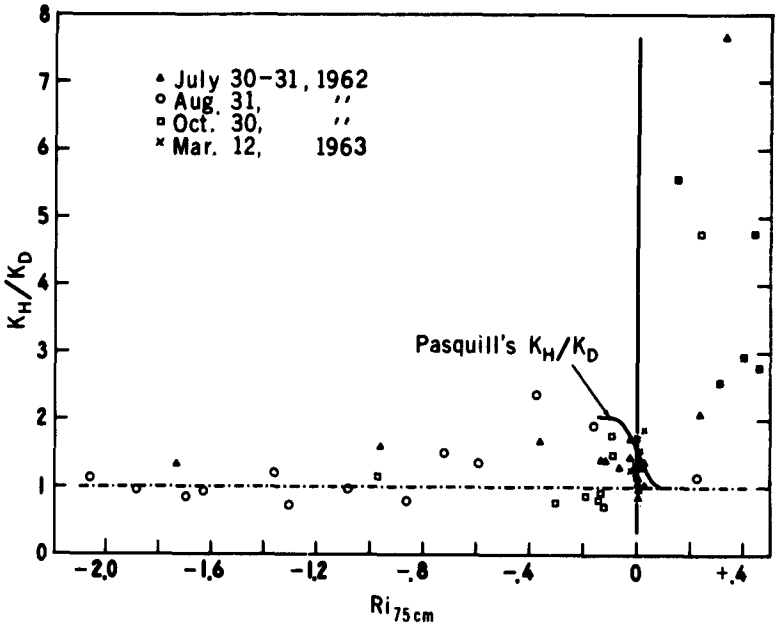

Figure III-11. The variation of the ratio K_H/K_D with Ri_{75}. Pasquill's (1949) relationship was replotted for comparison with 1962-63 Davis data. Solid circles or triangles are for cases of dew.

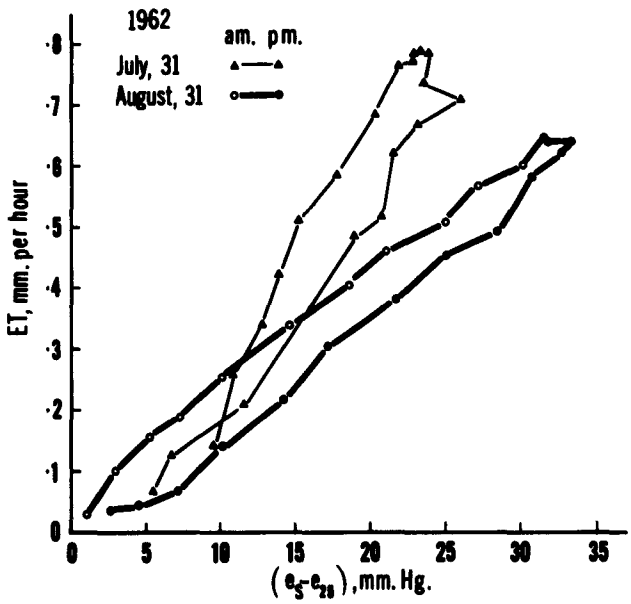

Figure III-12. Evapotranspiration versus the vapor pressure gradient from leaf surface to air at 25-cm level, $(e_s - e_{25})$ where e_s is the saturation vapor pressure at leaf temperature, T_s, and not a true measured surface vapor pressure.

uncertainty as to actual Ri values during these periods due to the difficulty of measuring very low wind velocities.

In general it is believed that the Davis results lend considerable support to a near equality of eddy diffusivity for water vapor and eddy conductivity for heat except under highly stable conditions. The good results in predicting ET reported in Chapter IV using the energy balance equation (which assumes $K_D = K_H$) offers further evidence of the above.

With the large variation noted earlier of the relationship of fluxes to gradients above the surface it should be interesting to compare in particular the flux of water vapor away from the surface as a function of the difference in vapor pressure of the evaporating surface and of the air just above the surface. The relationship of the pattern of ET to $e_s - e_{25}$ noted earlier in Figure III-8 suggests possible use of a Dalton type approach in estimating potential evapotranspiration from a full cover crop with unlimited water supply. Slatyer and McIlroy (1961) indicate that the Dalton approach has not been tried over land and suggested problems which could be expected.

When comparing the results in Figure III-12 with the results in Figure III-9, however one is struck with the much smaller effect on the ratio of $ET/(e_s - e_{25})$ of widely varying stability conditions encountered on August 31 as compared to the effect on the ratio of $ET/(e_{50} - e_{100})$.

For August 31 the plot in Figure III-12 still indicates greater morning transfer of moisture with a given gradient than in the afternoon hours. Since wind was fairly steady after 0900, this may be due to greater instability during the morning hours. If this is the case, the demands for correction for stability would still be much less stringent than that indicated by Figure III-9 where the gradients of moisture concentration between the 50-cm and 100-cm level were considered. Variation in stomatal resistance during the day may also be a factor.

If the data presented are typical, the requirements for accuracy in measurement of gradients would be considerably less stringent. At mid-day for example, the gradients from the surface to a 25-cm level were an order of magnitude greater than the gradients above the grass.

The data for July 31 in Figure III-12 are reversed from that of August 31. Although early morning relationships are similar on the two days, the effect of higher afternoon winds is probably two-fold. The level of stability reached in late afternoon of July 31 is not only much less but the wind provides better

turbulent transport of vapor away from the surface. Part of the reason for a higher maximum transfer rate on July 31 is the higher level of radiation. It should be noted here, however, that actual surface temperatures and vapor pressures remained lower due to the greater evaporative cooling.

In Figure III-13 a plot of $ET/(e_s - e_{100})$ versus wind speed at the 100-cm level has been made. In the Dalton-type equation for evaporation the form has normally been of the following

$$E = f(u_z)\ (e_s - e_z)$$

where e_s is surface vapor pressure, e_z is vapor pressure at some height z above the evaporating surface, and $f(u_z)$ is an empirically derived function of average wind speed at height z, commonly given in the form

$$f(u_z) = a(1 + bu).$$

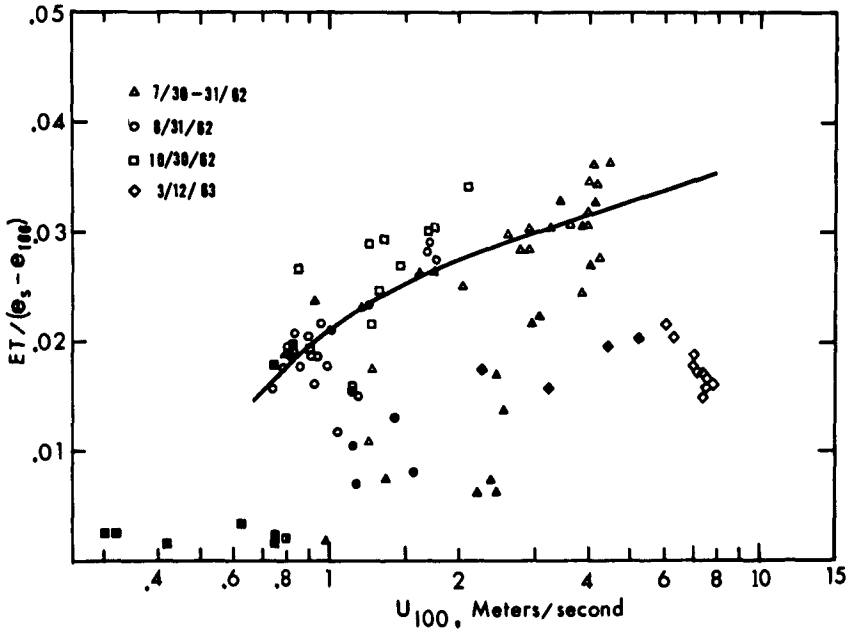

Figure III-13. The variation of the ratio $ET/(e_s - e_{100})$ with wind speed at the 100-cm level where e_s is the saturation vapor pressure at leaf temperature, T_s and not a measured surface vapor pressure.
Solid data points are for periods earlier than 1 1/2 hours after sunrise and later than 1 1/2 hours before sunset. Half-solid points indicate dew cases.

Except for the night-time and a few early-morning or late-afternoon hours, almost all of the 1962 data in Figure III-13 lie fairly close to the average relationship indicated by the eye-smoothed curve. Except for the dew cases, the lower values may be caused in part by restriction of transpiration due to partial or complete stomatal closure. Preliminary studies on diurnal variations in stomatal aperture of ryegrass as measured by infiltration techniques, indicate full stomatal opening is not attained until 1-3 hours after sunrise. As indicated in Chapter XI and in Chapter X of this report, plant resistances to water loss also increase during the afternoon indicating possible stomatal closure due to tensions within the plant or to some other factors.

A damping of turbulence due to the strong inversion in late afternoon may also be a factor in causing some of the low 1962 daytime values in Figure III-13. The low values at night for the cases of dew are probably due to this factor since stomatal behavior would be of no consequence at this time.

As indicated earlier, considerable plant control over transpiration was suspected for the March 12 date. Results in Figure III-13 provide a prime reason for such a conclusion. It is clearly evident that a true measure of effective surface vapor pressure was needed on this date and that the use of a saturated vapor pressure at measured leaf temperature was entirely unsatisfactory. This highlights one of the most difficult problems to overcome in the use of such an approach for cropped surfaces.

As indicated earlier, the Dalton approach has normally been used in a form which assumes a linear relationship between $E/(e_s - e_z)$ and the wind speed. Results in Figure III-13 show a relationship which appears to be curvilinear even on a semi-log plot.

Seasonal Variation of Evapotranspiration and Radiation

Seasonal variations in the relationship of evapotranspiration to solar and net radiation were reported earlier by Pruitt (1962). Additional data are available for 1961-62 and are given along with 1959-60 data in Figure III-14.

It is obvious that there are large seasonal changes in relationship between ET and solar radiation, R_c. However, if only the May-October period is considered, the range of ET/R_c ratios is only from about 0.48 to 0.58 whereas the annual range is from 0.24 to 0.58.

The ET/R_n relationships shown indicate the 1961-62 results corroborate earlier results with higher midsummer and fall ET/R_n ratios than in winter and spring months. This situation may be somewhat analogous to the relationships noted during diurnal cycles. In spite of similar radiation on spring and fall days, the surface temperature of the grass, at least during morning hours, must be warmer on the fall days than on spring days. Apparently the resulting higher surface vapor pressures must more than overcome the generally higher air humidity in the fall so that a greater gradient exists.

It should be noted that with a taller, more dense crop the cover would serve as a more effective insulation and leaf temperatures should be less affected by the soil surface temperature. The differences in leaf temperature between spring and fall would be less and the seasonal variation of ET/R_n ratios should therefore be lower. A crop with greater insulation effect should also decrease the diurnal variation of ET/R_n ratios noted for grass at Davis.

Another factor may be the tendency for higher stomatal resistance in afternoon hours, as noted by both Monteith in Chapter X and Aston in Chapter XI. Monteith in an analysis of previous year's data also indicates higher stomatal resistances in fall months than in spring months and concludes that if stomatal resistance remained constant the variation of ET/R_n ratios would be even greater from spring to fall months as well as between morning and afternoon hours.

There is some evidence, however, that the effect on the grass ET of seasonal variation of stomatal resistance is not very significant. With data for medium or high advection days excluded, the results shown in Figure III-15 indicate little if any significant seasonal change in the relationship of ET at Davis to evaporation from free water surfaces.

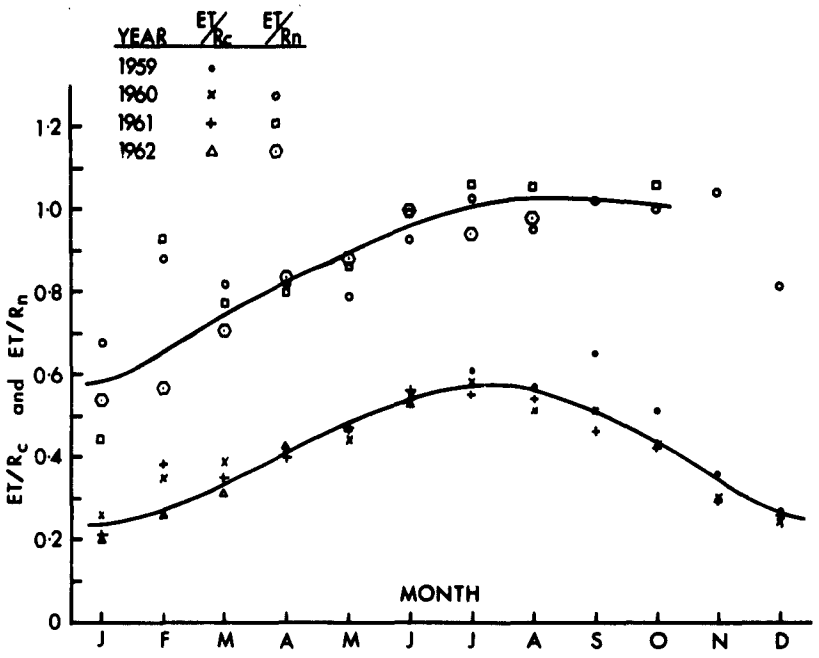

Figure III-14. The relationship of mean monthly evapotranspiration by ryegrass, ET to incoming solar radiation, R_c and net radiation, R_n. High advection days were excluded in the calculations.

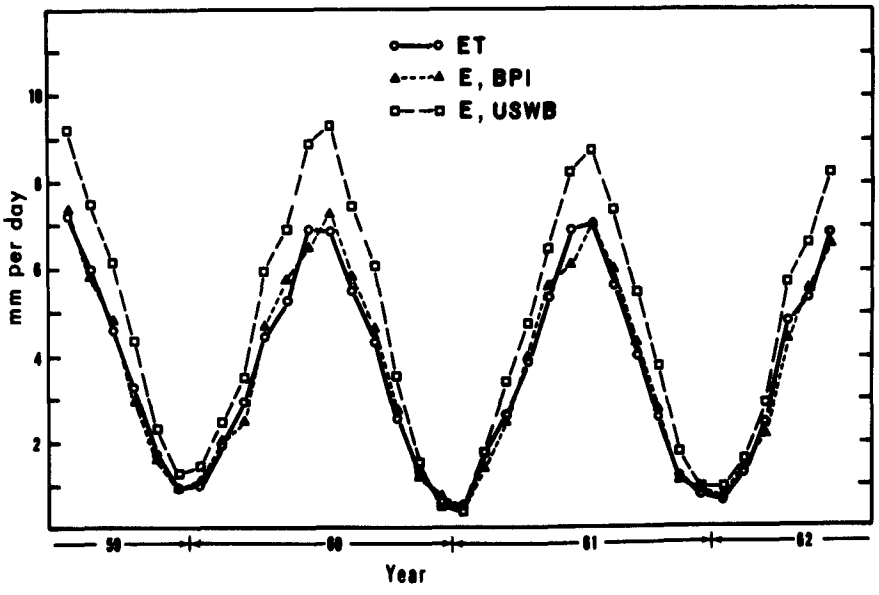

Figure III-15. Mean monthly evapotranspiration for ryegrass and evaporation from a USWB Class A pan and from a USDA-BPI pan. Both pans are located within the large irrigated grass field in which the lysimeter is located.
Note: High advection days excluded in calculations.

SUMMARY

The relationship between net radiation and the energy used in evapotranspiration from a well-irrigated grass surface was found to be quite complex and dependent upon a number of factors even in the absence of advective effects. The ratio of $L(ET)/(R_n + G)$ gradually increased from a low of around 0.5 two hours after sunrise to 1.0 by 1400-1500, with a sharper increase thereafter. This rather low use of R_n for evaporation during morning hours resulted in radiation heating of the surface considerably in excess of the rate of evaporative cooling and resulted in a development of a strong lapse rate between surface and the air with T_s exceeding T_{100} cm by as much as 8.3°C by 1030 on one very calm day. This produced a convective heat transfer away from the surface which almost equaled evaporative heat flux the first 2 or 3 hours of the day and at the time of peak flux rate at 1030-1100 accounted for about 36% of R_n.

On the continually calm day of August 31, 1962, leaf temperatures were fairly closely in phase with the pattern of ET while air temperature was well out of phase. Leaf temperatures were considerably higher in afternoon hours than in morning hours with equal radiation. This is likely the major factor in causing an out of phase relationship between ET and $R_n + G$ on such days. The gradient of vapor pressure between surface and air was almost in phase with ET. The saturation deficit, like air temperature, was well out of phase, reaching a peak as much as 3 to 4 hours after ET peaked. On the steadily calm day of August 31, the vapor gradients in the air above the surface gradually increased during morning hours corresponding to an increase in ET, but continued to rise or leveled off while at the same time ET dropped in a normal pattern. This was no doubt due to the development of strong stability conditions soon after 1500.

In a comparison of eddy diffusivities for water vapor, K_D and eddy conductivity for heat, K_H, the results support a concept of nearly equal transfer mechanisms for both water vapor and heat throughout a large range of unstable cases. K_H/K_D averaged somewhat greater than 1.0 at Ri numbers near zero and approached 2 to 3 under highly stable conditions. This trend is opposite to that suggested by results of Pasquill (1949).

Whereas the large variations in stability noted for calmer days indicate the need for a major correction factor for stability when using flux-

gradient formulas, the closeness of the relationship of ET to vapor gradients from the surface to the air suggest the possible use of a Dalton-type approach. Not only would requirements for accuracy be almost an order of magnitude lower, but only slight correction for stability variation is indicated. Such a method, however, would be possible for use only when the surface was acting nearly as a saturated surface. Results for March 12, 1963 provide a good example of a case where this was far from true.

The seasonal variation of ET--solar and net radiation relationships indicates a somewhat analogous situation to the diurnal variations. ET/R_c or ET/R_n ratios were generally lower in spring months as compared to fall months with an equivalent radiation.

ACKNOWLEDGEMENTS

The authors wish to express their appreciation to Dr. F. A. Brooks, Mr. T. V. Crawford and Dr. J. L. Monteith for their part in the July investigations and to Dr. Herbert Schultz for the use of solar radiation data.

The work of Mr. Fred Lourence, Mr. Wilson Goddard, Mr. Donald Addicott, Mr. Dennis Orr, Mr. Sergius von Oettingen, Mr. Houshang Esmaili and Miss Ellie Cornwall in collection and analysis of the data is also gratefully acknowledged.

Table III-1. Humidity of air; Temperature of soil, leaf surface, and air; and Wind Velocity at various levels (cm from soil surface), July 30-31, 1962

Time at Period's End	Air Humidity, gms/m^3					Soil, Leaf, and Air Temperature, °C							Wind Velocity, cm/sec			
	$\rho q_{11.4}$ 1/	ρq_{25}	ρq_{50}	ρq_{100}	ρq_{200}	T_{-1} 1/	T_s 1/	$T_{6\&12}$ 1/	T_{25}	T_{50}	T_{100}	T_{200}	U_{25}	U_{50}	U_{100}	U_{200}
7/30																
1400	14.28	12.12	10.88	9.94	9.19	23.6	31.8		28.86	28.81	28.75	28.68	176	238	291	335
1430	14.64	12.96	11.52	10.21	9.23	23.7	31.3		29.04	29.07	29.10	29.14	208	279	343	397
1500	12.72	11.49	10.52	9.65	8.91	23.6	29.6	27.3	28.94	29.09	29.24	29.35	230	321	400	459
1530	12.00	11.12	10.31	9.48	8.67	23.4	27.8	26.5	28.58	28.82	29.03	29.22	242	330	410	474
1600	12.00	11.13	10.40	9.72	9.15	23.2	26.9	26.3	28.27	28.58	28.85	29.07	254	340	418	480
1630	11.94	11.06	10.32	9.58	9.06	22.9	26.3	26.2	28.01	28.38	28.71	28.98	275	366	451	530
1700						22.7	25.6	26.1	27.68	28.13	28.51	28.83	219	291	363	434
1730	12.36	11.69	11.15	10.60	10.05	22.5	24.4	25.1	26.84	27.36	27.76	28.10	156	222	290	357
1800	12.46	11.86	11.39	10.94	10.57	22.3	22.4	24.4	25.44	25.96	26.40	26.81	241	322	402	478
1830	11.92	11.46	11.13	10.84	10.59	22.1	21.1	21.7	23.57	24.10	24.56	24.98	187	248	308	370
1900	11.04	10.95	10.81	10.63	10.44	21.8	18.8	19.0	21.99	22.48	22.92	23.34	138	197	246	288
1930	10.48	10.38	10.28	10.20	10.10	21.6	17.6	17.4	19.91	20.38	20.84	21.28	141	190	238	283
2000	9.88	9.80	9.70	9.65	9.66	21.2	16.4	16.0	17.71	18.13	18.53	18.90	146	197	245	288
2030	9.68	9.63	9.60	9.57	9.56	20.9	15.2	15.1	16.75	17.19	17.59	17.98	128	174	220	265
2100						20.7	14.8	14.7	16.12	16.46	16.78	17.08	181	240	298	354
2130						20.6	14.2	14.3	15.34	15.67	15.97	16.27	152	209	262	310
2200						20.3	14.1	13.7	14.68	15.00	15.34	15.65	145	192	238	284
2230						20.0	13.1	13.3	14.16	14.47	14.79	15.11	140	189	236	275
2300						19.9	12.9	13.0	13.88	14.19	14.51	14.82	136	187	234	277
2330						19.7	12.4	12.7	13.57	13.88	14.18	14.49	134	181	223	261
2400						19.6	12.0	12.3	13.04	13.36	13.68	13.98	121	166	208	247
7/31																
0030						19.4	11.0	12.0	12.63	13.00	13.34	13.66	92	121	150	180
0100						19.3	10.6	11.7	11.98	12.39	12.75	13.06	74	101	111	138
0130						19.1	10.9	11.4	12.08	12.39	12.67	12.91	87	106	128	156
0200	8.53	8.65	8.68	8.70	8.72	18.9	10.8	11.6	12.05	12.36	12.60	12.78	95	123	152	183
0230						18.8	10.1	11.2	11.63	12.00	12.30	12.53	75	99	124	150
0300						18.7	8.6	10.4	10.40	11.12	11.66	12.06	42	50	70	95
0330	7.45	7.75	7.96	8.19	8.17	18.5			9.92	10.66	11.24	11.67	29	33	38	44
0400	7.32	7.63	7.85	8.02	8.12	18.3			9.45	10.59	11.25	11.73	37	48	67	80

Table III-1. (continued)
July 30-31, 1962

Time at Period's End	Air Humidity, gms/m^3					Soil, Leaf, and Air Temperature, °C							Wind Velocity, cm/sec			
	$\rho q_{11.4}$ 1/	ρq_{25}	ρq_{50}	ρq_{100}	ρq_{200}	T_{-1} 1/	T_s 1/	$T_{6\&12}$ 1/	T_{25}	T_{50}	T_{100}	T_{200}	U_{25}	U_{50}	U_{100}	U_{200}
7/31																
0430	7.20	7.37	7.52	7.68	7.82	18.1			8.58	9.47	10.47	11.07	41	53	80	108
0500	7.40	7.57	7.68	7.79	7.89	17.9			8.94	9.77	10.55	11.11	54	56	63	74
0530						17.8	6.2	8.3	8.96	9.55	10.65	11.22	37	47	69	97
0600	7.56	7.58	7.62	7.64	7.67	17.7	9.9	11.3	10.84	11.11	11.36	11.65	68	78	98	127
0630	8.20	8.14	8.10	8.04	7.97	17.7	13.1	13.6	12.67	12.65	12.62	12.59	89	113	136	159
0700	9.02	8.56	8.27	8.07	7.97	17.8	16.3	15.1	14.45	14.24	14.02	13.80	87	106	123	140
0730	9.20	8.82	8.54	8.32	8.20	17.9	17.9	17.2	15.49	15.13	14.82	14.58	95	111	127	142
0800						18.1	20.4	21.1	16.92	16.51	16.12	15.74	96	115	132	148
0830	10.44	10.06	9.78	9.58	9.42	18.4	23.4	21.8	18.11	17.69	17.32	17.02	66	73	79	86
0900						18.8	25.2	23.8	19.61	19.09	18.66	18.33				
0930						19.3	27.4	25.7	21.08	20.58	20.19	19.91	66	74	82	90
1000	12.74	11.36	10.57	9.99	9.53	19.9	29.1	25.8	22.47	21.91	21.54	21.27	78	85	93	105
1030	14.21	12.05	11.15	10.49	9.93	20.6	30.6	27.1	23.79	23.25	22.82	22.51	92	104	118	135
1100	14.94	12.71	11.57	10.77	10.18	21.3	31.3	27.3	25.41	24.83	24.38	24.06	115	138	162	186
1130	15.38	12.95	11.83	10.98	10.22	22.0	32.3	28.6	26.44	25.93	25.51	25.16	125	150	175	200
1200	16.09	12.85	11.73	10.89	10.21	22.5	33.6	29.1	27.09	26.60	26.19	25.87	135	171	204	232
1230	15.38	13.08	11.83	10.90	10.12	23.0	32.5	28.8	27.81	27.49	27.18	26.89	178	231	279	318
1300		13.12	11.88	10.91	10.12	23.3	32.7	29.0	28.29	28.04	27.78	27.55	162	214	261	296
1330		12.58	11.32	10.28	9.40	23.4	32.2	28.3	28.73	28.58	28.43	28.28	197	265	328	380
1400		12.36	11.05	10.11	9.40	23.6	31.9	28.1	29.25	29.20	29.16	29.11	228	312	387	447
1430	15.32	11.95	10.64	9.71	8.99	23.4	31.6	28.1	29.76	29.76	29.78	29.80	221	294	363	423
1500	13.22	10.48	9.74	9.14	8.62	23.3	30.3	27.1	29.52	29.65	29.75	29.84	224	322	411	478
1530	13.57	11.10	10.49	9.88	9.26	23.2	29.7	26.6	29.57	29.74	29.87	29.96	228	318	398	460
1600	13.16	11.65	10.90	10.32	9.86	23.1	28.6	26.7	29.13	29.34	29.50	29.60	236	321	399	460
1630	13.38	11.78	10.99	10.42	9.97	22.9	27.2	25.6	28.31	28.57	28.76	28.89	234	315	387	442
1700	12.53	11.44	10.77	10.25	9.87	22.7	26.1	24.8	27.23	27.54	27.77	27.94	258	344	424	498
1730	12.00	10.66	10.12	9.73	9.47	22.5	24.8	23.4	26.35	26.72	27.04	27.31	226	311	388	452
1800	11.76	10.74	10.19	9.78	9.47	22.3	23.4	22.4	25.68	26.09	26.49	26.84	172	235	294	347
1830	10.70	9.72	9.38	9.12	8.90	22.1	21.6	20.7	24.10	24.64	25.16	25.63	148	203	256	304

1/ As measured - all other data from eye-smoothed profiles.

Table III-2. Humidity of air; Temperature of soil, leaf surface, and air; and Wind Velocity at various levels (cm from soil surface), August 31, 1962

Time at Period's End	Air Humidity, gms/m^3						Soil, Leaf and Air Temperature, °C								Wind Velocity, cm/sec			
	ρq_6 1/	ρq_{25}	ρq_{50}	ρq_{100}	ρq_{200}	ρq_{400}	T_{-1} 1/	T_s 1/	T_6 1/	T_{12} 1/	T_{25}	T_{50}	T_{100}	T_{200}	U_{25}	U_{50}	U_{100}	U_{200}
0600																		
0630	8.85	8.71	8.71	8.71	8.71	8.71	16.94	9.54	10.61		9.24	11.00	11.40	11.56	55.5	93.5	128.0	156.0
0700	10.51	9.83	9.76	9.70	9.67	9.66	17.00	12.27	12.09		12.00	12.10	12.18	12.20	113.2	146.7	176.8	201.0
0730	11.74	10.76	10.34	10.11	10.01	9.95	17.06	15.91	13.91		13.80	13.75	13.70	13.68	109.5	142.6	170.8	193.0
0800	12.57	10.92	10.66	10.52	10.43	10.36	17.22	18.55	14.28	14.52	14.35	14.00	13.90	13.96	109.0	137.0	162.6	182.7
0830	14.01	11.50	10.97	10.70	10.58	10.49	17.56	21.01	18.65	18.69	18.75	17.97	17.68	17.45	85.3	104.7	122.2	137.8
0900	14.49	11.73	11.18	10.78	10.54	10.38	17.89	24.25	19.78	20.18	19.58	18.82	18.52	18.25	76.5	89.5	101.0	109.5
0930	18.15	12.25	11.63	11.25	11.00	10.88	18.44	27.14	22.33	22.09	21.55	20.72	20.33	20.50	73.5	85.0	95.5	105.0
1000	18.44	12.38	11.62	11.18	10.92	10.77	19.00	29.46	25.01	23.75	23.18	22.30	21.63	21.15	62.6	72.2	80.3	86.7
1030	18.79	12.84	11.98	11.47	11.17	11.02	19.67	31.06	27.32	25.38	24.86	23.89	23.21	22.76	71.2	81.2	89.5	96.3
1100	18.72	13.12	12.07	11.56	11.27	11.09	20.33	33.19	28.52	26.70	26.28	25.53	24.91	24.96	63.4	73.0	82.7	91.2
1130	18.91	13.64	12.52	11.81	11.32	10.95	21.00	34.35	29.93	27.88	27.85	27.10	26.50	26.72	64.2	72.6	79.5	83.8
1200	18.88	14.17	12.97	12.17	11.62	11.23	21.56	35.94	30.56	29.37	29.09	28.35	27.76	27.86	73.3	82.3	90.7	94.4
1230	20.17	13.63	12.13	11.44	10.99	10.71	22.06	36.35	31.40	30.29	30.20	29.56	29.07	29.30	65.5	74.2	80.7	84.9
1300	23.72	14.06	11.85	11.18	10.73	10.43	22.44	36.50	32.89	31.22	31.20	30.61	30.04	30.28	73.7	85.2	94.6	102.0
1330	27.25	13.00	11.26	10.18	9.42	8.88	22.78	36.72	33.31	31.70	31.90	31.47	31.05	31.22	78.3	89.7	99.4	106.8
1400	27.07	12.64	10.93	9.83	9.05	8.53	23.00	36.33	32.85	32.01	32.60	32.23	31.85	32.30			78.0	
1430	26.35	12.17	11.02	10.21	9.65	9.26	23.17	35.29	33.64	32.59	33.40	33.00	32.63	33.05	67.3	77.6	85.9	91.9
1500	26.63	12.34	10.63	9.63	8.94	8.50	23.11	34.39	31.83	32.60	33.40	33.23	33.08	33.16	58.7	67.1	73.6	77.7
1530	25.42	12.94	11.12	9.96	9.16	8.56	23.06	33.11	30.69	32.38	33.40	33.38	33.36	33.85	70.5	82.6	92.4	99.4
1600	24.46	12.75	11.06	9.92	9.12	8.55	23.06	31.40	29.47	31.62	32.70	32.85	32.98	33.33	78.3	96.6	112.2	124.2
1630	22.79	13.54	11.83	10.57	9.56	8.68	23.00	29.44	28.41	30.95	32.05	32.38	32.60	33.11	78.0	97.5	116.8	135.7
1700	22.21	14.49	11.95	10.42	9.34	8.48	22.89	28.25	27.63	29.87	31.05	31.50	31.95	33.59	62.3	82.8	103.6	124.4
1730	19.14	14.20	12.30	10.83	9.58	8.43	22.67	25.44	25.55	28.06				33.53	58.0	85.0	113.8	148.8
1800	16.57	12.66	11.72	10.74	9.78	8.83	22.44	22.04	22.68	24.83				32.21	47.8	82.2	116.2	151.2
1830	13.70	11.05	10.69	10.35	9.93	9.47	22.11	18.16	19.31	21.21	23.65	25.59	27.37	29.05		121.0	156.5	
1900	12.70	11.15	11.05	10.95	10.85	10.75	21.78	16.10	17.48	19.30	21.30	23.04	24.69	26.30	64.2	102.0	140.9	184.0

1/ As measured - all other data from eye-smoothed profiles

Table III-3. Humidity of air; Temperature of soil, leaf surface, and air; and Wind Velocity at various levels (cm from soil surface), October 30, 1962

Time at Period's End	Air Humidity, gms/m^3					Soil, Leaf and Air Temperature, °C								Wind Velocity, cm/sec			
	ρq_6 1/	ρq_{25}	ρq_{50}	ρq_{100}	ρq_{200}	T_{-1} 1/	T_s 1/	T_6 1/	T_{12} 1/	T_{25}	T_{50}	T_{100}	T_{200}	U_{25}	U_{50}	U_{100}	U_{200}
0930						13.78	21.78	18.44	18.78	17.78	17.07	16.62	16.28	48	58	65	71
1000	13.18	11.97	11.58	11.23		14.17	21.72	18.94	19.89	18.86	18.04	17.52	17.21	56	69	80	90
1030	14.65	12.02	11.56	11.09		14.44	22.56	19.22	20.28	19.12	18.64	18.28	18.06	114	144	171	196
1100	14.38	12.93	12.42	11.82		14.72	23.33	20.17	21.39	19.95	19.47	19.00	18.53	138	176	209	242
1130	16.60 2/	12.62 2/	12.03 2/	11.57 2/		15.11	24.67	20.78	22.61	20.88	20.22	19.70	19.32	119	148	176	201
1200	15.08	12.78	12.22	11.76		15.50	25.39	22.00	23.56	21.64	20.93	20.42	20.05	88	112	134	155
1230	15.45	12.66	12.17	11.78		15.78	25.44	22.44	24.11	21.86	21.14	20.68	20.49	88	107	124	138
1300	16.19	12.60	12.13	11.67		16.11	25.94	22.56	24.22	22.70	22.00	21.57	21.29	98	123	147	166
1330	15.85	12.57	12.17	11.76		16.33	25.39	22.72	24.44	22.78	22.17	21.77	21.51	116	148	177	204
1400	16.21	12.66	12.14	11.71		16.50	25.39	22.56	24.00	22.89	22.32	21.90	21.62	91	112	131	149
1430	16.38	12.77	12.24	11.72		16.61	24.56	22.11	23.28	22.67	22.40	22.33	22.32	90	109	126	142
1500	16.30	13.03	12.38	11.97		16.67	23.56	21.39	22.50	22.44	22.41	22.38	22.35	62	77	90	102
1530	15.57	12.85	12.29	11.93	11.73	16.69	22.67	20.00	21.06	21.49	21.77	21.99	22.17	75	95	113	129
1600	15.89	12.87	12.39	12.06	11.88	16.69	20.00	19.06	19.72	20.71	21.08	21.37	21.52	52	63	74	84
1630	16.35	12.93	12.46	12.13	11.92	16.64	16.89	17.11	17.61	19.76	20.06	20.30	20.44	56	69	81	92
1700	15.85	12.35	12.26	12.22	12.29	16.60	12.83	14.00	14.56	16.60	18.03	18.66	19.02	36	52	66	78
1730	14.42 3/	11.61 3/	11.87 3/	12.03 3/	12.20 3/	16.41	10.06	11.89	11.56	14.79	16.77	17.56	18.00	28	46	63	78
1800						16.14	7.22	8.56	9.56	11.75	14.41	15.56	16.51	28	46	63	78
1830	15.03	10.65	11.42	11.93	12.27	15.72	6.78	8.00	8.06	10.67	13.04	14.77	16.19				
1900	14.81	9.94	10.75	11.43	12.00	15.56	6.44	7.50	7.67	9.74	11.88	14.00	16.11	12	46	80	112
1930	14.60	9.72	10.51	11.14	11.70	15.33	6.61	8.06	8.28	10.35	11.73	13.32	15.08	24	50	76	102
2000	13.42	9.86	10.65	11.27	11.80	15.14	6.44	7.78	8.33	10.30	12.18	13.68	14.98	29	52	76	99
2030	12.71	9.46	10.21	10.81	11.28	15.00	6.33	7.78	7.39	9.40	11.75	13.23	14.30	17	29	42	54
2100	11.79	8.76	9.62	10.34	10.92	14.83	5.39	6.28	6.28	8.10	10.73	12.38	13.60	18 1/		31 1/	
2130	11.47	8.57	9.48	10.20	10.79	14.67	5.06	5.83	5.78	7.52	10.33	12.00	13.25	13 1/		17 1/	
2200	11.13	8.78	9.55	10.22	10.74	14.47	5.11	6.39	6.44	8.00	10.38	11.68	12.61	17 1/		32 1/	

1/ As measured - all other data from eye-smoothed profiles
2/ 1100 - 1115 only
3/ 1700 - 1715 only

Table III-4 Humidity of air; Temperature of soil, leaf surface, and air; and Wind Velocity at various levels (cm from soil surface), March 12, 1963

Time at Period's End	Air Humidity, gms/m^3						Soil, Leaf and Air Temperature, °C								Wind Velocity, cm/sec			
	ρq_5 1/	ρq_{25}	ρq_{50}	ρq_{100}	ρq_{200}	ρq_{400}	T_{-1} 1/	T_s 1/	T_{11} 1/	T_{25}	T_{50}	T_{100}	T_{200}	T_{400}	U_{25}	U_{50}	U_{100}	U_{200}
1200	5.91	4.78	4.55	4.31			9.8	24.9	17.92	17.29	16.77	16.23	15.70	15.16	486	609	724	825
1230	5.87	4.79	4.57	4.33	4.14	4.09	10.1	25.2	18.03	17.37	16.88	16.37	15.86	15.34	526	665	788	894
1300	5.73	4.53	4.33	4.13	4.10	4.05	10.4	25.5	18.39	17.70	17.23	16.77	16.30	15.80	506	633	744	843
1330	5.83	4.78	4.44	4.24	4.14	4.11	10.6	25.2	18.20	17.52	17.06	16.60	16.16	15.70	517	648	766	868
1400	5.53	4.52	4.29	4.07	4.02	3.99	10.7	24.3	18.16	17.60	17.19	16.79	16.38	15.97	515	638	758	870
1430	5.47	4.48	4.23	4.05	3.98	3.91	10.8	23.2	18.40	17.78	17.48	17.16	16.84	16.49	502	626	740	843
1500	5.34	4.43	4.15	3.96	3.92	3.89	10.9	21.7	18.18	17.51	17.19	16.95	16.73	16.54	473	592	702	801
1530	5.33	4.54	4.30	4.07	4.00	3.98	11.0	19.7	17.69	17.24	17.11	16.99	16.86	16.73	480	598	707	802
1600	5.27	4.48	4.23	4.06	4.00	3.98	11.0	17.8	17.16	16.85	16.81	16.76	16.71	16.68	426	528	630	732
1630	5.21	4.43	4.22	4.06	4.04	3.99	10.9	15.7	16.38	16.59	16.62	16.64	16.65	16.64	408	508	605	700
1700	5.13	4.40	4.21	4.08	4.04	4.02	10.9	13.3	15.76	15.90	16.02	16.14	16.21	16.30	359	443	527	607
1730	5.21	4.62	4.38	4.25	4.21	4.14	10.8	10.8	14.40	14.76	15.02	15.26	15.48	15.68	303	373	443	513
1800	5.26	4.62	4.46	4.35	4.32	4.30	10.7	8.1	12.36	12.83	13.25	13.66	14.04	14.43	216	270	323	376
1830	5.12	4.69	4.59	4.53	4.48	4.44	10.5	3.6	8.75	9.54	10.21	10.86	11.49	12.12	142	182	226	275
1900							10.3	-0.2	5.03	6.55	7.60	8.66	9.72	10.78	78	1.2	153	197
1930							10.0	-0.8	5.38	6.54	7.65	8.75	9.83	10.87	123	165	211	260
2000	5.02	4.68	4.59	4.54	4.52	4.50	9.8	1.8	5.74	6.62	7.31	7.98	8.66	9.33	116	160	208	260
2030	5.01	4.55	4.47	4.42	4.39	4.37	9.6	-0.1	4.78	5.59	6.36	7.17	8.00	8.84	92	126	164	204
2100	4.99	4.47	4.39	4.32	4.29		9.4	-1.1	4.36	5.20	5.92	6.70	7.51	8.38	125	164	208	255

1/ As measured - all other data from eye-smoothed profiles

Table III-5. The Energy Balance. Measured net radiation, R_n; lysimeter evapotranspiration, L(ET): ground heat flux at 1 cm soil depth, G, and calculated convective heat flux using the energy balance equation,

$$R_n + G + LE + H = 0$$

Time at Period's End	R_n	G	LE	H
	langleys per minute			
July 30, 1962:				
1400	.873	-.028	-.754	-.091
1430	.811	-.023	-.779	-.009
1500	.725	-.018	-.735	.028
1530	.633	-.013	-.664	.044
1600	.527	-.010	-.575	.058
1630	.422	-.007	-.508	.093
1700	.308	-.005	-.442	.139
1730	.199	-.003	-.348	.152
1800	.090	-.002	-.252	.164
1830	-.005	.001	-.176	.180
1900	-.066	.004	-.097	.159
1930	-.089	.006	-.036	.119
2000	-.095	.007	-.028	.116
2030	-.095	.008	-.022	.109
2100	-.095	.009	-.022	.108
2130	-.094	.010	-.018	.102
2200	-.093	.010	-.022	.105
2230	-.092	.011	-.018	.099
2300	-.091	.010	-.012	.093
2330	-.091	.011	-.012	.092
2400	-.088	.012	.003	.073
July 31, 1962				
0030	-.083	.012	.009	.062
0100	-.083	.013	.009	.061
0130	-.084	.013	.009	.062
0200	-.086	.013	.012	.061
0230	-.081	.012	.006	.063
0300	-.071	.014	.006	.051
0330	-.061	.015	.006	.040

Time at Period's End	R_n	G	LE	H
	langleys per minute			
July 31 (cont'd)				
0430	-.063	.017	.006	.040
0500	-.062	.016	.006	.040
0530	-.050	.016	.006	.028
0600	-.022	.013	-.003	.012
0630	.048	.010	-.025	-.033
0700	.138	.007	-.064	-.081
0730	.247	.004	-.124	-.127
0800	.350	-.001	-.218	-.131
0830	.462	-.005	-.205	-.252
0900	.564	-.008	-.327	-.229
0930	.661	-.014	-.418	-.229
1000	.733	-.020	-.476	-.237
1030	.806	-.025	-.508	-.273
1100	.874	-.030	-.608	-.236
1130	.911	-.034	-.657	-.220
1200	.944	-.035	-.696	-.213
1230	.957	-.035	-.723	-.199
1300	.951	-.034	-.772	-.145
1330	.926	-.030	-.775	-.121
1400	.872	-.025	-.772	-.075
1430	.808	-.022	-.760	-.026
1500	.731	-.017	-.751	.037
1530	.640	-.016	-.672	.048
1600	.533	-.013	-.575	.055
1630	.426	-.009	-.502	.085
1700	.320	-.006	-.415	.101
1730	.206	-.004	-.333	.131
1800	.095	-.003	-.255	.163
1830	.003	-.001	-.140	.138

Time at Period's End	R_n	G	LE	H
	langleys per minute			
Aug. 31, 1962				
0630	-.036	.020	.003	.013
0700	.036	.010	-.030	-.016
0730	.143	.009	-.100	-.052
0800	.255	.004	-.154	-.105
0830	.373	.001	-.185	-.189
0900	.476	-.005	-.249	-.222
0930	.573	-.009	-.333	-.231
1000	.664	-.014	-.396	-.254
1030	.742	-.019	-.451	-.272
1100	.809	-.023	-.499	-.287
1130	.840	-.026	-.557	-.257
1200	.872	-.028	-.591	-.253
1230	.874	-.029	-.630	-.207
1300	.856	-.030	-.636	-.190
1330	.823	-.028	-.619	-.176
1400	.765	-.028	-.611	-.126
1430	.694	-.025	-.572	-.097
1500	.605	-.021	-.485	-.099
1530	.503	-.020	-.445	-.038
1600	.402	-.018	-.376	-.008
1630	.290	-.014	-.300	.024
1700	.178	-.012	-.212	.046
1730	.072	-.009	-.140	.077
1800	-.018	-.005	-.067	.090
1830	-.079	-.001	-.042	.122
1900	-.091	.001	-.036	.126

Table III-5, Contd. The Energy Balance

Time at Period's End	R_n	G	LE	H
	langleys per minute			
Oct. 30, 1962				
0930	.326	-.001	-.191	-.134
1000	.411	-.005	-.218	-.188
1030	.481	-.008	-.281	-.192
1100	.526	-.010	-.327	-.189
1130	.549	-.012	-.351	-.186
1200	.554	-.014	-.364	-.176
1230	.538	-.015	-.361	-.162
1300	.507	-.016	-.357	-.134
1330	.466	-.017	-.333	-.116
1400	.394	-.016	-.306	-.072
1430	.315	-.016	-.242	-.057
1500	.234	-.015	-.188	-.041
1530	.140	-.013	-.137	.010
1600	.047	-.011	-.097	.061
1630	-.025	-.009	-.045	.079
1700	-.066	-.006	-.006	.078
1730	-.067	-.002	.009	.060
1800	-.061	.000	.009	.052
1830	-.054	.005	.012	.037
1900	-.050	.006	.009	.035
1930	-.050	.008	.009	.033
2000	-.051	.009	.006	.036
2030	-.055	.008	.006	.041
2100	-.051	.010	.009	.032
2130	-.046	.010	.009	.027
2200	-.049	.011	.009	.029

Time at Period's End	R_n	G	LE	H
	Langleys per minute			
March 12, 1963				
0700	-.090	.016	-.011	.085
0730	-.024	.015	-.060	.069
0800	.070	.013	-.115	.032
0830	.187	.010	-.169	-.028
0900	.306	.007	-.199	-.114
0930	.419	.004	-.218	-.205
1000	.521	.001	-.245	-.277
1030	.610	-.002	-.275	-.333
1100	.681	-.005	-.303	-.373
1130	.732	-.007	-.324	-.401
1200	.760	-.008	-.330	-.422
1230	.770	-.010	-.330	-.430
1300	.754	-.011	-.317	-.426
1330	.720	-.012	-.314	-.394
1400	.667	-.012	-.309	-.346
1430	.600	-.011	-.297	-.292
1500	.513	-.011	-.275	-.227
1530	.408	-.010	-.249	-.149
1600	.292	-.007	-.230	-.055
1630	.175	-.006	-.202	.033
1700	.064	-.003	-.151	.090
1730	-.044	-.001	-.109	.154
1800	-.113	.001	-.061	.173
1830	-.125	.004	-.027	.148
1900	-.105	.006	-.011	.110
1930	-.116	.010	-.008	.114
2000	-.111	.011	-.008	.108
2030	-.111	.011	-.003	.103
2100	-.112	.011	-.003	.104

TABLE III-6. Eddy diffusivity for water vapor, K_D, for heat, K_H, and the ratio K_H/K_D. The two parameters K_D^* and K_H^* are equal to the eddy diffusivities divided by $z^2 \partial u/\partial z$. The Richardson Number, Ri_{75}, is also given. All calculations are based on the average gradient between the 50 and 100-cm levels.

End of Period	K_D	K_H	K_H/K_D	K_D^*	K_H^*	Ri_{75}
July 30, 1962						
1400	1133	5428*	4.80**	.190	.910*	-.004*
1430	840	--	--	--	--	+.001*
1500	1194	635**	0.53**	.134	.071**	+.004
1530	1129	619**	0.55**	.125	.069**	+.005
1600	1195	638**	0.55**	.136	.073**	+.007
1630	970	833	0.86	.101	.087	+.007
1700	--	1074	--	--	.133	+.012
1730	894	1114	1.28	.117	.146	+.019
1800	790	1087	1.37	.088	.121	+.011
1830	857	1140	1.33	.127	.169	+.021
1900	766	1047	1.37	.139	.190	+.030
1930	644*	743	1.15*	.119*	.138	+.033
2000	780*	829	1.06*	.144*	.154	+.029
2030	1017*	771	0.76*	.200*	.149	+.032
July 31						
0200	825*	708	0.86*	.250*	.217	+.049
0330	35	191	5.60	.062	.340	+4.003
0400	24	181	7.70	.011	.085	+.316
0430	53	111	2.08	.017	.037	+.236
0500	77	143	1.85	.098	.182	+2.692
0530	--	71	--	--	.029	+.391
0600	--	133	--	--	.059	+.108
0630	575*	3056*	5.27*	.222*	1.181*	-.010
0700	450	1023**	2.28**	.235	.535**	-.130
July 31, 1962 (continued)						
0730	795	1152**	1.45**	.442	.640**	-.206
0800	--	952	--	--	.498	-.228
0830	1452	1931	1.33	2.151	2.861	-1.731
0900	--	1516	--	--	--	- --
0930	--	1675	--	--	1.860	-1.003
1000	1155	1850	1.59	1.288	2.060	-.961
1030	1088	1839	1.69	.691	1.170	-.363
1100	1074	1504	1.41	.398	.557	-.128
1130	1092	1529	1.41	.388	.544	-.110
1200	1171	1521	1.30	.315	.410	-.062
1230	1099	1886	1.72	.204	.349	-.022
1300	1124	1635	1.45	.213	.309	-.019
1330	1052	2349**	2.22**	.148	.331**	-.006
1400	1160	5682*	5.00*	.137	.673**	-.001*
1430	1154	--	--	.149	--	+.001*
1500	1768	1107*	0.62*	.177	.111*	+.002*
1530	1557	1081**	0.69**	.173	.120**	+.003
1600	1401	1022**	0.73**	.160	.116**	+.004
1630	1245	1315	1.05	.154	.162	+.006
1700	1127	1300	1.15	.125	.144	+.008
1730	1208	1198	0.99	.139	.138	+.009
1800	877	1193	1.37	.132	.180	+.019
1830	758	772	1.02	.127	.129	+.031

*Not used in graphs because of large percentage errors possible when Δq was 0.1 grams per meter^3 or less, or when ΔT was 0.1°C or less.

**Not used because of possible large percentage errors in the energy balance calculation of convective heat flux, H, near neutral conditions.

TABLE III-6. (continued)

End of Period	K_D	K_H	K_H/K_D	K_D^*	K_H^*	Ri_{75}
August 31, 1962						
0630	--	90**	--	--	.023**	+.058
0700	717*	--	--	.212*	--	+.015*
0730	615	2887*	4.77*	.194	.910*	-.011*
0800	--	2917**	--	--	1.013**	-.026
0830	967	1852	1.92	.491	.940	-.160
0900	879	2102	2.38	.680	1.626	-.380
0930	1239	1689	1.37	1.049	1.430	-.592
1000	1273	1090	0.85	1.397	1.196	-1.697
1030	1250	1156	0.92	1.340	1.238	-1.629
1100	1383	1344	0.97	1.268	1.232	-1.082
1130	1109	1254	1.14	1.429	1.616	-2.058
1200	1044	1255	1.20	1.105	1.328	-1.359
1230	1291	1241	0.96	1.766	1.698	-1.878
1300	1341	983	0.73	1.267	.929	-1.304
1330	820	1243	1.52	.752	1.139	-.718
1400	785	783	1.00	--	--	--
1430	998	784	0.79	1.069	.839	-.859
1500	685	1964**	2.86**	.937	2.687**	-.568
1530	542	5275**	10.00**	.492	4.787**	-.033*
1600	465	--	--	.265	--	+.085
1630	336	328**	0.98**	.155	.151**	+.095
1700	196	304**	1.56**	.084	.130**	+.167
1730	134	--	--	.041	--	--
1800	96	--	--	.025	--	--
1830	175	200	1.15	.044	.050	+.231
1900	515*	222	4.30*	.118*	.051	+.180
October 30, 1962						
0930	--	838	--	--	1.065	--
1000	881	1023	1.16	.712	.827	-.972
1030	845	1509	1.78	.278	.497	-.094
1100	771	1141	1.47	.208	.307	-.085
1130	1078	1020	0.94	.342	.324	-.130
1200	1117	983	0.88	.451	.397	-.190
1230	1306	1007	0.77	.683	.527	-.300
1300	1095	899	0.82	.406	.333	-.140
1330	1149	832	0.72	.352	.255	-.120
October 30, 1962 (continued)						
1400	1005	496**	0.49**	.470	.232**	-.194
1430	657	2375*	3.57*	.344	1.242*	-.040*
1500	646	3778*	5.89*	.442	2.584*	-.029*
1530	536	133**	0.25**	.265	.066**	+.110
1600	417	607**	1.45**	.337	.491**	+.360
1630	194	943	4.76	.144	.699	+.240
1700	212*	351	1.67*	.135*	.223	+.539
1730	78	216	2.78	.041	.113	+.460
1800	--	128	--	--	.067	--
1830	32	60	1.89	--	--	--
1900	18	46	2.56	.005	.012	+.313
1930	20	58	2.94	.007	.020	+.403
2000	14	67	4.76	.005	.025	+.445
2030	14	77	5.56	.010	.053	+.150
2100	17	54	3.22	--	--	--
2130	17	45	2.63	--	--	--
2200	19	62	3.22	--	--	--
March 12, 1963						
1200	1909	2227	1.17	.147	.172	-.0069
1230	1909	2406	1.26	.114	.173	-.0057
1300	2202	2628	1.19	.176	.210	-.0063
1330	2182	2439	1.15	.164	.184	-.0056
1400	1947	2472	1.27	.144	.183	-.0047
1430	2288	2624	1.15	.178	.205	-.0042
1500	2010	2750	1.37	.162	.222	-.0033
1530	1501	3643	1.76	.122	.297	-.0017
1600	1877	3167*	1.69*	.163	.276*	-.0008
1630	1756	4300*	2.45*	.160	.394*	+.0004
1700	1615	2120	1.31	.170	.224	+.0029
1730	1164	1807	1.55	.147	.229	+.0083
1800	768	1182	1.85	.128	.198	+.0245
1830	637*	638	1.00*	.128*	.129	+.0582
1900	--	291	--	--	.063	+.1101
1930	--	295	--	--	.057	+.0901
2000	244*	453	1.86*	.045*	.094	+.0632
2030	82*	361	4.40*	.021*	.075	+.0767
2100	59*	375	6.37*	.012*	.076	+.0709

REFERENCES FOR CHAPTER III

Aston, Mervyn J. (1963). Resistance to water loss from plants. Chapter XI. Final Report. USAEPG Contract No. DA-36-039-SC-80334, University of California, Davis.

Brooks, F. A., W. O. Pruitt, D. A. Pope and H. B. Schultz (1962.) Smoothed diurnal curves of observed energy and moisture fluxes on cloudless days and comparison with Dyer's Evapotron measurements 28 October 1961. Chapter I, Second Annual Report, USAEPG Contract No. DA-36-039-SC-80334, University of California, Davis. P. 5-25.

Bowen, I. S. (1926). The ratio of heat losses by conduction and evaporation from any water surface. Physical Rev. 27:779-89.

Crawford, T. V. (1963). Eddy diffusivity for water vapor as a function of stability. Chapter V, Final Report, USAEPG Contract No. DA-36-039-SC-80334, University of California, Davis.

Ellison, T. H. (1957). Turbulent transport of heat and momentum from an infinite rough plane. Jour. of Fluid Mech. 2:456-466.

Monteith, J. L. (1963). Calculating evaporation from diffusive resistances. Chapter X. Final Report. USAEPG Contract No. DA-36-039-SC-80334. University of California, Davis.

Pasquill, F. (1949). Eddy diffusion of water vapour and heat near the ground. Proc. Roy. Soc. London. A198:116-40.

Pruitt, W. O. (1962). Diurnal and seasonal variations in the relationship between evapotranspiration and radiation. Second Annaul Report, USAEPG Contract No. DA-36-039-SC-80334. University of California, Davis. P. 27-45.

Pruitt, W. O. and Angus, D. E. (1960). Large weighing lysimeter for measuring evapotranspiration. Trans. ASAE 3(2):13-18.

Pruitt, W. O. and D. E. Angus. (1961). Comparisons of evapotranspiration with solar and net radiation and evaporation from water surfaces. First Annual Report, USAEPG Contract No. DA-36-039-SC-80334. University of California, Davis. P. 74-107.

Slatyer, R. O. and I. C. McIlroy (1961). Practical Microclimatology Commonwealth Scientific and Industrial Research Organization. Australia (UNESCO).

Tanner, C. B. and W. L. Pelton. (1960). Potential evapotranspiration estimates by the approximate energy balance method of Penman. J. Geophysical Res. 65:10, 3391-3413.

CHAPTER IV

APPLICATION OF SEVERAL ENERGY BALANCE AND AERODYNAMIC EVAPORATION EQUATIONS UNDER A WIDE RANGE OF STABILITY

W. O. Pruitt

INTRODUCTION

With the availability of profile and energy balance data for the period covered by this report it was deemed worthwhile to check the application of several aerodynamic and energy balance evaporation equations for half-hour periods. Although only 4 to 5 days of records were available, they represented widely varying air stability and surface moisture conditions as indicated by Chapter III of this report. The data used were presented in the Tables of Chapter III and the reader is referred to it for details.

RESULTS AND DISCUSSION

Aerodynamic Approaches

Thornthwaite and Holzman (1939) assuming a logarithmic form for the wind speed profile introduced an expression for evaporation involving the measurement of wind speed and humidity at two heights above a surface. This equation can be expressed as

$$E = k^2 \rho \frac{(q_1 - q_2)(u_2 - u_1)}{[\ln (z_2/z_1)]^2} \qquad (1)$$

where E is evaporation in gms/cm^2 sec; k is the von Karman constant, assumed equal to 0.4 in this Chapter; ρ is the air density in gms/cm^3; q_1 and q_2 are absolute humidities in gms water per gm of air at two heights, z_1 and z_2 cm above the surface; and u_1 and u_2 are the wind velocities in cm/sec at those same heights.

Since the wind profile tends to be logarithmic only under adiabatic conditions it has long been recognized that the Thornthwaite-Holzman equation has limited application.

The results shown in Figure IV-1 indicate the inadequacy of this approach except under the windier conditions realized on the afternoon of July 30 and 31, and on March 12. The predicted values seldom approach the measured evapotranspiration ET, on the calm, clear days of August 31 and October 30th. Pasquill (1949a) and Priestley (1959) indicate that

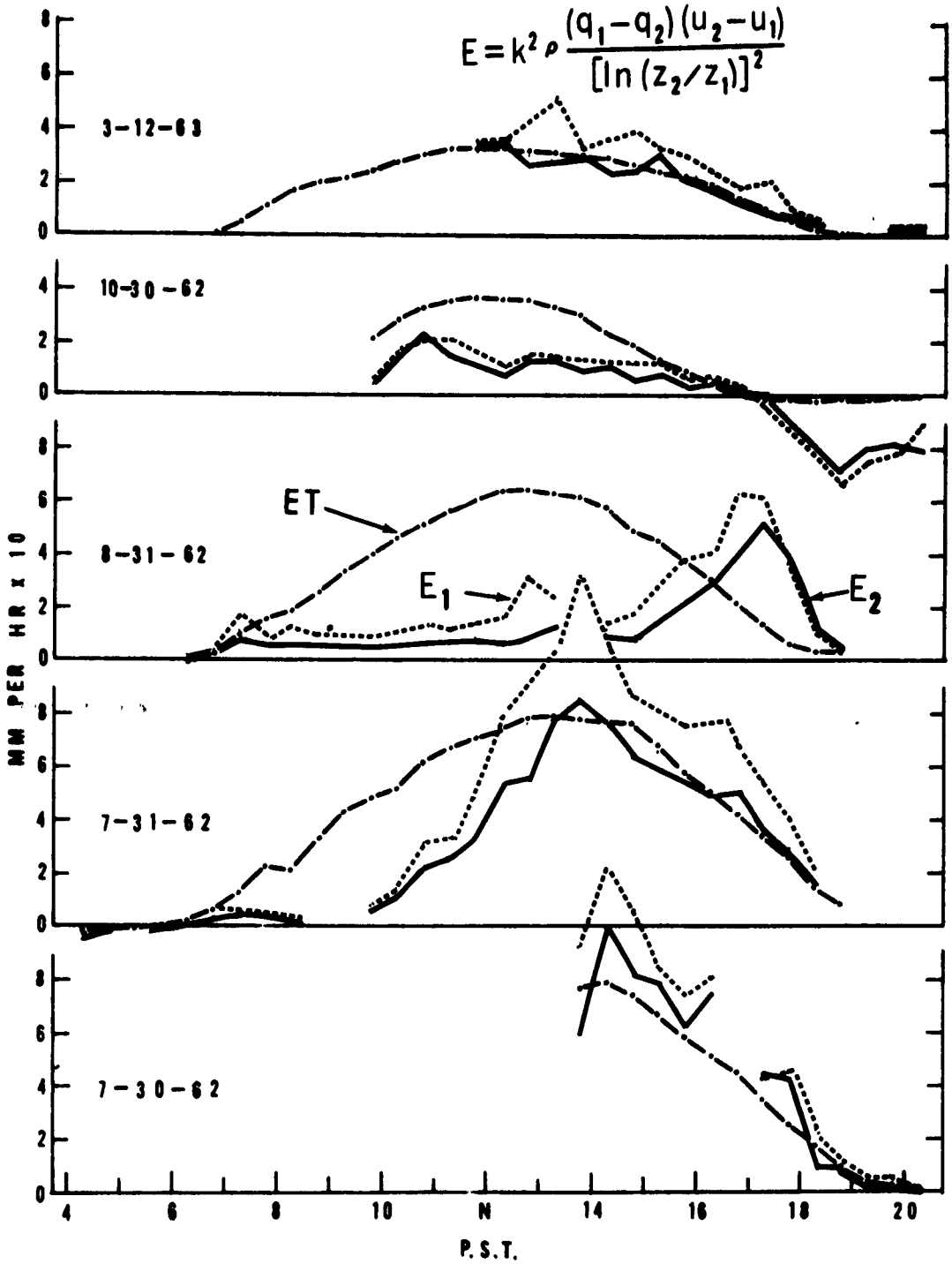

Figure IV-1. Measured evapotranspiration, ET for perennial ryegrass compared with calculated vapor flux E, using the Thornthwaite-Holzman (1939) equation (Eq. 1). E_1 based on measuring heights, z_1 and z_2 of 25 and 50 cm above the soil surface, with E_2 based on heights of 50 and 100 cm.

Equation (1) will underestimate evaporation in unstable conditions and over estimate evaporation in stable conditions. Results in Figure IV-1 indicate a very considerable underestimation during all three mornings of July 31, August 31 and October 30 under clear calm conditions when buoyancy must have been a very great factor. On the two latter days when the calm conditions prevailed all day, ET is seriously underestimated up until 1500 and seriously overestimated thereafter. It is also apparent that the evaporation estimate is strongly dependent upon the heights at which the measurements were taken (E_1 based on heights of 25 and 50 cm above the soil surface and E_2 based upon the 50 and 100 cm levels).

The observations on the night of October 31 may be of particular interest to some readers. The formula predicts a deposition of dew at the rate of 0.2 to 0.3 mm per hour when the actual rate was only around 0.01 mm per hour. The formula clearly fails on this night of high stability with wind speeds of only 50-80 cm/sec at a 1-meter height and a high rate of radiation cooling of the surface.

Various attempts have been made to revise the above method to make it usable under non-adiabatic conditions. Although Pasquill's (1949a) study provided evidence for the absolute validity of the Thornthwaite-Holzman equation under adiabatic conditions, it also demonstrated that very serious errors can result when this method is used under non-adiabatic conditions. This was shown to be especially true if the original measuring heights of Thornthwaite and Holzman were used (up to 7 1/2 meters). Pasquill suggested that the effects of thermal stratification could only be reasonably neglected if the gradient measurements of wind and humidity were confined to the first 50 cm above the surface. The Davis results, as indicated earlier, show that even with this restriction in measurement heights, the method can be highly inaccurate on calm, clear days.

In addition to suggesting the above, Pasquill simplified the form of the Thornthwaite-Holzman equation to one which for the purpose of this Chapter can be expressed as

$$E = \left\{ \frac{k^2 \left[1 - (u_1/u_2)\right]}{\left[\ln (z_2/z_1)\right]^2} \right\} \rho u_2 (q_1 - q_2) \qquad (2)$$

where all units are consistent with definitions given previously. The

expression in brackets serves as a constant, the ratio of u_1/u_2 being determined by careful observations made only under neutral conditions over the surface in question.

Within the range of stabilities encountered, Pasquill indicates errors exceeding 10 percent were seldom found during daytime periods. It is obvious from Figure IV-2 that much greater error can be expected when this method is used under stability conditions beyond the range covered in Pasquill's study in England.

As should be expected the results, except under calmer conditions, are almost identical to those in Figure IV-1 since the only real change of Equation 1 is the use by Pasquill of the ratio, u_1/u_2 determined under neutral conditions. The significant differences evident on the calmer days can be simply explained. u_1/u_2 normally is less under stable conditions and greater under unstable conditions than at times when the temperature profile is neutral. Thus the use of a u_1/u_2 for neutral conditions in the expression $(1 - u_1/u_2)u_2$ for all hours of the day gives lower estimates of E for stable conditions and higher estimates of E for unstable conditions than if the actual value of $u_1 - u_2$ had been used as in the Thornthwaite-Holzman equation. Although Pasquill anticipated some additional error due to this simplification of the formula, in effect it helps to compensate to some extent for the absence of a stability parameter. This is evidenced by a comparison of Figures IV-1 and IV-2 where the Pasquill equation results in a desirable trend with higher values of E on the morning of August 31 and lower values in late afternoon. A particularly significant improvement due to the above was the much closer estimate of dew on the night of October 30 by Pasquill's equation. E is still 2 to 3 times as great as the actual flux of vapor to the surface, however.

Deacon and Swinbank (1956) suggest that these difficulties may be relieved to a large extent by the determination, under neutral conditions, of a low-level drag coefficient from measurements of wind at two heights more easily identified than in the previous case. They suggest that in so far as the eddy diffusivity for water vapor, K_D and the eddy viscosity, K_M are equal and the low-level drag coefficient is independent of stability, the following equation should be reliable even when profiles are far from logarithmic:

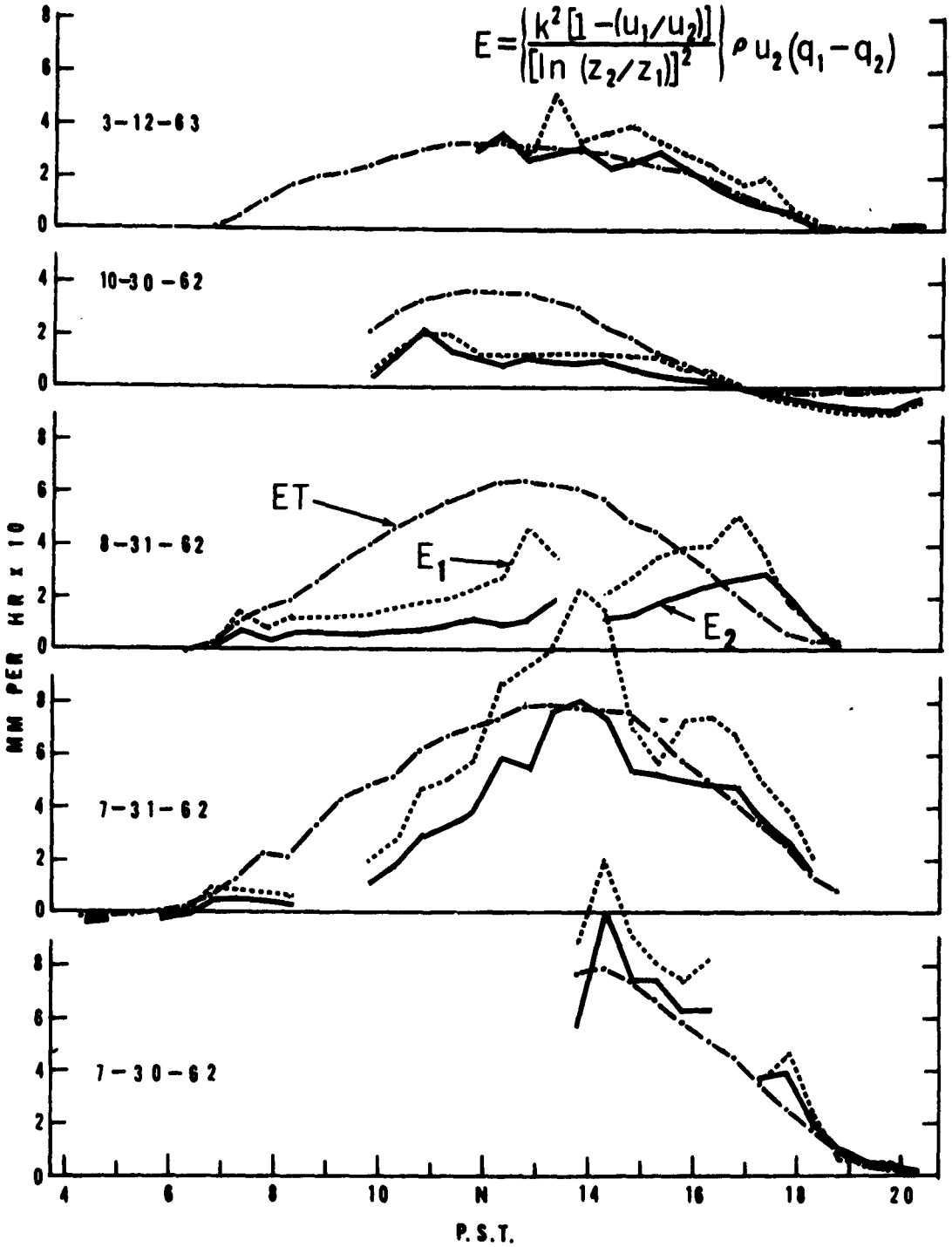

Figure IV-2. Measured ET compared with calculated vapor flux E, using Pasquill's (1949) equation (Eq. 2).

$$E = c_n \rho u_n^2 \frac{(q_1 - q_2)}{(u_2 - u_1)} \tag{3}$$

where c_n is the drag coefficient at the level n, near the surface (determined under neutral conditions) and u_n is the wind speed at level n, during any period being considered. Conveniently the levels z_n and z_1 can be the same level and z_2 chosen sufficiently high to allow desired accuracy in determination of $q_1 - q_2$ and $u_2 - u_1$.

In Figure IV-3 the improvement over previous results is very striking considering the simple changes in Equation 3 from the previous expressions. It should be recognized that only part of the variation in E values from one half-hour period to the next should be attributed to weaknesses of these formulas. A considerable part of the scatter, no doubt, is a reflection of the inability to fully achieve the extreme accuracy in gradient measurements required. The trends evident throughout each day, however, should be quite reliable.

For Equation 3 there is still some striking dependence of E on the height of measurement, especially on August 31. It is interesting that E_1 gave a very good estimate of ET up until noon on this day in spite of very great instabilities while E_2 seriously underestimated ET. In the afternoon hours E_2 was the best estimate with a serious overprediction by E_1.

Slatyer and McIlroy (1961), writing of the proposed method of Deacon and Swinbank state that "although requiring further confirmation, in particular over surfaces other than rough pasture, this appears at present to be the most practical application of the aerodynamic approach".

The Davis results lend considerable support to this statement although the method appears to be uncertain under clear, calm days with extreme changes in stability conditions.

The vast improvement over Equation (1) in prediction of dew on the night of October 30 is also striking, with E_2 ranging from -0.015 to -0.027 mm per hour compared to -0.01 mm per hour for the actual flux of vapor to the surface. Of course this still indicates a significant error in measurement of dew.

Another approach for improvement of the aerodynamic method under non-neutral conditions has been the inclusion of some stability parameter in

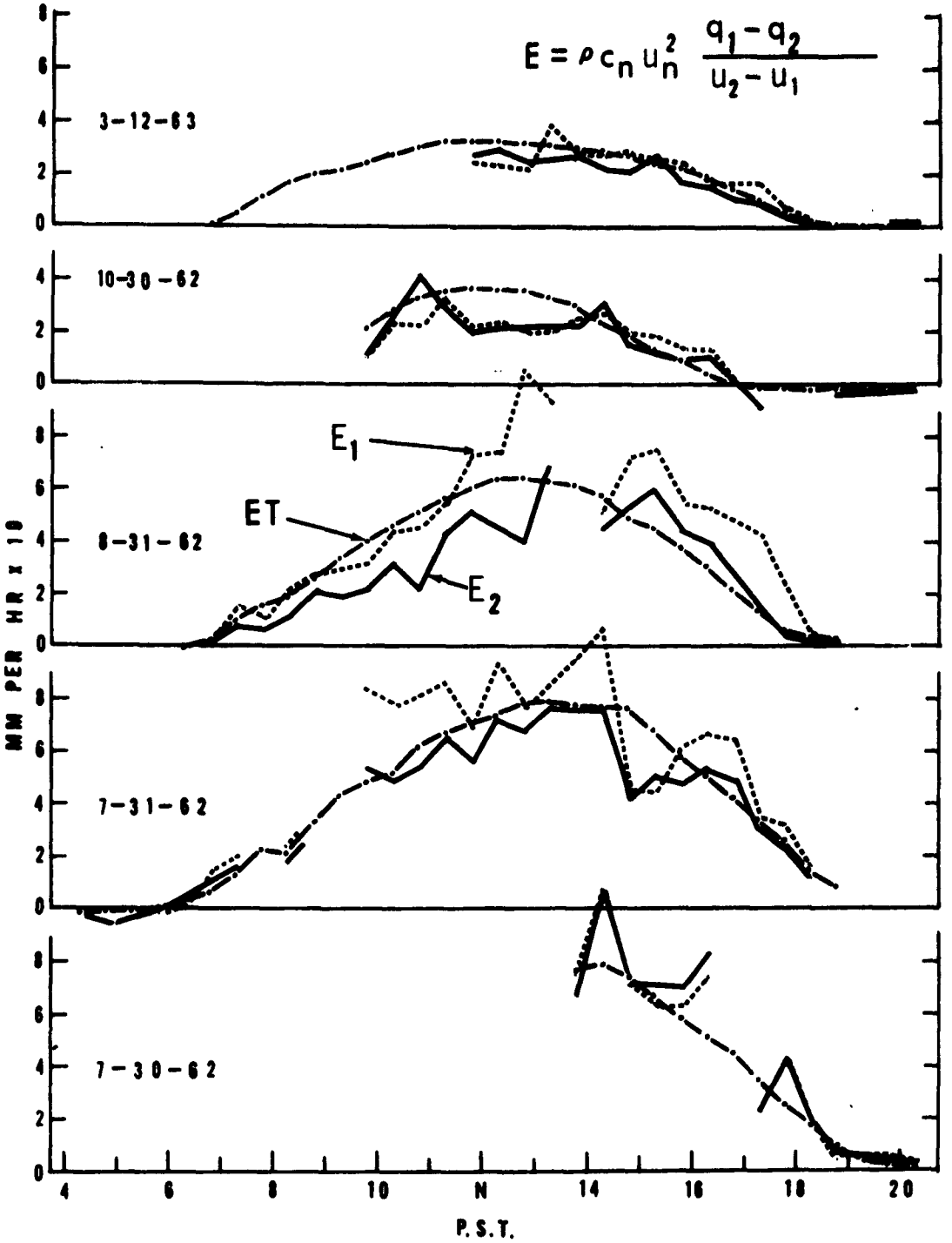

Figure IV-3. Measured ET compared with calculated vapor flux E_1 and E_2 using the Deacon-Swinbank equation (Eq. 3) where c_n is a low-level drag coefficient determined under neutral conditions.

defining the relationship between the flux of momentum and the velocity gradients. For example, Rossby and Montgomery (1935) proposed the expression for use under stable conditions of $K^*_M = k(1 + \sigma Ri)^{-1/2}$ where K^*_M is a dimensionless form of the eddy viscosity from which the neutral dependence of wind speed and height has been removed; σ is a constant and Ri is the gradient form of the Richardson number. This mathematical expression must fail in the more unstable conditions as σ Ri approaches -1.0. When pressed into use for estimating evaporation, this would be a serious disadvantage because evaporation would normally be high under just such conditions.

Holzman (1943) proposed the expression of $K^*_M = k(1 - \sigma Ri)^{1/2}$ which when pressed into use for prediction of moisture flux should be superior to the previous relationship since it would tend to fail only under the stable condition when σ Ri approached +1.0, a condition likely to occur only under fairly low evaporation conditions in late afternoon if the results in Chapter III can be considered as typical for cropped areas. This assumes a σ of approximately 8 to 12.

Neither of the above expressions can be adequate under all conditions. The fact that, when pressed into use by a number of workers, the value of σ has been found to have a wide range, indicates the mathematical form of the equation inadequately estimates the true effect of stability on the flux-gradient relationships.

In Figure III-10 of the previous Chapter, the relationship between a dimensionless form of the eddy diffusivity for water vapor K^*_D, and the Richardson number Ri, was presented based on results at Davis. An approximate average relationship under unstable and near-neutral conditions was easily determined while beyond Ri = +0.05 the average relationship indicated was highly uncertain.

It is proposed here that rather than using a mathematical expression to describe the relationship of K^*_D to Ri, the use of a graphed relationship or average curve to predict probable K^*_D values from calculated values of Ri, might provide an adequate estimate of evaporation. With an estimate of K^*_D, a computed value of eddy diffusivity $\left(K_D\right)_c$ could be derived from $\left(K_D\right)_c = K^*_D\, z^2\, \partial u/\partial z$ and evaporation then computed from

$$E = -\rho \left(K_D\right)_c \partial q/\partial z \qquad (4)$$

In so far as the Davis data are representative and the Richardson number can be relied upon to predict the effect of stability under various conditions, this approach should lead to an adequate estimate of evaporation within a wide range of stability. The uncertainty seems quite considerable, however, in the more stable cases represented by values of Ri > + 0.05. It also has one disadvantage over previous expressions in that an additional measurement is required since temperature gradients are needed to compute the Richardson number.

In Figure IV-4 the results indicate quite good estimation of the actual flux for most of the periods. A fairly definite exception is on the afternoon of August 31 when there were two rather high estimates just after noon. Also, during the half hour period of 1500-1530, with the temperature profile averaging almost neutral, E is less than half of ET. This may be partially due to the difficulty of getting a reliable Ri value at such times.

Other than for August 31 the results show good agreement. Even on August 31 when data for half-hour periods is scattered the total predicted E for the day is close to the daily ET total, exceeding it by only 8%.

One of the oldest of the aerodynamic methods of predicting evaporation can be attributed to Dalton. This method can be expressed as

$$E = f(u)\,(e_s - e_z) \tag{5}$$

where e_s is the saturated vapor pressure at surface temperature; e_z is the vapor pressure at some height z above the surface and f(u) is a function of the wind speed commonly given in the form of $f(u) = (a + bu_z)$ where u_z is the average wind velocity at height z and a and b are empirically determined constants.

This method has been checked many times over water surfaces. Slatyer and McIlroy (1961) indicate the Dalton approach has been established as thoroughly satisfactory for estimating lake evaporation [U. S. Geological Survey (1954), Harbeck, Kohler and Coberg (1958), and Webb (1960)].

In many studies of the Dalton approach daily totals of evaporation were considered. By contrast Webb (1960) introduced an equation for three-hour periods. The Davis data provide an opportunity to test a Dalton approach for even shorter periods although the use of surface temperature measurements of vegetation to deduce an effective surface vapor pressure is highly

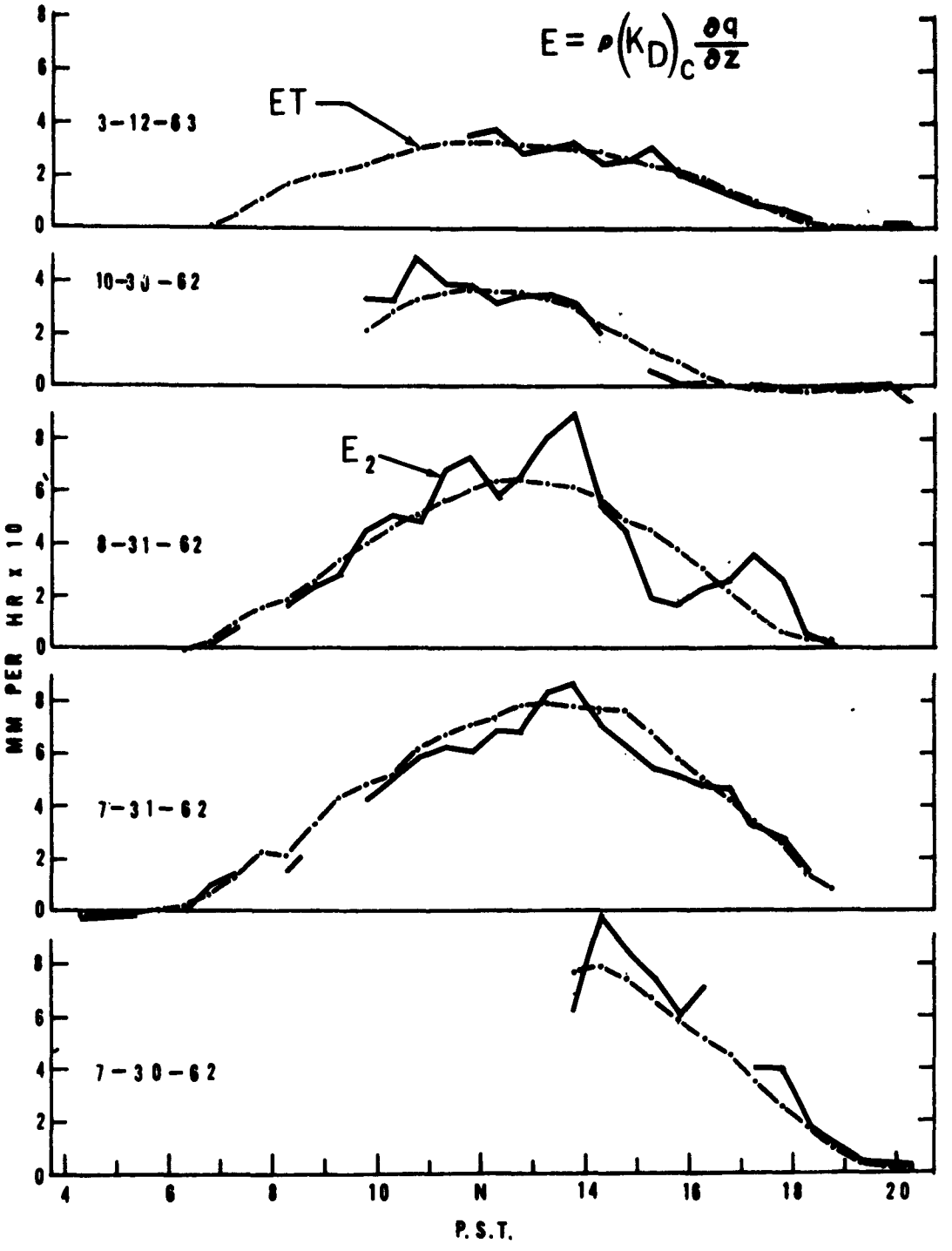

Figure IV-4. Measured ET compared with calculated vapor flux (Eq. 4) where the eddy diffusivity $(K_D)_c$ is calculated from a value of K_D^* obtained from the average relationship of K_D^* and Richardson numbers. Data are based on measurements at 50 and 100 cm.

questionable under some conditions. This is indicated by the results reported in Chapter III where a possible stomatal closure during low light periods and during all hours of a strong, dry-wind day, produced a very great scatter in a plot of ET/ $(e_s - e_{100})$ versus wind speed. Nevertheless, with the exception of the above, there was a fairly small degree of scatter in the data.

If it could be presumed that there was little stomatal resistance change within the range of wind speeds studied (excluding the March 12 data and the low-light hours of the other days) the results indicate a non linear relationship for the wind function f(u). As yet the Davis data have not been used to test any of the previously derived constants in an assumed linear relationship. However, in order to illustrate trends throughout the day of the relationship between $ET/(e_s - e_{100})$ and wind, values of this ratio were picked off of the curve in Figure III-13 for the various levels of wind speed for each 1/2-hour period. Since this curve represents an average f(u), the values determined from the curve were used in Equation 5 to calculate estimates of E. The original units of ET used in Figure III-13 were in mm per hour, thus E in equation 5 would also be in mm per hour.

It could be argued that with the data already presented in Figure III-13 it would be superfluous to use the same data in Equation 5 (the same also applies to the previous method discussed). However, by taking this approach it becomes possible to determine any definite trends of departure of the actual relationships from the average during various times of each day.

The results in Figure IV-5 on all but March 12 indicate that a Dalton method may offer considerable promise over cropped surfaces even when surface vapor pressures are based on an assumed saturated surface at leaf temperature. Except for the afternoon of August 31 excellent agreement between E and ET is evident for 1962 data. On this very calm day there is apparently some influence of high stability from mid-afternoon on; or greater stomatal resistance caused a lower effective surface vapor pressure than that calculated from surface temperature. It is obvious from Figure III-13 that early morning and late afternoon ratios of $ET/(e_s - e_{100})$ tend to run well below other daytime periods with equivalent wind.

The data for March 12, a strong, dry wind day provide an excellent example of the dangers of using assumed surface vapor pressures rather than measured values in a Dalton type approach. On this day there must

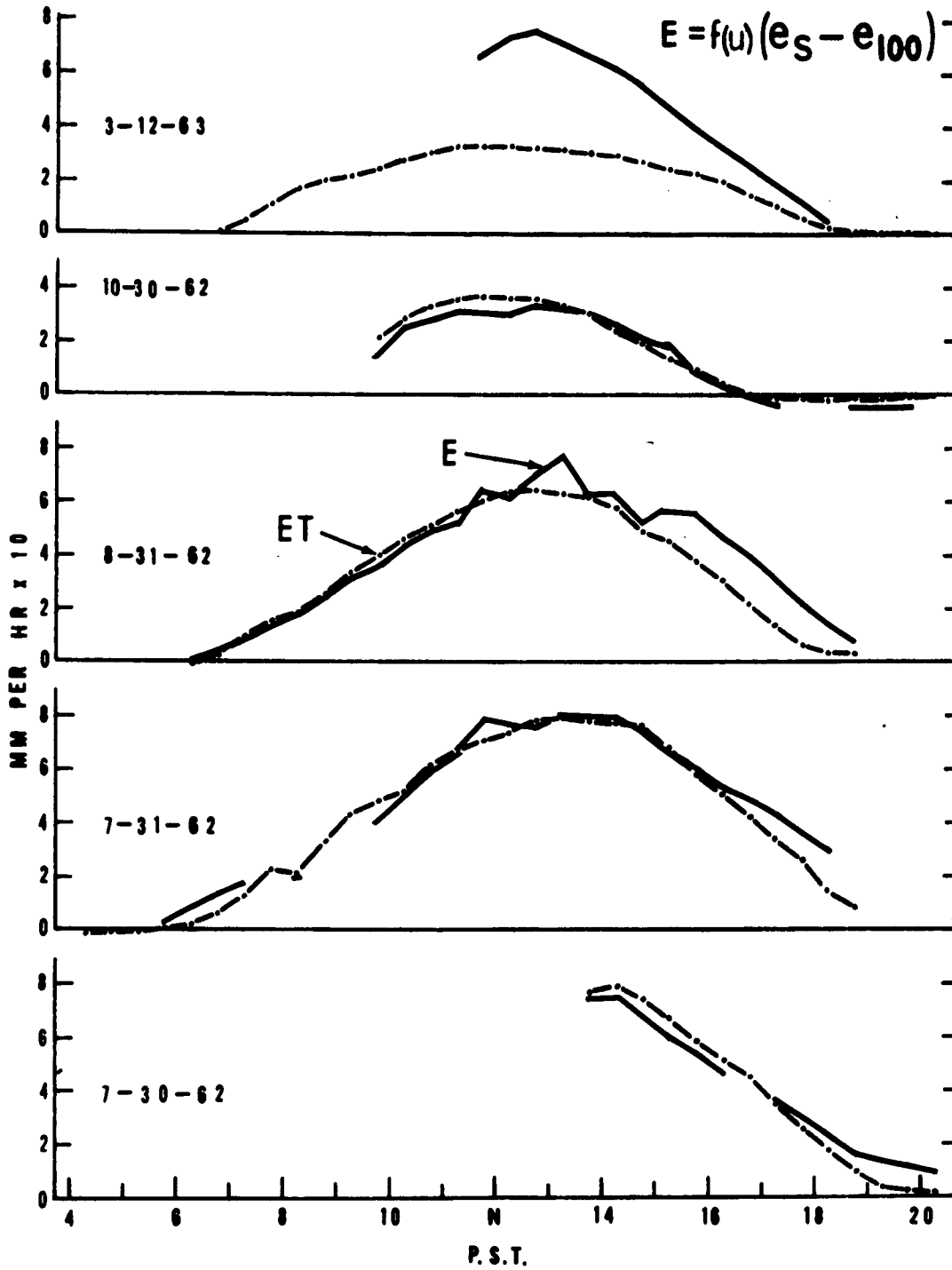

Figure IV-5. Measured ET compared with calculated vapor flux (Eq. 5) where f(u) is obtained from the graph in Figure III-13. Measurement heights for E were from the crop surface to 100 cm above the soil surface.

have been a very definite plant control of transpiration as indicated in Chapter III.

One of the attractive features of a Dalton approach is the accuracy reqirement. The Davis results indicate the vapor gradients between surface and 100 cm were almost an order of magnitude greater than the gradients between 50 and 100 cm much of the time. A reasonably accurate humidity and wind speed measurement at a single height above the surface along with a surface temperature measurement might provide better accuracy than the more sophisticated aerodynamic methods which require very precise gradient measurements of wind and temperature. If the surface was not responding essentially as if it were saturated some way of obtaining an effective surface vapor pressure would be required, however. When using surface temperature measurements there would always be the danger that some unsuspected factor might be producing significant stomatal control of transpiration.

Energy Balance Approach

The energy balance at the surface can be expressed as $R_n + G + LE + H = 0$ where R_n is the net radiation, G is the soil heat flux, LE is the evaporative heat flux and H is the convective heat flux. In this form G, LE, and H are negative if the flux is away from the surface.

If it were convenient to measure R_n, G and H, the energy going into evaporation could be calculated from the above equation. Althouth R_n and G can now be determined with adequate accuracy, obtaining a measurement of H is probably as difficult as measuring LE itself. A common approach then, has been to measure R_n and G and resort to the use of some suitable method of partitioning the remaining energy between evaporation and heating of the air. This can be arrived at by taking the expressions for H and LE of

$$H = \rho c_p K_H \partial T/\partial z \quad \text{and} \quad LE = L \rho K_D \partial q/\partial z$$

where H and LE are in cal/cm^2 sec; c_p is the specific heat of the air at constant pressure in cal/gm^{o}C; L is the latent heat of evaporation; and K_H and K_D are the eddy conductivity for heat and the eddy diffusivity for water vapor respectively in cm^2/sec.

Assuming $K_H = K_D$, an expression for H/LE in terms of measured gradients is

$$\frac{H}{LE} = \frac{\rho c_p K_H \, \partial T/\partial z}{L \, \rho K_D \, \partial q/\partial z} \quad \frac{c_p}{L} \frac{\partial T/\partial z}{\partial q/\partial z}$$

This can be approximated using measurements of temperature and humidity differences at two heights giving

$$\frac{H}{LE} = \frac{c_p}{L} \frac{T_2 - T_1}{q_2 - q_1} = \beta$$

where β is commonly known as the Bowen ratio, although Bowen's (1926) expression for β was in terms of vapor pressure gradients rather than specific humidity and included barometric pressure. His expression for β gives somewhat lower values than the one above.

To obtain E from the previous equation it is rewritten in the form

$$E = \frac{R_n + G}{L} \left(\frac{LE}{H + LE} \right) = \frac{R_n + G}{L} \left(\frac{1}{1 + \beta} \right) \tag{6}$$

This method has had wide use over water surfaces but more recent work has been over cropped surfaces. Suomi and Tanner (1958) found good agreement between calculated E using the above method and measured ET using lysimeters. Results of extensive work by Angus at the Davis, California site in 1959 have been included in a PhD dissertation Angus (1962) . Good agreement between calculated and measured ET was obtained except under strong advection conditions. Also under highly unstable cases, Angus found that evaporation may be over-estimated by 50 to 100 percent.

On the other hand, Pasquill's (1949b) results indicated poor agreement especially in unstable atmospheric conditions. Priestley (1959) indicates that simultaneous measurements of H and E by Swinbank have failed to corroborate this method.

Results in Figure IV-6 indicate the energy balance approach gave the best overall results of any of the methods included in this Chapter. There was serious disagreement between ET and E_1 or E_2 only at times when β approached a value of -1.0 and these were at times of the day when vapor

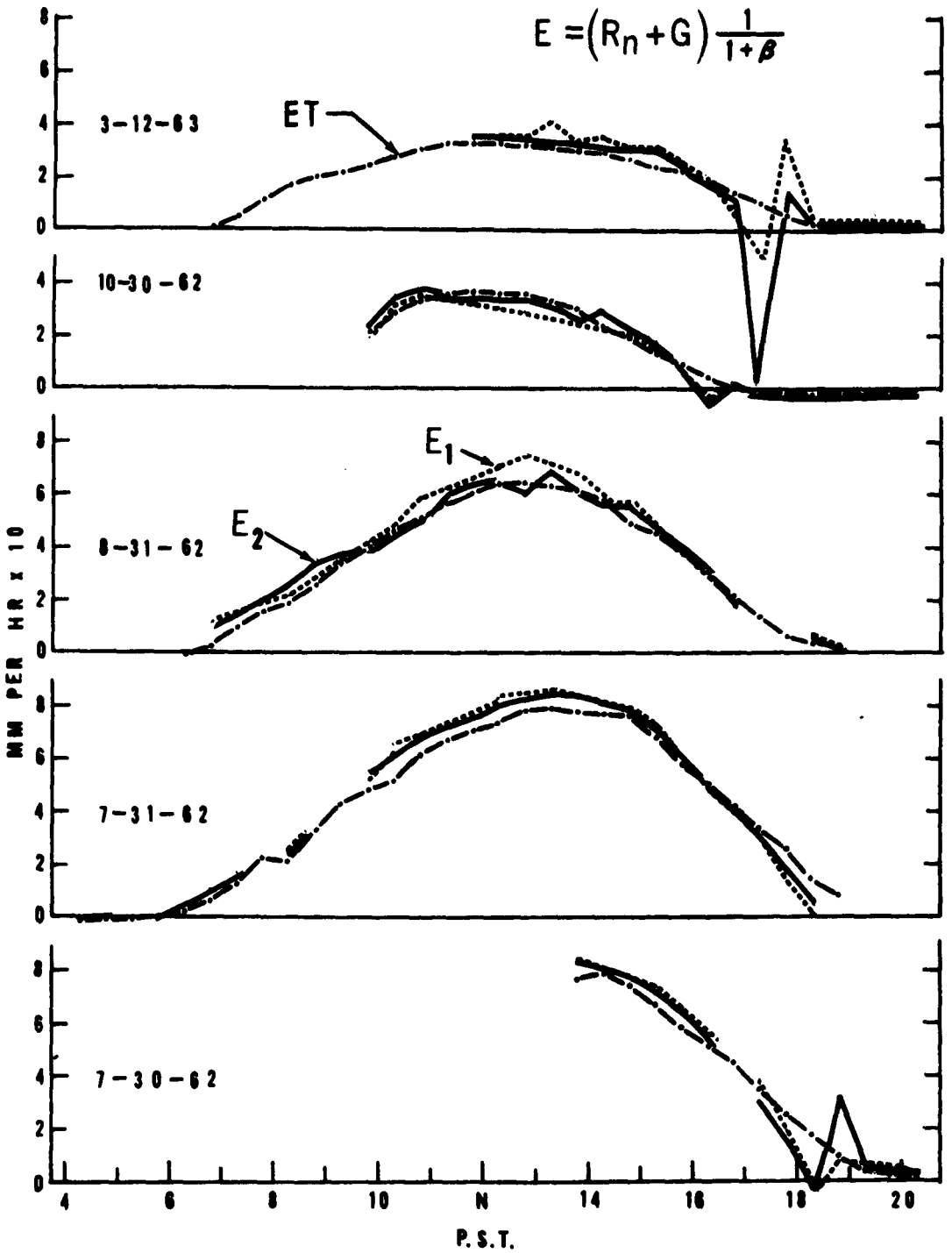

Figure IV-6. Measured ET compared with calculated vapor flux (Eq. 6) using the energy balance (or Bowen Ratio) approach. Measurement heights for E_1 and E_2 were 25 to 50 and 50 to 100 cm respectively.

flux was quite low anyway. In contrast to all other methods checked, this approach gave excellent estimates of ET throughout the wide range of stability encountered on August 31. Little tendency to over-estimate ET under highly buoyant conditions was noted.

Also of importance is the fact that E_1 and E_2 gave very similar results. The energy balance approach also gave one of the better estimates of dew on the night of October 31 although E still exceeded actual vapor flux to the surface by about 100%.

SUMMARY

Five aerodynamic approaches to estimating water vapor flux away from a surface were tested over half-hour periods using the wind, temperature and humidity data reported in Chapter III. Also tested was the energy balance approach (or Bowen Ratio Approach).

The Thornthwaite-Holzman gradient equation proposed in 1939 as well as a modified form of this equation as suggested by Pasquill in 1949 was shown to be highly inadequate except under wind conditions of 3 to 4 meters per second or more. Both equations gave very similar estimates. Only slight improvement was noted in the Pasquill approach.

The equation proposed in 1956 by Deacon and Swinbank making use of a low-level determination of a drag coefficient during neutral conditions proved to give a very much improved estimate of ET although difficulty was noted for two very calm, clear days. Also, results depended somewhat upon the level at which the measurements were made.

A method proposed by the writer using an empirically determined relationship between a common stability parameter (the Richardson number) and a dimensionless form of the eddy diffusivity for water vapor, indicated a method for accounting for the effects of widely varying stability in the aerodynamic approach. Considerable uncertainty was evident at Ri values > +0.05 but the results in general gave good estimates most of the time on all five days investigated.

An average relationship between the ratio of vapor flux to vapor gradient from surface to 100 cm, as a function of wind speed, was described in Chapter III. The function of wind speed thus obtained was used in a Dalton approach with good results except for a strong, dry-wind day when stomatal resistance of the plant must have kept the surface from being

effectively near saturation. In general, the results indicate the Dalton approach might be very successfully used over cropped surfaces, especially if an effective surface vapor pressure measurement could be obtained.

The use of an energy balance approach proved to be highly satisfactory on all five days tested. The only serious discrepencies occurred when the Bown Ratio β, approached -1.

ACKNOWLEDGEMENTS

The author wishes to express his appreciation to Mr. Mervyn Aston for much of the leaf and air temperature data and to other members of the project for their part in the July investigations. The Technicians and Assistants listed at the end of Chapter III also deserve much credit.

REFERENCES FOR CHAPTER IV

Angus, D. E. (1962). The influence of meteorological and soil factors on the rate of evapotranspiration of a crop. PhD Dissertation, University of California, Davis. 128 pages.

Bowen, I. S. (1926). The ratio of heat losses by conduction and by evaporation from any water surface. Physical Rev. 27:779-89.

Deacon, E. L. and W. C. Swinbank (1956). Comparison between momentum and water vapour transfer. Proceedings of the Canberra Symposium. Climatology and Microclimatology. Arid Zone Research, UNESCO, p. 38-41.

Harbeck, G. E., M. A. Kohler and G. E. Coberg (1958). Water loss investigations: Lake Mead studies. U. S. Geological Survey Paper 298.

Holzman (1943). The influence of stability on evaporation. Ann New York Acad. Sci., 44:13-18.

Pasquill, F. (1949a). Some estimates of the amount and diurnal variation of evaporation from a clayland pasture in fair spring weather. Quart. J. Royal Met. Soc. v. 75, 249-56.

Pasquill, F. (1949b). Eddy diffusion of water vapour and heat near the ground. Proc. Roy. Soc. London, A, 198:116-40.

Priestley, C. H. B. (1959). Turbulent Transfer in the Lower Atmosphere. Chicago University Press.

Rossby, C. G. and R. B. Montgomery (1935). The layer of frictional influence in wind and ocean currents. Papers in Physical Oceanography and Meteorology, M.I.T. and Woods Hole Oceanographic Institution, Vol. 3, No. 3.

Slatyer, R. O. and I. C. McIlroy (1961). Practical Microclimatology. Commonwealth Scientific and Industrial Research Organization, Australia. (UNESCO).

Suomi, V. E. and C. B. Tanner (1958). Evapotranspiration estimates from heat-budget measurements over a field crop. Trans. Amer. Geophys. Union 39:298-304.

Thornthwaite, C. W. and B. Holzman, (1939). The determination of evaporation from land and water surfaces. Monthly Weather Rev. 67:4-11.

U. S. Geological Survey (1954). Water loss investigations. Lake Hefner Studies, Geological Survey Paper 269.

Webb, E. K. (1960). An investigation of the evaporation from Lake Eucumbene. C.S.I.R.O. Aust. Div. Meteorological Physics. Tech. Paper No. 10.

CHAPTER V

EDDY DIFFUSIVITY AS A FUNCTION OF STABILITY

Todd V. Crawford

INTRODUCTION

Methods of estimating evaporation from gradient measurements, such as those proposed by Thornthwaite and Holzman (1939), Pasquill (1949a), and Deacon and Swinbank (1956), utilize an eddy diffusivity or drag coefficient obtained from wind profile data under neutral conditions. In this case the log-law representation of the wind profile is satisfactory. Pasquill (1949b) and Deacon and Swinbank (1956) have shown that the eddy diffusivities of water vapor and momentum are equal in near-neutral conditions with moderate wind, but Pasquill (1949b) indicates that this is not true in non-neutral conditions.

Because truly neutral conditions occur for only two relatively short periods (near sunrise and sunset on clear, high-evaporation days), this paper examines the variation of the eddy diffusivity of water vapor as a function of stability.

THEORY

By using the exchange coefficient hypothesis and neglecting molecular transfer terms, the vertical fluxes of momentum, sensible heat, and water vapor can be represented by the following equations:

$$\tau = \rho K_M \frac{\partial u}{\partial z} \tag{1}$$

$$H = - \rho C_p K_H \frac{\partial T}{\partial z} \tag{2}$$

$$E = - \rho K_D \frac{\partial q}{\partial z} \tag{3}$$

The definitions and units of the above terms are standard. The adiabatic lapse rate has been neglected in equation (2) because of its small effect over the range of heights involved. In addition, the following discussion will assume that the fluxes are constant with height.

By using mixing length or similarity concepts, and assuming fully rough flow, the well-known log law for representing the velocity profile can

be derived.

$$\frac{\partial u}{\partial z} = \frac{u_*}{kz} \tag{4}$$

or

$$u = \frac{u_*}{k} \ln \left(\frac{z}{z_o}\right) \tag{5}$$

Observations have shown that this law fits the data quite closely under neutral conditions and with a von Karman's constant (k) equal to approximately .4. From equations (1) and (4) it is possible to show that

$$K_M = k^2 z^2 \frac{\partial u}{\partial z} = kzu_* . \tag{6}$$

Because the log law does not fit the data under non-neutral conditions, various proposals --- Rossby and Montgomery (1935), Holzman (1943), Monin and Obukhov (1954), Businger (1959), etc. --- have been made to modify equations (4) - (6) for stability effects. However, most of these modifications are small corrections applicable only to near-neutral conditions. Even these stability-modified forms of eddy viscosity have not generally appeared in the formulas for estimating evaporation.

The turbulence that causes a turbulent transfer of water vapor down its concentration gradient can be either mechanically or thermally generated. For mechanically generated turbulence, where the influence of buoyancy is negligible, the preceding equations are applicable. However, for the case of sensible heat flux, where the flux is due to the turbulence generated by the buoyant elements themselves, Priestley (1959) has proposed, from dimensional reasoning, the following equation:

$$H = h \rho C_p \left(\frac{g}{T}\right)^{1/2} z^2 \left|\frac{\partial T}{\partial z}\right|^{3/2} \tag{7}$$

to which he refers as heat transfer under a regime of free convection. If one still retains the exchange coefficient concept, then by using equations (2) and (7), it is possible to obtain the following form for the eddy conductivity under the free-convection regime:

$$K_H = hz^2 \left(\frac{g}{T} \left| \frac{\partial T}{\partial z} \right|\right)^{1/2} \tag{8}$$

Ellison (1957) predicts, theoretically, that the turbulent transport of any neutral density substance must take place in exactly the same manner as the turbulent transport of sensible heat because the concentration and density fluctuations in turbulent flow are correlated. Applied here, this means that $K_D = K_H$ under all extremes of stability. However, Pasquill (1949b) has reported data that show K_H approaches $2K_D$ under unstable conditions. To help resolve this conflict, it is convenient to define the following nondimensional evaporative flux, E*, and then investigate its variation with changes of stability.

$$E^* = \frac{E}{\rho \left(\frac{g}{T}\right)^{1/2} \left| \frac{\partial T}{\partial z} \right|^{1/2} z^2 \frac{\partial q}{\partial z}} \tag{9}$$

Under near-neutral conditions ($K_D = K_M = K_H$), the use of equations (3) and (6) in equation (9) gives:

$$E^* = k^2 \left| Ri \right|^{-1/2} \tag{10}$$

where Ri is the gradient form of the Richardson number, Richardson (1920). Ri is defined by:

$$Ri = \frac{g}{T} \frac{\frac{\partial T}{\partial z}}{\left(\frac{\partial u}{\partial z}\right)^2} \tag{11}$$

and represents the ratio of the kinetic-energy increase (or decrease) of an eddy due to buoyancy forces to the kinetic-energy input to the eddy from the working of the Reynolds stresses against the mean-velocity profile. Batchelor (1953) has shown that Ri is the sole governing parameter for frictionless non-adiabatic atmospheric flow. Negative values are associated with unstable conditions and positive values are associated with stable conditions.

In the regime of free convection, equations (3) and (8), with $K_H = K_D$, are used to represent the evaporation. Substitution in equation (9) for E gives:

$$E^* = h \tag{12}$$

With slightly stable conditions, E* should follow the form given in equation (10). In extremely stable conditions the turbulence must decay

completely and then the evaporative flux must only be due to molecular diffusion. The molecular diffusion of water vapor can be represented by an equation exactly like equation (3), with K_D replaced by κ, which is the molecular diffusivity. Then E* becomes:

$$E^* = \frac{\kappa}{\left(\frac{g}{T}\right)^{1/2} \left| \frac{\partial T}{\partial z} \right|^{1/2} z^2} \tag{13}$$

or

$$E^* = \frac{\kappa}{(Ri_{crit.})^{1/2} \frac{\partial u}{\partial z} z^2} \tag{14}$$

$Ri_{crit.}$ is the critical value of the Richardson number which is characteristic of the atmosphere after the turbulence has completely decayed.

COMPARISON WITH DATA

Data obtained at the Davis test site on July 30-31, 1962, August 31, 1962, and October 30, 1962 were used to investigate E* as a function of Ri. The evaporative-flux data were obtained from the 20-foot diameter weighing lysimeter. Absolute humidity (ρ q) data were obtained by sequential sampling at six heights between the surface and 4 meters, then analyzing the absolute humidity of the sample with the infrared hygrometer. Temperature data were available from aspirated thermocouple masts. The July temperature data were obtained from nine heights between 10 cm and 6 m above the ground; those in August and October were obtained from four heights between 25 cm and 2 m. Wind profile data at four heights between 25 cm and 2 m were obtained with Thornthwaite cup anemometers.

All of the data were averaged over half-hour periods -- about the minimum period needed to obtain accurate evaporative flux data with the lysimeter -- and then all of the half-hourly profiles were plotted on semi-log paper. Smooth curves were drawn through the data points. Values were picked from these smoothed profiles (wind, temperature, and absolute humidity) at heights of 25, 50, 100, and 200 cm.; these values are tabulated elsewhere in this report (Pruitt and Aston 1963).

Even though the Davis lysimeter site is very uniform, the presence of a road and a drier alfalfa field influenced the temperature profile above one meter on August 31 when there were light northeast winds. Thus, to

avoid any effect of horizontal inhomogeneity (Crawford and Dyer 1962) and to be consistent for all of the days involved, the profile gradients at 75 cm. above the ground were approximated by finite differences between 100 cm. and 50 cm. However, it should be pointed out that the relationships between E* and Ri determined at 75 cm are applicable to other heights as long as the vertical fluxes remain constant. Even though Ri increases almost linearily with height, it is the magnitude of Ri which characterises the turbulence. Thus, height, per se, will not influence the relationships between E* and Ri. The data were used to compute E* and Ri from their defining equations and hence to prepare Figure V-1. Although E* is plotted as a function of $|Ri|$, the open circles correspond to $Ri < O$ and the dots to $Ri > O$. An inspection of these data indicated a general change of the functional dependence of E* on -Ri. This change seemed to take place at about Ri = -.02 to -.03. Therefore, logarithmic regression lines were fitted to the data for all data in the range of $-.022 < Ri < +.022$ and for $Ri < -.03$. These lines are represented by dashed lines in Figure V-1. As indicated by equations (10) and (12), the functional dependency of E* on Ri used over the same Ri ranges gives the logarithmic regression lines indicated by the solid lines in Figure V-1. The extension of the one curved regression line beyond $Ri = |.03|$ will be discussed later.

These data indicate that the evaporative flux takes place under a regime of forced convection (buoyancy effects negligible) for $Ri < |.02|$. Then there is a region of transition and finally the evaporative flux takes place under a regime of free convection for $Ri < -.03$. This transition from one type of regime to another must be continuous, but the limiting forms for E* specified by equations (10) and (12) do represent the processes taking place quite well over a large range of Ri. The slopes of the dashed regression lines are greater than the solid regression lines whose slope was fixed by equations (10) and (12). However, this result may be due to sparse data for $O > Ri > -.1$. The forced convection regime is predominantly determined by data collected under stable conditions; when the Richardson number approaches the value appropriate for the transition to a regime of free convection, one would expect E* to be larger than for the same $|Ri|$ under stable conditions. Additional data would hence change the slope of the regression line more to that indicated by equation (10). This additional data would also increase the value of k, which is .365 for the dashed regression line and .387 for the solid

line, and bring it closer to the accepted value of .4. The possibility that the differences between the observed and the theoretically predicted slopes are real should not be overlooked. If they are real, it would indicate that the turbulent transfer coefficient goes through a minimum value as the ratio of thermally to mechanically generated turbulence increases. A similar effect has been noted in the heat transfer from a hot-wire anemometer by Hulkill (1941) and Coulbert (1952).

In practice, at Davis, it is difficult to obtain small negative Richardson numbers over the irrigated lysimeter field. It is more desirable, for accuracy reasons, to make Ri small by increasing the denominator than by decreasing the numerator. In fact, data associated with $\Delta T < \left|.1^{o}C\right|$ and $\Delta(\rho q) < .1\ g/m^3$ between 100 and 50 cm were not used in this work. Over the lysimeter field lapse conditions occur only during the morning and early afternoon and at this time the winds are usually light. The late afternoon winds are associated with temperature inversions. This diurnal cycle is especially true of the summer months which are relatively unaffected by frontal systems and which have high evaporation rates.

A similar analysis of a dimensionless sensible heat flux has been reported by Priestley (1959). It is defined by:

$$H^* = \frac{H}{\rho C_p \left(\frac{g}{T}\right)^{1/2} \left|\frac{T}{z}\right|^{3/2} z^2} \tag{15}$$

and has exactly the same limiting forms for the regimes of forced and free convection as E*. Thus, inasmuch as the turbulent transfers of sensible heat and water vapor are considered to be governed by the same mechanism, comparisons can be drawn between the results obtained by Priestley and those reported in this paper. Eddy correlation measurements of H and temperature- and wind-profile data were used to prepare a graph of H* versus -Ri (Priestley 1959, p.44). The shape of this graph is identical to Figure V-1 and shows a regime of predominantly forced convection which changes into one of free convection at a Ri of -.02 to -.03. Realising that H may be underestimated by the eddy correlation technique of measurement, Priestley suggests a value of h = .9 which is higher than that given by his data. The value of h from the E* data is 1.05. It could be that Priestley's allowance for the underestimation of the sensible heat flux was not sufficient,

or perhaps this discrepancy could be accounted for by the fact that the density stratification over an evaporating surface is greater than that indicated by the temperature gradient alone. If the virtual temperature gradient had been used instead of the actual temperature gradient in defining E*, the values of E* would have been reduced by a few percent.

The point of transition from forced to free convection can also be examined by investigating the temperature profile shape. This shape characteristic is defined by the following expression:

$$\frac{\partial T}{z} \propto z^{-\beta} \tag{16}$$

where β = 1 for forced convection
= 4/3 for free convection
= 2 for natural convection

The value of $\beta = 2$ corresponds to the shape characteristic predicted theoretically by Malkus (1954) and observed experimentally in the laboratory by Townsend (1959) for pure convection, i.e. no horizontal wind. Townsend (1962) introduces the term natural convection for this regime and tries to reconcile the laboratory measurements with some in the atmosphere to show that at a large instability there should be a transition from a regime of free convection (which Townsend prefers to call mixed convection) to one of natural convection. He estimates that this transition should occur at $Ri \simeq -1$.

The tabulated temperature-profile data referred to previously was used to obtain a temperature gradient, by the method of finite differences, at 37.5 cm, 75 cm, and 150 cm above the ground. These values were plotted versus height on log-log paper and β determined graphically from a straight line of best fit drawn through the data points. These values of β are plotted as a function of -Ri at 75 cm in Figure V-2. The solid lines are the predicted lines of $\beta = 1$ and $\beta = 4/3$ and the dashed lines are logarithmic regression lines, with assumed zero slope fitted to the data. These give $\beta = 1.05$ in the forced convection regime and $\beta = 1.29$ in the free convection regime. There is no indication of a transition to a value of 2 at $Ri < -1$. The difference between the observed and predicted forms of β in the free and forced convection regime is not significant. The use of β to characterize the transition between the different regimes of turbulence is more subject to errors than the use of H* or E* because it is essentially the second

derivative of temperature with respect to height.

Townsend (1962) also suggested that

$$H^* \propto \left| Ri \right|^{+1} \tag{17}$$

in the regime of natural convection. Priestley's (1959) H* data only extends to a Ri = -.7, but the E* data in this paper show no evidence of a regime of natural convection for -Ri as large as 2 (see Figure V-1 again).

Under the stable conditions (+ Ri) in Figure V-1, it appears that the regime of forced convection extends past Ri $\simeq \left| .02 \right|$ which is the limiting point for unstable conditions. As the Richardson numbers increase positively, finally a value is reached at which turbulence begins to decay. Townsend (1957) and Ellison (1957) have estimated the value of this lower critical Richardson number to be about .1. At this point turbulence begins to decay, but the flow is still turbulent. Finally, an upper-critical Richardson number is reached that characterizes the flow after the decay has been completed. This upper-critical Richardson number cannot be estimated theoretically without taking into account molecular effects. This has not been done. However, Businger (1959) reports some observations of a wind-profile shape, similar to β above, as a function of Ri which suggests a marked change in the character of the flow at Ri $\simeq$ .20. Townsend (1957) reports laboratory observations of a complete decay of turbulent mixing at Ri = .3. Extensive scintillation measurements over long path lengths reported by Portman, Elder, Ryznar, and Noble (1962) also indicate a marked change in the character of the flow at Ri $\simeq$ .35. Thus it is hypothesized, in extending the solid curve in Figure V-1 past Ri .03, that the forced convection regime for stable conditions extends to Ri $\simeq$ .1 and then decreases rapidly to the value of E* appropriate for molecular diffusion of water vapor as Ri $\rightarrow$ +.35. For $Ri_{crit.} \simeq .35$, E* is of the order of 10^{-4}. The limited data under large positive Richardson number suggest that this picture of the behavior of E* may be correct but certainly no definite conclusions can be reached.

CONCLUSIONS

The eddy diffusivity for water vapor varies with the local Richardson number in exactly the same way as does the eddy conductivity for sensible heat through the forced- and free-convection regimes. This result is in direct contradiction to the results reported by Pasquill (1949b). The explanation may be that his evaporative and sensible heat fluxes, which were determined from repeated weighing of small moist soil containers and the energy balance approach respectively, were not as accurate as the flux measurements used in this paper and by Priestley (1959). There was no evidence of a natural convection regime in these data, which extended to negative Richardson numbers as large as 2. Evaporation under stable conditions has been shown to decrease rapidly with increasing positive Richardson numbers. This decrease seems to be consistent with some estimates of the Richardson numbers characteristic of the initiation and completion of turbulence decay.

Once having established the form of E* versus Ri for both stable and unstable conditions (more data than are available at this writing should be used), this approach will have the practical usefulness of estimating E under all extremes of stability from such a graph, and gradient measurements of wind, temperature and moisture. If the data in Figure V-1 can be considered typical for Davis, the importance of being able to allow for extremes of stability in estimating E from gradient data is obvious.

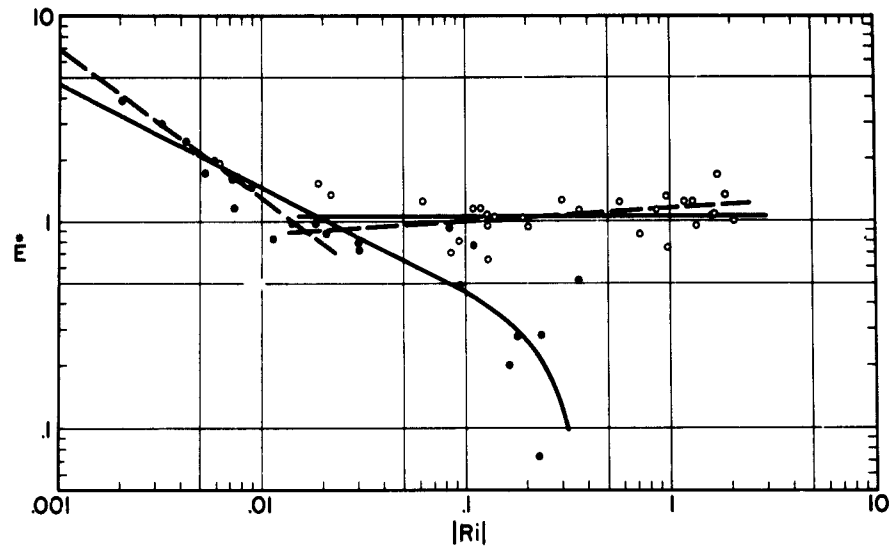

Figure V-1. Nondimensional evaporative flux as a function of Richardson numbers; o refer to -Ri and • refer to +Ri.

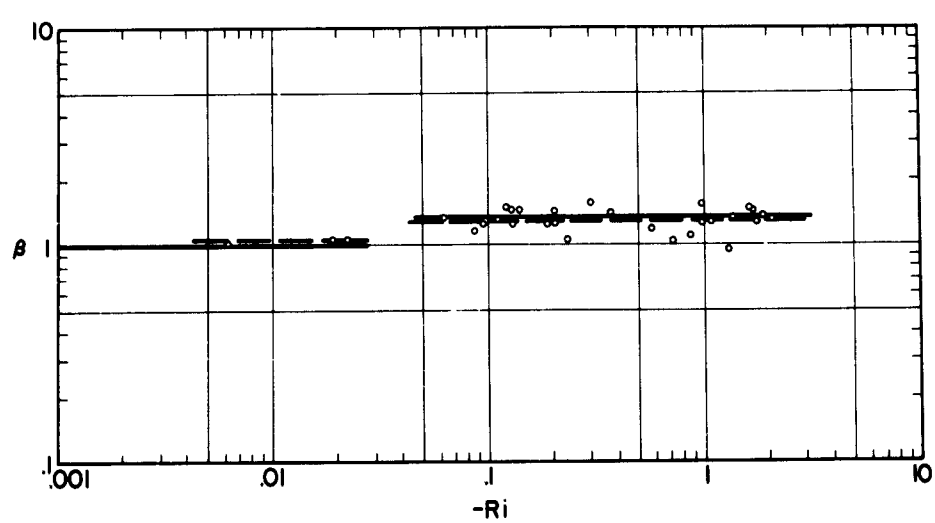

Figure V-2. The temperature-profile shape characteristic as a function of negative Richardson numbers.

LITERATURE CITED

Batchelor, G. K., 1953: "The conditions for dynamical similarity of motions of a frictionless perfect-gas atmosphere", Quart. Jour. Roy. Meteorol. Soc., 79:224-35.

Businger, J. A., 1959: "A generalization of the mixing length concept", Jour. of Meteorol. 16:516-523.

Coulbert, C. O., 1952: "Mach-Zehnder interferometer applications", Amer. Soc. Mech. Engr. Paper No. 52-A-9, 6 pages.

Crawford, T. V. and A. J. Dyer, 1962: "The vertical divergence of evaporative and sensible heat fluxes", Second Annual Report, Investigations of Energy and Mass Transfers Near the Ground Including Influences of the Soil-Plant-Atmosphere System, U.S. Army Contract No. DA-36-039-SC-80334.

Deacon, E. L. and W. C. Swinbank, 1956: "Comparison between momentum and water vapor transfer". Paper No. 2, Australia-UNESCO Symp. Arid Zone Climatology. Published in 1958 with the Proceedings of the meeting.

Ellison, T. H., 1957: "Turbulent transport of heat and momentum from an infinite rough plane", Jour. of Fluid Mech., 2:456-466.

Holzman, B., 1943: "The influence of stability on evaporation", Ann. New York Acad. Sci. 44:13-18.

Hulkill, H. V., 1941: "Characteristics of thermocouple anemometers" in "Temperature, its Measurement and Control in Science and Industry". Reinhold Pub. Co., New York, pp. 666-672.

Malkus, W.V.R., 1954: "The heat transport and spectrum of thermal turbulence", Proceedings of the Roy. Soc. of London, A. 225:196-212.

Monin, A. S., and A. M. Obukhov, 1954: "Basic regularity in turbulent mixing in the surface layer of the atmosphere", U.S.S.R. Acad. Sci., Geophys. Inst., No. 24.

Pasquill, F., 1949a: "Some estimates of the amount and diurnal variation of evaporation from a clayland pasture in fair spring weather", Quart. Jour. Roy. Meteorol. Soc., 75:249-56.

Pasquill, F., 1949b: "Eddy diffusion of water vapour and heat near the ground", Proceedings of the Roy. Soc. of London, A., 198:116-140.

Portman, D. J., Elder, F. C., Ryznar , E., and V. E. Noble, 1962: "Some optical properties of turbulence in stratified flow near the ground", Jour. of Geophy. Res., 67:3223-3235.

Priestley, C.H.B., 1959: "Turbulent Transfer in the Lower Atmosphere", The Univ. of Chicago Press, p. 130.

Pruitt, W. O. and Mervyn J. Aston, 1963: "Atmosphere and surface factors affecting evapotranspiration", Chapter III, Final Report, USAEPG Contract No. DA-36-039-SC-80334, University of California, Davis, California.

Richardson, L. F., 1920: "The supply of energy from and to atmospheric eddies", Proceedings of the Roy. Soc. of London, A. 97:354-73.

Rossby, C. G. and R. B. Montgomery, 1935: "The layer of frictional influence in wind and ocean currents", Papers in Physical Oceanography and Meteorology, M.I.T. and Wood Hold Oceanographic Institution, Vol. 3, No. 3.

Thornthwaite, C. W. and B. Holzman, 1939: "The determination of evaporation from land and water surfaces", Monthly Weather Rev. 67:4-11.

Townsend, A. A., 1957: "Turbulent flow in a stably stratified atmosphere", Jour. of Fluid Mechanics 3:361-372.

Townsend A. A., 1959: "Temperature fluctuations over a heated horizontal surface", Jour. of Fluid Mechanics, 5:209-241.

Townsend, A. A., 1962: "Natural Convection in the earth's boundary layer", Quart. Jour. Roy. Meteorol. Soc., 88:51-56.

CHAPTER VI

BOUNDARY LAYER TRANSPORT UNDER CONDITIONS OF SINUSOIDAL DOWN WIND SURFACE FLUXES

H. F. Poppendiek

SUMMARY

This paper considers transport in the atmospheric boundary layer under the condition that the vertical fluxes at the earth surface vary sinusoidally in the down wind direction. An idealized transport model is proposed and a corresponding solution derived. The results, which are applicable to both heat and mass transfer, are used to examine a specific example. The solution is also compared to some experimental boundary layer temperature measurements.

INTRODUCTION

The influence of non-uniform heat and mass flux distributions at the air-ground interface on the corresponding transport processes in the boundary layer requires investigation. For example, how is a non-uniform earth surface temperature distribution in the down wind direction reflected in the vertical air temperature profiles? If vertical convective heat fluxes are being measured at various elevations above the ground at a given station, what variations in the measurements are to be expected under these conditions? Some attention has been given to this problem in the literature. Philip* has presented a number of step function type boundary layer diffusion problems. Step function boundary concentrations and fluxes were specified. Power law velocity and eddy diffusivity profiles were used. The analysis presented in the present report differs from Philip's in that the case of a periodic or sinusoidal boundary concentration or flux is considered. A simplified two-dimensional transport model is presented, evaluated and utilized to specify the prime micrometeorlogical variables that control this problem.

---

* Philip, J. R. "The Theory of Local Advection": I, Journal of Meteorology, Vol. 16, No. 5, pp 535-547, Oct. 1959.

ANALYSIS

Idealized System

The idealized, two-dimensional heat transport model* is defined by the following postulates:

1. The non-uniform earth surface temperature varies sinusoidally in the direction of the wind velocity (one dimensional variation).
2. The wind velocity profile is uniform.
3. The vertical eddy diffusivity profile is uniform.
4. Lateral eddy transport is small compared to lateral convection.
5. Steady state exists.

In the following paragraphs, this model is used to derive temperature and heat flux solutions for an atmospheric boundary layer with a sinusoidal heat flux or temperature distribution at the earth surface. In a later section, a more refined diffusion model is considered.

Derivation

The boundary value problem to be solved is defined by the following differential and boundary equations:

$$u \frac{\partial T}{\partial x} = \varepsilon \frac{\partial^2 T}{\partial z^2} \tag{1}$$

$$T\,(z=o,x) = T'_o \cos 2\pi x/x_o + T_o \tag{2}$$

$$\frac{\partial T}{\partial z}(z = \infty, x) = - \frac{(q/A)_o}{\gamma c_p \varepsilon} \tag{3}$$

---

* This model and the subsequent solution also apply to mass transport by making the usual variable changes.

where, u, uniform wind velocity

T, potential temperature

T'_o, amplitude of the sinusoidal boundary temperature distribution in the down wind direction

T_o, mean boundary temperature

x, down wind position

x_o, wave length of the sinusoidal boundary temperature distribution

z, elevation above the ground

ε uniform eddy diffusivity or conductivity

$(q/A)_o$, mean, vertical heat flux in boundary layer

γ air density

c_p, air heat capacity

Equation (1) is the well known transport relation including the idealizations described previously for this model. Equation (2) defines the sinusoidal boundary temperature distribution in the down wind direction. Equation (3) states that the temperature gradient at great distances above the boundary is equal to the mean gradient based on the mean vertical heat flux in the boundary layer.

It can be shown that the solution of Equations (1), (2) and (3) is equal to the sum of the solutions of the following two boundary value problems:

Problem 1

$$o = \frac{\varepsilon}{u}\frac{\partial^2 T_1}{\partial z^2} \tag{4}$$

$$T_1\,(z = o, x) = T_o \tag{5}$$

$$\frac{\partial T_1}{\partial z} = \frac{(q/A)_o}{\gamma c_p \varepsilon} \tag{6}$$

Problem 2

$$\frac{\partial T_2}{\partial x} = \frac{\varepsilon}{u}\,\frac{\partial^2 T_2}{\partial z^2} \tag{7}$$

$$T_2(z = o, x) = T'_o \cos 2\pi\,\frac{x}{x_o} \tag{8}$$

$$\frac{\partial T_2}{\partial z}\,(z = \infty\,,\, x) = o \tag{9}$$

The subscripts 1 and 2 refer to problems 1 and 2, respectively.

Problem 1 represents an atmospheric boundary layer with a uniform inter-face temperature or heat flux. The simple temperature solution* is,

$$T = T_o - \frac{(q/A)_o}{\gamma c_p \varepsilon} z \tag{10}$$

Problem 2 represents an atmospheric boundary layer with a sinusoidal boundary temperature distribution in the down wind direction. The mean boundary temperature is zero and the temperature gradient at great distances above the boundary is also equal to zero. Equations (7), (8) and (9) are similar to the ones for the classical problem of periodic heat conduction in a slab. The solution can be obtained by the separation of variables technique. The resulting complex equation is reduced to a real function to satisfy the real periodic boundary condition at z = o,

$$T = T'_o e^{-B\frac{z}{x_o}} \cos\left(2\pi \frac{x}{x_o} - B\frac{z}{x_o}\right) \tag{11}$$

It is more convenient to express temperatures and vertical heat fluxes in dimensionless form. The dimensionless temperature equation is

$$\bar{T} = e^{-BZ} \cos(2\pi \bar{X} - BZ) \tag{12}$$

where, $\bar{T} = \frac{T}{T'_o}$

$\bar{Z} = \frac{z}{x_o}$

$\bar{X} = \frac{x}{x_o}$

$B = \sqrt{\frac{\pi u x_o}{\varepsilon}}$

The dimensionless vertical temperature gradient which is proportional to the vertical convective heat flux is,

---

* If the uniform eddy diffusivity is replaced by one that increases linearly with height z, the classical logarithmic temperature profile is obtained instead of the simplified linear profile (Equation (10)).

$$\frac{\partial \bar{T}}{\partial \bar{Z}} = - Be^{-B\bar{Z}} \left[\cos(2\pi\bar{X} - B\bar{Z}) - \sin(2\pi\bar{X} - B\bar{Z})\right] \tag{13}$$

The temperature solution to the boundary value problem defined by Equations (1), (2) and (3) is the sum of the temperature solutions given by Equations (10) and (11). Thus temperature and vertical heat flux profiles for an atmospheric boundary layer with a sinusoidal boundary temperature distribution in the down wind direction are defined.

RESULTS

An illustrative example depicting temperature and vertical heat flux profiles in a boundary layer with a sinusoidal boundary temperature distribution has been evaluated for neutral stability conditions ($(q/A)_o = o$). The temperature and heat flux results for the study are shown in Figures VI-1, VI-2 and VI-3 for the specific condition, B = 100. Figure VI-1 presents profiles of the dimensionless temperature, $\bar{T}$, as a function of the dimensionless vertical and down wind positions. Similarly, Figure VI-2 shows profiles of the dimensionless vertical temperature gradient, $\partial\bar{T}/\partial\bar{Z}$. Note that the contour plumes create variable vertical temperature and heat flux profiles as a function of down wind position. A graph of the ratio of the vertical heat flux at a given elevation to the heat flux at the boundary (denoted as Q) can be seen in Figure VI-3; this figure shows large variations in vertical heat flux that can be encountered for the case of neutral stability in a boundary layer with a periodic earth surface temperature distribution. Such variations become significantly smaller, of course, for stable and unstable atmospheres (where mean, negative or positive heat fluxes exist in the boundary layer). The dimensionless temperature profiles as a function of down wind position are shown in Figure VI-4 for the neutral case.

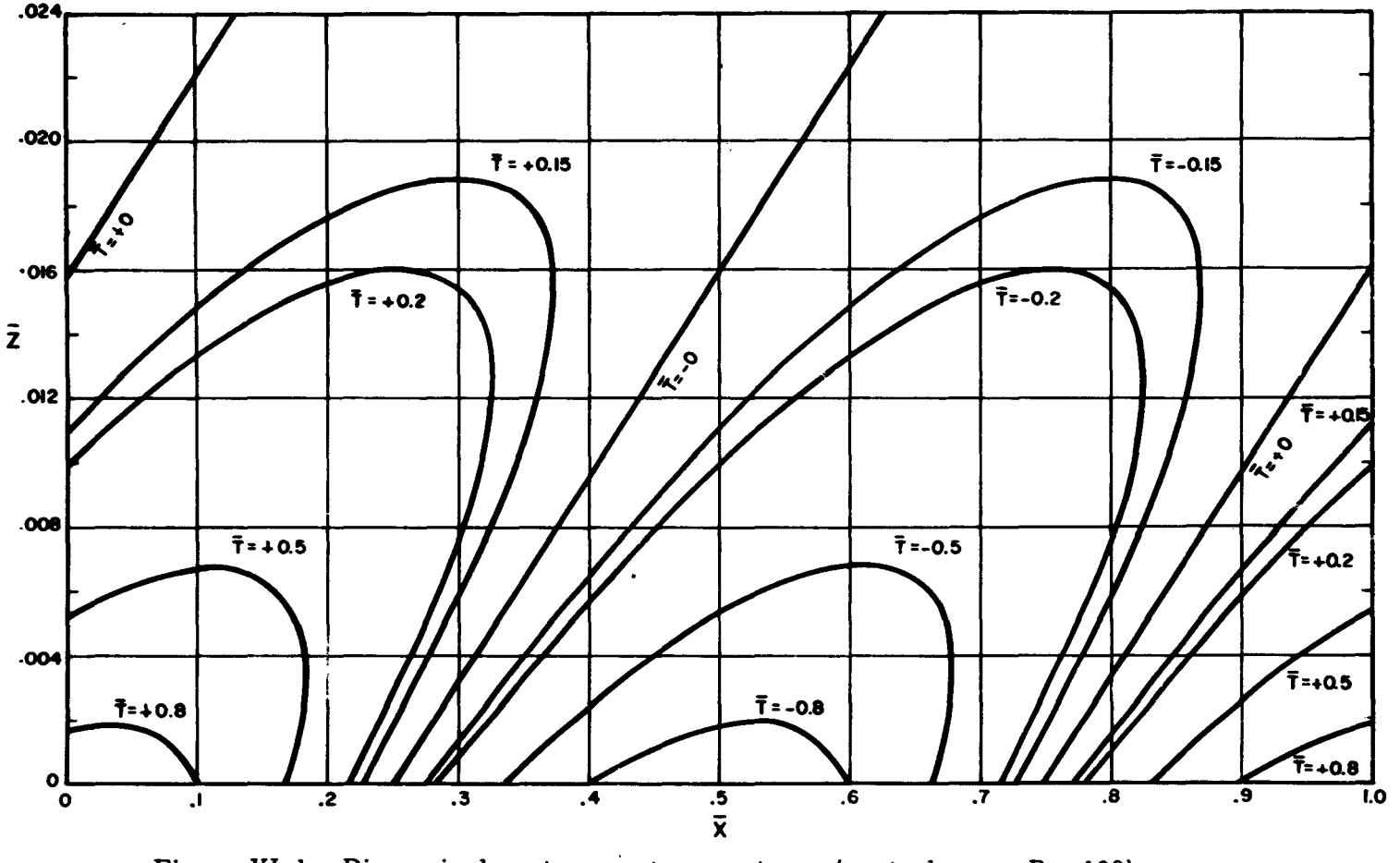

Figure VI-1. Dimensionless temperature contours (neutral case, B = 100).

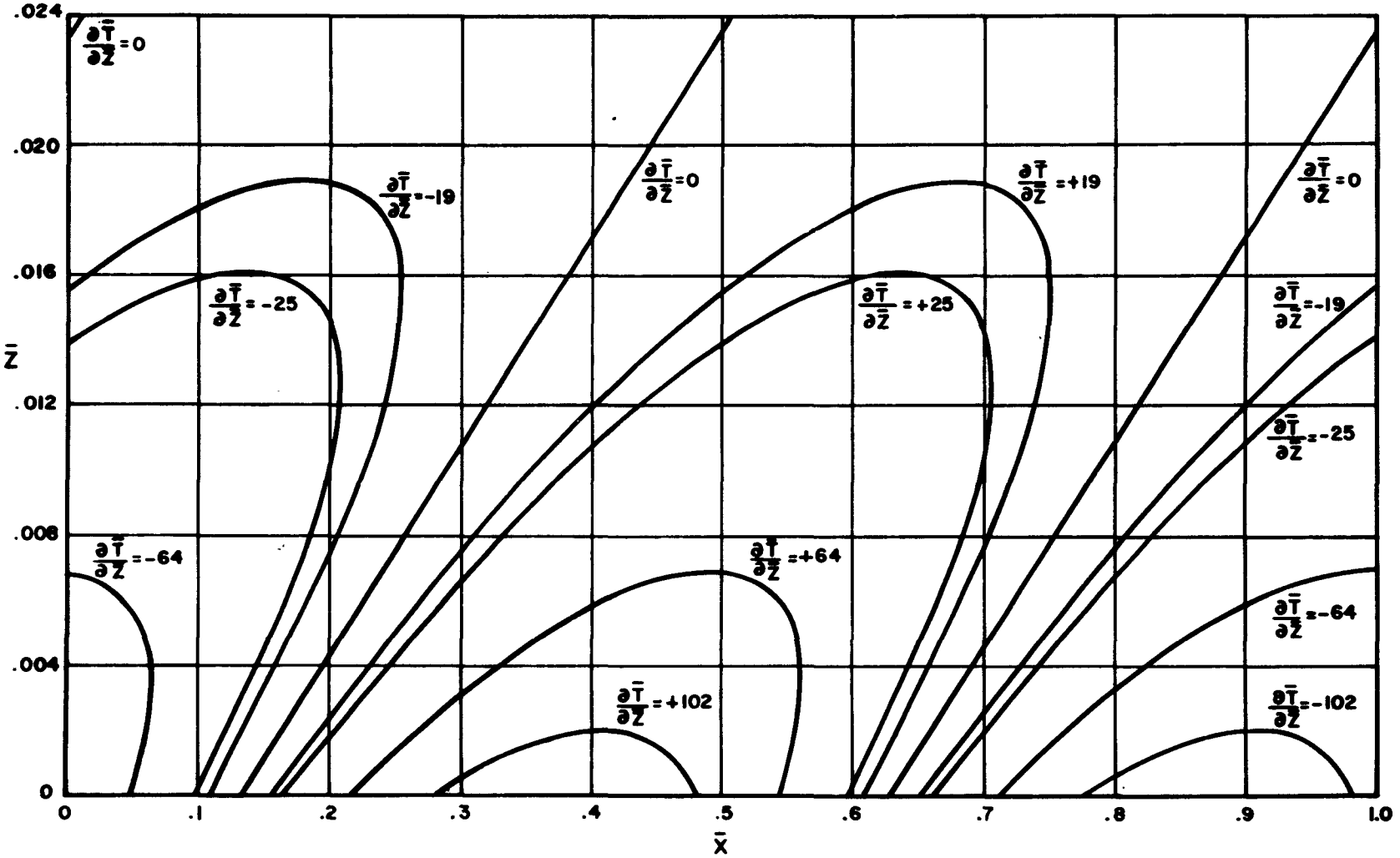

Figure VI-2. Dimensionless vertical temperature gradient contours (neutral case B = 100).

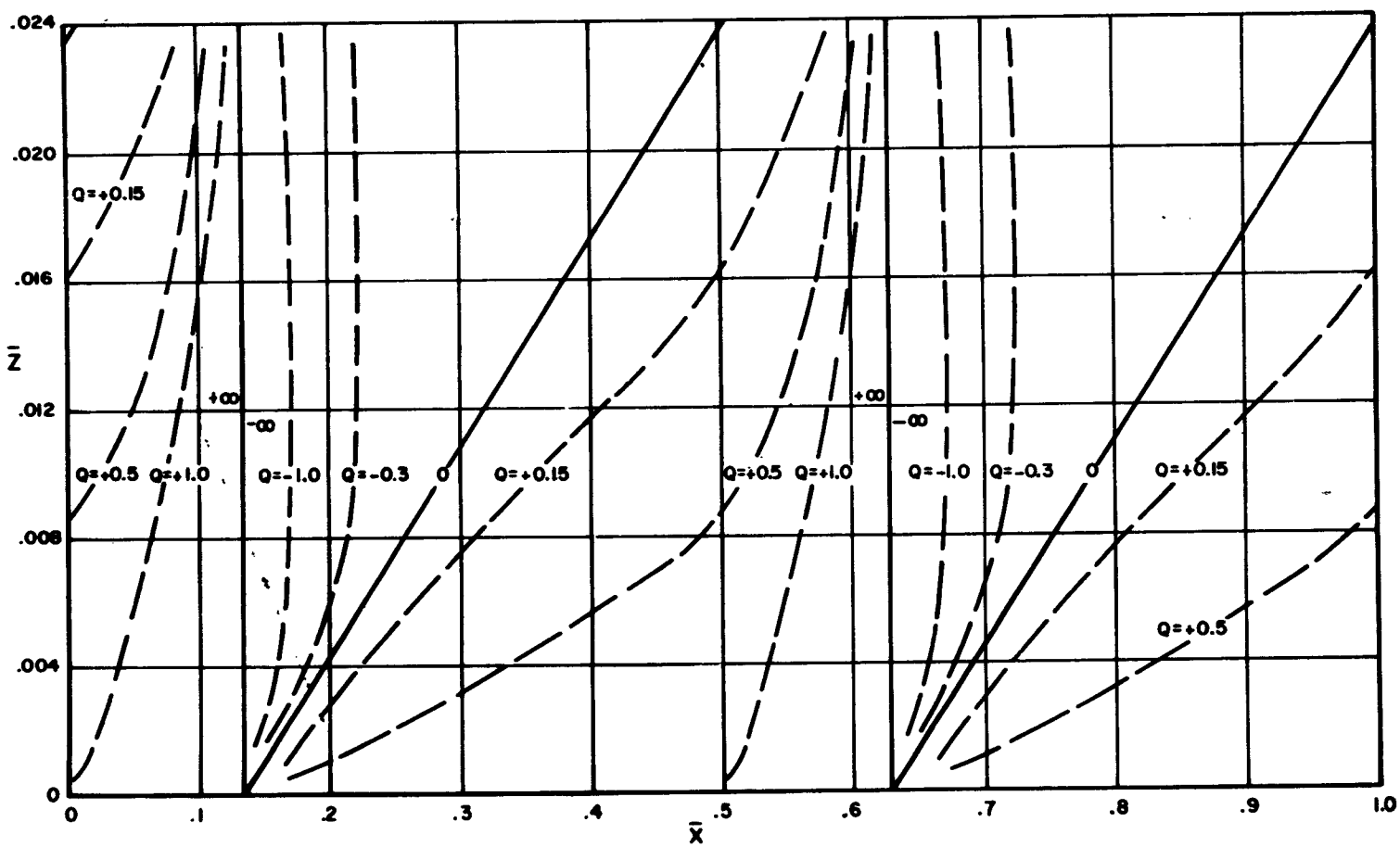

Figure VI-3. Dimensionless vertical heat flux contours (neutral case, B = 100).

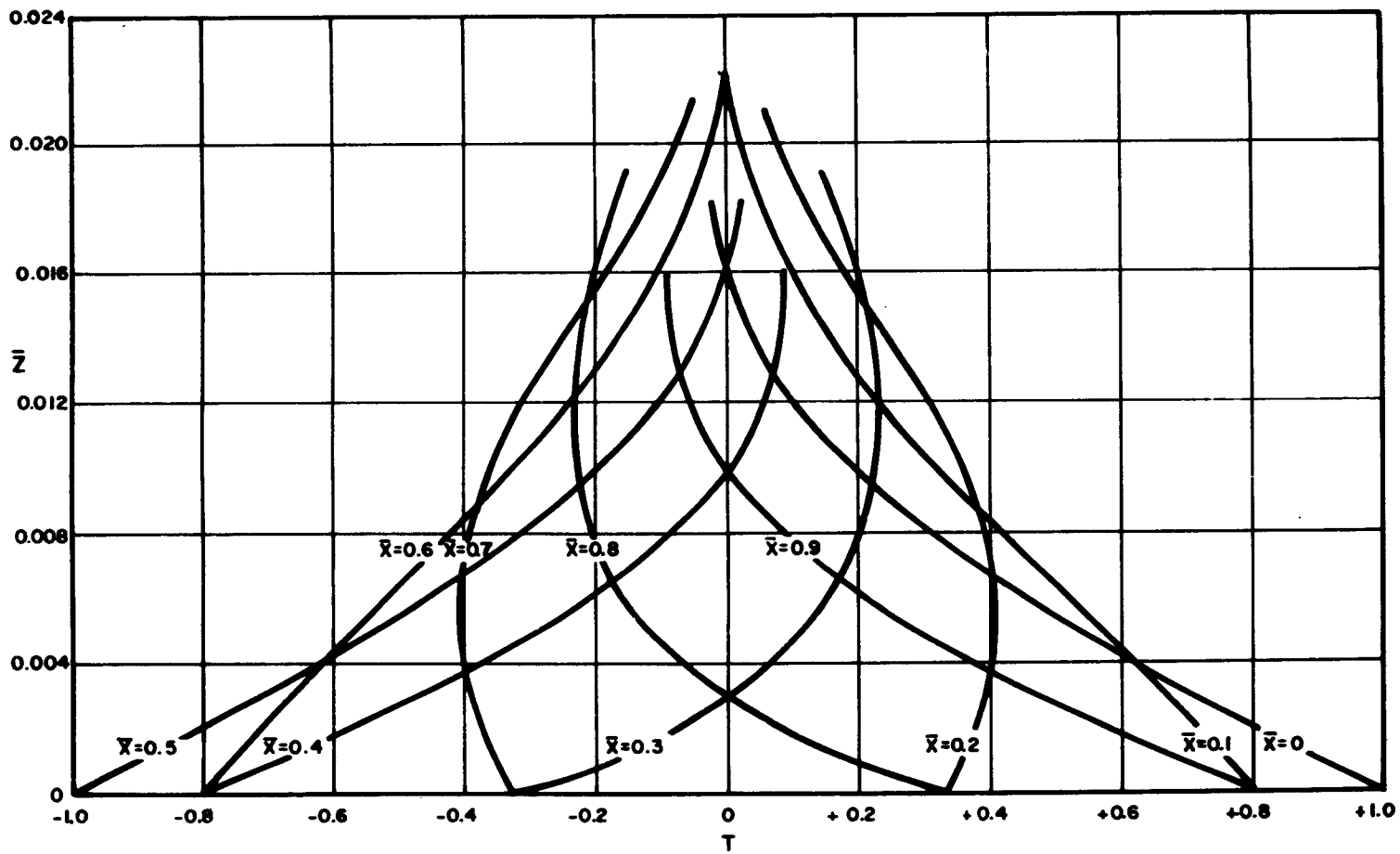

Figure VI-4. Dimensionless temperature profiles as a function of $\bar{X}$ (neutral case, B = 100).

CONCLUDING REMARKS

At the University of California climatological site, Davis, California, dry bulb temperature profile measurements* were made over a large grass field with down wind variations in temperature and humidity. Typical measurements are shown plotted in Figure VI-5. It was not possible to specify the complete boundary temperature distribution for the field and

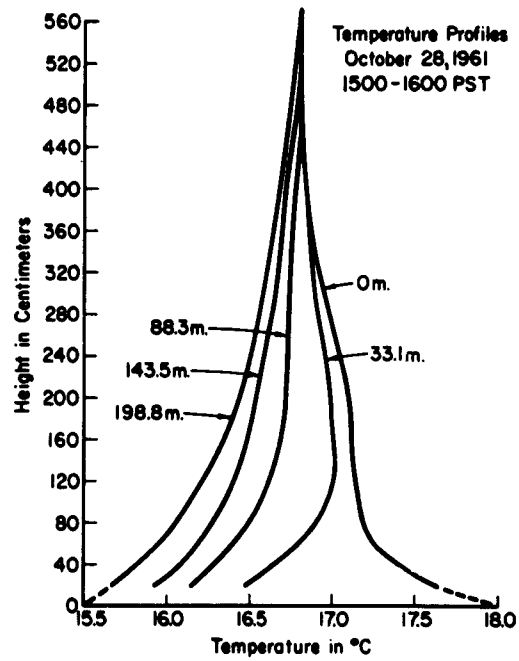

Figure VI-5. Temperature Profiles, 28 October 1961: 1500 - 1600 PST

its surroundings. In the light of the up wind variations in terrain and the shapes of the experimental temperature profiles in Figure VI-5, it is felt that the boundary temperature distribution may be approximated by a cosine. The mean experimental temperature amplitude decay was found to be about 0.12 at a height of 310 cm. The wind velocity was about 7.0 meters/sec and x_o

---

* Brooks, F. A., Pruitt, W. O., Nielson, D. R. and Vaadia, Y., "Investigation of Energy and Mass Transfers Near the Ground Including the Influences of the Soil-Plant-Atmospheric System;" Second Annual Report (Task 3 A99-27-005-08), University of California, Davis, California, Feb. 1962.

was about 200 meters. From Vehrencamp's shear-stress measurements over Grassland, the surface stress at Davis was estimated to be about 0.30 dynes/ cm^2. This quantity was used to calculate the eddy diffusivity from the elementary relation,

$$\varepsilon = \sqrt{\frac{\tau_o}{\rho}}\ K(z + z_o) \tag{14}$$

where, τ_o, boundary layer shear stress
ρ, mass density of air
K, Karman constant
z_o, roughness parameter

For a height of 310 cm, the eddy diffusivity was found to be about 7000 ft^2/hr. This value was in satisfactory agreement with earlier measurements reported in the literature under somewhat similar conditions. The predicted temperature amplitude reduction, e^{-BZ}, in Equation (11) was calculated to be 0.093 in comparison to the experimental value of 0.12. This agreement is considered to be better than expected because the actual earth surface temperature variation with down wind position is only approximately periodic in character.

The elementary boundary layer transport model described in this report has been extended to include variable wind velocities and eddy diffusivities. A temperature solution has been outlined which is defined by a height dependent velocity,

$$u = C\,(b_1 + b_2\,z) \tag{15}$$

and a height and down wind dependent eddy diffusivity

$$\varepsilon = (b_1 + b_2\,z)\,(1 + b_3 \cos \frac{2\pi x}{x_o}) \tag{16}$$

where C, b_1, b_2 and b_3 are constants. The solution of this boundary value problem closely follows a periodic (time dependent) convective heat transfer solution.*

* Poppendiek, H. F., "A Periodic Heat-Transfer Analysis for an Atmosphere in Which the Eddy Diffusivity Varies Sinusoidally with Time and Linearly with Height," Journal of Meteorology, Vol. 9, No. 5, Oct. 1952, pp. 368-370.

CHAPTER VII

INTRODUCTORY MEASUREMENTS OF SHEAR-STRESS ACROSS RYE GRASS SOD

W. B. Goddard

In December 1962 a series of micrometeorological tests were conducted in which a shear-stress lysimeter was used to measure air drag. The measurements were of a preliminary nature because the lysimeter was not yet filled with soil. However, the measurements do give an indication of the system's potential and are, therefore, worth reporting.

Description of Shear-Stress Measuring Equipment - December 1962

The lysimeter was in floating condition, lacking only the soil and drainage system. This stage of construction permitted its use as a shearmeter, giving the opportunity to collect preliminary shear-stress data and allowing a study of the system's dynamic response. Note that at that time the lysimeter weighed approximately 5,200 pounds as compared to a final soil filled weight of 105,000 pounds. The larger weight and correspondingly higher water level will dampen the dynamic response somewhat but will not alter the average values nor change the basic method of use.

A temporary floor was constructed and covered with rye grass sod 7 cm. in thickness. The sod cover was obtained from the field site and closely approximated the surrounding cover. The ground surface adjacent to the lysimeter had to be raised 3 1/2 cm. to match the height of the floating rye grass. This surface was tapered down to field lever over an outward distance of one meter and properly sodded. The few disturbed areas near the lysimeter were leveled and also covered with sod. See Figure VII-1.

A mast was erected 17 meters east of the lysimeter with a Friez anemometer at the 15 meter height. The wind velocity was continuously recorded on a 20 pen Esterline-Angus recorder. A shear-stress transducer was especially designed and built for the tests. It consisted of a sight read jeweled bearing Starrett dial indicator actuated by an interchangeable spring. The dial was easily read to .001 inches and had a one inch travel. A vibrating system consisting of a D.C. relay operated on 1/2 wave A.C. helped overcome static friction. Two springs were made to fit the device, one having a spring constant of 752 grms. per inch and the other

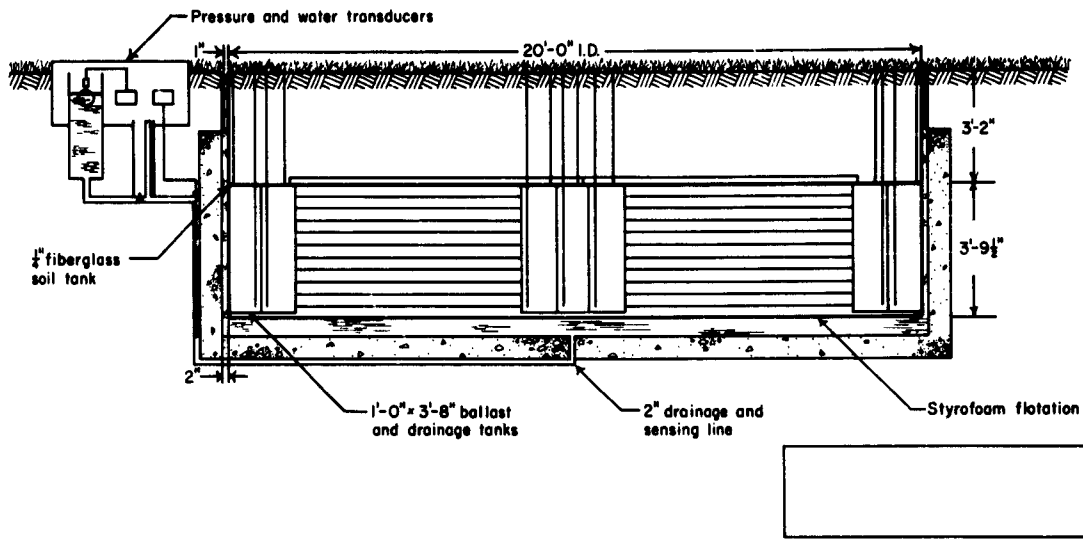

Figure VII-1. Shear-stress lysimeter design.

of 2,685 grms. per inch. It was found that during the test wind conditions allowed us to use the lighter, more sensitive spring. See Figure VII-2.

Shear-Stress Lysimeter Preliminary Operation Procedure.

Visual reading of the shear-stress transducer was accomplished by using a standard surveyor's level which enabled the reader to be about 8 meters across wind from the lysimeter. The transducer was placed directly upwind and attached by a light string to a 5 inch peg fastened in the middle of the lysimeter. The string then continued downwind to the outside and over a light pulley where a 50 grm. counter-weight was hung. The counter-weight served to position the float and establish a positive, non-moving zero reading. See Figure VII-3.

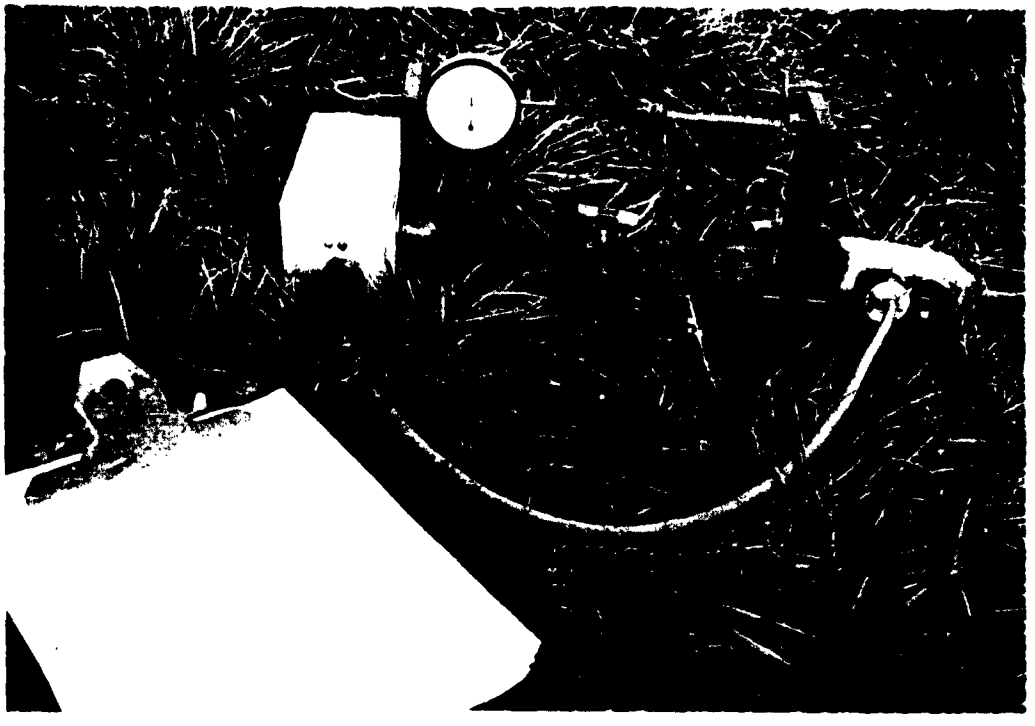

Figure VII-2. Introductory shear-stress transducer.

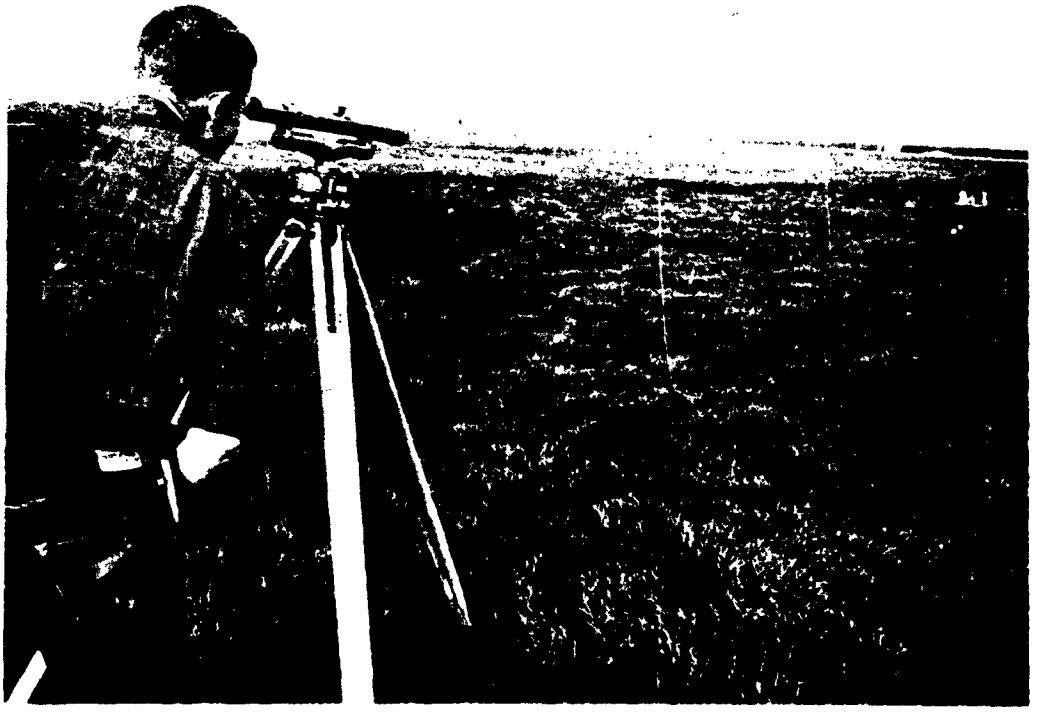

Figure VII-3. Field site reading of introductory shear-stress transducer. The outlined area shows the rye grass sod on the floating lysimeter.

Sampling Procedure

1. Upwind position of shear-stress transducer checked and vibrator turned on.
2. Distance between the float and rim checked to make sure the float was free.
3. Sample starting time recorded.
4. Readings recorded (at least 25 per sample period).
5. Sample stopping time recorded.
6. Float-rim clearance re-checked and vibrator turned off.

The sample period took from two to four minutes depending on the dial fluctuations. The wind velocity record was continuously timed so that the sample periods and wind record would accurately correspond. Further tests were conducted in February 1963 using the same transducer design but equipped with a linear differential transformer whose output monitored the spring movement. These tests were used to determine the overall time response of the system. Figure VII-4 shows a section of the output record where the response of air drag with a change in wind profile occurs during a two minute period.

Interpretation of Results

Boundary shear-stress is basic to any mass and energy transfer across an interface. Its role is of major importance in determining the friction velocity, the drag coefficient, and the Karman constant. Air drag together with wind velocity profile give a direct method for determining the above coefficients.

The shear-stress transducer was calibrated both before and after the test, and its converted response was applied to the average of the 25 or more readings taken during each sampling period. The transducer's response converted to air drag is as follows:

$$\tau = \frac{\text{spring constant x average reading + intercept}}{\text{lysimeter area}}$$

which reduces to

$$\tau = 2.4573 - 2.5268 \text{ x average reading, dynes per cm}^2$$

The determination of coefficients involving shear-stress and wind velocity necessitates accurately determining the time interval between an increase in wind velocity and the resulting increase in air drag. The cause

and effect type of record shown in Figure VII-4 enabled us to establish the time delay as 40 seconds.

The defining formulas used in calculating the following coefficients are:

$$\text{drag coefficient } C_D = \frac{\text{air drag force}}{\text{air density x (wind velocity at 15 meters)}^2}$$

where the air density is taken for standard atmosphere

$$\rho = .001293 \text{ grms./cm}^3$$

$$\text{friction velocity, } u_* = \left(\frac{\text{air drag force}}{\text{air density}}\right)^{1/2}$$

drag force, wind velocity at 15 meters

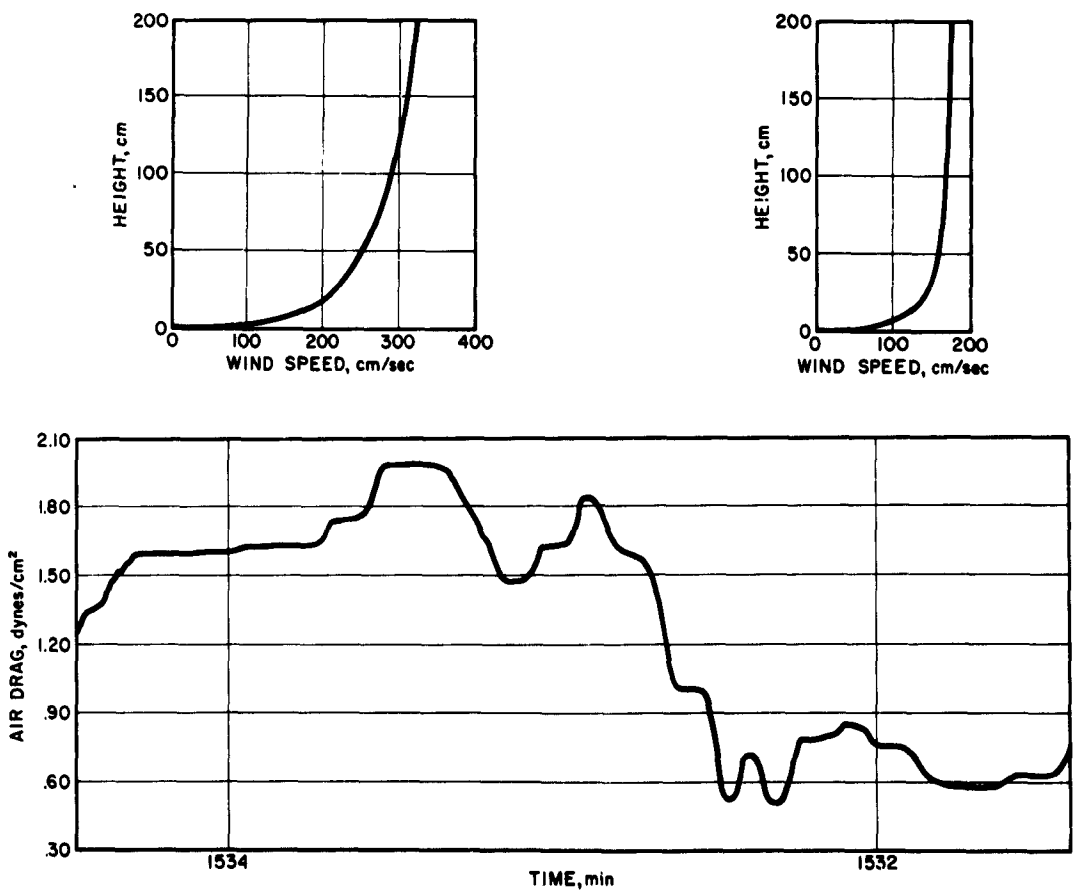

Figure VII-4. Shear-stress transducer output record.

A value for von Karman's constant, k_u, was calculated for each shear meter sampling period by using the Thornthwaite anemometer wind profile to get u_* from its tangent. Then from u_* from the shear meter a value of $\overline{k_u}$ k_u was determined. The calculated values when averaged into early evening 2015 to 2315, late evening to early morning 2315 to 0545 and late morning 0545 to 1145 ranged from .496 to .465 to .515 respectively. This appears to show a rise from stability change. Friction velocity, drag coefficient and von Karman constant are listed in Tables VII-1 and VII-2 for 13-14 December 1962. These results compare very well with the following researchers:

Researcher	C_D with U_{15} meters	Surface
Poppendiek	.0015	disked flat ground
Pasquill	.0025	uniform grain field
Sheppard	.005	rough row cropland

There is still a stability correction for shear-stress that has not yet been determined. F. A. Brooks believes that this correction will be in the order of .2 for strong stability and 3.0 for strong thermal convection. Using the shear-meter on tests covering the whole diurnal cycle, including various climatic conditions, and supported by the usual mass and energy parameters measured by this project, many hitherto unanswered questions will be resolved. The future use of this shear-meter will undoubtedly help put our mass and energy transfer interpretations on a more firm foundation.

Table VII-1. Summary of introductory shear-stress measurements for 13-14 December 1962

Date	Time	Wind velocity at 15 meters cm/sec	Shear-stress τ dynes/cm^2	Friction velocity u_*, cm/sec	Drag coefficient C_D
12/13/62	1553	458	.9386	27.0	.0035
	1606	454	.9503	27.1	.0036
	1614	378	.9020	26.4	.0049
	1624	420	1.0342	28.2	.0045
	1635	444	1.1532	29.9	.0045
	1644	444	1.1305	29.6	.0044
	1648	412	1.1494	29.8	.0052
	2030	435	.6531	22.4	.0027
	2058	355	.5612	20.8	.0034
	2128	325	.4679	19.0	.0034
	2236	400	.5739	21.0	.0028
	2304	310	.3899	17.4	.0031
	2331	298	.3068	15.4	.0027
12/14/62	0005	368	.4617	18.9	.0026
	0034	340	.3823	17.2	.0026
	0103	355	.4199	18.0	.0026
	0145	298	.3777	17.1	.0033
	0207	270	.3780	17.1	.0040
	0306	330	.6027	21.6	.0043
	0352	355	.4682	19.0	.0029
	0429	355	.5162	20.0	.0032
	0500	546	.5140	20.0	.0013
	0616	330	.4972	19.6	.0035
	0645	245	.2991	15.2	.0039
	0713	220	.2640	14.3	.0042
	0743	268	.3745	17.0	.0040
	0816	355	.5083	18.8	.0031
	0846	325	.6004	21.5	.0044
	0916	268	.3343	16.1	.0036
	0946	245	.2928	15.0	.0038
	1029	220	.4912	19.5	.0078
	1111	210	.2832	14.8	.0050
	1144	145	.0773	7.7	.0028

Table VII-2. Summary of introductory shear-stress measurements for 12-13 December 1962 (including non Karman constant)

Date	Time	Thornthwaite anemometer $\frac{u_*}{k_u}$ cm/sec	von Karman constant k_u
12/13/62	2015	58.7	.388
	2045	43.5	.495
	2115	33.1	.596
	2145	37.0	.527
	2215	36.5	.562
	2245	41.7	.480
	2315	38.3	.431
	2345	37.0	.446
12/14/62	0015	37.8	.483
	0045	35.2	.497
	0115	45.6	.389
	0145	35.7	.482
	0215	34.8	.510
	0245	43.5	.457
	0315	38.3	.549
	0345	35.7	.544
	0415	51.3	.385
	0445	42.2	.475
	0515	46.5	.430
	0545	45.6	.433
	0615	40.0	.487
	0645	30.0	.516
	0715	23.9	.617
	0745	28.7	.593
	0815	45.2	.421
	0845	45.6	.466
	0915	35.1	.456
	0945	30.4	.493
	1015	28.3	.645

Table VII-2. Summary of introductory shear-stress measurements for 12-13 December 1962 (including non Karman constant) (Continued)

Date	Time	Thornthwaite anemometer $\frac{u_*}{k_u}$ cm/sec		von Karman constant k_u
12/14/62	1045	29.1		.602
	1115	21.8		.630
	1145	22.6		.341
			Total	15.826
			Average k_u	$\frac{15.826}{32} = .495$

CHAPTER VIII

AUTOMATIC DATA RECORDING SYSTEM

F. Lourence

INTRODUCTION

The Automatic Data Recording System has been in operation since May of 1962 following the major System modification at the Electro Instruments factory in San Diego. This report will cover four areas regarding the System with the first being the accuracy of the System under field conditions. The second discussion will cover the reliability of the System over the past year. The third topic will give the results of a test designed to check the Automatic Data Recording System's ability to record varying input signals. The last area to be discussed in this report will concern the D-C preamplifier performance in the System.

SYSTEM ACCURACY

The accuracy of the Automatic Data Recording System has been of vital concern since the System was originally designed by W. T. Kyle in 1960. In the original proposal (First Annual Report, 1962, p. 68), the minimum System resolution was specified as 10 microvolts with an input range from 0 to .9999 volts. The maximum error was given as $\pm$ 20 microvolts. When the decision to use thermocouples as the basic transducer was made, the System required a 1 microvolt resolution with an absolute accuracy of $\pm$ 10 microvolts. In order for the Electro Instruments' equipment of the System to measure these low level signals with 1 microvolt resolution and the required accuracy, the Digital Voltmeter had to be operated on its 10 volt range with the D-C preamplifier on a gain of X 1000. The Crossbar Scanner Switch had to be operated on a 3-wire switching mode thus reducing the number of inputs from the original 300 channels to 200 channels.

The basic voltage calibration procedures set forth by W. T. Kyle required some changes in order to provide calibration signals known to 1 microvolt absolute accuracy. The basic voltage standard of the calibration system consists of two N.B.S. certified Eppley Unsaturated Standard Cells. One microvolt steps, by comparing the standard cells directly to the 6-decade Kelvin-Varley voltage divider, are not possible. By using an indirect comparison method by a voltage dividing circuit comprised of accurately

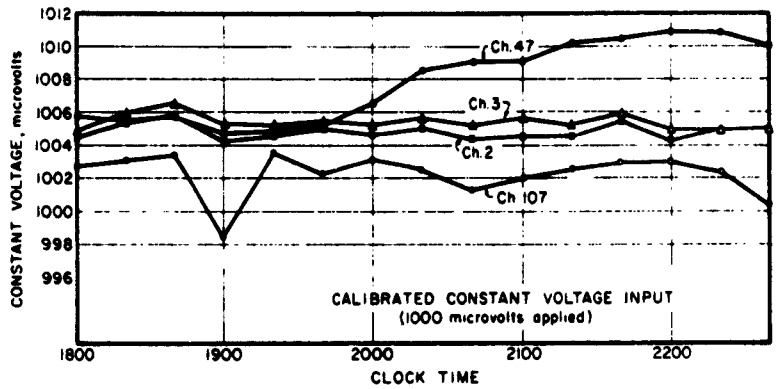

Figure VIII-1. Calibrated constant voltage input.

calibrated resistors, the required calibration voltages traceable to N.B.S. are possible. The following sketch shows the circuit used.

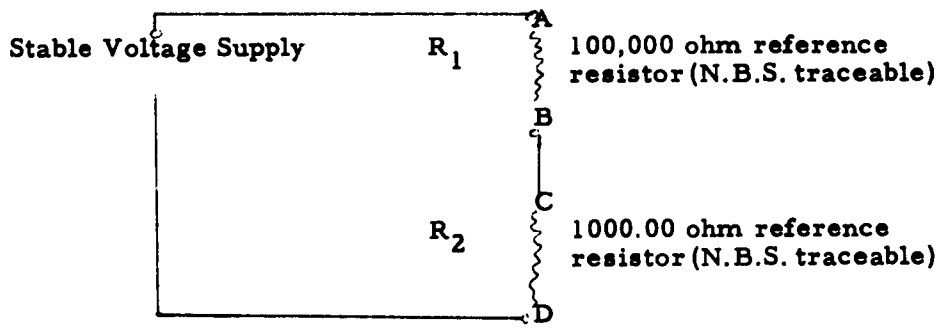

By measuring the potential across (e_1) R_1 at points A and B to 0.001% in the circuit, the voltage potential (e_2) across R_2 at points C and D may be calculated by the relationship:

$$e_2 = \frac{e_1 R_2}{R_1}$$

e_2 is then used to calibrate the 6-decade Kelvin-Varley voltage divider which now provides it with 1 microvolt steps in the last decade. The method is essentially the same as that of a Lindeck potentiometer. The greatest difficulty of providing accurate calibration voltages at these low level potentials is caused primarily by the presence of thermo-electric potentials.

From the major run made in December of 1962, the means and variances of the fixed voltage inputs and the shorted channels were computed. Figure VIII-1 shows how four channels of identical fixed voltages were read and recorded by the Automatic Data Recording System over a 4 1/2-hour period. Three of the shorted channels are listed in Table VIII-1, and in Table VIII-2 the variances of the fixed voltage channels are listed over the same 4 1/2-hour period. All of the points listed represent a 20-minute averaging period. The adverse variations within the same channels and between different channels with time is caused primarily by thermal-electric potentials development within the crossbar scanner unit. The high variances of channel 107 shown in Table VIII-2 are typical of the second one hundred channels because the thermal-electric potentials are greater in the second one hundred channels than in the first one hundred. The thermal-electric potentials can produce as much as 6 microvolts difference on the same channel and between different channels over a 20-minute period of time. This 6 microvolt error corresponds to a 0.15°C difference between thermocouple inputs.

Even though the stray thermal-electric voltages are within the $\pm$ 10 microvolt required absolute accuracy, work is being done to reduce them to a minimum.

TABLE VIII-1. SHORTED INPUT CHANNELS - 20-MINUTE MEANS, Microvolts

Time	Channel 1	Channel 21	Channel 109
1800	0.8	4.6	2.6
1820	1.0	4.6	3.0
1840	1.2	4.8	6.0
1900	1.2	4.4	6.2
1920	0.3	3.5	3.5
1940	1.1	3.6	3.8
2000	0.6	3.6	3.9
2020	0.8	2.6	4.8
2040	0.8	3.0	4.0
2100	1.8	3.5	4.0
2120	0.8	2.6	2.2
2140	3.0	4.6	4.0
2200	0.1	4.0	3.0
2220	2.0	4.0	3.6
2240	0.0	5.0	3.4

TABLE VIII-2. VARIANCES FOR FIXED VOLTAGE CHANNELS, Microvolts

Time	Channel 2	Channel 3	Channel 47	Channel 107
1800	0.15	0.75	0.20	4.20
1820	0.60	1.30	0.40	4.20
1840	2.60	2.40	1.10	5.40
1900	0.40	1.20	0.60	6.50
1920	0.40	1.90	0.25	8.50
1940	1.40	1.25	1.10	9.60
2000	0.45	1.40	6.10	8.48
2020	2.60	3.10	8.52	9.10
2040	0.25	1.40	5.20	8.75
2100	0.20	1.78	6.25	8.60
2120	0.55	0.90	3.40	6.50
2140	0.25	0.20	2.75	4.50

SYSTEM RELIABILITY

The Automatic Data Recording System has shown poor reliability. Some of the malfunctions which have occurred since May 1962 are:

1) Occasionally punched cards have double punches occurring in the clock time and scan number columns.

2) The digital clock gained time at the rate of 0.5 minutes per hour.

3) The I.B.M. punch relays interconnecting some signals to the Electro Instruments System became faulty and occasionally caused such conditions as digital clock stoppage at the end of a scan cycle.

Some of the less serious malfunctions which have occurred and have been completely repaired are:

1) Resistors in the scanner control unit power supply failed.

2) The parallel output control unit had a transistor failure in its I.B.M. punch starting circuitry.

3) The digital voltmeter polarity indicator failed due to faulty circuit components.

4) The I.B.M. punch failed due to loose connections.

5) The parallel output control unit failed due to faulty solder connections.

6) The digital printer drive clutch spring failed.

7) The differential amplifier showed instability due to environmental warming. The unit later failed completely and had to be returned to the factory for repairs.

This shows that the System's reliability leaves much to be desired. It was irritating to find that a good portion of the malfunctions were traced to loose or poor solder connections. As a possible means of reducing the number of malfunctions, shock mounts have been placed under the equipment racks, and the System is operated on a test-running schedule at least two hours per week in order to prevent relay contacts and connectors from corroding from lack of continual use.

DATA RECORDING SYSTEM RESPONSE TO VARYING VOLTAGE INPUTS

All of the field transducers' outputs change in emf over a given time period. A test was designed to determine two characteristics of the Automatic Data Recording System's ability to measure and record changing potentials. The test first determined the largest change in applied emf

over a period of time that the System could successfully record. Secondly, the test established the tracking accuracy on a changing potential.

A low frequency signal generator was used to provide an input to the System in the form of a triangle wave. Figure VIII-2 shows the readings recorded by the System. The System recorded without any forced prints a triangle wave form that was changing at the rate of 50 microvolts per

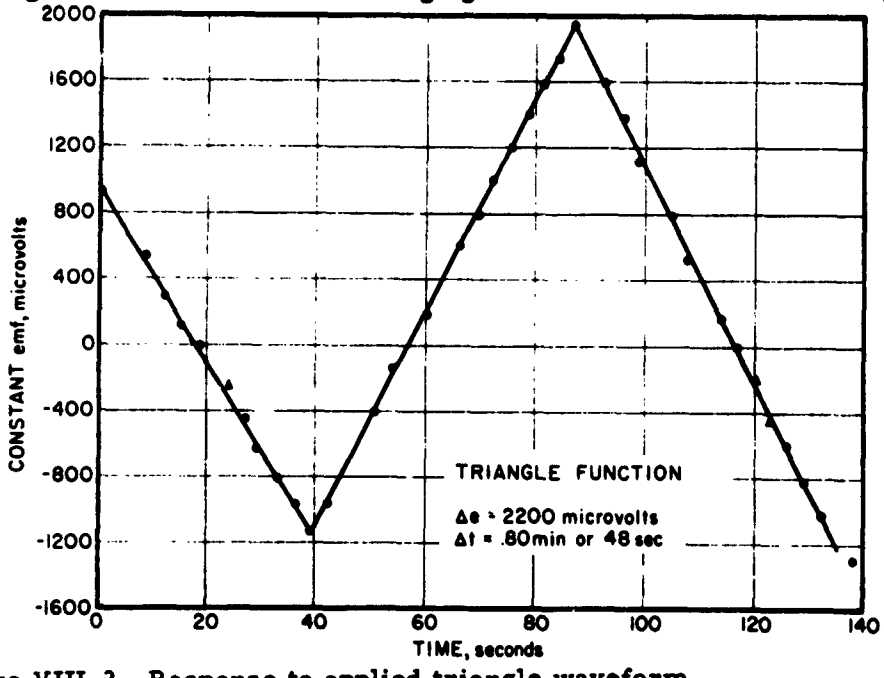

Figure VIII-2. Response to applied triangle waveform.

second. This was with the D-C preamplifier in the circuit on a gain of X 1000, and voltmeter sensitivity control at 80% of maximum. With the preamplifier on X 1000, the digital voltmeter actually was presented with a signal changing at the rate of 50 millivolts per second. When the digital voltmeter had a triangle wave applied to it directly, i.e. without the preamplifier, it would successfully record a potential changing at the rate of 3 volts per second. Thus the D-C amplifier causes a considerable reduction on the digital voltmeter's ability to null on a changing potential.

The tracking accuracy of the System with a 50 microvolt per second signal applied is shown in Figure VIII-3. The tracking accuracy was completely satisfactory with never more than about 2 microvolts deviation from the mean of the continually changing input triangular wave.

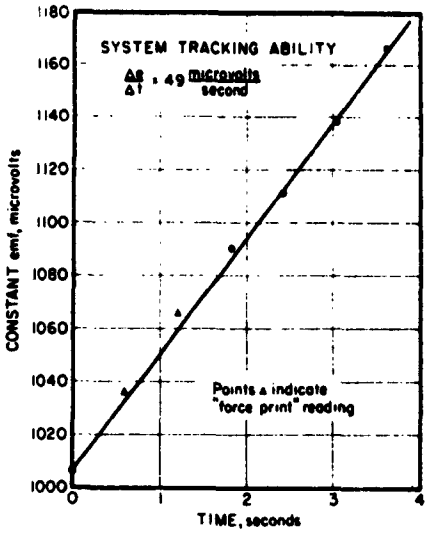

Figure VIII-3. Ability of the system to track on a changing signal.

An additional test was made applying a sine wave signal instead of a triangular wave. The digital voltmeter was able to null on the peaks of the sine wave when the signal had 10 times the frequency of the corresponding triangular wave form.

Another characteristic that the digital voltmeter exhibited during the tests was that it could null a decreasing potential changing at the rate of 120 microvolts per second while a null could not be achieved on an increasing potential changing more than 50 microvolts per second. This characteristic is due to the inherent searching pattern of digital voltmeter.

THE AUTOMATIC DATA RECORDING SYSTEM D-C PREAMPLIFIER

The D-C preamplifier required a gain of X 10 in W.T. Kyle's original design, but in order to provide 1 microvolt resolution, the required gain was increased to X 1000. This modification was made in the major System modification at the San Diego Electro Instruments factory. In addition, input and output R-C filters were installed in the preamplifier's input and output.

The purpose of the input and output filters is to filter the spurious noise that becomes amplified at the high levels of amplifier gain. Errors in measuring voltage potential can result from the effects of the capacitors in the filter networks not being allowed to charge or discharge fully in

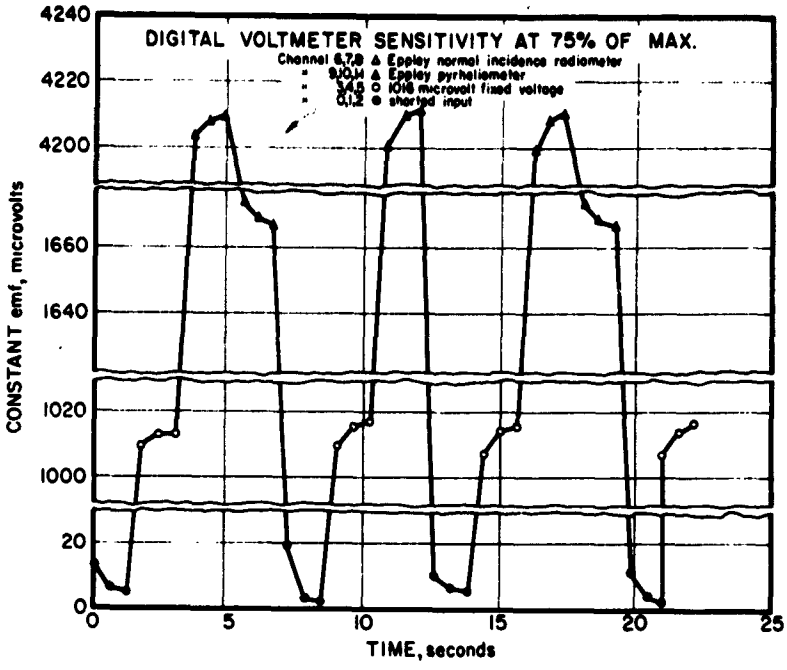

Figure VIII-4. Digital voltmeter sensitivity control set at 75% of maximum.

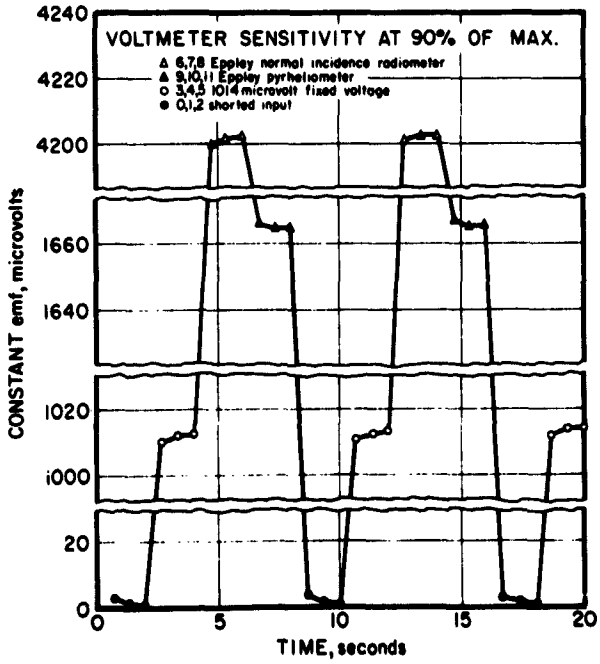

Figure VIII-5. Digital voltmeter sensitivity control set at 90% of maximum.

going from one channel to another. These "carry over" effects are especially noticeable whenever there are large voltage changes between sequential channels being scanned, and when the digital voltmeter does not have its sensitivity control turned to as near maximum as possible. Figure VIII-4 shows the effects of the capacitor "carry-over" effect on a typical scan covering 12 channels. The digital voltmeter sensitivity control was increased in the plot shown in Figure VIII-5 covering the same 12 channels. The first reading of each group of identical inputs is within tolerance of the final reading of the group, but the System speed suffers as the result of increasing the voltmeter sensitivity by 20%, i.e. the rate of scanning is reduced from 100 channels per minute to about 80 channels per minute.

The Electro Instruments A-16 D-C preamplifier displayed instability in operation whenever the amplifier temperature rose to greater than 35°C. Shortly after this condition was noticed, the unit had a major malfunction. Meanwhile another D-C amplifier was borrowed from Cohu Electronics. The borrowed amplifier was found to operate more satisfactorily than the Electro Instruments A-16 amplifier. The borrowed amplifier was of a narrow-band type as opposed to the A-16 wide-band unit. For a low-frequency D-C system there is little need for a wide-band D-C amplifier. Much of the spurious higher frequency electrical noise is not allowed to pass the narrow-band amplifier's band-pass characteristic. Using the narrow-band-pass amplifier, transducers with input impedances up to 10,000 could be measured and recorded, something that the System has not previously been able to do.

The Cohu Kin Tel 114C narrow-band differential amplifier showed that it could produce a system speed of 90 channels per minute on field transducers with the digital voltmeter sensitivity control at a higher setting than that of the Electro Instrument's amplifier. The Electro Instrument's amplifier produced a system speed of 80 channels per minute on the same transducers. The 114C amplifier was purchased for the System in December 1962.

CHAPTER IX

DATA PROCESSING AND COMPUTER PROGRAMMING*

F. A. Brooks and F. V. Jones

To go beyond the usual limits of personal analysis of the micrometeorological complex, it is essential to record and process the extensive research data automatically. Only as a first step are the observations from 4 or more masts simplified to single horizontal mean magnitudes from which central vertical profiles are constructed. The next requirement calls for interpretation of horizontal differences as in advection studies anticipated by Brooks (1961) and by Poppendiek in Chapter VI of this report. Difference studies require much finer accuracy than mean profiles and in the naturally highly variable outdoor conditions this calls for time smoothing of means, each composed of many repetitive measurements. In writing the programs for the automatic computer, therefore, a completely corrected tape with no omissions is essential. The various procedures to create this tape from punched cards having various errors and omissions is described below.

A series of computer programs has been developed to process the basic data acquired primarily through the use of the Electro Instrument digital system. Certain other data, recorded on continuous strip charts or recorded by hand, will also enter the system via key punched Hollerith cards. At present the IBM 1410 of the University of California, Davis, Computer Center is used by the project. A 40K IBM 1710 computer system is also available. Plans for expansion of the Computer Center facilities include the replacement of the IBM 1410 with an IBM 7040 computer. These changes will take place in the fall of 1963. Some reprogramming will be required to match this new facility configuration.

Editing and Error Checking of Original Punched Card Data. Unavoidable electronic noise plus various malfunctions in the acquisition system require thorough screening of the crude data before its use in automatic analysis. So-called errors or "bad" data fall into the following categories and correction or rejection is accomplished at present in subsequent programs:

1. Bad Scan: Flagged with a "-" sign preceding scan number field. Produced by a numeric double punch which cannot be read by the

* This Center is partially supported by National Institutes of Health Grant Number FR-00009.

computer; usually coming from occasional excessive electronic noise.

2. Bad Card: Flagged with a "-" sign preceding card time field. These are blanks, skips, or multiple punches in individual readings or scan times.
3. Duplicate Scan: Last value accepted and counted.
4. Skipped Scans: Occasionally the E.I. equipment will skip a scan number and its data. Such a skip results in a piece of missing data. However, this does not cause erroneous readings or computational errors. The results are affected only to the extent of a smaller count and reduced amount of data.
5. Out-of-sequence Scan Number: Rejected. Sometimes a spurious digit appears, usually in the second-order position.
6. Out-of-sequence Time: Rejected. These come usually from erratic clock signals, but occasionally are due to misfiled cards.
7. Multiple Time Punches: Rejected. Clock stops occasionally while recording of data continues.
8. Time greater than 24 hours: Rejected.
9. Incorrect polarity: Absolute value accepted for temperatures regardless of polarity; polarity as recorded accepted for other variables.
10. Wild Data: Occasionally an erroneous digit appears in the data field resulting in extremely high or low readings. Even though completely outside the acceptable range these are included in first calculations.

To judge the performance of data acquisition system, the above errors are counted and listed for each mean period.

Card-to-tape Conversion (Program #1). The primary purposes of this program are (1) to convert the E-I output to tape media for higher input speed and condensed storage and (2) to edit the data for errors of type 1 and 2.

As noted in the discussion of type 2 errors, a single piece of bad data of this type results in the rejection of all other scans on the card, 9 of which might be good. In reprogramming using the "Column Binary" reading capability of the IBM 1410, only the one piece of objectionable data would be rejected. Several other types of card errors can also be eliminated in new programs, such as cards with "good" time fields and first data fields but with all following fields blank. Some of these are now accepted in subsequent

processing and are counted into sums used to calculate means, variances, and standard deviations. In converting from cards to tape, Program #1 provides a detailed listing of all card records for initial inspection to trace errors and permit error analysis.

Calculation of Means and Variances (Program #2). While quite similar to the previous computer program used to calculate means and variances, the new program serves several other purposes. The editing function eliminates erroneous data from the computation and provides counts of the aforementioned errors. Options have been provided to select 10-, 20-, or 30-minute time periods for calculation of the means. A simple technique has been developed to check all readings against a moving reference (the mean of the immediately preceding time period), using appropriate criterion for rejection of "wild" items. The scope has been expanded to accept as many as 10 masts plus an increased number of scan points. The output of this program is (1) a listing with appropriate headings for greater clarity and (2) a working file of magnetic tape instead of punched cards. The tape increases input speed and saves on storage space.

Interpolation. Because of missing data needed to be filled in for any smoothing operation or because of rejected "wild" readings in the initial computations, an interpolation procedure is needed. Such erroneous readings are readily detected since they tend to make the mean deviate considerably from adjacent means, and their variance is extreme. In simple cases linear interpolation timewise is used. When, however, the missing data are in a curved section, parabolic interpolation is calculated or else an average is used based on simultaneous changes at several levels, a rigid procedure being followed to avoid personal bias. Need for this interpolation will be greatly reduced, if not entirely eliminated, using the technique described above in the mean and variance program.

Smoothing Techniques (Program #3). As mentioned previously, natural eddy parcel variations and occasional gusts of air of different physical qualities make it impossible for a nearly instantaneous vertical series of measurements, no matter how precise, to provide a profile useful for close analytical interpretation. We usually assume that vertical rates are constant with height. There are, however, continual and fluctuating transfers in all directions between various-sized air parcels which are meaningful

only in their average effects over discrete intervals of time. Furthermore, during periods of rapid change as, for instance, at sunrise, the conditions at the bottom of a mast change measurably within the time interval required to scan the transducers upwards on two masts. Therefore, our scan schedule also calls for downward scans in reverse order so that in each roundtrip all the observations will average, at one design instant (Fig. IX-1), very near the center of a few slow-changing observations.

Two procedures have been used for time smoothing of observations centered on 2-minute and 4-minute scan sequences. Fourier harmonic smoothing was used for the flux measurements reporting the 1961 tests. This powerful technique organizes all observations (up to 720 per cycle) into a few major harmonic cycles and is most useful in preserving the full noontime maxima in the diurnal cycles of radiation and evapotranspiration. To avoid the higher harmonics which induce spurious oscillation in derivative curves, the 24-hour day was analyzed in two halves discontinuous at sunrise and sunset. This year, to provide continuous, smoothed curves through these two periods of rapid changes in the 4-component energy balance, 5- and 9-point parabolic smoothing has been applied to arithmetic averages of successive 30- or 20-minute periods respectively. The smoothing procedure by fourth differences has been used as described by Lanczos (1956). This technique is the least squares parabola counterpart of the French-curve graphical smoothing by eye. The example for temperature data (see Chapter I, Fig. I-8) used 5-point smoothing ($2k+1$ where $k = 2$ neighbors to the point being smoothed), but the program has been generalized to permit the option of 7-, 9- and more points ($k = 3, 4$ and n). This procedure has been applied rigorously to velocity, temperature and humidity observations at each level in order to reduce scatter before the vertical profiles are automatically determined as curved logarithmic regression lines suiting equations 7 in Table II-2.

The most difficult mechanical smoothing procedure concerns the weight-loss of the lysimeter which automatically prints the weight of the 50-ton soil sample every 4 minutes to a least measurement of 2 pounds or about 1 per cent of total daily loss. If a continuing running mean difference is used instead of first derivative of a smoothed curve, the single change of 2 pounds on a quiet night with nearly zero loss will appear over a time period twice the time interval of the running mean. This sudden hump in the

curve of evaporation rate then has to be smoothed in a subsequent calculation. Thus to follow rapid changes near sunrise yet smooth out widely spaced nocturnal response and normal daytime scatter, the composite-day weight-loss record for 28-29 October 1961 shown in Fig. I-6 was processed as follows. First, an overlapping linear average over 9 points was made on 20-minute centers (mainly to reduce irregular readings due to wind gusts). Secondly, this continuous sequence of 20-minute means was smoothed by the 9-point parabolic technique which weights the center point by the constant 702 and the radially neighboring points by the constants 648, 468, 168, and -252 with a constant divisor of 2772. Linear differences were then taken between the smoothed means spanning the centerpoint plus and minus 20 minutes. This follows the common practice of using the finite difference over plus and minus one interval to represent the derivative at the center point. Then the 9-point parabolic smoothing is applied to these differences (rates) to determine the smoothed evapotranspiration rate curve of 72 points for the 24 hours. Verification is possible in reverse by integrating the evaporation rates over the 72 intervals and comparing with the known total weight loss in the 24 hours.

The whole essence of any rigorous smoothing procedure is to use the same mathematical smoothing technique and the same time spans for all the micro-meteorological factors so that with the same degree of time smoothing the time lags relating to significant perturbations will not be altered. This concept is inherent in Fourier harmonic analysis, and we believe has been retained in the continuous smoothing procedures described above.

Data Transfer and Conversion Programs. These are intended to provide convenience in manipulation and processing of selected portions of the data as well as converting from microvoltages to dimensional units. Three types of programs are used:

(a) Data Transfer (Program #4) permits any set of scan numbers and associated readings to be rapidly extracted from the master data tape (output of program 1) and transferred to another tape for subsequent processing. This results in reduced main frame computer time.

(b) Tape-to-Card Conversion (Program #5) permits the use of cards for small segments of data which are to be given specific study or can be more

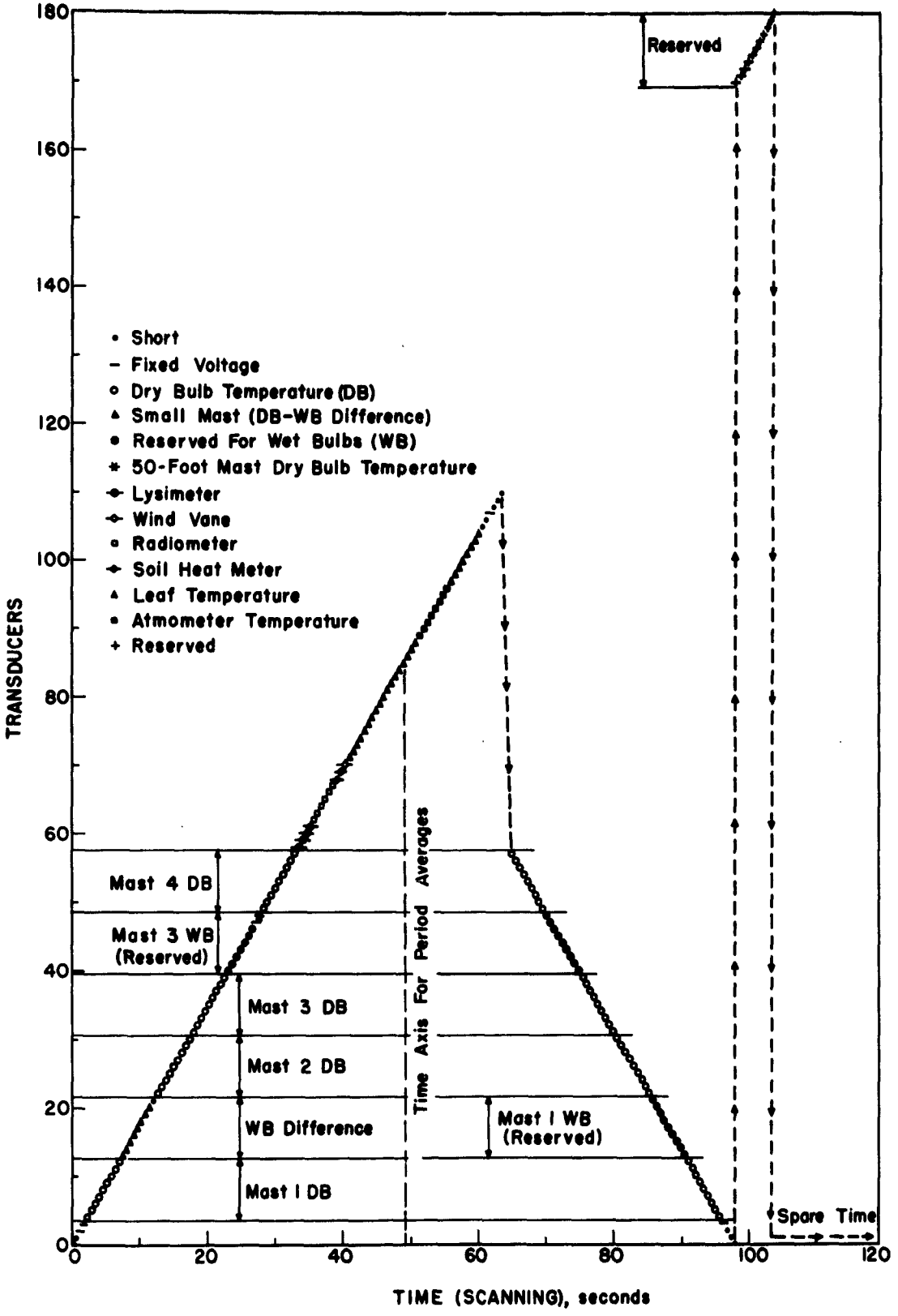

Figure IX-1. Scanning Schedule For Transducers to Center in Middle of Each Round-Trip. 13-14 December 1963.

readily and less expensively handled by some type of off-line processing.

(c) Dimensional Conversion (Program #6). All computations are made in microvolt units. The last program applies the necessary conversion constants and formulae to convert to the true dimensional units. An additional function is that of format control to prepare final tabulated copy for publication.

Vertical Profiles (Program #7). This program employs a curvilinear regression fit to the logarithmic gradient and square root functions of z (height above soil surface) for velocity, temperature, and moisture. The basic formulae (see Table II-2) are reduced to a more computable form for input to the program and the $\beta_{1,2,3}$ and $\partial_{1,2,3}$ calculated from the regression coefficients. The formula for velocity takes the form:

$$\bar{u}_* = \beta_1 \ln z' - \beta_1 \ln z_o - 2\partial_1 \beta_1 \sqrt{z'}$$

The program, prepared by Walter Mara of the Computer Center, is one of several new library programs used by the Center. The logarithms and square roots of z' (= z-d) are computed and punched into a deck of cards for input to this program.

Comments regarding the acceptability of the results of this approach at this stage are included in Chapter II.

CONCLUSION

Without automatic data processing and computing the scope of this complex research project would have to be severely reduced. The automatic interpretation obtains higher reliability from experimental observations by its capacity to use larger samples of all factors of the environment than would be possible in conventional procedures. Furthermore, the vagueness due to natural irregularity can be largely eliminated by consistent machine smoothing of data. This permits close comparisons of natural phenomena in magnitude, rate of change and timing.

REFERENCES FOR CHAPTER IX

Brooks, F. A., 1961. "Need for measuring horizontal gradients in determining vertical eddy transfers of heat and moisture", Jour. of Meteoro., Vol. 18, No. 5, pp. 589-596, October.

Lanczos, Cornelius, 1956. Applied Analysis, Prentice-Hall, Inc., New Jersey. (pp. 316-322).

CHAPTER X

CALCULATING EVAPORATION FROM DIFFUSIVE RESISTANCES

J. L. Monteith

Theoretical

Assuming that the flux of water vapour above a surface is constant with height the surface evaporation rate is

$$E = -K(z)\partial\chi/\partial z = (\chi_o - \chi)/r_a \qquad (1)$$

where χ_o and χ are the water vapour concentration (g/cm^3) at the surface and at a convenient height z, and the diffusive resistance r_a (sec/cm) is a simple function of the diffusive coefficient for water vapour K (cm^2/sec) integrated between the surface and z. Similarly, the upward flux of sensible heat C, in the regime of forced convection is

$$C = \rho c_p (T_o - T)/r_a' \qquad (2)$$

where r_a' is the appropriate resistance for heat transfer and ρc_p is the volume thermal capacity of air (cal/cm^3). The surface concentrations χ_o and T_o cannot normally be measured, but can be eliminated from equations (1) and (2) as shown by Penman (1953), introducing a third equation for the heat balance of the surface and a quantity that specifies its "effective wetness" by relating χ_o to T_o. An appropriate surface parameter r_s (sec/cm) can be found from the evaporation rate and the saturation deficit at the surface, writing

$$E = \left(\chi^* (T_o) - \chi_o\right)/r_s \qquad (3)$$

where the star denotes saturation at T_o. In the special case of transpiring vegetation, with leaf temperature T_o, $\chi^*(T_o)$ is the concentration of water vapour within sub-stomatal cavities; χ_o is the concentration at leaf surfaces; and r_s defined by equation (3) is a stomatal resistance. This concept of stomatal resistance is fundamental to an understanding of the balance between weather and soil-plant factors in determining crop evaporation.

If R is net radiation and G soil heat storage (both in cal cm^{-2} per unit time) and λ is the latent heat of evaporation (= 580 cal/g) the heat balance of the surface is

$$R = C + \lambda E + G \tag{4}$$

and following Penman's analysis it can be shown that the elimination of T_o and χ_o from equations (1) to (4) gives

$$\lambda E = \frac{\Delta R + \gamma \lambda \left(\chi^*(T) - \chi\right)/r_a'}{\Delta + \gamma\,(r_a + r_s)/r_a'} \tag{5}$$

where Δ is the slope of the saturation vapour pressure curve evaluated at the wet bulb temperature and γ is the psychrometer constant in the same units. By differentiating equation (5) with respect to r_a^{-1} and assuming that r_a'/r_a is constant, it can be shown that the evaporation rate will be independent of r_a, and hence of wind speed and surface roughness, when

$$R = \lambda \left(\chi^*(T) - \chi\right)\left(\Delta + \gamma\right)/\Delta r_s \tag{6}$$

Substituting for R in equation (5) it can be shown that the Bowen ratio assumes the value

$$C/\lambda E = \gamma/\Delta \tag{7}$$

As a useful corollory to be exploited later, when equation (7) is satisfied, stomatal resistance can be found from equation (6) without knowing the value of r_a.

In adiabatic conditions the value of r_a can be determined from a variant of the familiar aerodynamic expression for evaporation from a surface with roughness Z_o (cm), viz

$$E = k^2 u\,(\chi_o - \chi)/(\ln z/z_o)^2 \tag{8}$$

where k is von Karman's constant (=0.41), u (cm/sec) is wind speed at height z, and χ_o is a surface concentration to be found by plotting χ against u at

several heights to give a straight line intercepting $u = 0$ at $\chi = \chi_o$ (Covey 1959) Monteith 1963). From equation (8) and an analagous expression for heat transfer, it follows that

$$r_a = r_a' = \left[(\ln z/z_o)^2 / k^2 u\right] \tag{9}$$

In non-adiabatic conditions, equation (8) is invalid, but provided the transfer coefficients for water vapour and momentum are equal at all stabilities as experimental evidence suggests, χ will be a linear function of u and the diffusive resistance r_a will still be defined by equation (1). When the departure from neutral stability is serious, T will no longer be a linear function of u, and r_a' will become difficult to determine accurately from T_o and equation (2).

In the rest of this chapter, values of r_a and r_s determined from profile measurements are used in equation (5) to estimate the diurnal and seasonal variation of evaporation from grass on the experimental field.

Analysis of 30-31 July 1962

Mean hourly values of χ_o and T_o were found from smoothed profiles of temperature, vapour pressure, and wind speed at four heights over grass on the experimental field from 25 to 200 cm (see Chapter III). Given net radiation, soil heat flux, and evaporation from the 20-ft. lysimeter, sensible heat transfer was calculated by difference from equation (4) and diffusive resistances for $z = 2$ m were found from equations (1) and (2). In non-neutral conditions, the values of r_a' are approximate, but with strong instability on the morning of 31 July they are significantly smaller than r_a because sensible heat transfer by mechanical turbulence was enhanced by buoyancy (Table X-1). The smoothed wind profiles derived from a combination of Thornthwaite and Casella anemometer measurements gave a zero plane displacement of about 10 cm, and z_o about 1 cm, whereas the original unsmoothed data from the Thornthwaite anemometers alone gave z_o about 3 cm with no zero-plane correction. Because of this uncertainty in the derivation of roughness from wind profiles alone, a working value of z_o was obtained from equation (8), inserting values of $(\chi_o - \chi)$ and E during near-neutral hours to give a mean value of $z_o = 2.3$ cm. The third column of Table X-1 was then calculated using this value in equation (9). In non-neutral conditions, differences between the 'observed' values of r_a (from equation (1) and the calculated values

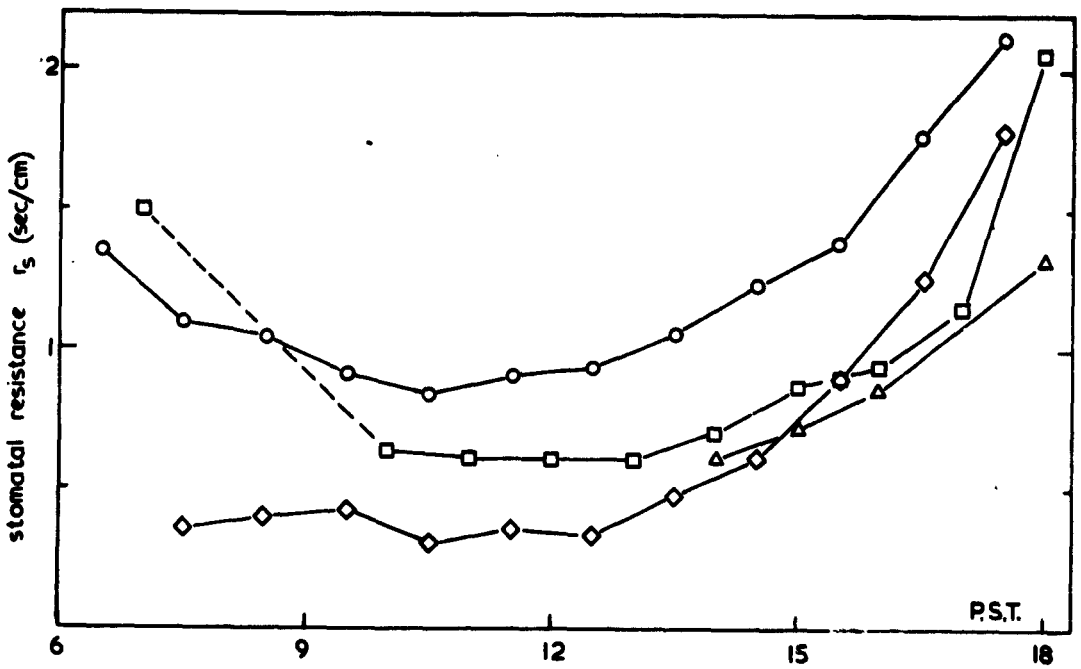

Figure X-1. Diurnal variation of stomatal resistance
(a) from equation (1)
△ 30 July 1962
□ 31 July 1962
(b) from equation (5)
◊ 28 May 1960
○ 1 June 1960

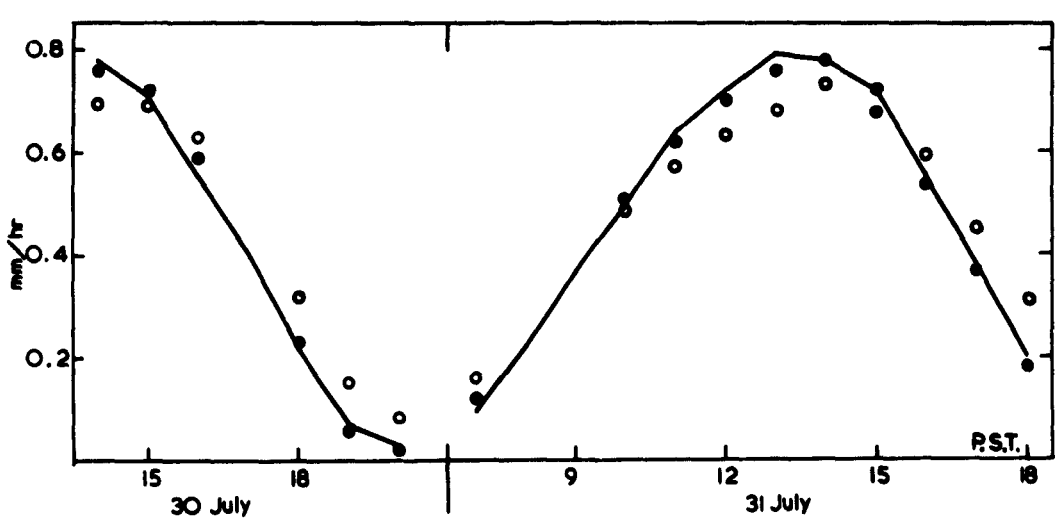

Figure X-2. Evaporation on 30 to 31 July, 1962.

——— recorded by 20 foot lysimeter

● calculated from equation (5) with r_s values taken from Table 1

○ calculated from equation (5) with r_s = 0.7 sec/cm

were often large, but seemed uncorrelated with Richardson number.

Values of stomatal resistance calculated from equation (3) reached a minimum value of about 0.6 sec/cm in the middle of the day and rose steadily during the afternoon, presumably in response to growing moisture deficits within the plants (Fig. X-1). The decrease in resistance between 7 and 10 P.S.T. on 31 July is more difficult to explain but may be exaggerated by the error in determining r_s in the early morning when E is very small.

Fig. 2 compares the observed evaporation rate with values calculated from equations (5) and (9) using the hourly values of r_s in Table X-1. Fortunately, on the morning of the 31st when equation (9) is invalid because the air was very unstable, the Bowen ratio is close enough to γ/Δ to make the value of E insensitive to error in r_a and r_a'. Hence the calculated evaporation agrees excellently with observation throughout the period. In practice, the diurnal variation of stomatal resistance will not be known a priori but the evaporation rate can still be calculated with tolerable accuracy if the mean stomatal resistance is known. For the 24-hour period beginning 1400 on 30 July, the weighted mean value of the stomatal resistance was $\Sigma r_s E/\Sigma^E = 0.7$ sec/cm. When this constant value was used in equation (5), evaporation was underestimated in the afternoon, but integrating over a day the error in total evaporation was negligible and Table X-2 shows close agreement between observed evaporation and values calculated from hourly or mean values of stomatal resistance.

Analysis of other data

For 29 May and 1 June 1960, analysed in detail in previous reports, [Pruitt (1962)] diurnal variation of r_s was calculated from equation (5) using measured values of evaporation rate, saturation deficit, temperature, and wind speed. Figure X-1 shows that although the diurnal pattern of r_s repeated the pattern of 1962, the resistance was much larger on 1 June than three days previously. This increase could be ascribed to increasing soil moisture deficit but it is probably more significant that 1 June was an "advection" day with hot dry winds of 6-7 m/sec creating a very large potential evaporation rate which the grass was unable to meet.

At much smaller evaporation rates, Makkink (1956) in the Netherlands found that for a given soil moisture deficit, the actual rate of evaporation for grass increased less rapidly than the potential rate, presumably because

moisture stress within the plants induced stomatal closure. Despite the relatively high stomatal resistance, the evaporation on 1 June was the largest observed over a period of almost 4 years.

A similar analysis for 21 March and 23 September 1961 was only partly successful, probably because the wind was so light that it was impossible to allow properly for instability and for the large increase of roughness at low wind speeds reported by Monteith (1963) for a similar surface. For these two days, values given in Table X-3 were obtained from equation (6) when the Bowen ratio was approximately γ/Δ.

Table X-2 suggests that the stomatal resistance of grass on the experimental field may vary between a minimum of about 0.4 sec/cm and a maximum of 0.9 sec/cm or more depending on reserves of soil moisture and on the potential evaporation rate. Although the resistance on 23 September seems to be unaffected by cutting on the 20th, shock closure of stomata or diminished leaf area after cutting might increase the resistance for several days and cause differences of evaporation between different lysimeters. This may explain some of the anomalies in the downwind variation of the evaporation rate examined in the Second Report because most of the analysis covers the five days after cutting on 27 October 1961.

Annual evaporation

Equation (5) can be used to estimate seasonal changes of evaporation rate assuming that evaporation is confined to hours of daylight. Small amounts of evaporation are observed on dry windy nights when water vapour diffuses through incompletely closed stomata and through leaf cuticles; but on calm, clear nights, the surface gains moisture by condensation. In most months, the net moisture exchange at night is probably two orders of magnitude below daytime evaporation. Assuming further that wind speed is uncorrelated with temperature and saturation, daily evaporation may be calculated from daily means $\overline{R}$, $\overline{T}$, $\overline{X}$, and r_a in equation (5), multiplying the saturation deficit $\left(X^*(\overline{T}) - \overline{X}\right)$ by the number of hours of daylight.

Net radiation and wind speed in 1960 were available for Davis and mean daytime air and dew-point temperatures at 5 feet were taken from published records for Sacramento airport. (The mean 1000 PST screen temperatures at Sacramento and Davis are usually the same within 1°C.) The seasonal variation of evaporation at Davis in 1960 was then calculated for a surface with a roughness of 2.3 cm and stomatal resistances of 0.4

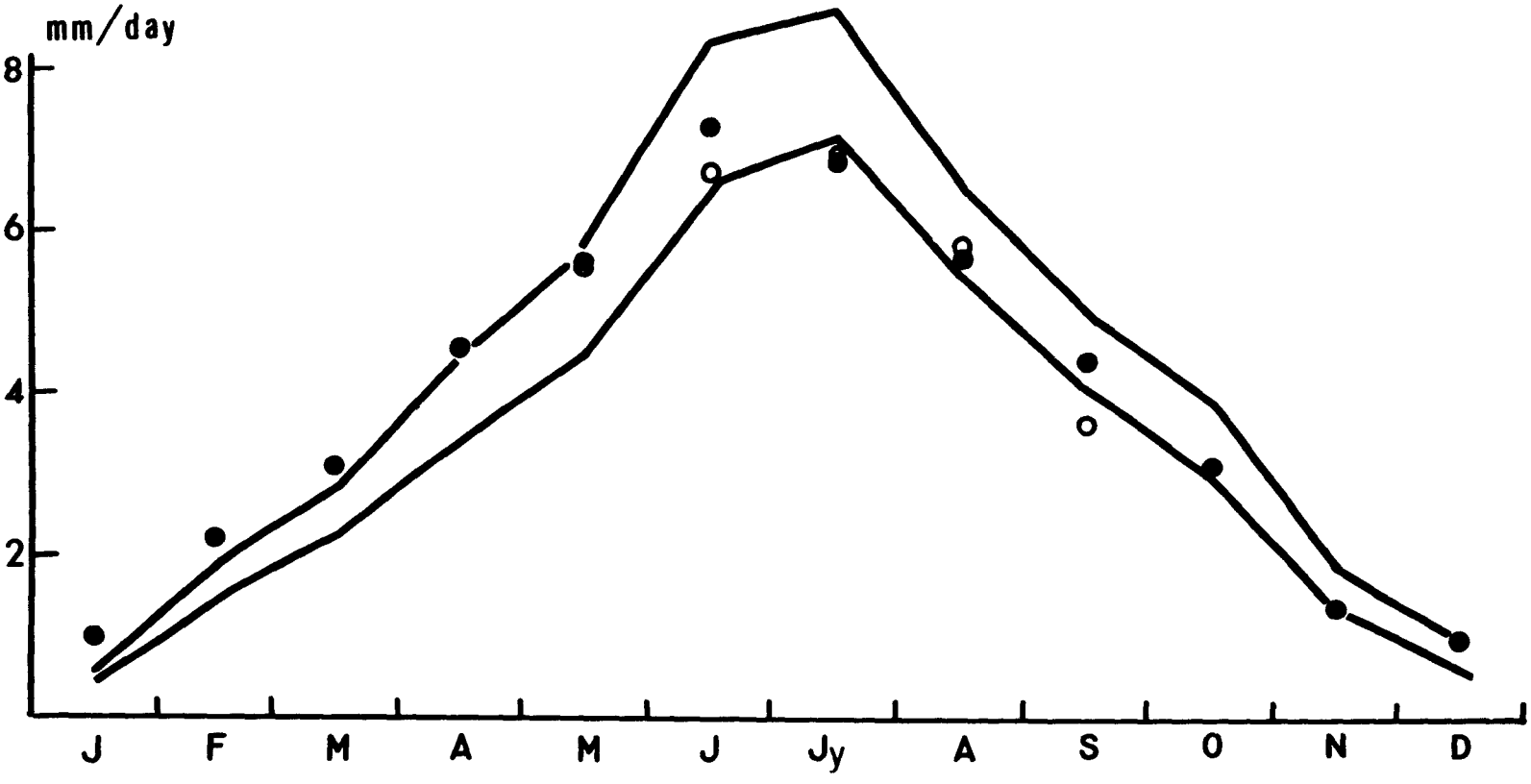

Figure X-3. Seasonal variation of grass evaporation at Davis, 1960

Upper curve from equation (5) with r_s = 0.4 sec/cm

Lower curve from equation (5) with r_s = 0.8 sec/cm

● recorded by 20 foot lysimeter

O water use by irrigated alfalfa (Veihmeyer)

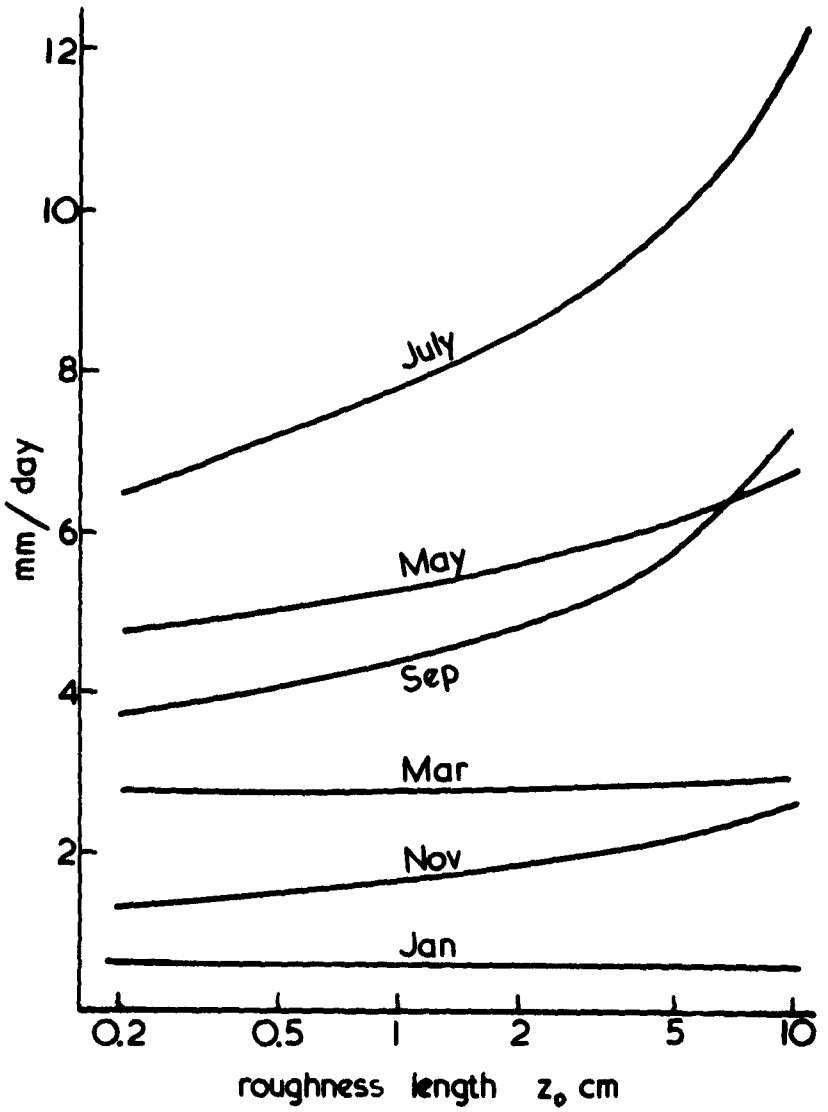

Figure X-4. Evaporation at Davis in 1960 as function of surface roughness assuming r_s = 0.4 sec/cm and same weather at 2 m above zero plane of all surfaces.

and 0.8 sec/cm (Fig. X-3). Evaporation measured with the 20 foot lysimeter agrees well with estimates for $r_s \approx 0.4$ from January to May and for $r_s = 0.8$ sec/cm from June to December. There are at least two possible reasons for this increase of resistance. From June to October the grass was cut (and irrigated) about every 10 days and regrowth between cuts during the hotter summer months may have been too slow for stomatal resistance to reach a smaller value. However, the larger resistance from June onwards may be a response to very high rates of evaporation imposing a severe water stress even on vegetation that is frequently irrigated.

Measurements reported by Halkias, Veihmeyer, and Hendrichson (1955) of summer evaporation from alfalfa (open circles, Fig. X-3) agree with estimates for $r_s = 0.8$ sec/cm but the resistance could probably have been smaller if periods immediately after cutting had been excluded from the analysis.

Change of evaporation with roughness

Assuming that $r_s = 0.4$ represents a minimum value of stomatal resistance for most mesophytes, monthly evaporation rates at Davis were calculated for roughnesses between 0.2 cm (e.g. mown grass) and 10 cm (e.g. maize) (Fig. 4). The change of evaporation rate with roughness depends on the difference between daily mean values of $C/\lambda E$ and γ/Δ. When the two quantities are almost equal as in January and March, evaporation is almost independent of r_a and hence of windspeed and roughness, but as the saturation deficit increases later in the year, γ/Δ exceeds $C/\lambda E$ and evaporation rate increases with roughness. For z_o between 1 and 5 cm, representing most common agricultural crops, the largest absolute variation in evaporation rate is ±1.1 mm/day about a mean of 8.9 mm/day in July. In a more humid, maritime climate, the Bowen ratio will be larger during the summer and changes with crop evaporation with roughness smaller than those of Fig. X-4. This is consistent with field experience reviewed by Penman (1963) that when crops with different height and structure are grown in the same climate, differences in evaporation rate are small.

Conclusions

Many features of evaporation at Davis described in previous reports can be explained in terms of diffusive resistances and the Penman formula. For example, the loops found when λE is plotted against R either on a daily

or on a seasonal basis are predicted by equation (5) because the two terms in the denominator are out of phase. The ratio of the aerodynamic term to the radiative term increases during the day and during the year and if stomatal resistance remained constant, instead of increasing towards the end of the day and during summer and autumn, the arms of each loop would be even more widely separated. Similarly, a failure to estimate evaporation assuming that surface air is saturated can be explained by the very low surface humidites in Table X-1. This assumption of surface saturation is one of the weakest features of current analytical attacks on the advection of hot, dry air over irrigated vegetation. More realistic solutions await the incorporation of a stomatal parameter, recognizing that the physiological behaviour of plant surfaces may control evaporation, even when soil moisture is maintained by frequent rainfall or irrigation.

Acknowledgements

I should like to thank Dr. F. A. Brooks, Mr. W. O. Pruitt, Dr. H. B. Schultz and staff of the Signal Corps Project for providing material for this analysis, for many fruitful discussions, and for their friendship during my short stay in Davis.

TABLE X-1

MEAN HOURLY RESISTANCES, SURFACE HUMIDITY, AND EVAPORATION RATES 30-31 JULY 1962

TOTALS FOR 31 JULY ONLY

TIME P.S.T. centre of hour	RESISTANCES (sec/cm x 10^2) $r_a' = \frac{\rho c_p (T_o - T)}{C}$	$r_a = \frac{\chi_o - \chi}{E}$	$r_a = \frac{\left[\ln \frac{z}{2.3}\right]^2}{k^2 u}$	r_s	SURFACE HUMIDITY (per cent) $\frac{\chi_o}{\chi^*(T_o)}$	EVAPORATION (mm/hr x 10^2) measured	eqn. (8) $z_o = 2.3$	eqn. (5) $z_o = 2.3$ r_s column 4	eqn. (6) $z_o = 2.3$ $r_s = 80$
30 July									
1400	--	32	33	62	54	78	76	76	69
1500	22	26	26	73	49	71	71	72	69
1600	23	27	24	87	49	55	63	59	62
1800	22	35	28	133	62	22	28	23	31
1900	30	40	42	350	65	7	7	6	14
2000	35	32	43	510	74	3	2	2	8
31 July									
0700	24	71	85	150	72	10	8	12	15
1000	30	55	99	64	66	50	27	51	49
1100	25	42	62	61	61	64	43	62	57
1200	22	32	43	61	57	72	54	70	63
1300	22	30	35	61	52	79	67	76	68
1400	--	29	28	71	50	78	82	78	73
1500	10	16	26	88	42	72	47	68	71
1600	13	28	26	95	48	55	57	54	59
1700	12	26	25	116	50	38	39	37	45
1800	22	36	37	206	51	20	20	18	31
						538	444	526	531

TABLE X-2

STOMATAL RESISTANCE AND RELEVANT DATA ON SELECTED DAYS

Date	Minimum r_s sec/cm	Mean Wind (u) m/sec	Approx. Moisture Deficit (cm)[1]	Previous Cutting	Previous Irrigation
29 May 1960	0.4	2.4	2.9	4 May	20 May[2]
1 June 1960	0.9	7.0	5.3	31 May	20 May[2]
21 March 1961	0.5	1.6	1.5	13 Mar.	Previous Fall[3]
23 Sept. 1961	0.4	1.1	4.5	20 Sept.	12 Sept.
31 July 1962	0.6	3.5	4.5	25 July	23 July

1/ Calculated for the upper 45 cm of soil at noon. The available moisture in this zone is about 7.5 cm. On 29 May and 1 June it may be of significance that the lower 45 cm of soil was at the wilting point due to a failure of two previous irrigations to re-wet this zone following a severe dry-down run ending on May 9.

2/ A 1.5 cm rain fell on 23-24 May.

3/ Heavy rains on 15 March brought the upper 75 cm of the soil profile to field capacity. Light rain on 19 March re-wet the surface again.

REFERENCES

Covey, W. (1959) Testing a hypothesis concerning the quantitative dependence of evapotranspiration on availability of moisture. M. Sc. Thesis, Agricultural and Mechanical College of Texas.

Halkias, N. A., Veihmeyer, F. J. and Hendrickson, A. H. (1955) Determining water needs from climatic data. Hilgardia 24:9 pp. 207-233.

Makkink, G. F. and van Heemst, H. D. J. (1956) The actual evapotranspiration as a function of the potential evapotranspiration and the soil moisture tension. Neth. J. Agrig. Sci., 4 pp. 67-72.

Monteith, J. L. (1963) Gas exchange in plant communities. Proceedings of Canberra Symposium on Environmental Control of Plant Growth, New York, Academic Press (in the press).

Penman, H. L. (1953) The physical basis of irrigation control. Rpt. 13th Int. Hort. Congr. 2, pp. 913-914.

Penman, H. L. (1963) Vegetation and Hydrology. Technical Communication No. 53, Commonwealth Bureau of Soils, Harpenden.

Pruitt, W. O. (1962) Diurnal and seasonal variations in the relationship between evapotranspiration and radiation. Chapter II, Second Annual Report, USAEPG Contract No. DA-36-039-SC-80334. pp. 27-45.

CHAPTER XI

RESISTANCE TO WATER LOSS FROM PLANTS

Mervyn J. Aston

INTRODUCTION

The need for the inclusion of a plant factor, in evapotranspiration studies, has long been known. However, attempts to use a unique plant correction value have met with little success, particularly in short term observations.

Micrometeorologists, concerned mainly with what occurs above the plant, usually ignore the plant and the effects it may have in limiting, or assisting the flow of water from the soil to the atmosphere. There has, therefore, been a great need for studies concerned with the effect of this organism on water loss from the soil surface and from a crop cover.

Water flow from soil to atmosphere can descriptively be considered in three phases, viz.

1. Through the soil to the plant root,
2. Into the plant root and through the plant to the atmosphere, and
3. Movement in the atmosphere away from the plant.

The second phase will be the only one considered in this report, although some attempt is made at correlating the observed plant variables with changes in the surrounding environment. Flow within the plant can be considered as being through the roots, stem, and leaves the latter being considered in the fluid phase within the leaf tissues, and gaseous phase from within the substomatal cavity to the atmosphere. There has been considerable argument and discussion as to the relative resistances offered to water flow in different parts of the plant (Van den Honert 1948, Allerup 1960, Brouwer 1961) however it is beyond the scope of these observations to consider each separately.

Assuming the effect of root pressure on transpiration and water flow through the plant to be relatively small*, it can be considered that the main force for water movement through the plant is situated at the cell wall surfaces in the substomatal cavity (Levitt 1956). The forces causing flow

* This may quite well be an erroneous assumption, but laboratory experiments by Vaadia and Aston (unpub. data) indicate the assumption to be correct. The interpretation of principles is, however, not greatly affected even if this assumption were not true.

furthermore could be expected to be influenced by the conditions which exist between the leaf and the surrounding environment. Therefore, we can consider the flow of water through the plant from soil to atmosphere in analogous terms to the flow of electricity and Ohms law, i.e.

$$E = \frac{\Delta P}{R}$$

where E = evaporation loss (gm. sec^{-1}. cm^{-2})
ΔP = potential difference
R = resistance to flow

In this form, it can be seen that water flow through the plant, with its consequent loss as evaporation is affected by the gradient inducing flow, and the resistances to this flow imposed by the plant. It is not necessary to specify where these resistances exist, whether they are in the roots, leaves, or stomates, they may be considered in total as affecting flow through the whole plant.

In these studies the ΔP gradient has been expressed as an absolute moisture gradient rather than a vapor pressure gradient. In this case

$$E = \frac{x_1 - x_2}{R}$$

or

$$R = \frac{x_1 \quad x_2}{E}$$

where x_1, x_2, are the absolute water contents in $gm.cm^{-3}$. In this case R has the units of $sec.cm^{-1}$.

The gradient for water loss has been considered as being between the cell surfaces of the sub stomatal chamber and the surrounding air. For the purpose of the studies it has been assumed that saturation exists at these surfaces, and the x value then is that for saturation at the temperature of the leaf. Therefore, (x_1 - x_2) is (x(T) Leaf - x Air). In order to remove the obvious effect of leaf area variations on the resistance, the evaporation values are expressed for each square centimeter of leaf surface.

Considering flow through the plant in this manner does, however, neglect the effects of the very thin air layer which exists around each leaf. It has been shown that resistance to flow through this layer is high (Van den

Honert 1948, Kuiper 1961) and may constitute a major portion of the resistance values calculated in the above manner. Ideally, therefore, the x air value should be measured at an infinitessimally small distance outside the stomates. This, of course, is not possible. An estimate of the resistance within this layer, and in the surrounding mass of air can be obtained by considering a wet surface essentially free from internal resistances, in which case the resistance present is due to the surrounding air layers. In this case -

$$R_{plant} = R_{total} = R_{air}$$

i.e.

$$R_{plant} = \left(\frac{x \text{ leaf} - x \text{ air}}{E \text{ plant}} \right) - \left(\frac{x \text{ wet surf.} - x \text{ air}}{E \text{ wet surface}} \right)$$

Ideally the wet surface should be physically similar to the leaf as close as possible.

METHODS

The studies were carried out on a perennial ryegrass sward, (Lolium perenne), the 20 ft. weighing lysimeter being used for the measurement of water loss. Sward leaf areas were measured by means of an airflow planimeter (Jenkins 1959). Leaf temperatures were measured with copper-constantan thermocouples, made from 40 gauge wires, inserted into the leaf. Wet and dry air temperature measurements were made with wet and dry 20 gauge copper-constantan thermocouples which were shaded and aspirated at an air velocity of 900 feet per minute. A black atmometer mounted within the sward was used as the wet surface for R_{air} calculations. The surface temperature of the bulb was measured with the fine thermocouples. In order to correlate the surface occurences with variation in the air mass above the grass, use was made of the calculated resistance in the air above the award, calculated by Monteith's (1962) method. Assuming that the transfer conditions of water vapor and momentum are equal under conditions of stability and that the vertical fluxes are constant with height, he shows that:

$$Ea = \frac{u\, k^2 (x - x_o)}{[\ln((z-d) / zo)]^2}$$

where k(0.41) is von Karmen's constant, x and u (windspeed) are measured at height Z, and x_o is the surface vapor concentration. Zo is the roughness parameter and d is the zero plane displacement.

Considering $R_A = \frac{(x - xo)}{Ea}$

and introducing a correction for air stability, then

$$RA = \frac{\left[\ln\left(\frac{Z - d}{Zo}\right)\right]^2}{uk^2 (1 - oRi)}$$

where Ri is the Richardson Number given by

$$Ri = \frac{g \, \partial t / \partial Z}{T (\partial u / \partial z)^2}$$

T is the absolute temperature, and σ is a constant determined empirically, here taken to be equal to 10. Ri was measured between 100 and 25 cm and u at 100 cms. The units of RA are based on the square area of ground surface and hence are not the same as those of R_{air} or R_{plant}, but variations in RA may be correlated with those of R_{air} and R_{plant}.

RESULTS AND DISCUSSION

To date complete results have been obtained for only two and a half days and consequently it is difficult to draw conclusions from the data.

Although the net radiation level for 31 August 1962 was lower than 30/31 July 1962 the resulting leaf and air temperatures were 3-4 deg C higher on the former day (Figure XI-1 a-b). This phenomenon is most likely due to the wind conditions prevalent on these days (Figure XI-1 a-b). During 30/31 July the wind increased during the day to 4 meters per sec., completely dying down in the evening. During 31 August the wind was essentially calm at about 1 meter per second. Richardson numbers for these periods demonstrate the wind effect, and during the July days varies little, while a wide variation of Richardson number on 31 August shows a dependence almost entirely on the prevailing temperature gradients. (cf Table III-6).

The plant resistances and sward air resistances are shown in Figures XI-2a, b, c. Here the effect of the light wind can be seen to decrease the resistance of the sward air from around 2.5-3 to 0.5-1. The plant values

on both days are approximately the same. The plant resistance values show no correlation with conditions in the air layers above the ground which certainly indicates that the plant is exerting a separate and independent influence on water loss.

During both July days the plant resistance values were higher than those for the surrounding air. The sudden rise in resistance towards sunset, appears to be correlated with a corresponding rise in the RA (Figure XI-2) values at that time. There is, however, a possibility that part of this resistance rise may be associated with stomatal closure around sunset, this causing a restricted flow while the potential gradient for vapor flow is still reasonably high. There appears to be a gradual increase in resistance during the day, which would be expected as tensions within the plant increase. A similar increase in resistance throughout the day has been shown for beans and long grass in English studies (Monteith 1962) approaching this problem from a micrometerological viewpoint (cf Chapter X).

The resistance values for 31 August are more difficult to interpret. On this day the R_{air} values are greater than R_{plant} indicating that the main controlling resistance to water flow is in the surrounding air. It is, however, interesting to note that the two resistance values behave oppositely to each other, viz as R_{air} increases, R_{plant} decreases and vice versa. These results could be interpreted as meaning the controlling resistance is in the surrounding air with the plant resistance having an almost equal effect. As R_{air} decreases the influence of the plant increases and it exerts a greater influence on water flow, as R_{air} increases, this control becomes less and consequently R_{plant} decreases.

In general it is hard to draw any firm conclusions, but there certainly appears to be an independent plant effect in controlling water loss. There would appear to exist, a balance between the resistance to flow offered by the surrounding air layers, and the plant. Under conditions of low potential gradient, for water loss and poor atmospheric vapor transfer the resistance is primarily in the air layers, but as the potential gradient increases and transfer in the surrounding air layers increases the influence of the plant becomes significant.

The use of a black atmometer bulb as a wet surface is subject to criticism, because of its bulk, colour, shape and inflexibility. In future

studies, small evaporimeters made from green blotting paper strips will be used in an attempt to approach sward conditions. The results obtained from the bulbs in these two studies do, however, indicate that they give good relative measurements.

It is intended to continue these studies throughout the year with additional instrumentation and measurements of internal water status of the plant. Laboratory experiments have also been designed with the aim of defining the specific areas of resistance within the plant, and to assessing the effect of individual environmental factors.

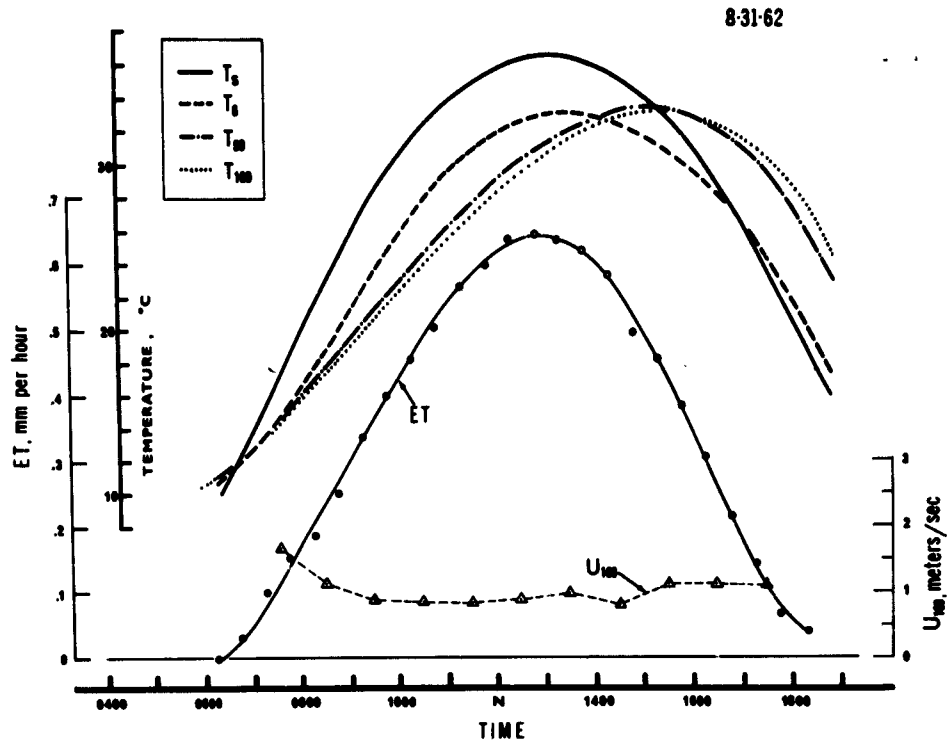

Figure XI-1a. Daily fluctuations of evapotranspiration, 100 cm wind speed (U100), leaf temperature (T_s), air temperature within the sward (T_6), at 50 cm height (T_{50}), and 100 cm height (T_{100}).

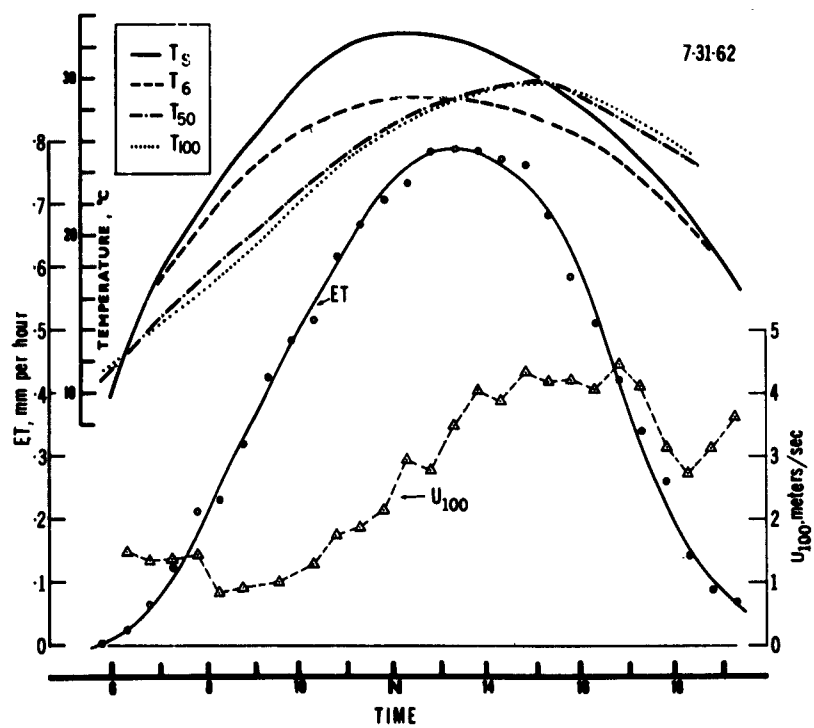

Figure XI-1b. Daily fluctuations of evapotranspiration, 100 cm wind speed (U100), leaf temperature (T_s), air temperature within the sward (T_6), at 50 cm height (T_{50}), and 100 cm height (T_{100}).

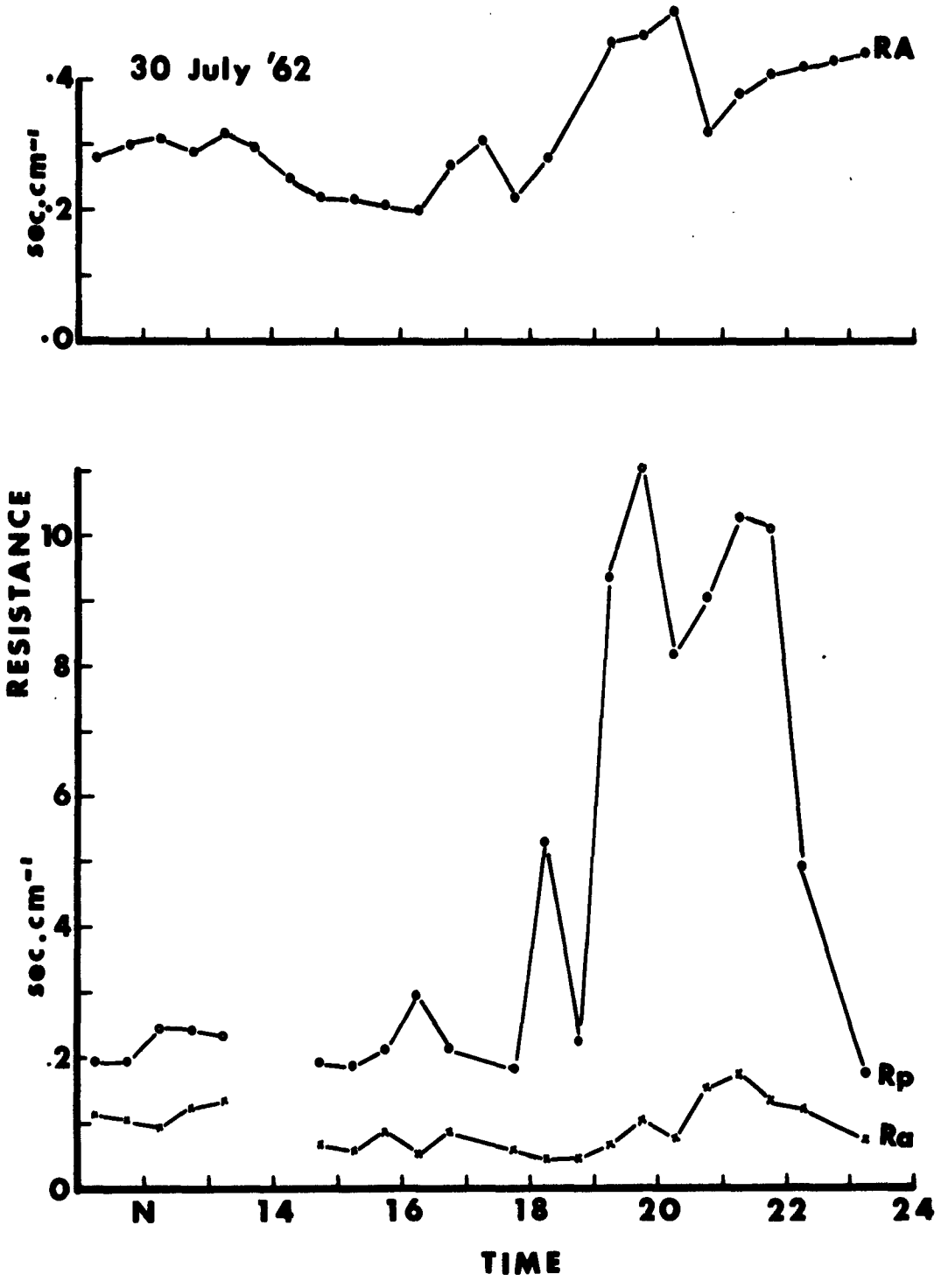

Figure XI-2a. Daily fluctuations of plant resistance (R_p - sec. cm^{-1} cm^{-2} leaf surface), resistance of surrounding air (Ra - sec. cm^{-1} cm^{-2} bulb surface, resistance of air (after Monteith 1962) above sward (RA - sec. cm^{-1} cm^{-2} ground area).

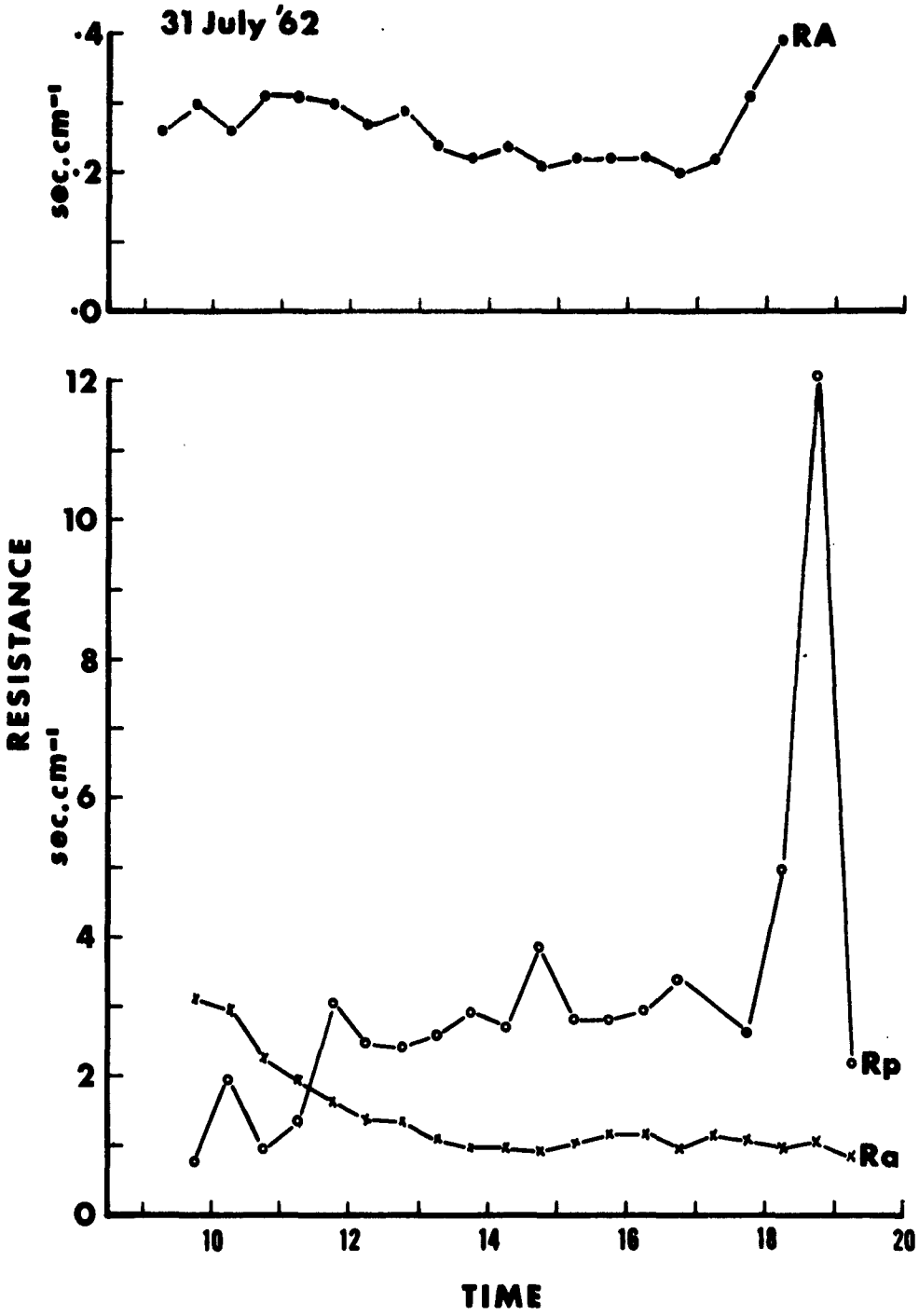

Figure XI-2b. Daily fluctuations of plant resistance (R_p - sec. cm^{-1} cm^{-2} leaf surface), resistance of surrounding air (Ra - sec. cm^{-1} cm^{-2} bulb surface), resistance of air (after Monteith 1962) above sward (RA - sec. cm^{-1} cm^{-2} ground area).

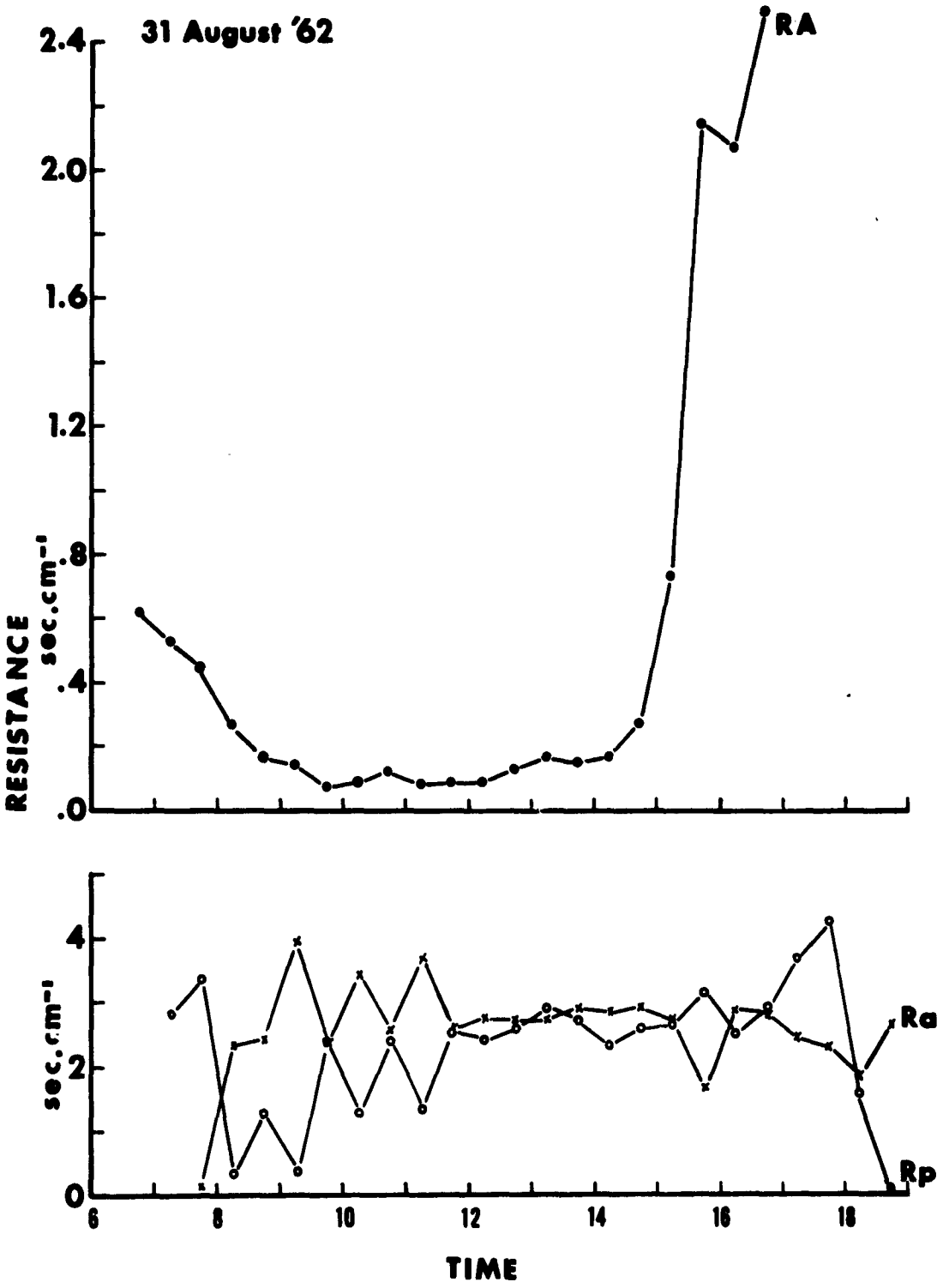

Figure XI-2c. Daily fluctuations of plant resistance (R_p - sec. cm^{-1} cm^{-2} leaf surface), resistance of surrounding air (Ra - sec. cm^{-1} cm^{-2} bulb surface), resistance of air (after Monteith 1962) above sward (RA - sec. cm^{-1} cm^{-2} ground area).

LITERATURE CITED

Allerup, S. 1960. Transpiration Changes and Stomatal Movements in Young Barley Plants. Physiol. Plant V. 13 (1):112-19.

Brouwer, R. 1961. Water Transport Through the Plant. JAARB I.B.S. Meded 150:11-24.

Van den Honert, T. H. 1948. Water Transport in Plants as a Catenary Process Faraday Soc. Disc. No. 3:146-53.

Jenkins, H. V. 1959. An Airflow Planimeter for Measuring the Area of Detached Leaves. Plant Physiol. V. 34 (5):532-6.

Kuiper, P.J.C. 1961. The Effects of Environmental Factors on the Transpiration of Leaves, with Special Reference to Stomatal Light Response. Meded Landbouwhogeschool Wageningen V. 61 (7):1-94.

Levitt, J. 1956. The Physical Nature of Transpiration Pull. Plant Physiol. V. 31:248-51.

Monteith, J. L. 1962. Gas Exchange in Plant Communities. Paper presented at Canberra Symposium on Controlled Environment.

CHAPTER XII

MOVEMENT AND DISTRIBUTION OF THO IN TISSUE WATER AND VAPOR TRANSPIRED BY SHOOTS OF HELIANTHUS AND NICOTIANA

Franklin Raney and Yoash Vaadia[1/]

INTRODUCTION

We recently reported (8) on the use of THO-enriched water (tritiated water) as a tracer of water movement in the roots of sunflowers in the presence and absence of transpiration. Subsequent studies reported here relate to the use of THO for appraising the pattern of movement and distribution of THO in sunflower and tobacco stems and leaves, and their transpired water vapor.

METHODS

The plants used were grown and selected in the manner reported previously (8).

Measurement of THO in Shoot Tissues

Influx and efflux of THO was followed in intact 30-day-old sunflower (*Helianthus annuus*) plants raised from seed in tritiated nutrient solution (THO-grown plants) and in plants raised from seed in water without added tritium (HHO-grown plants). In addition, influx and efflux of THO were traced in detached shoots of THO-grown plants cut beneath the surface of the THO solution.

At harvest, stem segments, the first- and second-order leaf veins, and the residual leaf-blade material between the second-order veins (hereafter referred to as mesophyll) were analyzed for tritium.

When an intact plant was being studied, the root system was blotted with filter paper and the leaves were removed at the stem end of the petiole with a razor blade. The petioles were then severed at the base of the leaf blade. The entire stem and attached root system was then segmented into 2-cm pieces with one stroke of a multibladed knife with the outside blade positioned at the cotyledonary node. The leaf blades were then dissected with a sharp razor blade to separate the midvein and the first-order lateral veins from the mesophyll, which of course contained numerous

1/ Present address: Department of Plant Physiology, Arid Zone Research Institute, Beersheva, Israel.

higher-order veinlets. Immediately after stem segmentation and leaf dissection, the tissue was stored in tightly-corked cylindrical (15 x 45 mm) vials. The vials of tissue were then frozen in dry ice for storage. This entire process required about five minutes.

McDermott (7) observed that in some cases the water content of plant tissues depends on the method used for cutting the tissue. One trial was therefore made to determine the effect of cutting technique on the amount of tritium in the water of plants exposed to a THO solution in the light for 6 hours. Leaves were dissected under three conditions: 1) after the petiole was severed at the base of the blade; 2) with the leaf still attached to the stem; and 3) with the leaf frozen on a block of dry ice and dissected while still frozen. Since tritium content was not affected by the cutting condition, the multibladed dissection system was considered to be reliable.

Measurement of THO in Transpired Vapor

Fully grown 80-day-old flowering tobacco plants (*Nicotiana rustica*) that had been raised on tritiated nutrient solutions were sealed in a 9-liter glass chamber and supplied with 800 ft-c of incandescent light. Air, pre-dried with three dry-ice freeze-out fingers and two P_2O_5 columns, was coursed through the chamber at various speeds and periods. The transpired water vapor was captured periodically by passing the outgoing current of moist air through a series of freeze-out tubes submerged in dry ice. THO contents were determined for the transpired vapor, the rooting medium, and the leaf-tissue water. In one experiment, the transpiration rate was automatically recorded with an infrared hygrometer and the THO activity of transpired vapor was measured by capturing the vapor as before.

Influx of THO Vapor into Intact Plants

Leaf guttation occurred during initial experiments when 7-day-old sunflower seedlings were transferred from the germinating medium to tritiated nutrient solution. Since guttating plants of the same age were growing adjacently in non-tritiated nutrient solution, this was an opportunity to observe whether THO vapor in the air would appear in the guttation water or in the tissues of the plants guttating from non-tritiated solution. Some absorption of THO did occur (Figure 1), the guttation water from HHO-grown seedlings increasing in THO activity. Either the tritium was moving root-ward from the cotyledon, or the hypocotyl itself was absorbing THO.

However, no gain in THO was detected in the roots or nutrient solution in 48 hours. Consequently, the ventilation rate of the chamber where the plants were transpiring tritium was increased so that the THO vapor would be removed more efficiently.

RESULTS

Movement of THO in Shoot Tissues

In general, the pattern of influx and efflux of THO in comparable tissues (stem, Figure XII-2; veins, Figure XII-3; mesophyll, Figure XII-4) was similar regardless of whether or not the shoot was attached to the root system.

Both influx and efflux were slower for the apical stem segment (25 cm above the cotyledonary node; Figure XII-2) than for the segment at 8 cm, just above the node bearing the first true leaves, and THO was not completely lost from the apical segment by 24 hours. The segment at 8 cm effluxed completely in about 4 hours, as did the veins (Figure XII-3).

Figures XII-2, XII-3, and XII-4 show that the lag in THO movement between the bottom of the shoot (8 cm) and the top of the shoot (24 cm) was greatest in the stem tissues. This lag was also by far the greatest in THO-grown shoots whose roots had been removed before efflux and reinflux of THO (Figure XII-2) had occurred. From Figure XII-5 can be gained an idea of the rate of equilibration of stem tissues in an HHO-grown sunflower influxing THO.

The pattern of THO influx and efflux in the stem and leaf veins was strikingly similar in both THO-grown and HHO-grown intact plants (Figures XII-2 and XII-3). The influx pattern for leaf veins (Figure XII-3) was similar for leaves at both the 8- and 24-cm level on the plant, and approached completion in one light-dark cycle.

Mesophyll tissue (Figure XII-4) reached only 55 to 80% of solution THO activity (C/C_o = 0.55 to 0.80) even after the plant had been grown in THO from seed to an age of 30 days. THO reinflux differed markedly in pattern from the preceding efflux from the leaf. The efflux of THO from the mesophyll in the basal (8 cm) set of true leaves did resemble the efflux of the apical (24 cm) set of true leaves. However, after 24 hours, reinflux of THO into these leaves was asymptotic to a value of C/C_o = 0.5 rather than to the value 0.80, from which the initial efflux began.

In HHO-grown plants (Figure XII-4), the water in the mesophyll tissue equilibrated at nearly the same rate in both the oldest (8 cm) and the youngest leaves (24 cm), in 24 hours asymptotically approaching a value of 55% of equality with the external solution. A longer study of HHO-grown plants (Figure XII-6) showed that the radioactivity of whole-leaf tissue (veins plus mesophyll) did not exceed 75% of external activity even after eight days with the roots in tritiated water.

Since there is always the possibility that these results may depend in both pattern and absolute values on the kind of plant studied, distribution of THO was examined in tobacco plants raised for 80 days in tritiated Hoagland solution. At analysis the plants were setting seed. The data (Figure XII-7) show that the various tissues departed to differing degrees from equality with the THO of the external solution:

1) Stem tissue of tobacco equilibrated at about 97%, veins at 92%, and mesophyll at 62% (much like in sunflower).
2) In tobacco, as in sunflower, the youngest stem tissues tended to fall shorter of equality with the external medium than did the older stem tissues.

In addition, at various levels in the plant there was distinctly more THO in the mesophyll of the leaf than in the leaf tip (Figure XII-8).

Efflux of THO in Transpired Water Vapor

The tritium content of water vapor transpired by Helianthus and Nicotiana enclosed in sealed chambers and served by a stream of dry incoming air is of great interest (Figure XII-9).

The THO content of leaf tissue was sampled only at the beginning and the end of the period over which the THO content of the transpired vapor was measured. Nevertheless, although the hour-by-hour THO content of the leaf water is not known, the concentration in leaf tissue rose over a twelve-hour period (in light) from 65 to 95% of the tritium concentration in the Hoagland solution bathing the roots.

During the same period, the THO content of the transpired water vapor rose from a value below that of the leaf-tissue water, matched the initial THO content of the leaf water after about four hours had elapsed, and for the remaining eight hours rose steadily to reach a value of 95%, equal to that in the leaf-tissue water.

During the entire period of 12 hours, the rate of transpiration, measured by an infrared hygrometer, declined as the THO content of the leaf tissue and the THO content of the transpired vapor continued to increase.

Flow rate and the THO activity of transpired water were correlated inversely (Figure XII-10).

Entry of Atmospheric Vapor into Leaves

The fact that the THO in tissue does attain the external concentration when the shoot is exposed to predried air suggests that the exchange of water molecules between atmospheric vapor and tissue water can be considerable in an open system. Figures XII-11 and XII-12 present data on the exchange of water between the leaf and its environment. Figure XII-11 presents a long record of THO absorption from the atmosphere by HHO-grown plants growing adjacent to THO-grown plants. The THO in the atmosphere came from the vapor transpired by THO-grown plants and by direct evaporation from the nutrient solution. The concentration of THO in the atmospheric vapor was not measured, but because of high ventilation rates must have been very low. However, the results show that THO did enter the HHO-grown plants and was most concentrated in the cotyledons and leaves, where vapor exchange would be expected to take place. Other organs usually contained much less THO.

Figure XII-12 characterizes THO concentrations in excised leaves of THO-grown plants during equilibration with a saturated HHO atmosphere at 20°C in diffuse laboratory light. Whole leaves lost THO to an HHO atmosphere rapidly, with a half-time of about three hours. The veins tended to lag behind the mesophyll a little, but the entire leaf had completely lost its THO content before 24 hours had elapsed.

DISCUSSION

The lower, mature stem internodes of the leaf veins of sunflower gained and lost THO in a pattern the same as the leaf veins and reached equality with the external THO solution in one 24-hour period (Figures XII-2 and XII-3). This tends to contradict the existence in the stem of a sizable fraction of water that is inaccessible for long-term turnover. These stem tissues exhibited an initial rapid phase in THO intake requiring three hours for an intact transpiring Helianthus plant. This state reached 90 to 100% of external

concentration of THO and may have involved all of the apoplast as well as the amorphous regions of the cellulose macro-molecules. The steepness of the flux curves for this first phase suggests that the pathways for water movement in the stem are of large size, with little net tortuosity, and that radial dispersion of the tracer is rapid.

Interpretation of the data from leaf tissues, young stem tissues, and veins in young leaves is more complicated. As noted earlier, leaf tissues did not equilibrate with external THO concentration even over extended periods. This observation has been made previouly by other workers (1, 2, 4, 10). Biddulph et al. (1) attributed this to direct flux of the transpiration stream from the xylem to the surrounding atmosphere, with little mixing in the mesophyll. However, they did not analyze the transpired vapor for THO. Their contention that a considerable fraction of water in the leaf did not exchange was not experimentally supported.

Our studies of vapor transfer between atmospheric water and the leaf tissue (Figures XII-11, XII-12) show that the lack of equilibration of the leaf tissue results from a dilution of THO in the leaf with unlabeled atmospheric vapor.

Transpiration is known to be proportional to the difference in vapor pressure between the leaf and the atmosphere (6). As in any other diffusion process, the net transpiration rate (T) represents the difference between outward diffusion (d_1) and inward diffusion (d_2). Each component is proportional to the vapor pressure at its source. Therefore, transpiration is predicted by:

$$T = d_1 - d_2 = \frac{P_1 - P_2}{R} \tag{1}$$

where P_1 and P_2 are respectively the vapor pressures in the leaf and the atmosphere (at the two ends of the diffusion path) and R is the resistance of the path, assuming a proportionality constant that is identical regardless of the direction of diffusion.

Under steady-state conditions, when transpiration equals absorption the leaf THO concentration does not vary with time, the following relation holds:

$$(d_1 - d_2)\, C_o = d_1\, C_1 - d_2\, C_2 \tag{2}$$

where C_o, C_1, and C_2 are respectively the THO concentrations in the external solution, the leaf, and the atmospheric vapor. Since ventilation is continuous in these experiments, C_2 is very small. Thus, neglecting C_2 and rearranging equation (2):

$$\frac{C_1}{C_o} = 1 - \frac{d_2}{d_1} \tag{3}$$

Since $d_1 = P_1$ and $d_2 = P_2$, equation (3) can be rewritten as

$$\frac{C_1}{C_o} = 1 - \frac{P_2}{P_1} \tag{4}$$

where P_2 is the vapor pressure of the atmosphere and P_1 is the vapor pressure of the tissue water.

If P_1 is assumed to be the saturation vapor pressure under isothermal conditions, P_2/P_1 represents the relative humidity. According to equation (4), when the environmental relative humidity is 50%, as in our experiments, C/C_o for THO at steady state in the leaf tissue should be about 0.5, somewhat lower than our results. However, since the ventilation of transpired THO was not quite complete (as evidenced by some entry of THO from transpired vapor into leaves of HHO-grown plants) (Figure XII-11), the observed values should exceed somewhat those predicted by equation (4).

Under conditions were P_2 is near zero, the steady-state concentration of THO in the leaf should approach the external concentration. This is confirmed in Figure XII-9, where the shoots were continuously exposed to predried air.

Data for 80-day-old THO-grown tobacco plants showed that young stem tissue did not attain as high a THO concentration as older stem sections, and that various parts of the inflorescence assume THO concentrations intermediate between those of the stem and the mesophyll (Figure XII-7). Also, within a given leaf the leaf base reaches higher C/C_o values than the leaf apex (Figure XII-8). These observations can be hypothetically explained by the formulation just developed. According to this formulation, any factor affecting the vapor pressure of the atmosphere surrounding the leaf and that of the tissue water itself would tend to influence C/C_o at steady state. If the atmospheric vapor pressure is controlled, C/C_o would vary from variations

in the vapor pressure of the tissue itself. This may be due either to differences in leaf temperatures or to differences in tissue-water potential. Leaf temperature is affected by ambient temperature, incident radiation, and transpiration rate. It is well known that leaf temperatures may vary widely on different parts of a plant (9) and possibly even within one leaf. Such differences are also found in tissue-water potential, but, since large changes in potential are associated with small changes in vapor pressure, this variation is of lesser importance. Since neither leaf temperature nor tissue-water potential is constant at all points in a given plant, we should not expect to C/C_o values at these various points to be the same. A leaf of higher temperature should be expected to attain a higher C/C_o value than a leaf of lower temperature. Young tissues tend to have higher transpiration rates than older leaves (5), and therefore possibly lower temperatures.

No detailed measurements of plant temperature were made during the investigations reported here. However, leaf temperatures were measured when the composition of the transpired vapor was determined. At 1400 hours when the transpiration rate decreased abruptly an increase in temperature of 2° occurred. At the same time THO in the transpired vapor increased substantially.

The above discussion, supported by the observations that leaf mesophyll can equilibrate with external THO concentration around the roots (Figure XII-9) and that an excised leaf would lose its THO content completely to saturated HHO water vapor (Figure XII-12), contradicts the existence in the leaf of a sizable fraction of water that is inaccessible to turnover.

Some evidence for preferential water pathways in the leaf can be obtained from data on the pattern of increase of THO in the mesophyll of leaves transpiring into dry air (Figures XII-9 and XII-10). The THO concentration was lower in transpired vapor than in tissue water. This could have resulted from unexpelled HHO in the chamber and tubes during the early part of the experiment. However, such HHO still trapped in the system would have been removed at a faster rate than that indicated in Figure XII-9. Therefore, it is possible that, under the prevailing high transpiration rates, water with a lower THO concentration than that in composited leaf water was first to be withdrawn by transpiration. This possibility is supported by Figure XII-10, which shows that the THO concentration of the vapor being lost into

dry air during transpiration depends on the air velocity in the chamber, and therefore on the transpiration rate itself. THO concentrations were always higher at low flow rates than at rapid flow rates. This relation may be explained, but further experimental support is necessary. At high transpiration rates, the transpired vapor may contain water with a low THO concentration derived from the mesophyll cells during a partial leaf dehydration. At low transpiration rates, the contribution is proportionately larger from veins containing a high concentration of THO, increasing the THO concentration in the transpired vapor. This interpretation could be confirmed by data (not yet available) on the THO concentration in the mesophyll throughout the experiment.

Since only tissue water and transpired water vapor were analyzed in these experiments, nothing can be said concerning the capture of tritium by metabolic substrates. Such a capture would be accelerated by the transport of tritiated metabolites to storage sites or other locations where respiration may or may not break tritium bonds. A certain percentage of the translocated and subsequently respired tritium would be reincorporated into other materials. This circulation of tritium in the plant was not studied during these experiments. However, Cline (4) has shown that the amount of incorporated tritium in young Phaseolus plants is generally small in comparison with the amount of tritium in the incoming water.

Usefulness of Tritium as a Tracer for Plant Water Movement

The value of a material as a tracer depends, of course, on the degree to which it behaves like its analog. For a number of reasons, no better single tracers than DHO, THO, or H_2O^{18} will probably be found for following water movement in organisms. Since these materials are little ionized and their mass ratios with respect to their common analog are not far from one, only a 5-10 percent difference in their rates of diffusion would be expected on the basis of physical considerations.

Interpretation of the rates of water movement from the behavior of these tracers is likely to be straightforward only so long as:

1. Only mass flow or self-diffusion is occurring.
2. Little or no exchange occurs en route.
3. The porous medium has a fixed pore-size distribution.
4. Dead-end pores or inaccessible compartments are either absend or have a known effect.

5. Conditions are at least quasi-steady-state.

Living organisms, and specifically higher plants, present a complex medium for the flow of water. They present a gamut of pore sizes ranging from the relatively large pores of conducting tissues to the much smaller pores of protoplasmic membranes. Each cell contains several regions of basically different physical characteristics, such as the cell wall, the cytoplasm, and the vacuole. Furthermore, steady-state conditions are cyclicly disturbed by endogenous and environmental factors. For these reasons, it is obvious that none of the above conditions can be met exactly, and as a consequence, the interpretation of tracer experiments will not be simple. Difficulties in the interpretation of water-tracing experiments are actually due not so much to differences between the tracer molecule and water as to the large measure of similarity between them. For example, if we were to measure flow rates in just the xylem, the tracer selected should not diffuse laterally during transport or exchange into the structural molecules of the xylem. THO or other water tracers, like water, obviously cannot meet this requirement.

When assessing the usefulness of tritium as a tracer, the objectives of the study must be clear. THO cannot be used for exact prediction of the precise rates of net water movement. However, because its behavior is similar to that of water molecules, its quasi-steady-state distribution in the tissue and variations in this distribution can yield important information concerning the pathways of water movement in plant tissues and the factors that can regulate and control these pathways (3). Experiments with THO should be designed with these conditions in mind.

SUMMARY

The distribution of THO in sunflower plants in light with roots in THO was studied as a function of time. In one 12-hour light period, THO concentrations in the stem tissue and petioles of mature leaves approached equality with the THO concentration of the nutrient solution. The increase in concentration in the stem as a function of distance from the root-stem junction was exponential.

The approach to equality was much slower in the terminal several nodes and the internodes that were still elongating and in tissue that was still expanding. In fact, the apical two nodes and internodes, bracts,

inflorescence parts, and seeds never reached equilibrium even when the plants had been grown from seed to seed maturity in THO.

The THO concentration of the external medium. Although the veins themselves equilibrated in a manner similar to that of the mature stem and petiole, the interveinal tissue did not reach THO equality with major veins, the stem, or external solution. The tissue water of the interveinal tissue was stable for long periods at 70% of external concentration. The results obtained were similar in pattern in sunflower and tobacco.

The THO in leaf-tissue water and vapor transpired by the canopy of an intact sunflower plant raised from seed in THO and treated with a stream of dry air inside a closed chamber increased over a 12-hour period. At the end of this period, interveinal tissue water and THO in the transpired vapor reached 95% of external concentration about the roots. It was also shown that the lack of equilibration in interveinal tissue may be due to vapor exchange between the leaf and the surrounding unlabeled vapor of the atmosphere. The results contradict the reported existence of a sizable fraction of tissue water that is inaccessible for turnover.

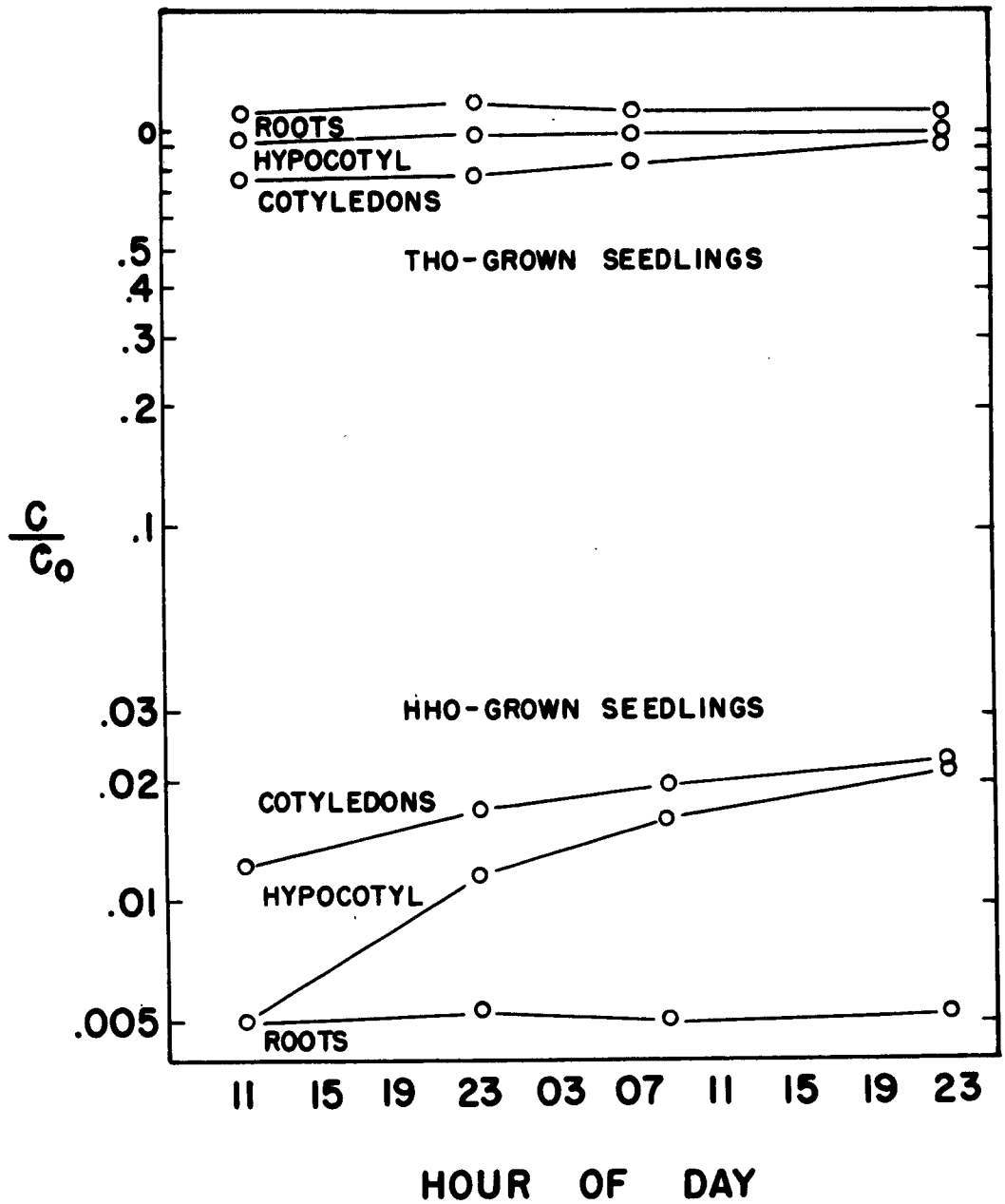

Figure XII-1 Absorption of THO from vapor by tissues of 7-day-old HHO-grown sunflower seedlings and water guttated by them compared to the THO content (C) of THO-grown seedlings of the same age. C_o represents external THO concentration for THO-grown seedlings.

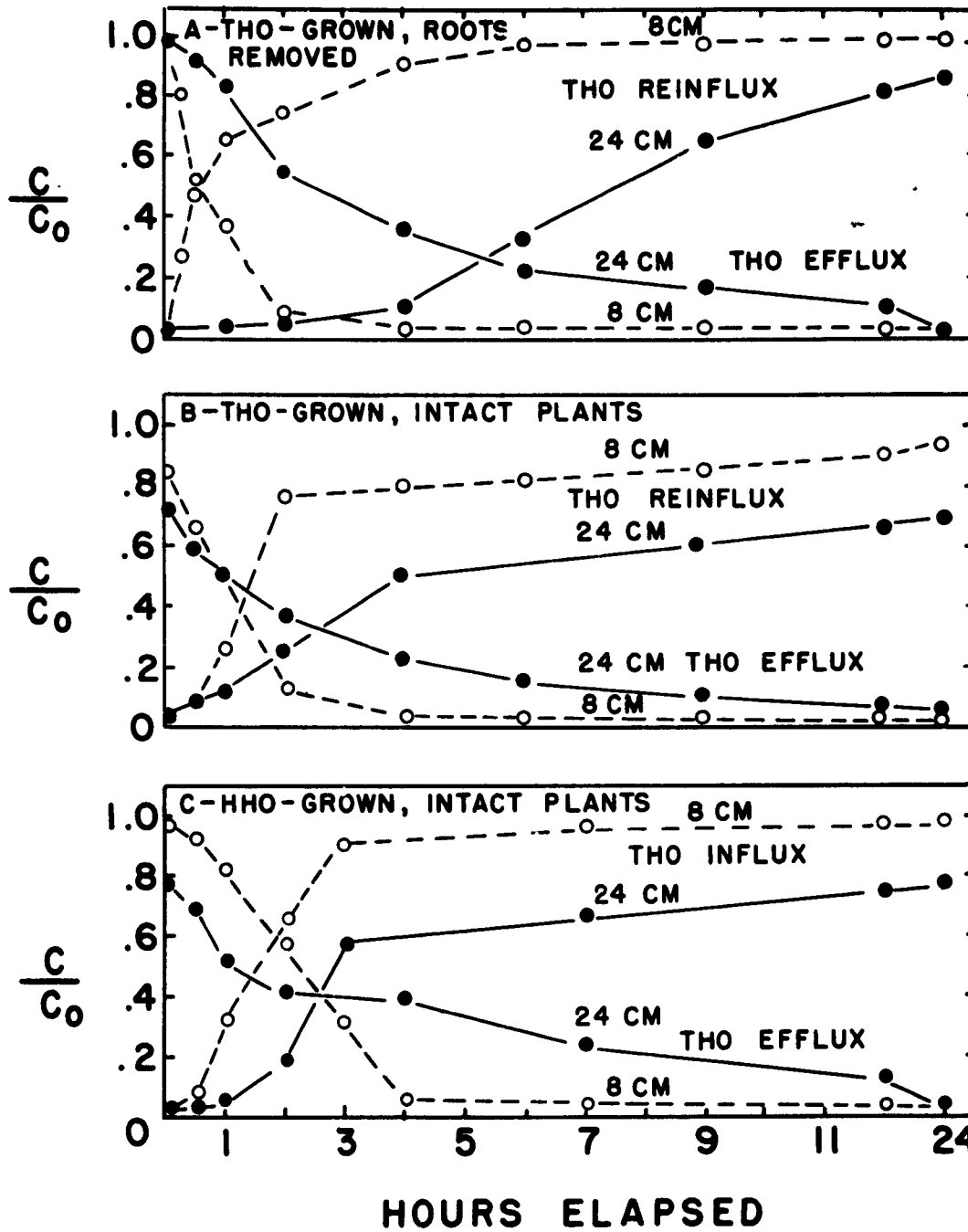

Figure XII-2 Influx and efflux of THO in stem tissue of THO- and HHO-grown sunflower plants 30 days old. Influx preceded efflux in HHO-grown plants. Efflux preceded influx in THO-grown plants. Measurements were made on 2-cm-long sections of stem tissues at 8 cm and 24 cm heights.

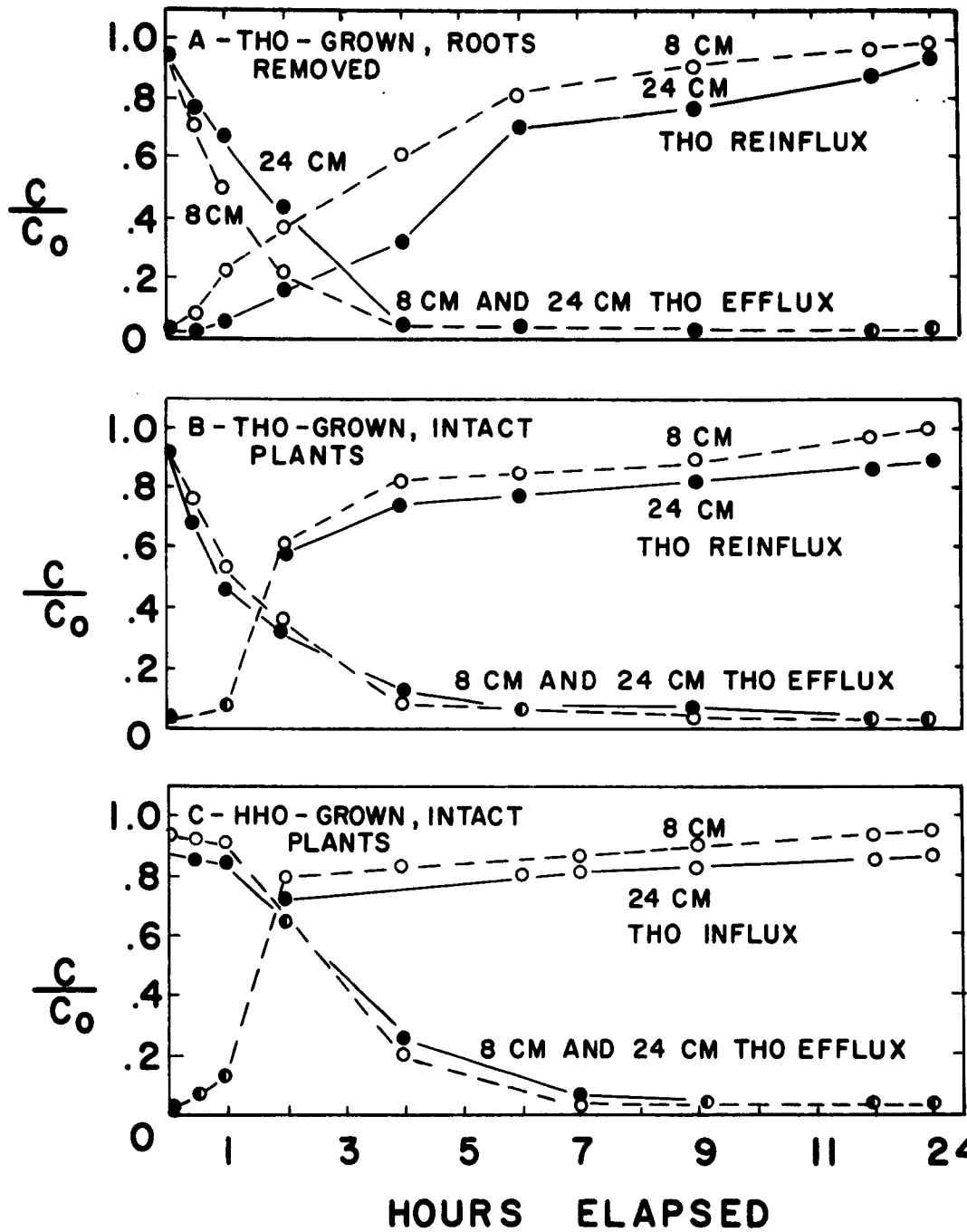

Figure XII-3 Influx and efflux of THO in veins of THO- and HHO-grown sunflower plants 30 days old. Influx preceded efflux in HHO-grown plants. Efflux preceded influx in THO-grown plants. Veins were taken from leaves at heights of 8 and 24 cm.

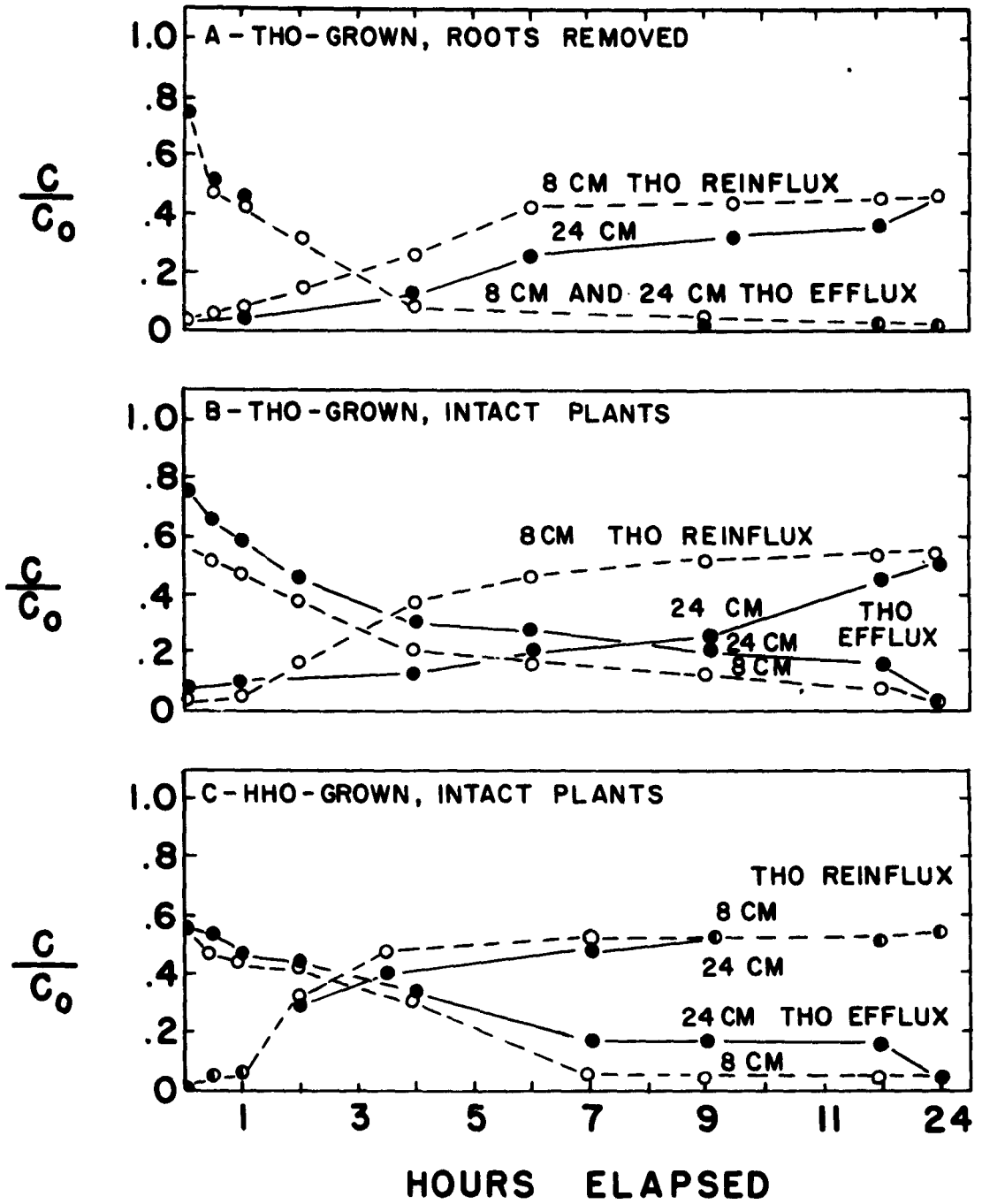

Figure XII-4 Influx and efflux of THO in mesophyll of THO- and HHO-grown sunflower plants 30 days old. Influx preceded efflux in HHO-grown plants. Efflux preceded influx in THO-grown plants. Mesophyll samples were taken from leaves at heights of 8 and 24 cm.

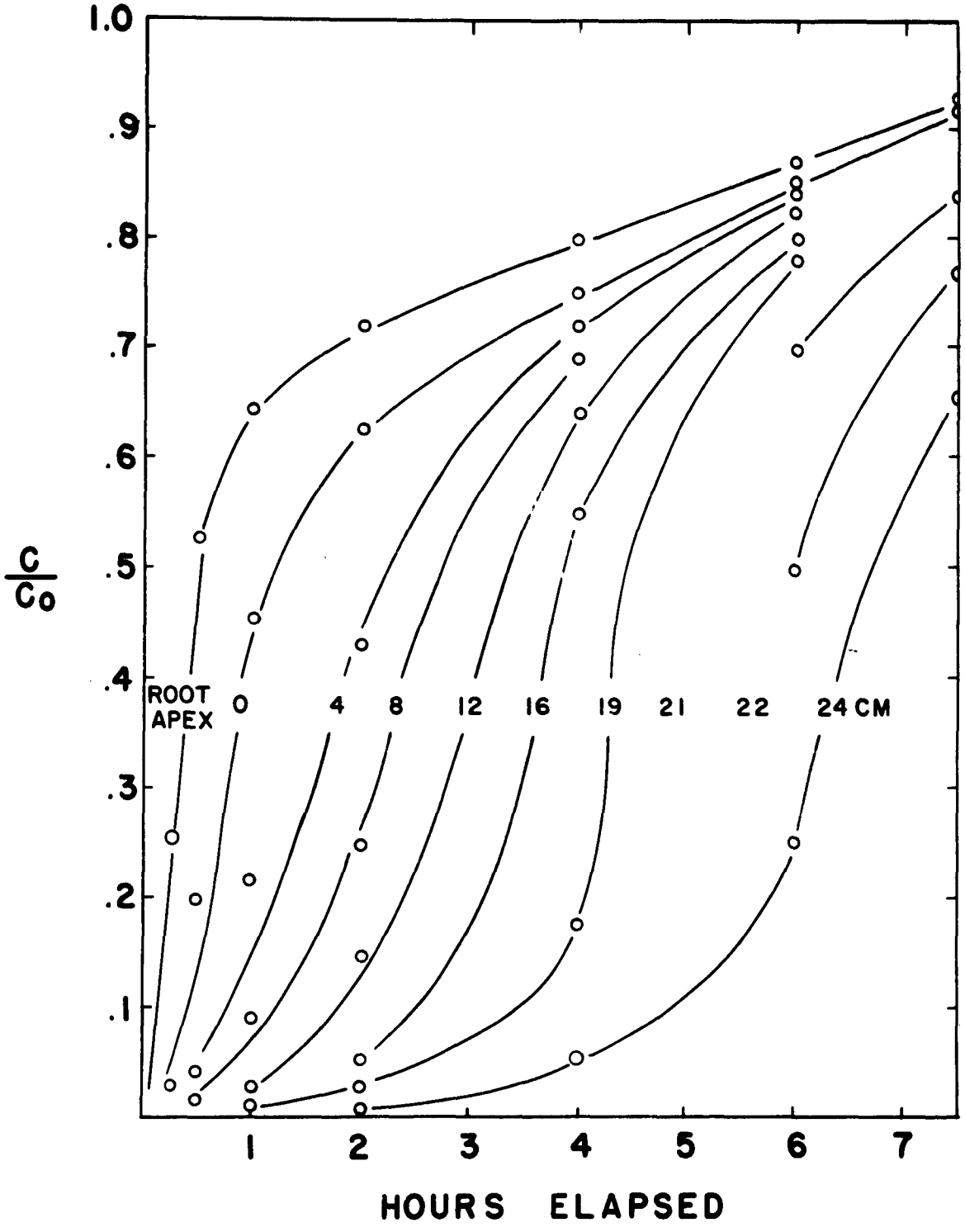

Figure XII-5 Influx of THO into root and stem tissue of HHO-grown sunflower plants 30 days old. The numbers in the curves indicate the height of the tissue sample above the cotyledonary node.

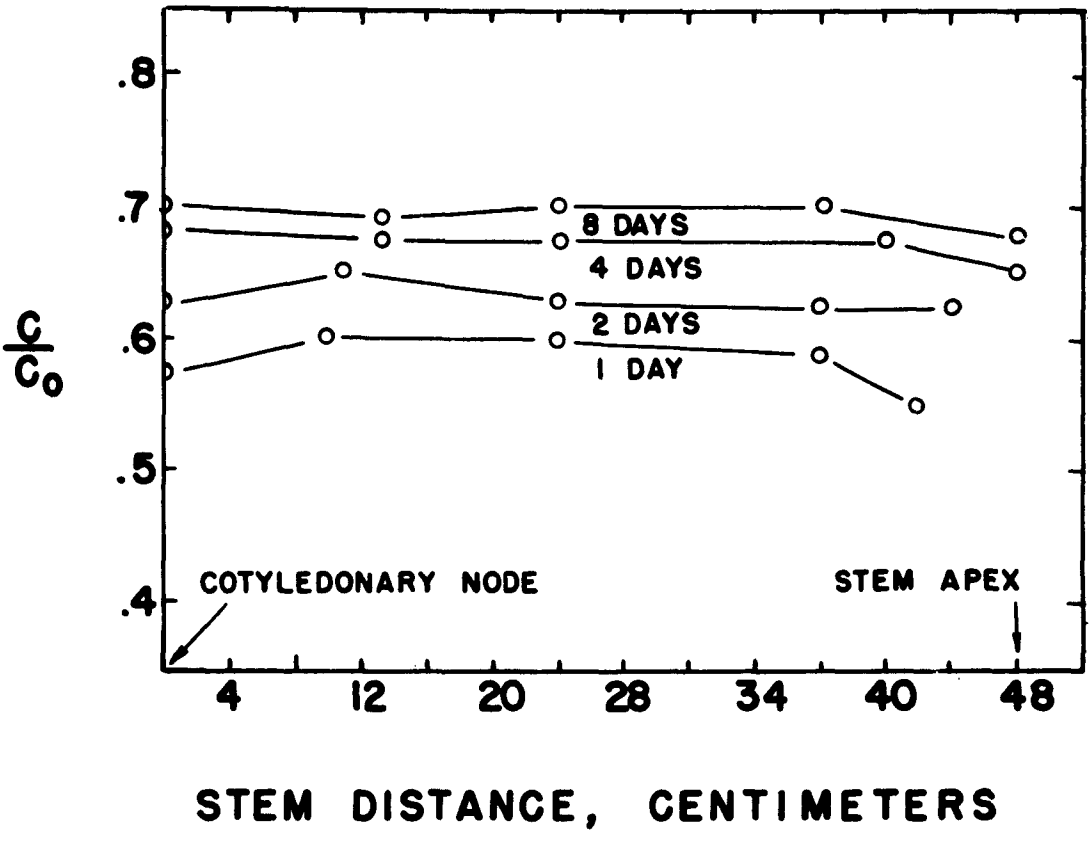

Figure XII-6 Gain of THO by mesophyll of HHO-grown sunflower plants 80 days old with roots submerged in THO over an 8-day period.

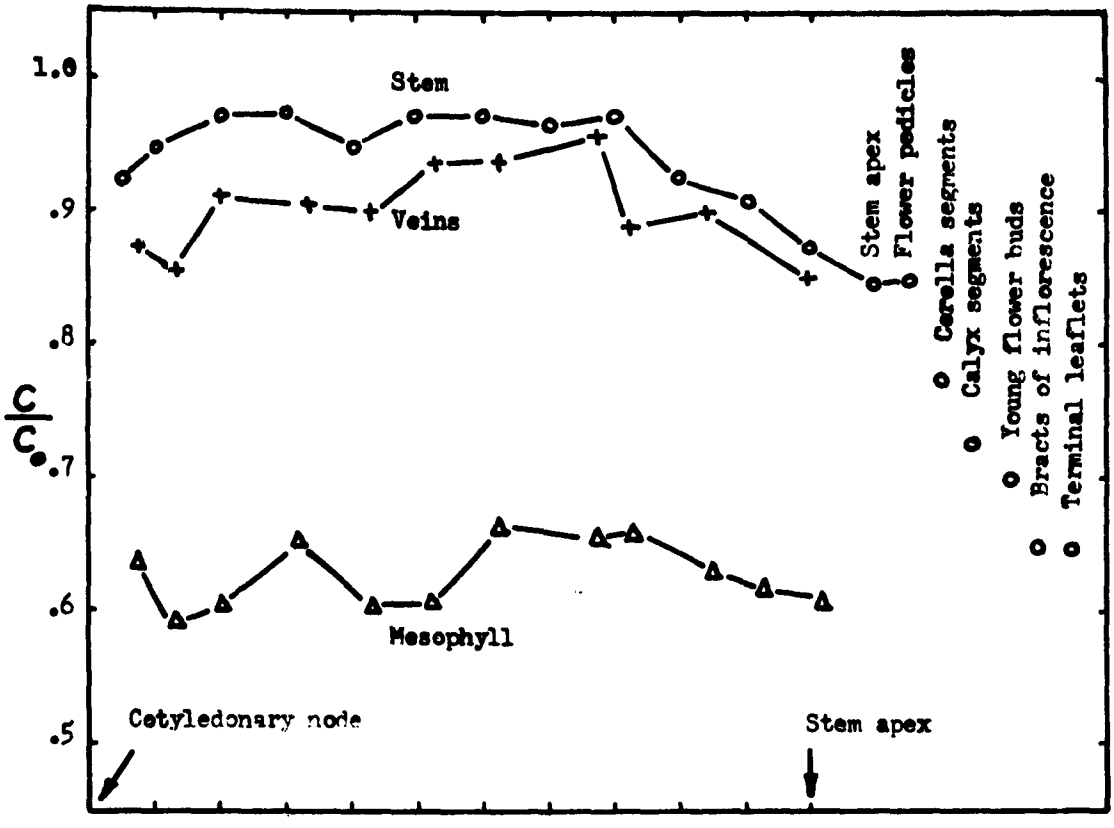

Figure XII-7 Distribution of THO in various tissues of THO-grown tobacco plants 80 days old.

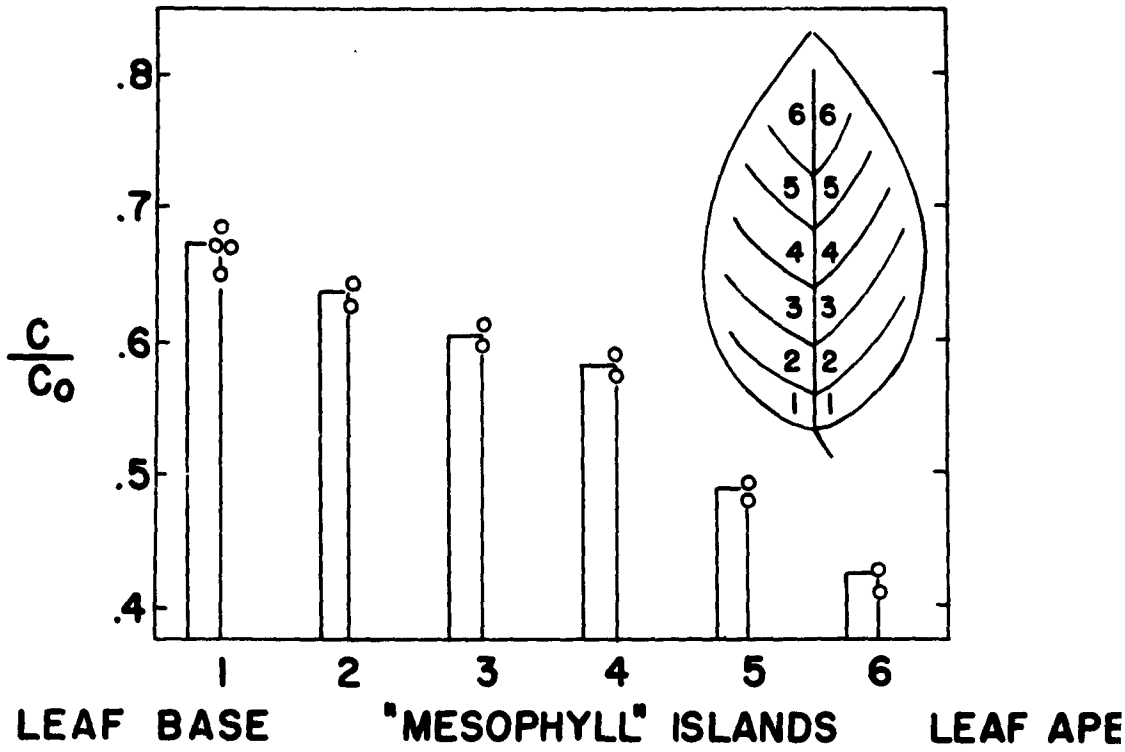

Figure XII-8 Amount of THO in tissue water of leaf discs from THO-grown tobacco 80 days old. Mesophyll islands refers to discs taken between the major lateral leaf veins of a fully-expanded leaf half way up the stem.

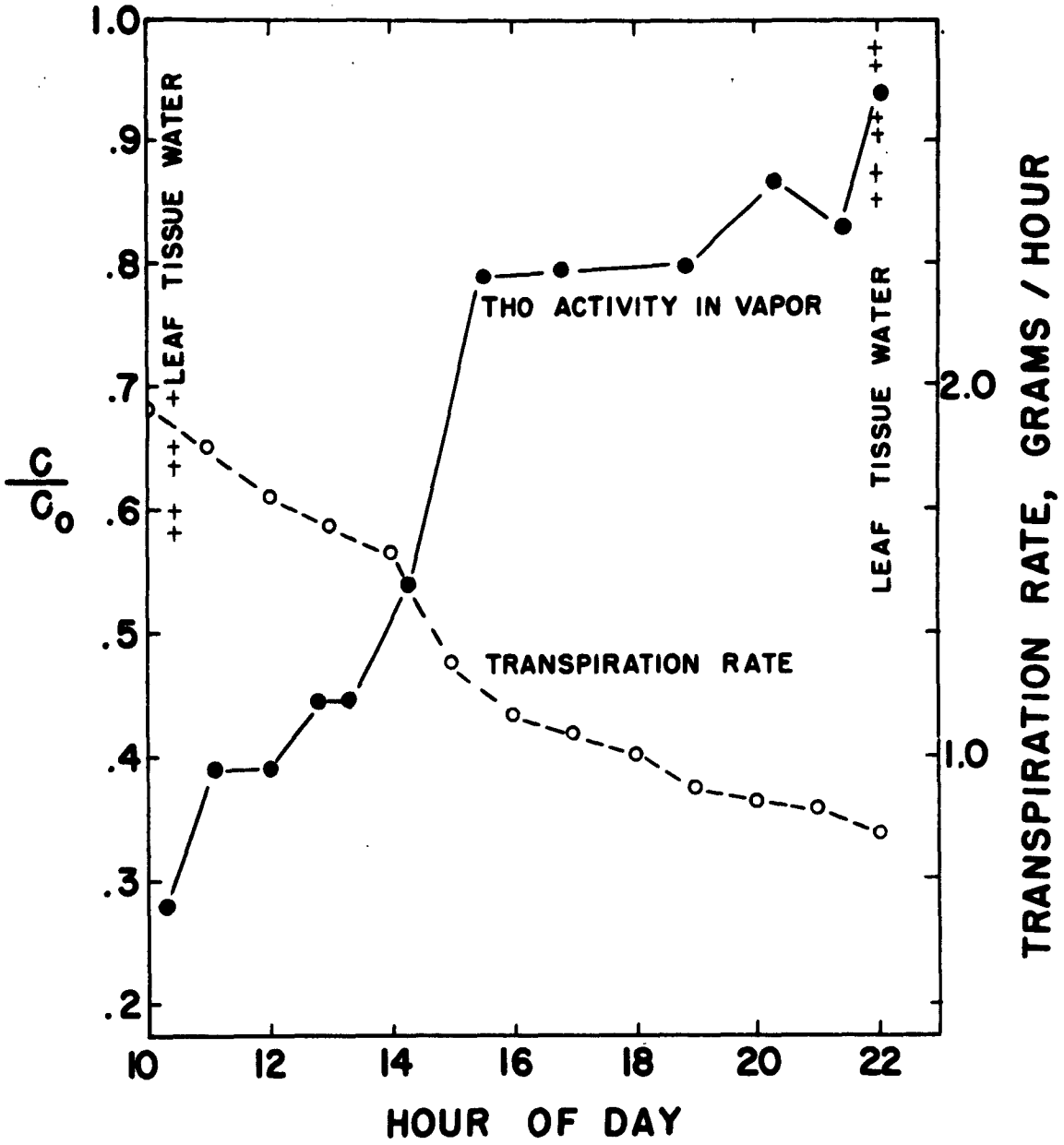

Figure XII-9 Relation between transpiration rate and THO activity of transpired water vapor from sunflower plants confined in a closed chamber with dry air admitted at a rate of 13 liters/min. Plants illuminated with 800 ft-c throughout the experiment.

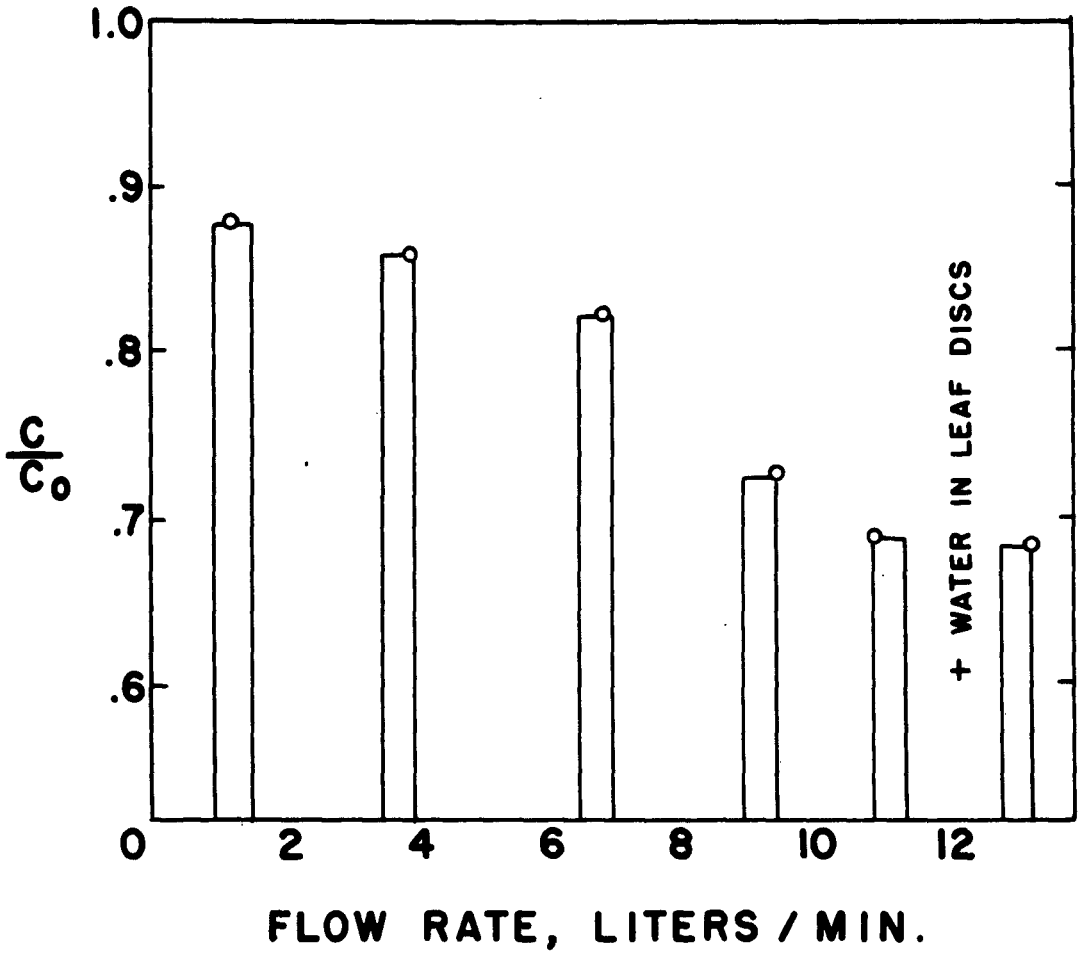

Figure XII-10 Trend of THO activity in water vapor transpired from leaves of THO-grown tobacco plants in a closed chamber (9-liter volume), 800 ft-c, and dry air entering at various rates for contiguous periods of 10 minutes preceded by 1 hr. at the given flow rate.

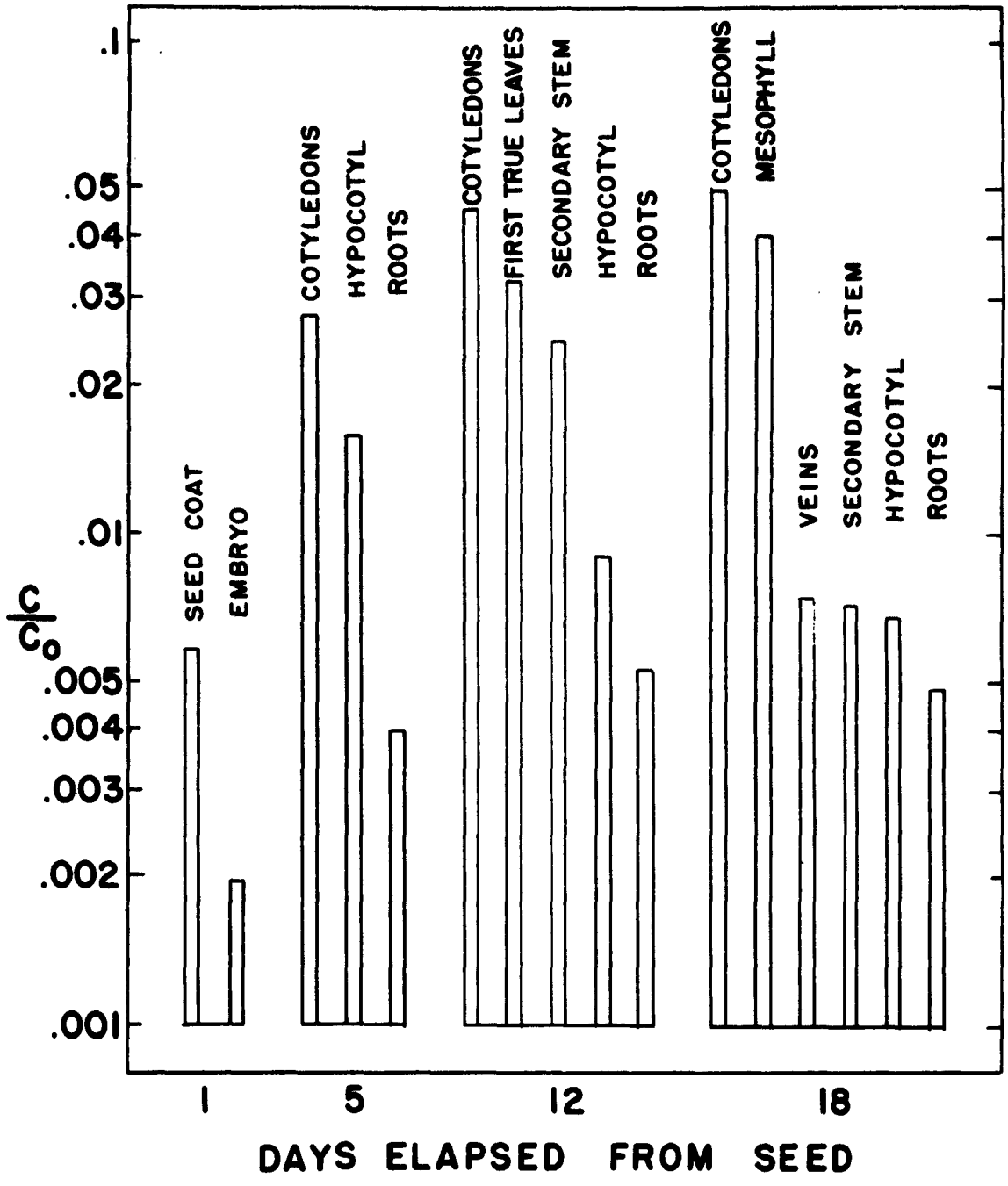

Figure XII-11 Absorption of THO (C) from vapor by shoot tissues of HHO-grown sunflower plants of increasing age. C_o represents external THO concentrations of the growing medium supplied to adjacent THO-grown plants.

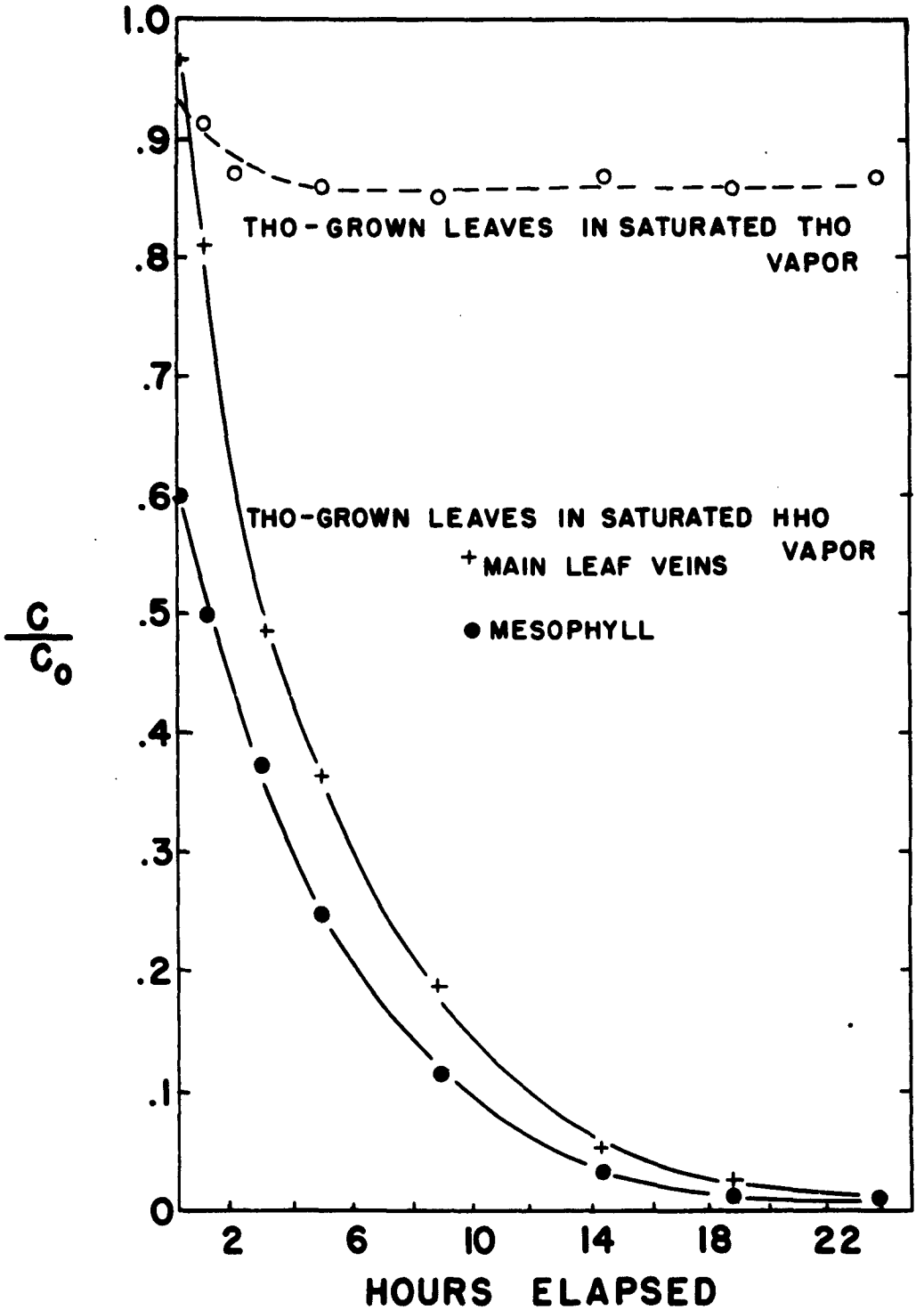

Figure XII-12 Efflux of THO from leaves of THO-grown sunflowers into saturated vapor of THO and HHO at 20°C under diffuse light.

REFERENCES FOR CHAPTER XII

Biddulph, O., F. S. Nakayama and R. Cory. 1961. Transpiration stream and ascension of calcium. Plant Phys. 36:429-436.

Biddulph, O., and R. Cory. 1957. An analysis of translocation in the phloem of the bean plant using THO, P^{32} and C^{14}. Plant Physiol. 32:608-619.

Canny, M. J. 1960. The rate of translocation. Biol. Rev. 35:506-532.

Cline, J. F. 1953. Absorption and metabolism of tritium oxide and tritium gas by bean plants. Plant Physiol. 28:717-723.

Kramer, P. J. 1959. Transpiration and the water economy of plants. In: Plant Physiol. II:607-726. Ed: F. C. Steward. Academic Press, N. Y.

Kuiper, P. J. C. 1961. The effects of environmental factors on the transpiration of leaves, with special reference to stomatal light response. Meded. Landbouwogeschod. Wageningen. 61:1-49.

McDermott, J. J. 1941. The effect of the method of cutting on the moisture content of samples from tree branches. Am. J. Bot. 28:506-508.

Raney, F., and Y. Vaadia. 1962. Movement of THO in the root system of Helianthus annuus in the presence or absence of transpiration. Plant Physiol. (in press).

Raske, K. 1960. Heat transfer between the plant and the environment. Ann. Rev. Plant Physiol. 11:111-126.

Vartapetyan, B. B., and A. L. Kursanov. 1959. A study of water metabolism of plants using water containing heavy oxygen, H_2O^{18}. Fiziol. Rast. 6:154-159.

CHAPTER XIII

THE MEASUREMENT AND DESCRIPTION OF INFILTRATION INTO UNIFORM SOILS

D. R. Nielsen, J. M. Davidson, and J. W. Biggar[1/]

Fluid movement in porous media is perhaps one of the most consequential phenomena governing the activities of the human race. The understanding and description of fluid moving within porous media therefore shares an interest with many fields other than agriculture. In agriculture, it is necessary to know changes in soil water content throughout the year under the influence of rainfall or irrigation, evapo-transpiration, and drainage. To predict water content changes, a mathematical description of the physical processes involved should be obtained. It is the purpose of this paper to present experimental data for water moving through soils and to examine how well existing mathematical equations describe the water movement.

The mathematical equations used in this investigation are those commonly employed in present day research in soil-water movement. Because the derivation of these equations are generally understood by many investigators, it is usually not necessary to redevelop them. However, in this manuscript it is convenient to have all derivations including pertinent assumptions closely at hand since the primary purpose of this study is to scrutinize and compare the theoretical and experimental behavior of a soil-water system. With the exception of two non-agricultural porous materials [Youngs, 1957], no work under constant environmental conditions of the laboratory has been reported involving this description of water moving vertically downward through soils.

The simplest type of fluid flow exists when the medium is saturated or all pores are filled with the same fluid. For saturated sand, Darcy (1856) observed a linear relation between the volume flux of water and the gradient of the hydraulic head. A generalization made from that observation is Darcy's Law:

$$\bar{v} = -K \bar{\nabla} \Phi \qquad (1)$$

1/ The contents of this chapter have been submitted for publication in Hilgardia, a publication of the California Agricultural Experiment Station.

where Φ is the hydraulic head (L), $\bar{v}$ is the volume flux of water (LT^{-1}) and K the proportionality constant (LT^{-1}) commonly called hydraulic conductivity. This relation has received general acceptance for hydraulic gradients when laminar flow exists under steady-state conditions.

The more complex but most common type of fluid flow in agriculture is that which takes place through soil partially filled with water. Because the soil pores not only contain water but also air and other gases and vapors, water movement is complicated by their presence. The air phase may be at pressures above or below atmospheric pressure regardless of its continuity of distribution within the soil. The pressure of the soil water is related to the surface tension and the radii of curvature present at the air-water interfaces within the partially filled pores of the soil. This relation is not analytic owing, among other things, to the presence of dissolved constituents in the soil water. Nevertheless, progress has been made by assuming that a definite relation exists between the soil water content and the soil water pressure. By definition, soil water pressure is equal to that gauge pressure to which water must be subjected in order to be in hydraulic equilibrium, through a porous permeable wall, with the water in the soil.

Childs and Collis-George (1950) performed an experiment to test the validity of Darcy's Law for unsaturated flow. By measuring the flux of water passing through partially saturated columns oriented to several positions between the vertical and horizontal, they concluded equation (1) was valid for steady-state conditions. For unsaturated flow, the hydraulic conductivity is commonly called the capillary conductivity (Richards, 1952).

In 1931, Richards used equation (1) in the equation of continuity:

$$\frac{\partial(\rho\,\theta)}{\partial t} = -\bar{\nabla} \cdot \rho\bar{v} \tag{2}$$

where θ is the water content ($L^3\ L^{-3}$), and ρ the fluid density (ML^{-3}) and t the time. It was assumed that changes in water content and pressure would take place slow enough so that a steady state relation used in equation (2) could describe the soil water system. The use of equation (1) in (2) yields:

$$\frac{\partial(\rho\,\theta)}{\partial t} = \bar{\nabla} \cdot (K\rho\bar{\nabla}\Phi) \tag{3}$$

For soils, the hydraulic head Φ is generally considered the sum of two terms, $\psi + x$, where ψ is the soil water pressure head and x the gravitational head. It has been mathematically convenient to consider the fluid density ρ constant and that a single-valued relation exists between water content and soil water pressure. This consideration allows the water content θ to be the dependent variable of equation (3). Recognizing hysteresis is most evident in the water content-pressure relation between wetting and drying processes, Childs and Collis-George (1948) introduced the following mathematics for a wetting process or a drying process, but not for both processes together:

$$K(\theta)\frac{\partial\psi(\theta)}{\partial x} = K(\theta)\frac{d\psi(\theta)}{d\theta}\frac{\partial\theta}{\partial x} = D(\theta)\frac{\partial\theta}{\partial x} \tag{4}$$

where $D(\theta)$ is called the soil water diffusivity. The capillary conductivity $K(\theta)$ is assumed to be a single-valued function of θ. Some evidence that supports the use of this assumption has been found by Nielsen and Biggar (1961). Substituting the soil water diffusivity in equation (3) for flow in the x-direction downward we have:

$$\frac{\partial\theta}{\partial t} = \frac{\partial}{\partial x}\left[D(\theta)\frac{\partial\theta}{\partial x}\right] - \frac{\partial K}{\partial x} \tag{5}$$

For horizontal movement the last term on the right-hand-side of equation (5) is omitted as it represents the external body force gravity. Without gravity, equation (5) takes the identical form of the well-known diffusion equation, where the diffusivity $D(\theta)$ is concentration dependent. This does not, however, imply that the mechanism of fluid movement is diffusion in the same sense as diffusion in gases, liquids, or solids due to random molecular motion. The diffusion equation is commonly used to describe soil water problems because of the ease of measuring water contents and its solutions are analogous to ordinary diffusion or heat flow equations.

This paper will present data for water at below atmospheric pressure entering air-dry soils. Measured soil water profiles for vertical and horizontal columns will be compared with those calculated from the solution of equation (5). Also presented is a method of measuring capillary conductivity for different water contents.

THEORETICAL

Horizontal and Vertical Soil Water Profiles

Philip (1955-1957a) has presented a numerical solution of equation (5) for infiltration into a semi-infinite homogeneous soil column either in the vertical or horizontal position. The initial soil water content is assumed constant with depth, and during the wetting process it is assumed that a greater constant water content exists at the soil surface. Thus, we have

$$\begin{aligned} \theta &= \theta n, \quad t = 0, \quad x > 0 \\ \theta &= \theta o, \quad t > 0, \quad x = 0 \end{aligned} \tag{6}$$

where $\theta o > \theta n$. For these boundary conditions, the solution of equation (5) for the vertical case is

$$x = \lambda(\theta)t^{1/2} + \chi(\theta)t + \psi(\theta)t^{3/2} + \omega(\theta)t^{2} + \ldots \tag{7}$$

where λ, χ, ψ, ω, etc. are single-valued functions of θ to be determined by the numerical analysis of Philip.

For the horizontal case, the first term of the right-hand-side of equation (5) is the only one used leaving the solution

$$x = \lambda(\theta)t^{1/2} \tag{8}$$

Equation (5) with its solution (7) or (8) may describe soil water movement provided certain assumptions are fulfilled, in addition to those made previously. (1) There must be no rearrangement of soil particles upon wetting; (2) The air movement does not influence the water movement. This condition requires water movement to be analogous to heat flow where consideration is given to only a single phase; (3) The properties of the water are uniform regardless of the position occupied by water; (4) An isothermal condition exists.

If all the assumptions and boundary conditions are fulfilled, a λ single-valued in θ satisfying equation (8) can be found experimentally. If a constant water content may be visually observed at the wetting front of a horizontal column, the distance to the wetting front divided by the square root of time

should yield the constant value λ. Still, a better means of ascertaining the existence of a unique λ versus θ relation is to measure the water content distribution in a horizontal column at different times. If $\lambda(\theta)$ exists, plots of $x/t^{1/2}$ versus θ will be identical for all times.

Equation (7) provides a theoretical formula for obtaining a curve of x versus θ for comparing calculated and experimental values of water content in vertical columns. Another expression is needed for the net amount of water that infiltrates into the soil surface. Upon integrating with respect to θ and differentiating with respect to t, equation (7) becomes

$$v_o = 1/2\, t^{-1/2} \int_\lambda + \int_\chi + K_n + 3/2 t^{1/2} \int_\psi + \ldots \tag{9}$$

where $$\int_\lambda = \int_{\theta_n}^{\theta_o} \lambda d\theta,\ \int_\chi = \int_{\theta_n}^{\theta_o} \chi d\theta,\ \int_\psi = \int_{\theta_n}^{\theta_o} \psi d\theta, \text{ etc.} \tag{10}$$

The term K_n is the capillary conductivity for the water content θ_n. For boundary condition (6) to be maintained ($\theta = \theta_n$ to great depth), a flux equal to K_n must be supplied at the soil surface in addition to that derived from equation (7).

Knowing the infiltration velocity v_o, the volume of water per unit area which has infiltrated into the profile at time t is

$$i = \int_o^t v_o dt \tag{11}$$

or in view of equation (9) it is

$$i = t^{1/2} \int_\lambda + t \left[\int_\chi + K_n \right] + t^{3/2} \int_\psi + \ldots \tag{12}$$

The right-hand-side of equation (12) gives the water stored in the profile plus that which has leaked out the bottom of the profile at great depth.

Equations (7), (9), (11) and (12) are asymptotic infinite series, that is, they fail to converge for large values of t. For these values a decreasing exponential curve is matched to that obtained by equation (9). The exponential curve assumed for times greater than t_1 minutes is

$$v_o = K_o + (V_1 - K_o) \exp\left[-a(t-t_1) \right] \tag{13}$$

where α is a constant to be obtained and V_1 is the value of v_o at $t = t_1$ minutes. To obtain α the derivative of equation (13) at $t = t_1$ minutes yields the value of the slope $-\alpha(V_1 - K_o)$ which is equal to derivative with respect to t of equation (11). The value of the derivative of (11) is known and hence, α may be calculated. Thus, equations (9) and (13) supply a single theoretical curve of v_o versus t for all times. Integration of v_o with respect to t yields the cumulative infiltration. For $t < t_1$ equation (12) applies. For $t > t_1$, integration of equation (13) yields the following cumulative infiltration expression:

$$\int_{t_1}^{t} v_o dt = K_o(t - t_1) + \frac{1}{\alpha}(V_1 - K_o)\,(1 - \exp[-\alpha(t - t_1)]) \qquad (14)$$

A theoretical expression for x versus θ for times greater than t_1 minutes corresponding to equation (7) is obtained by assuming that the shape of the profile for these times is the same as that when time is infinite, Philip (1957c). If the profile between θ_o and θ_1 is assumed to be linear, x_1 (associated with θ_1) may be computed from equation (9) by

$$i = K_n t + \int_{\theta_n}^{\theta_1} x'_\infty \, d\theta + x_1 (n - 1/2)\,\delta\theta \qquad (15)$$

where x'_∞ is the distance defined by $x = x_1 + x'_\infty$. The value of i is known theoretically for any time from equation (12) and (14). Once x_1 is found, the entire soil water profile is known for any time, it is the shape and position of these calculated profiles that will compare to the experimental profiles measured in the laboratory for the vertical cases.

Capillary Conductivity

For large times and boundary conditions (6) for the vertical case the value of the infiltration velocity approaches that of K_o as seen in equation (13). Physically, for these large times, a constant water content θ_o establishes itself over that portion of the profile near $x = 0$. For infiltration, where $\theta_o > \theta_n$, θ_o may take on any value of an unsaturated to saturated condition. For example, if θ_o were 0.35 cm^3/cm^3, the infiltration velocity would approach K_o, the capillary conductivity at a water content of 0.35 cm^3/cm^3.

It is of interest to notice for these times that a steady-state condition exists in the upper part of the profile. Thus, it is only necessary to assume equation (1) is valid, not equation (5). This method of obtaining the capillary

conductivity is similar but experimentally less difficult to perform that that presented by Childs and Collis-George (1950).

EXPERIMENTAL

The porous materials were Columbia solt loam, a recent alluvial soil bordering t ɔ Sacramento River; and Hesperia sandy loam, derived mainly from granitic alluvial sediments and occupying evenly sloping alluvial fans in the Bakersfield area.

Air-dried soils sieved to pass 1 mm screen were packed into clear plastic cylinders 3.2 cm in diameter, composed of 1 cm wide sections. The sections were supported in a V-shaped container made from a 4'' x 6'' piece of lumber. To uniformly pack the column, soil was added in small amounts through a 1.5 cm powder funnel connected to a 1 cm diameter rubber tube. The rubber tube rested on the top of the previously added soil and as more soil was added, the funnel and tube was raised and rotated simultaneously. After each addition of soil, the wood container that held the plastic column was systematically tapped with a rubber mallet.

The water used in all experiments was 0.01 N $CaSO_4$ made from deaerated distilled water. The pressure of the water entering the soils was controlled by a fritted glass bead plate described by Nielsen and Phillips (1958). The plate was filled with water and the desired pressure applied prior to placing the plate in contact with the porous material. Using the constant head buret shown in Figure XIII-1, the pressure at $x = 0$ was precisely controlled. Measurement of time in all experiments commenced the instant contact was established between the wetted plate and the soil. For each run the pressure was held constant at the value existing when the initial contact was made. The pressure drop across the plate and the soil-plate interface was initially in the order of 0.1 millibars and diminished to lesser values for longer times. This small pressure drop was made possible by using different size fritted beads and always using the fritted bead plate that remained just saturated at the desired pressure. It will be shown in figures to be presented that the water content at $x = 0$ remained constant for all observed times. This condition is required for the solution of the equation (5) using boundary conditions (6).

Water entering the columns was measured volumetrically in the constant head buret. Measurements of distance to the wetted front were

visually observed. When flow had proceeded for a desired time the fritted plate was removed from the soil, the column was segmented, and the water content of each 1 cm section gravimetrically determined. These gravimetric values were converted to θ using the average bulk density of the entire column. The ability to pack columns to equal average bulk density values has been discussed previously by Nielsen, et al. (1962).

Boundary conditions (6) were imposed on both horizontal and vertical soil columns. A complete discussion of the experimental boundary conditions for horizontal flow through the soils of this study and other porous materials has been presented (Nielsen, et al. 1962). Some of these data for horizontal flow through Columbia and Hesperia will be given here to make calculations of and comparisons with vertical profiles. The initial water contents θ_n of Columbia and Hesperia soils were 0.031 and 0.026 cm^3/cm^3, respectively. Values of θ_o will be given in the RESULTS. For these values, the soil water pressure at $x = 0$ ranged between -100 to -2 mb. The length of time t_o during which boundary condition (6) was maintained before gravimetrically determining the soil water distribution ranged from a few minutes to three weeks.

Capillary conductivity measurements were made on Columbia soil by the method outlined in the THEORETICAL. Values of θ_o maintained by pressures of -100, -75, -50, and -2 mb at $x = 0$ of vertical columns were 0.325, 0.35, 0.425 and 0.45 cm^3/cm^3, respectively. For these conditions, all columns were allowed to wet until the wetting front reached a depth of 75 cm. For all cases except those samples wetting at -100 mb, the infiltration velocity approached a constant value K_o. These values of capillary conductivity will be compared to those obtained for steady-state conditions using the more common two-plate method (Richards, 1931).

Soil water diffusivity (defined in equation (4)) versus water content relations were obtained by the method of Bruce and Klute (1956). This method is based upon the assumption that equation (8) exists for horizontal flow under conditions (6). Upon intergration of equation (5) without its right-hand term, the soil water diffusivity D is calculated from the soil water profiles using the following equation:

$$D(\theta) = -\frac{1}{2t_o}\frac{dx}{d\theta}\int_{\theta_n}^{\theta} x\,d\theta \qquad (16)$$

Soil water diffusivity values were obtained for both Columbia and Hesperia soils for values of θ_o corresponding to -2 mb. Diffusivity relations calculated for other values of θ_o have been reported elsewhere (Nielsen, et al., 1962).

Values of capillary conductivity for Columbia soil at water contents less than 0.30 cm^3/cm^3 were calculated using the method of Childs and Collis-George (1950). These values together with those determined with equation (13) for large times provided a complete K versus θ relation. This relation together with the diffusivity data above was used to obtain the solution of equation (5) for the vertical case. For the Hesperia soil, the necessary K versus θ relation was determined from the above diffusivity relation and the soil water profile developed under conditions (6) for t_o = 97 minutes.

RESULTS

Horizontal

If equation (5) is capable of describing soil water movement for conditions (6), a λ single-valued in θ will exist (equation (8)). Thus, any water content between θ_n and θ_o would proceed along the horizontal proportionally to the square root of time. Under the experimental conditions of this investigation, two means are available to ascertain the existence of a unique λ versus θ relation. The first is to divide the distance to the wetting front by the square root of time. If these ratios are constant during the experiment, they define the value of λ corresponding to the water content immediately ahead of the wetting front. The second means - and more conclusive - water content distributions for different times should reduce to a common λ versus θ relation if the distances are divided by the square root of the time each sample was allowed to wet. For Figure XIII-2 and Figure XIII-3 it has been assumed that the water content immediately in front of the visually observed wetting front is constant and that the distances to the wetting front divided by the square root of time are values of λ for that water content. For Columbia soil where θ_o at x = 0 equals 0.45 cm^3/cm^3, λ does exist at a value of 2.75 cm $min^{-1/2}$ as shown in Figure XIII-2. However, for θ_o = 0.425 and 0.325 cm^3/cm^3, a constant relation does not exist. Similar results were found for Hesperia soil. For θ_o = 0.385 corresponding to an applied soil water pressure of -2 mb., λ was 1.92 cm $min^{-1/2}$. For

smaller values of θ_o, the values of distance to the wetting front divided by square root of time decreased during the experiment.

After water had entered the Columbia soil with $\theta_o = 0.45$ for three time periods, the soil water content distribution with distance was measured. These distances when divided by the square root of each corresponding time period t_o, are the values of λ with their corresponding water contents θ described by equation (8). Equation (8) is apparently a physical reality for the Columbia soil water system given in Figure XIII-4, because plots of the experimental data for all three time periods yield the same λ versus θ relation. In Figure XIII-5 for $\theta_o = 0.325$, the λ versus θ relation is not unique for three time periods. Although not presented, the same was found for $\theta_o = 0.425$. A comparison of the values of λ in Figure XIII-2 and those near the wetting front in Figures XIII-4 and XIII-5 reveals that the assumption regarding the observation of a constant water content in front of the wetting front is reasonable.

Only for $\theta_o = 0.385$ cm^3/cm^3 (applied soil water pressure equal to -2 mb) was there a unique λ versus θ relation for different time periods of wetting Hesperia soil (Figure XIII-6). When the soil was allowed to wet at a smaller pressure producing a value of θ_o equal to 0.30 cm^3/cm^3, results similar to those of Columbia were measured, i.e. a unique λ versus θ relation did not exist (Figure XIII-7).

Values of soil water diffusivity were calculated (only when λ existed) from the measured soil water distribution curves using equation (16). Diffusivity values for Columbia soil allowed to wet at $\theta_o = 0.45$ cm^3/cm^3 are plotted against water content in Figure XIII-8. Values for Hesperia soil which was wet at $\theta_o = 0.385$ are given in Figure XIII-9. The successful prediction of horizontal soil water movement using these exact relations has been reported previously (Nielsen, et al., 1962).

Vertical

Observations of the wetting front advance into Columbia silt loam and Hesperia sandy loam for both horizontal and vertical movement are given in Figures XIII-10 and XIII-11. For the Columbia soil data shown in Figure XIII-10, the values of θ_o were 0.45, 0.425, 0.35 and 0.325 cm^3/cm^3. The distance the wetting front advanced in the vertical direction is always equal to or greater than that in the horizontal direction. For a given θ_o, the initial rates of advance are identical for both directions. Similar results for

Hesperia soil wet at θ_o equal to 0.385 and 0.30 cm^3/cm^3 are given in Figure XIII-11. It is of interest to observe for both soils that the effect of the gravitational field is more obvious as θ_o is decreased. For example, when water entered Columbia soil at 0.45 cm^3/cm^3, the time required for the wetting front to advance 50 cm horizontally was 1.4 times greater than that vertically. But when water entered at 0.425 and 0.325 cm^3/cm^3, the time required to advance 50 cm horizontally as compared to 50 cm vertically was 1.9 and 2.1, respectively.

Columbia soil water profiles developed during time periods of 64, 226, and 467 minutes where θ_o was 0.45 cm^3/cm^3 are presented in Figure XIII-12. At a time in the neighborhood of 225 minutes, a constant water content over approximately the first 30 cm depth is established. Profiles for θ_o equal to 0.425 cm^3/cm^3 are similar except that the times involved are greater. A time greater than 500 minutes is required to develop a 'θ-straight' (Philip 1957c) at 0.425. For water entering at the least water content of 0.325 cm^3/cm^3, a 'θ-straight' is being approached but is not established after 30,200 minutes of nearly 3 weeks. Hesperia soil water profiles developed for θ_o equal to 0.385 and 0.30 cm^3/cm^3 are given in Figures XIII-15 and XIII-16. For the greater water content a 'θ-straight' exists after 300 minutes while for the smaller water content such a condition failed to completely establish for the deepest profile.

The soil water profiles shown in Figures XIII-12 through XIII-16 differ from those reported by Bodman and Colman (1943) which have been the subject of considerable discussion (Baver, 1956; Philip, 1957d; Youngs, 1957). Their profiles were S-shaped having a sharp reduction in soil water content a few centimeters from $x = 0$. The profiles given in this paper are not S-shaped and without exception tend to develop a 'θ-straight' with time.

Capillary conductivity values for Columbia soil determined by the method described in this paper and by the two-plate method (Nielsen and Biggar, 1961) are given in Table XIII-1. Values of capillary conductivity taken equal to the infiltration velocities measured for soil columns wet to 75 cm depth compare favorably with those obtained using the two-plate steady-state method. The method provides a simple means of obtaining capillary conductivities for high soil water contents for the imbibing process, heretofore, a difficult measurement to make.

Table XIII-1 Measured values of capillary conductivity of Columbia silt loam by two methods.

θ	K_a	K_b
cm^3/cm^3	cm/min	cm/min
0.45	0.0464	-------
0.44	------	0.0215
0.425	0.0193	0.0150
0.35	0.00294	0.00260
0.30	0.000623	-------

K_a from this report

K_b from Nielsen and Biggar, 1961

The capillary conductivity relation for Columbia soil measured for water contents between 0.45 to 0.30 cm^3/cm^3 by the above method and calculated by the method of Childs and Collis-George (1950) for water contents less than .30 cm^3/cm^3 is given in Figure XIII-8. The capillary conductivity relation of Hesperia sandy loam given in Figure XIII-9 was calculated from the soil water profile for t_o 97 minutes presented in Figure XIII-15 by the method of Philip (1957b) outlined in the THEORETICAL.

Figures XIII-17 and XIII-18 show the parameters λ, χ, and ψ of equation (7). The λ and diffusivity relations are those obtained from the horizontal flow studies. The values of χ and ψ were calculated using the iterative procedure of Philip (1955, 1957a). It should be noted for both soils that the ordinate scales are not the same for each parameter and that χ and ψ are much smaller than λ.

Figure XIII-19 presents Columbia soil water profiles calculated from the above parameters for infiltration times of 64, 226 and 467 minutes for θ_o equal to 0.45 cm^3/cm^3. Agreement exists between the measured and theoretical plots for all three infiltration times. For Hesperia soil having θ_o equal to 0.385, the soil water profiles are successfully predicted for infiltration times of 286 and 482 minutes using the capillary conductivity relations calculated from the profile measured at 97 minutes.

Soil water profiles given in Figures XIII-13, XIII-14 and XIII-16 could be calculated using the solution of equation (5). This solution depends upon the calculation of a unique λ versus θ relation based upon measurements made on the horizontal samples. These relations were not unique as shown in Figures XIII-5 and XIII-7.

DISCUSSION

When water under near atmospheric pressure entered Columbia or Hesperia soil, soil water profiles were described by equation (5) subject to (6) for both the horizontal and vertical cases. However, when the soil water pressure was reduced causing a reduction in water content at $x = 0$, soil water profiles neither horizontal nor vertical could be predicted. The failure of the equation to describe horizontal flow for these soils and sandstone wet with not only water but oil has already been partially discussed (Nielsen, et al., 1962). Based upon experimental evidence it was concluded that rearrangement of soil particles or clay migration or swelling could not account for the lack of agreement between the measured and calcualted profiles. Further evidence showed that bacterial activity was not responsible. The above would suggest that assumption (1) given in the THEORETICAL section be fulfilled.

Consider assumption (2) which requires water movement to be analogous to heat flow where only a single phase is studied. Experimentally, the cylinder that supported the soil being composed of 1 cm segments allowed air to be displaced between those segments and also out the open end of the column. It would at first seem logical with the large differences in viscosity between that of water and air that this assumption might be fulfilled. Miller and Miller (1955) have discussed the wetting and drying of soils with particular emphasis given to hysteresis occurring in a single pore or sequence. The heterogeneous nature of the size, shape, composition and arrangement of soil particles complicates the task of physically describing the addition or removal of soil water at different rates. The contact angles between the water and the various surfaces would vary and would also depend upon rate of movement (Biggar and Taylor, 1960). The discontinuity of air and the possibility of its displacement is recognized at water contents near saturation. Once continuous air passages exist within the soil, further consideration of air movement has been generally neglected. With visual observation of a Christianson filter (Davidson, et al., 1962) having air as one of its fluids, it is easily recognized that the water distribution within a porous material is not unique for a given fluid content. Depending upon the position of the source of air and the rate at which the air is allowed to displace the original fluid, different fluid distributions occur. The particular distribution of air within the mass will again influence

subsequent displacements. In the transient condition of soil water movement, a sudden emptying of a relatively large pore sequence connected to the bulk soil mass by only smaller necks or openings will produce a disturbance that persists long enough to influence the draining of other pores in close proximity. A comparison made by Elrick (in press) of transient and steady-state water flow in unsaturated sand also suggests the same description. A suitable experiment to perform concerning the movement of the second phase would be the following: Subject samples of equal initial water content but of unequal lengths to identical increments of applied soil water pressure and observe rate of water content change. In addition, for equal soil lengths, a study of the water content relations for unequal pressure increments applied over the same pressure range would yield further insight to the problem. It is also possible to study water movement with the total air pressure reduced below normal atmospheric pressure although the use of gases other than air would probably be more convenient.

The third assumption states the properties of the fluid or water do not vary. It seems reasonable from work such as that of Anderson and Low (1958) that the physical state of water in films of considerable thickness differs markedly from that in bulk quantities. The presence of ions in the soil solutions also works against the validity of this assumption. The surface properties of the soil colloids together with their residual charge, are responsible for a non-uniform ion distribution within the liquid phase. Moreover, these distributions depend upon the pore diameter or the liquid film thickness. Experimental evidence of the behavior of water and aqueous solutions flowing through small capillaries of great length would be helpful in ascertaining the limits of applicability of this assumption.

Anderson and Linville (1962) have measured substantial temperature fluctuations in initially dry porous materials during water infiltration. For 35 u diameter glass beads, the accompanying temperature change was greater than 0.1° C while for bentonites changes have been measured as high as 40° C. Temperature increases of 2 to 5° C are commonly measured on air-dry agricultural soils. Because the Columbia and Hesperia soils were initially air-dry, it would be expected that significant temperature fluctuations occurred during infiltration. These fluctuations would influence the water movement to a greater degree as values of θ_o became substantially less than saturation.

In addition to the above assumptions, it is worthwhile to compare these experimental data with previously published data. Vertical soil water profiles reported by Bodman and Colman (1943) and horizontal profiles reported by Bruce and Klute (1956) have sharp increases in water content near $x = 0$. This increase is not peculiar to vertical nor horizontal water movement. Such an increase is not found in Figures XIII-12 through XIII-16. It is of interest to note that it is possible to produce such a water content distribution in Columbia and Hesperia soils with the apparatus shown in Figure XIII-1. By merely initiating flow with a slight instantaneous positive pressure or by pinching off the flexible tubing of the porous plate to cease flow at time t_o, the water content near $x = 0$ is increased. Such experimental artifacts demonstrate the necessity of additional carefully planned and executed experiments. With such information at hand, the physical processes revealed could be described.

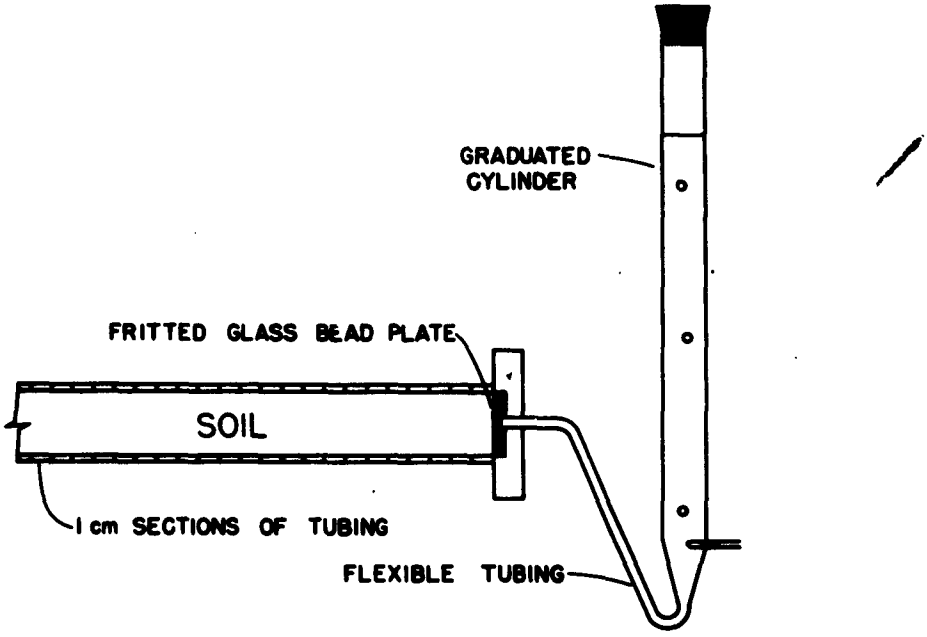

Figure XIII-1. Schematic diagram of apparatus used for horizontal and vertical soil water movement.

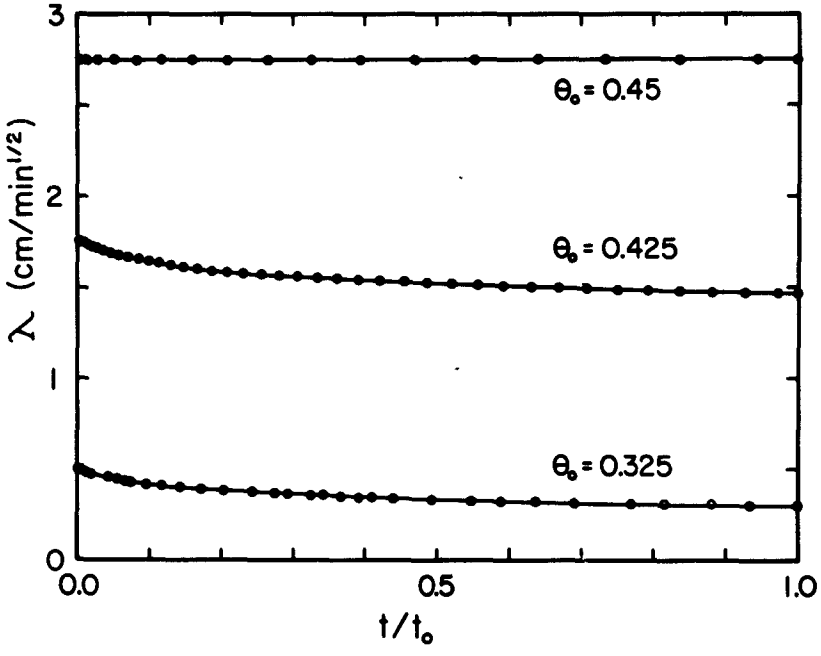

Figure XIII-2. Values of λ determined by visual distance to the wetting front divided by the square root of time for water infiltrating air-dry Columbia silt loam. θ_o is the soil water content at $x = 0$, the inflow end of the column.

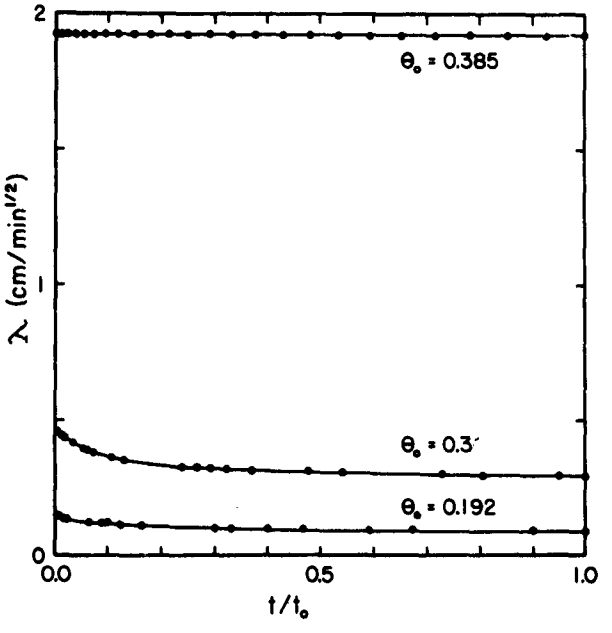

Figure XIII-3. Values of λ determined by visual distance to the wetting front divided by the square root of time for water infiltrating air-dry Hesperia sandy loam.

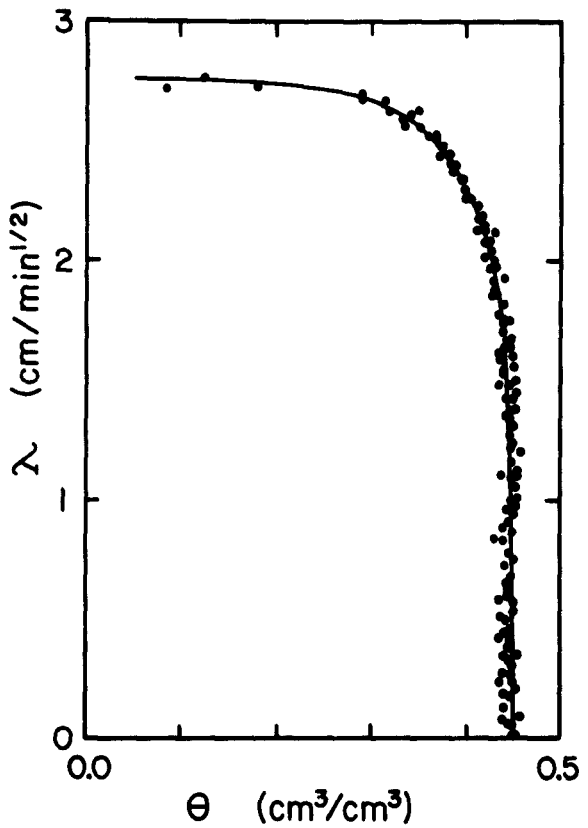

Figure XIII-4. Values of λ for Columbia soil determined from water content distributions measured for three time periods of infiltration with θ_o = 0.45 cm^3/cm^3.

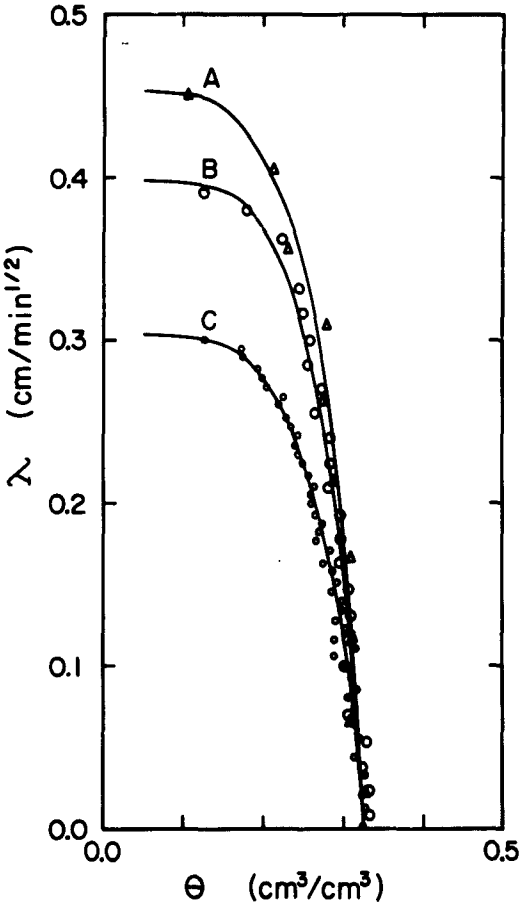

Figure XIII-5. Values of λ for Columbia soil determined from water content distributions measured for three time periods of infiltration with θ_o = 0.325 cm^3/cm^3. Curves A, B, and C correspond to times t_o equal to 441, 4182 and 28224 minutes, respectively.

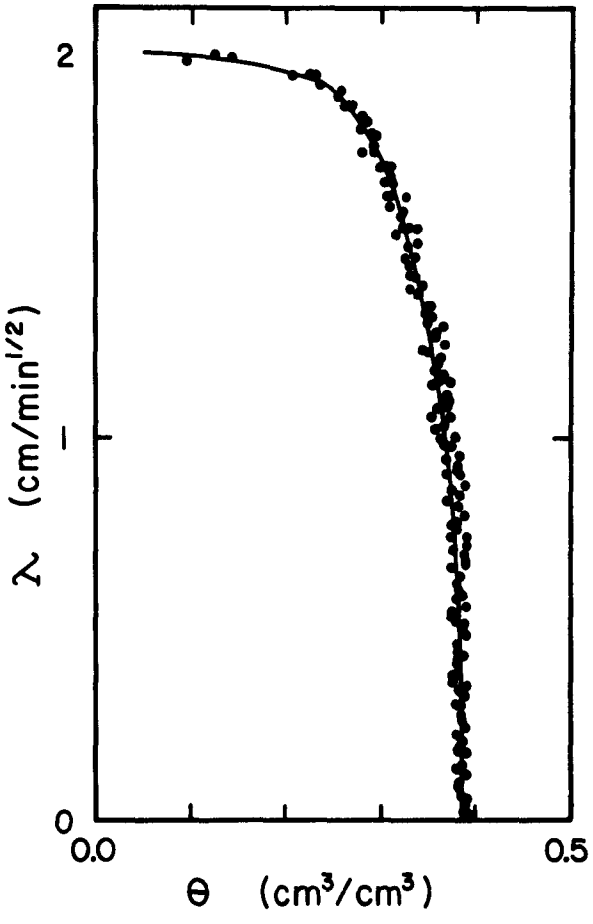

Figure XIII-6. Values of λ for Hesperia soil determined from water content distributions measured for three time periods of infiltration with θ_o = 0.385 cm^3/cm^3.

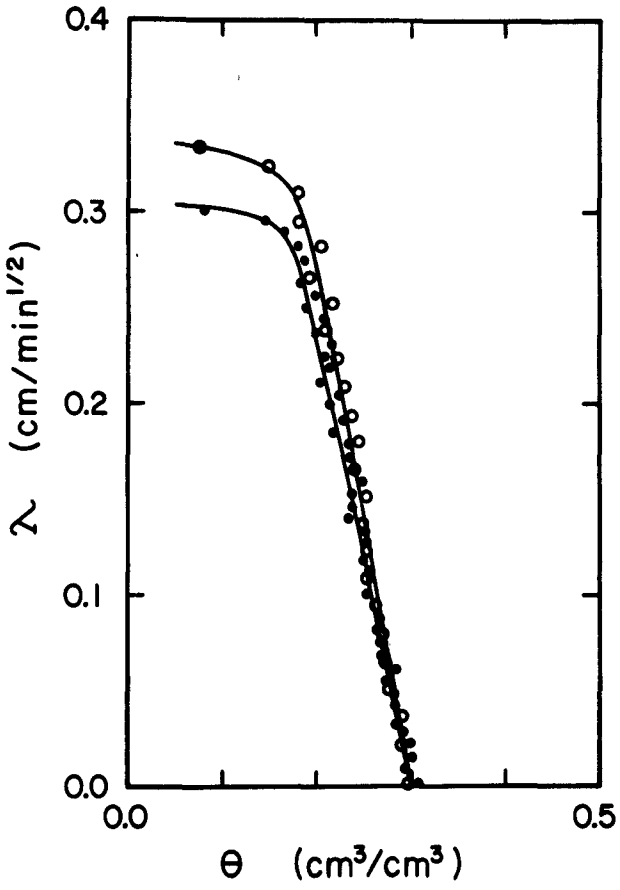

Figure XIII-7. Values of λ for Hesperia soil determined from water content distributions measured for two time periods of infiltration with $\theta_o = 0.30\ cm^3/cm^3$. Solid points and open circles represent data corresponding to times t_o equal to 4820 and 23677 minutes respectively.

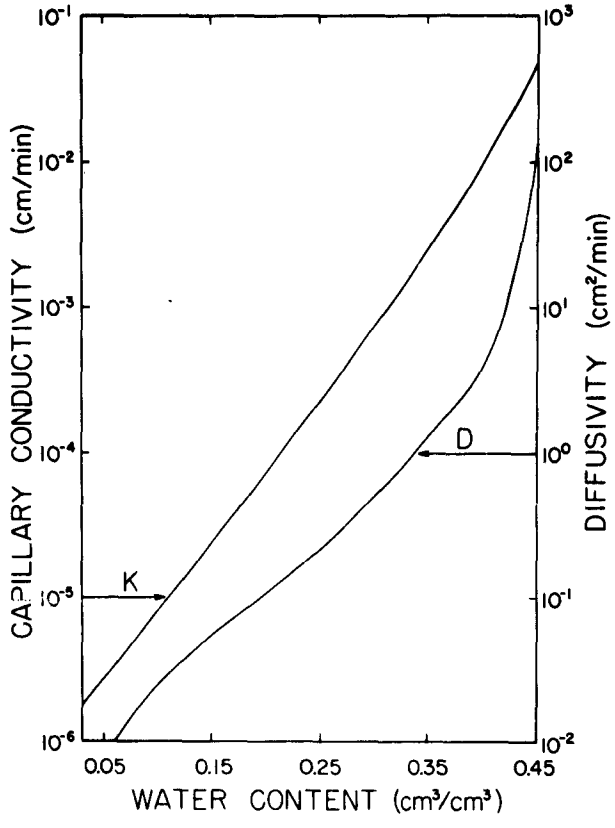

Figure XIII-8....Experimental values of capillary conductivity K and soil water diffusivity D for Columbia silt loam used to calculate vertical soil water movement.

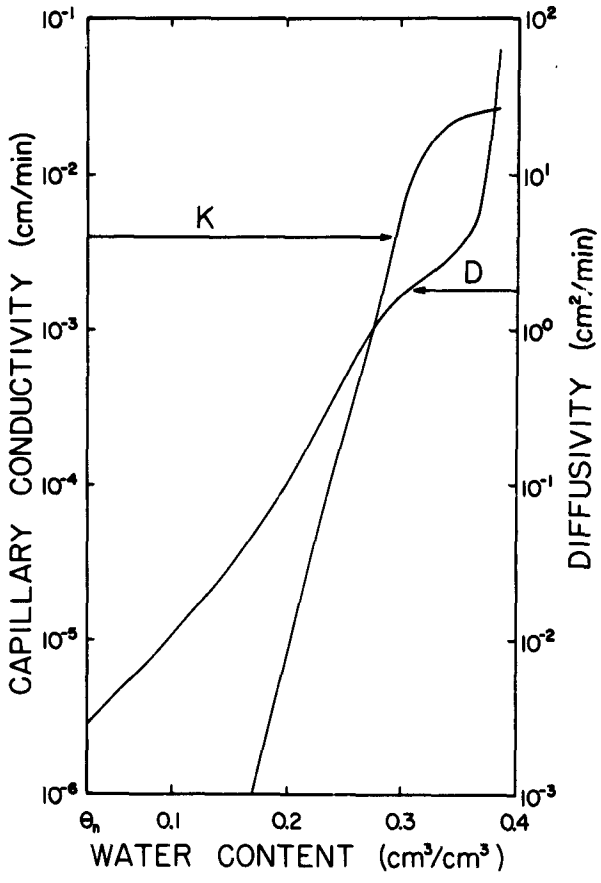

Figure XIII-9. Experimental values of capillary conductivity K and soil water diffusivity D for Hesperia sandy loam used to calculate vertical soil water movement.

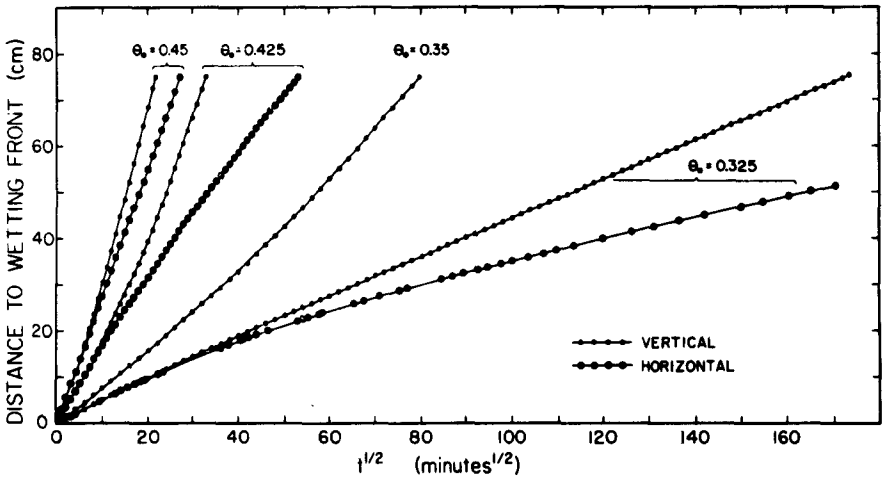

Figure XIII-10. Distance to the wetting front of air dry Columbia silt loam versus square root of time for horizontal and vertical movement.

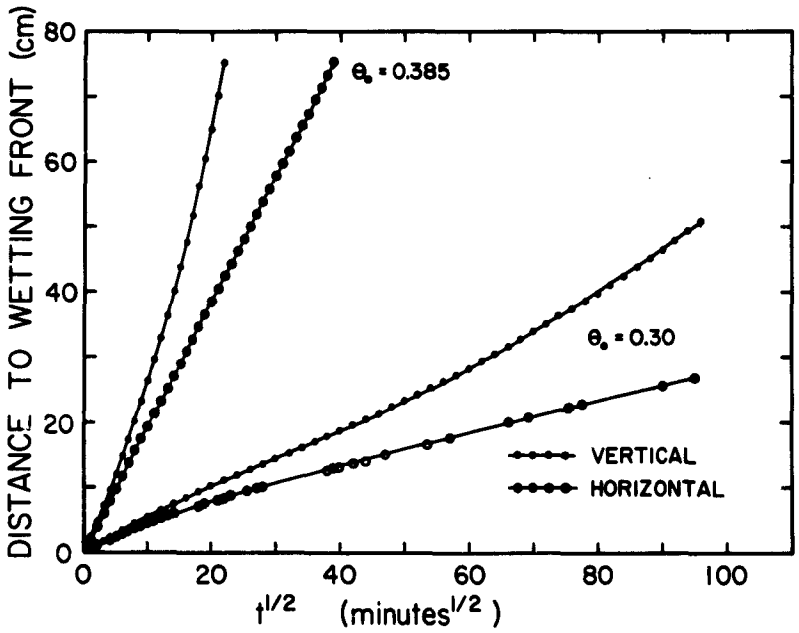

Figure XIII-11. Distance to the wetting front of air-dry Hesperia sandy loam versus square root of time for horizontal and vertical movement.

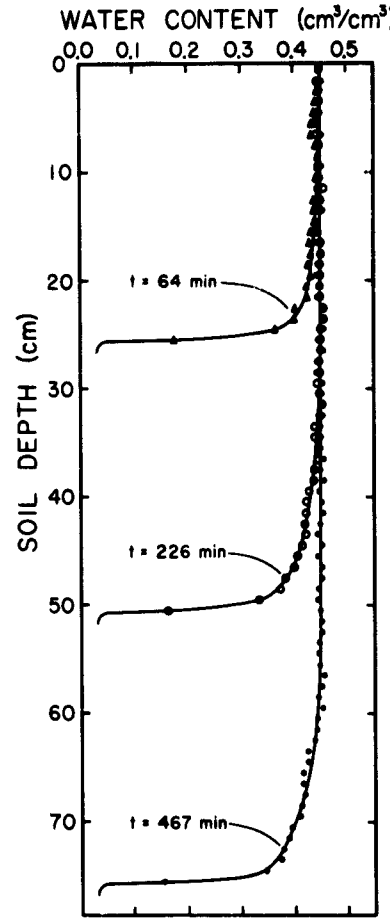

Figure XIII-12. Columbia soil water content distributions for vertical profiles developed in air-dry soil with $\theta_o = 0.45\ cm^3/cm^3$.

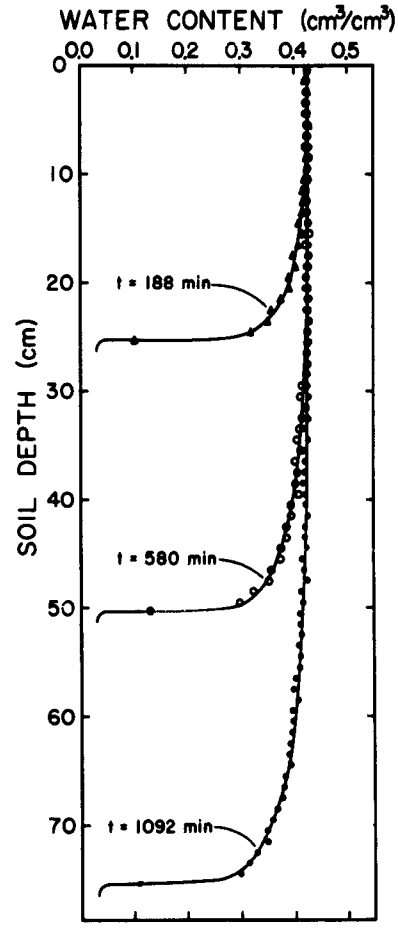

Figure XIII-13. Columbia soil water content distributions for vertical profiles developed in air-dry soil with θ_o = 0.425 cm^3/cm^3.

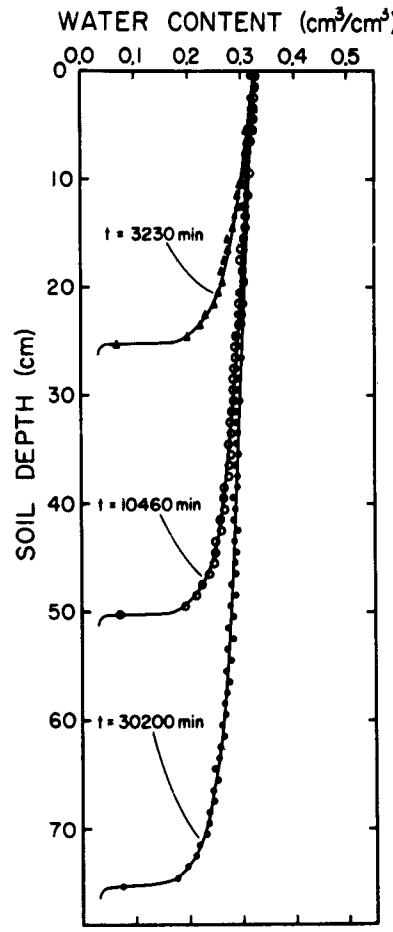

Figure XIII-14. Columbia soil water content distributions for vertical profiles developed in air-dry soil with θ_o = 0.325 cm^3/cm^3.

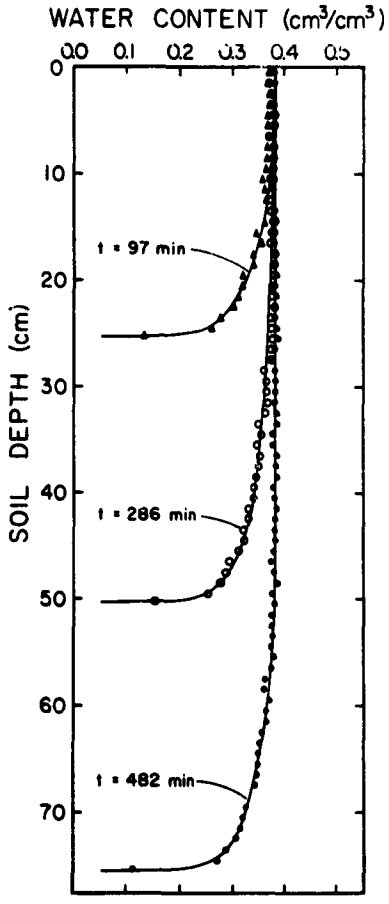

Figure XIII-15. Hesperia soil water content distributions for vertical profiles developed in air-dry soil with θ_o = 0 385 cm^3/cm^3.

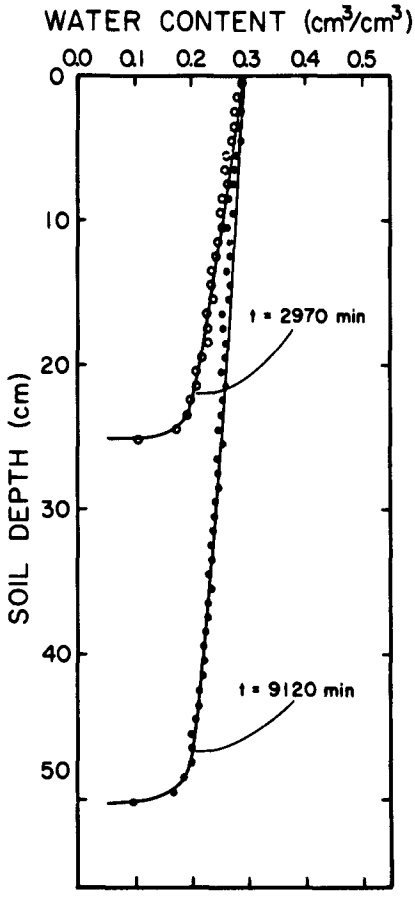

Figure XIII-16. Hesperia soil water content distributions for vertical profiles developed in air-dry soil with θ_o = 0.30 cm^3/cm^3.

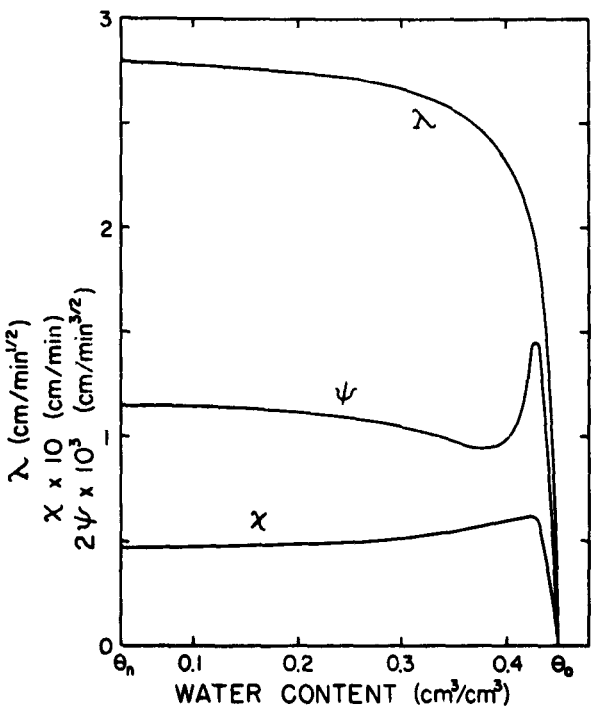

Figure XIII-17. Calculated values of λ, χ, and ψ defined in equation (7) for Columbia silt loam.

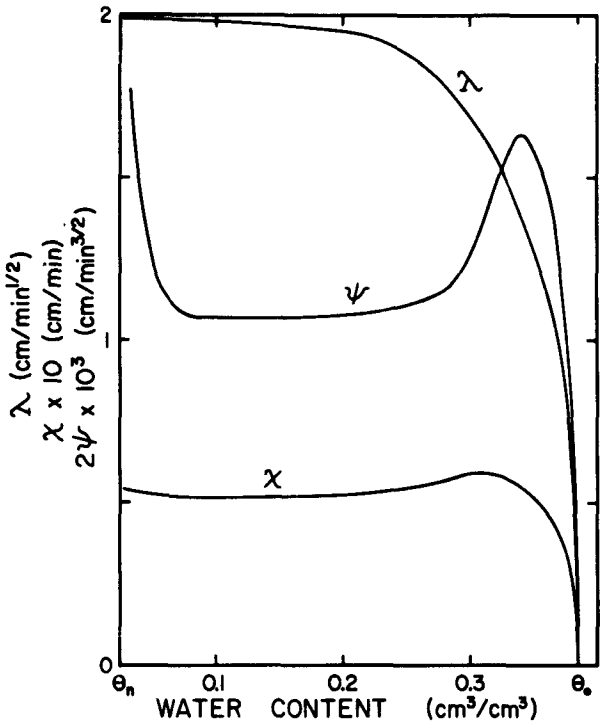

Figure XIII-18. Calculated values of λ, χ, and ψ defined in equation (7) for Hesperia sandy loam.

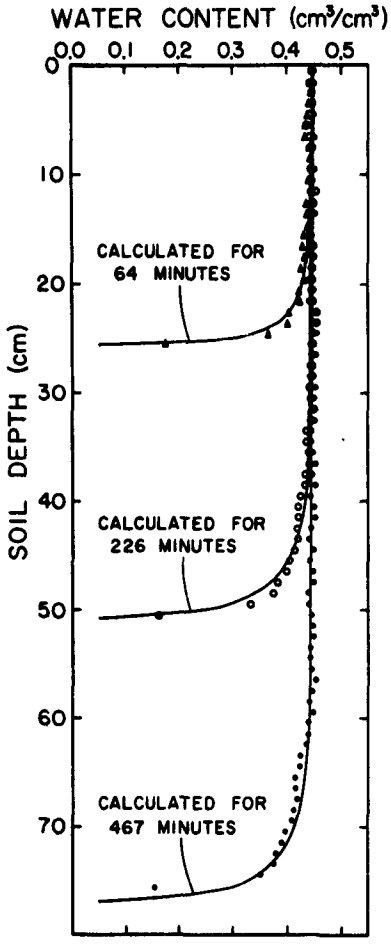

Figure XIII-19. Calculated and measured soil water profiles for air-dry Columbia soil allowed to wet at θ_o = 0.45 cm³/cm³.

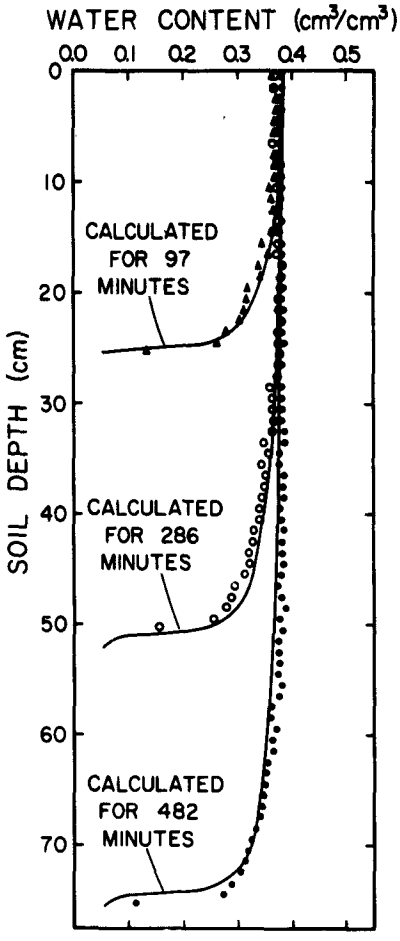

Figure XIII-20. Calculated and measured soil water profiles for air-dry Hesperia soil allowed to wet at θ_o = 0.385 cm^3/cm^3.

LITERATURE CITED IN CHAPTER XIII

Anderson, D. M., and Low, P. F. 1958. The density of water adsorbed by lithium-sodium-, and potassium-bentonite. Soil Sci. Soc. Am Proc. 22:99-103.

Anderson, D. M., and A. Linville. 1962. Temperature fluctuations at a wetting front: I. Characteristic temperature-time curves. Soil Sci. Soc. Amer. Proc. 26:14-18.

Baver, L. D. 1956. Soil Physics. John Wiley and Sons, Inc., New York.

Biggar, J. W., and S. A. Taylor. 1960. Some aspects of the kinetics of moisture flow into unsaturated soils. Soil Sci. Soc. Am. Proc. 24:81-85.

Bodman, G. B., and E. A. Colman. 1943. Moisture and energy conditions during downward entry of water into soils. Soil Sci. Soc. Am. Proc. 8:116-122.

Bruce, R. R., and A. Klute. 1956. The measurement of soil moisture diffusivity. Soil Sci. Soc. Am. Proc. 20:458-462.

Chilcs, E. C., and N. Collis-George. 1948. Soil geometry and soil water equilibrium. Disc. Faraday Soc. 3:78-85.

Childs, E. C., and N. Collis-George. 1950. The permeability of porous materials. Proc. Roy. Soc. London A201:392-405.

Darcy, H. 1856. Les fountaines publiques de la ville de Dijon. Dalmont Paris.

Davidson, J. M., J. W. Biggar, and D. R. Nielsen. 1962. A model for teaching students how water and air move through soil. Soil Sci. Soc. Am. Proc. 26:302-303.

Elrick, D. E. In press. Unsaturated flow properties of soils. Australian Jour. Soil Research 1:_____.

Miller, E. E., and R. D. Miller. 1955. Theory of capillary flow: 1. Practical implications. Soil Sci. Soc. Am. Proc. 19:267-271.

Nielsen, D. R., and R. E. Phillips. 1958. Small fritted glass bead plates for determination of moisture retention. Soil Sci. Soc. Am. Proc. 22:574-575.

Nielsen, D. R., and J. W. Biggar. 1961. Measuring capillary conductivity. Soil Science 92:192-193.

Nielsen, D. R., J. W. Biggar and J. M. Davidson. 1962. Experimental consideration of diffusion analysis in unsaturated flow problems. Soil Sci. Soc. Am. Proc. 26:107-111.

Philip, J. R. 1955. Numerical solution of equations of the diffusion type with diffusivity concentration-dependent. Trans. Faraday Soc. 51:885-892.

Philip, J. R. 1957a. Numerical solution of equations of the diffusion type with diffusivity concentration - dependent: 2. Australian Jour. Phys. 10:29-42.

Philip, J. R. 1957b. The theory of infiltration: 1. The infiltration equation and its solution. Soil Science 83:345-357.

Philip, J. R. 1957c. The theory of infiltration: 2. The profile at infinity. Soil Science 83:435-448.

Philip, J. R. 1957d. The theory of infiltration: 3. Moisture profile and relation to experiment. Soil Science 84:163-187.

Richards L. A. 1931. Capillary conduction of liquid through porous media. Physics 1:318-333.

Richards, L. A. 1952. Report of the sub-committee on permeability and infiltration, committee on terminology, Soil Science Society of America. Soil Sci. Soc. Am. Proc. 16:85-88.

Youngs, E. G. 1957. Moisture profiles during vertical infiltration. Soil Science 84:283-290.

APPENDIX A

LIST OF INSTRUMENTS AND TABLE OF PROPERTIES OF DRY AIR AND THE WET-BULB COMPUTATION OF MOISTURE CONTENT

Table A-1. INSTRUMENT LIST FOR RESEARCH IN HEAT AND MOISTURE TRANSFERS
University of Calif. Signal Corps Project

Modes of Heat Transfer	Symbol	Instrument	Independent Verification	Eq. # FAB	page CHBP*
RADIATION (above surface)	I	1. Eppley pyrheliometers			
		(1a) New model "normal incidence"	Evap. pans (approx.)	2-20a	
	W_z	(1b) Unshaded regular (Weather Sta.) Eppley, facing upward		2-24	
		(1c) Inverted regular Eppley			
	I_z, diffuse				
		(1d) Shaded regular Eppley			
		2. Radiometers			
net exchange	R_n	(2a) Unshaded whole-spectrum radiation exchange (B&W net radiometer)		2-14	
		(2b) CSIRO net radiometer		2-28	
		(2c) Shaded whole-spectrum G&D net		II-R	
		(2d) Unshaded whole-spectrum single hemisphere (B&W) with bottom shield		App. A	
CONDUCTION (below surface)	G	3. Soil Thermometers	(3) vs (4)	3-4	
		(3a) Plain thermocouples		3-3b	
		(3b) Suomi distributed resistance thermometers		3-5 3-6	
		(3c) Thermocouple in heat flow meter			
		4. B & W Heat Flow Meters	approx. sum	3-14	
CONVECTION (sensible heat above surface)	H_c	5. CSIRO Eddy Correlation Meters		4-8	2.2
		(5a) CSIRO eddy corr. meter for momentum transfer		4-14	4.4
		(5b) CSIRO eddy corr. meter for dry-bulb temp.			
		(5c) CSIRO eddy corr. meter for wet-bulb temp. Residual heat balance		4-7	
air drag		11. Shear Stress Meters	(5a)		
		(11a) Floating lysimeter			
		(11b) 30-inch Vehrencamp meter			
velocity profiles		12. Anemometers		7.4	p.91
		(12a) Cup anemometers -Thornthwaite		3.9	p.25
		(12b) Cup anemometers -Casella			
		(12c) Cup anemometers -Boller-Chivens			
		(12d) Cup anemometers -Fries			
		(12e) Hot wire anemometers			
temperature profiles		(13a) Aspirated thermocouples - dry		4-14	4.2
aerosol concentration		(15) Line source			
		(16) Detectors (photocells)			
MOISTURE TRANSFER soil moisture change	E_v	6. 20-foot Lysimeters			
		(6a) 20-ft. weighing lysimeter			
		(6b) 20-ft. floating lysimeter	(5c)	4-11	
soil moisture content		(7) Tensiometers (Pruitt's)		5-2	
		(8) Soil sampling for moisture content			
moisture profiles		(13b) Aspirated thermocouples - wet		3-3b	7.3
		(14) Moisture profiles by optical meters (spectrographic)			
convection above surf.			(11)+(12)+(14)		
PHOTOSYNTHESIS above surface		(9) Weight gain - cuttings Diurnal curve est. from (1)+(13a)			
RESPIRATION below surface		(10) Estimated from soil temp.			

* PRIESTLEY, C.H.B. "Turbulent Transfer in the Lower Atmosphere", 1959.
BROOKS, F.A. "Introduction To Physical Microclimatology", 1960.

TABLE A-2. QUALITIES OF DRY AIR, 0 to 39.9°C

DRY AIR DENSITY, $\rho_a = \rho_o \frac{273.16}{273.16+t}$

KINEMATIC VISCOSITY ν $cm^2 sec^{-1}$	TEMP. t °C	$gm_m cm^{-3}$ (ρ_o = .0012923) 0.0	0.1	0.2	0.3	0.4	0.5	0.6	0.7	0.8	0.9
.1322	0.0	.001292	.001292	.001291	.001291	.001290	.001290	.001290	.001289	.001288	.001288
.1331	1.0	.001288	.001287	.001287	.001286	.001286	.001285	.001285	.001284	.001284	.001283
.1340	2.0	.001283	.001282	.001282	.001282	.001281	.001280	.001280	.001280	.001279	.001279
.1349	3.0	.001278	.001278	.001277	.001277	.001276	.001276	.001276	.001275	.001275	.001274
.1358	4.0	.001274	.001273	.001273	.001272	.001272	.001271	.001271	.001271	.001270	.001270
.1366	5.0	.001269	.001269	.001268	.001268	.001267	.001267	.001266	.001266	.001265	.001265
.1375	6.0	.001264	.001264	.001264	.001263	.001262	.001262	.001262	.001261	.001261	.001260
.1384	7.0	.001260	.001260	.001259	.001259	.001258	.001258	.001257	.001257	.001256	.001256
.1393	8.0	.001256	.001255	.001255	.001254	.001254	.001253	.001253	.001252	.001252	.001252
.1402	9.0	.001251	.001251	.001250	.001250	.001249	.001249	.001248	.001248	.001248	.001247
.1411	10.0	.001247	.001246	.001246	.001245	.001245	.001244	.001244	.001244	.001243	.001243
.1420	11.0	.001242	.001242	.001241	.001241	001240	.001240	.001240	.001239	.001239	.001238
.1429	12.0	.001238	.001238	.001237	.001237	.001237	.001236	.001235	.001235	.001234	.001234
.1438	13.0	.001234	.001233	.001233	.001232	.001232	.001231	.001231	.001231	.001230	.001230
.1447	14.0	.001229	.001229	.001228	.001228	.001228	.001227	.001227	.001226	.001226	.001226
.1456	15.0	.001225	.001225	.001224	.001224	.001223	.001223	.001222	.001222	.001222	.001221
.1465	16.0	.001221	.001220	.001220	.001220	.001219	.001219	.001218	.001218	.001217	.001217
.1474	17.0	.001217	.001216	001216	.001215	.001215	.001214	.001214	.001214	.001213	.001213
1483	18.0	.001212	.001212	.001212	.001211	.001211	.001210	.001210	.001210	.001210	.001209
.1492	19.0	.001208	.001208	.001207	.001207	.001207	.001206	.001206	.001205	.001205	.001204
.1502	20.0	.001204	.001204	.001203	.001203	.001202	.001202	.001202	.001201	.001201	.001200
.1511	21.0	.001200	.001200	.001199	.001199	.001198	.001198	.001198	.001197	.001197	.001196
.1520	22.0	.001196	.001196	.001195	.001195	.001194	.001194	001194	.001193	.001193	.001192
.1529	23.0	.001192	.001192	.001191	.001191	.001190	.001190	.001190	.001189	.001189	.001188
.1538	24.0	.001188	.001188	.001187	.001187	.001186	.001186	.001186	.001185	.001185	.001184
.1548	25.0	.001184	.001184	.001183	.001183	001182	.001182	.001182	.001181	.001181	.001180
.1557	26.0	.001180	.001180	.001179	.001179	.001178	.001178	.001178	.001177	.001177	.001176
.1566	27.0	.001176	.001176	.001175	.001175	.001174	.001174	.001174	.001173	.001173	.001172
.1576	28.0	.001172	.001172	.001171	.001171	.001171	.001170	.001170	.001169	.001169	.001169
.1585	29.0	.001168	.001168	.001168	.001167	.001167	.001166	.001166	.001166	.001165	.001165
.1594	30.0	.001164	.001164	.001164	.001163	.001163	.001162	.001162	.001162	.001161	.001161
.1604	31.0	.001161	.001160	.001160	.001159	.001159	.001159	.001158	.001158	.001158	.001157
.1613	32.0	.001157	.001156	.001156	.001156	.001155	.001155	.001154	.001154	.001154	.001153
.1622	33.0	.001153	.001153	.001152	.001152	.001152	.001151	.001151	.001150	.001150	.001150
.1632	34.0	.001149	.001149	001148	.001148	.001148	.001147	.001147	.001147	.001146	.001146
.1641	35.0	.001146	.001145	.001145	.001144	.001144	.001144	.001143	.001143	.001132	.001142
.1651	36.0	.001142	.001141	001141	.001141	001140	.001140	.001140	.001139	.001139	.001138
.1660	37.0	.001138	.001138	.001137	.001137	.001137	.001136	.001136	.001136	.001135	.001135
.1670	38.0	.001134	.001134	.001134	.001133	.001133	.001133	.001132	.001132	.001132	.001131
.1680	39.0	.001131	.001130	.001130	.001130	.001129	.001129	.001129	.001128	.001128	.001128

WET-BULB COMPUTATION OF MOISTURE CONTENT

From Smithsonian Meteoro. Tables p. 365 the dry-bulb/wet-bulb relation is:

$$\text{(A-1)} \qquad A = \frac{e' - e}{p(t-t')} = 0.000660\ {}^{\circ}C^{-1} \left\{1 + 0.00115\ {}^{\circ}C^{-1}\ t'\right\}, \qquad {}^{\circ}C^{-1}$$

$$\text{Namely} \qquad \frac{e}{.00066p} = \frac{e'}{.00066p} - \left\{1 + .00115\ t'\right\}(t-t'), \qquad {}^{\circ}C$$

Where

- e', mb, = saturated vapor pressure at the wet-bulb temp. t'
- e, mb, = actual vapor pressure in air
- p, mb, = barometric pressure (std. sea-level press. = 1013.25 mb)
- t, $^{\circ}C$, = dry-bulb temp.
- t', $^{\circ}C$, = wet-bulb temp.

Since a power-law representation of the psychrometer curve formula involves the 6.15 power of a fraction, and a difference formula calls for a graph of psychrometer curve slope vs. wet-bulb temp., we might more easily use the following log formula, Figure A-1 for saturated vapor pressure Then:

$$\text{(A-2)} \qquad e_z = 8.108\ \text{antilog}_{10}\,(.0247\ t'_z) - 2.0 - .00066p\left\{1 + .00115\,t'_z\right\}(t_z - t'_z), \text{mb}$$

Thus we need wet-bulb temp. t' twice and wet-bulb depression $(t-t')$ once.

<u>Determination of Virtual Temperature Gradient to find the Times of Neutral Stability</u>. Neutral stability is not defined by zero gradient in potential temperature when considerable gradient in specific humidity exists. This is significant in the eddy transfer tests of 30-31 July 1962 when dry-bulb temperature gradients were weak most of the day because the latent heat taken up in evapotranspiration from the grass turf used practically all the net radiation. Two procedures are available to determine the times of neutral stability: 1) determination of times when virtual temperature gradient equals the dry adiabatic (Γ = 1.0°C/100m); and 2) when there is zero change in potential density with height. Using the first, virtual temperature is calculated from dry-bulb temperature by the common formulas:

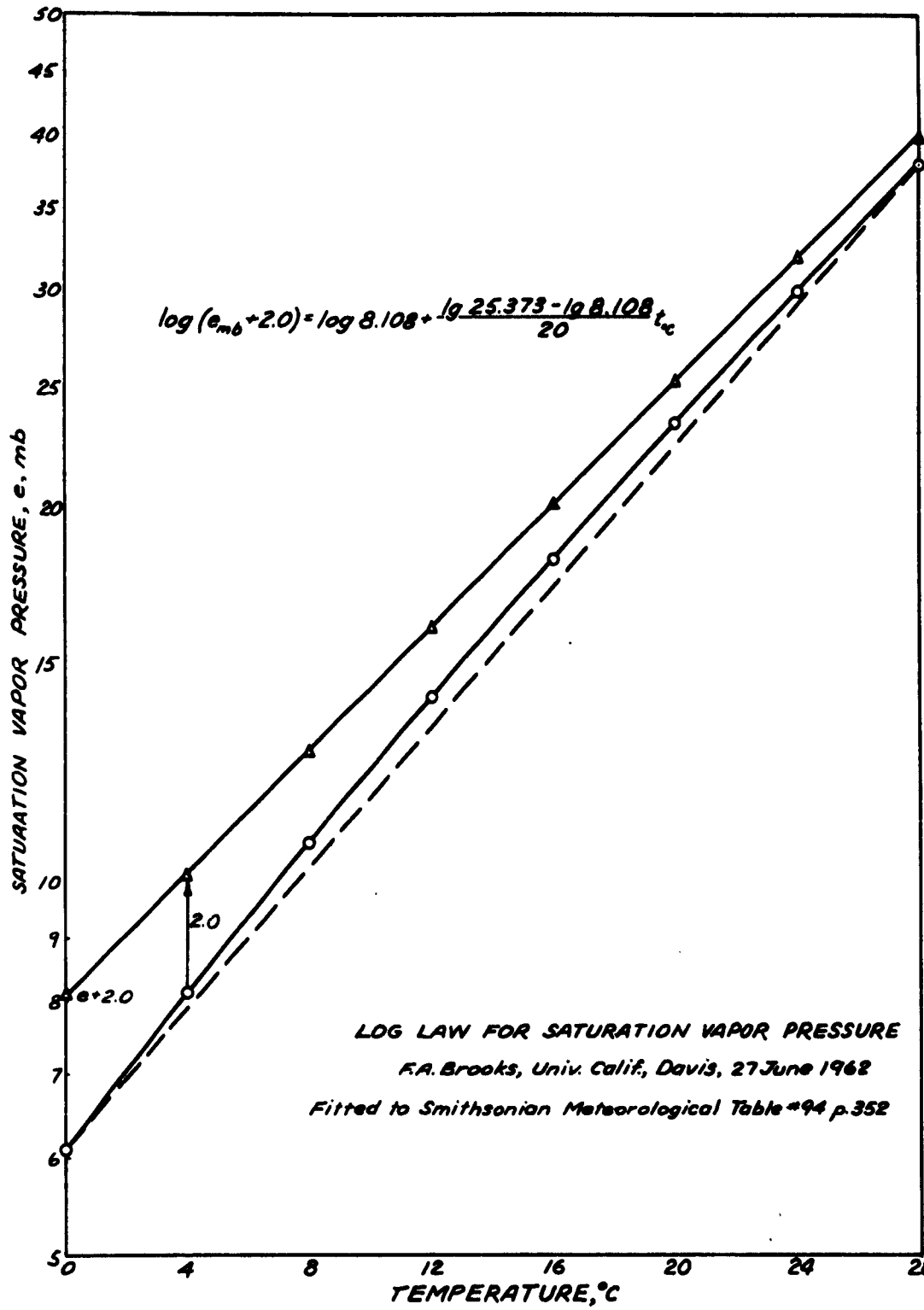

Figure A-1. Log law for saturation vapor pressure.

(A-3a) $$T' = \frac{T}{1.0 - 0.378\, e/p_a} \quad , \quad {}^{o}K \quad ,$$

(A-3b) $$T' = T\,\frac{1.0 + \dfrac{\rho w/\rho a}{0.622}}{1.0 + \rho w/\rho a} = (1.0 + 0.61\, \rho w/\rho a)\, T, \quad {}^{o}K.$$

In the first form (A-3a), the volumetric fraction occupied by the water vapor is ratio of partial pressures and this fraction is less dense than dry air by the deficiency in molecular weight $\frac{29 - 18}{29} = 0.378$. In the second form (A-3b), when a mixing ratio, $\text{gram}_{H_2O} / \text{gram}_{air}$, describes moisture content, a gram of water vapor occupies $\frac{29}{18} = 1.61$ times the volume of a gram of dry air. This means that the excess volume is $0.61\, \rho_w / \rho_a$. For the usual small ratios of e/p_a or ρ_w / ρ_a the moist air pressure or density is used namely e/p or ρ_w / ρ.

APPENDIX B

RADIOMETER CALIBRATION

The necessity of field checking the factory calibration of radiometers became apparent when it was found that net radiation values reported by Pruitt and Angus in Chapter 6 of the 1961 Annual Report were in error. Considering simultaneous readings of shortwave radiation, the error appeared to be 10% to 20%, too high. A comparison-shading technique has been developed which appears capable of determining all radiometer calibration factors to within 2% of their correct values.

An Eppley Normal Incidence Radiometer is the standard to which the radiometers under test are compared. First, the radiometer under test is exposed to both the sky and the direct incoming solar radiation. Approximately 30 readings of each radiometer are recorded in a 1 minute period by the Electro Instruments Automatic Data Recording System. The radiometer under test is then shaded by a shade so designed that it subtends the same solid angle of the sky that is being viewed simultaneously by the Normal Incidence Radiometer. After the shaded radiometer comes to equilibrium, approximately 30 readings are taken again of the two radiometers by the recording system. The solar elevation angle of the sun is read to the nearest 5 minutes from the shade-holding arm. The shade is then removed and an unshaded series of readings is again made. All of the calibrations are performed within 30 minutes of solar noon and the 3 sets of test readings are made within a 5 minute period. After converting the Normal Incidence Radiometer to a horizontal radiation flux, the k factor of the radiometer under test is readily determined.

Table B-1 lists some of the results of the calibration tests. For the Eppley Pyrheliometer that was checked, a scatter of $\pm$ 3% occurred in the tests conducted over a 5 month period. When a series of tests was performed on any one day, the scatter seldom exceeded 1%. Temperature and cosine corrections must be applied where applicable. From the appearance of the scatter of the field calibration factors, more attention should be given to the cleanliness of the pyrheliometer glass bulb. Also, the solar altitude angle measurements should be refined somewhat. For black plate radiometers, this method assumes that the upper and lower plates are equally balanced and exactly level.

TABLE B-1

REPEATABILITY IN FIELD CALIBRATIONS OF RADIOMETERS

Date	Type of Radiometer	Serial Number	Latest Factory Calibration	Field Calibration
Nov. 16	Eppley Pyrheliometer	2422	.4350	.4250
Nov. 19		2422	.4350	.4250
Jan. 5		2422	.4350	.4370
Feb. 22		2422	.4350	.4353
Feb. 27		2422	.4350	.4380
Mar. 7		2422	.4350	.4434
Mar. 19		2422	.4350	.4465
Feb. 28	Beckman-Whitley Net	262	.107	.1035
Mar. 7		262	.107	.1039
Mar. 19		262	.107	.1052

APPENDIX C

ANEMOMETER CALIBRATION AND NEW PULSE COUNTER

At low windspeeds non-similar performance can be seen in the profile array of cup anemometers. This makes it necessary to calibrate each anemometer with its output transducer. Also noticeable is occasionally erratic performance of the common electromagnetic counters. This defect usually comes from too narrow an operating range of voltage applied to the transducer and the relays. The previous permissible voltage range of about 10 per cent has been expanded to 50 per cent as described later.

To determine starting speeds of cup anemometers, a whirling-arm calibration apparatus is essential. This system requires two corrections, however, (i) the difference in radius to the driving cup depending on clockwise or counter clockwise rotation of the arm, and (ii) the circulating velocity of the air in the path of the anemometers. The first problem is completely handled by running all calibrations in both directions. This reversible rotation also settles the question of adding or subtracting a fractional count per rotation to allow for the inertia of the cups. The second problem of allowing for the circular flow of air following the anemometer is corrected in two ways: measuring the circulating airspeed by a stationary anemometer just beyond the one on the arm, and by comparing the test response with a performance curve interpolated below wind-tunnel ranging from 50 to 200 cm/sec. Figure C-1 shows how the two methods of calibration run together very well for two Thornthwaite anemometers. The resulting correction curve for the 3.5-meter whirling-arm, however, shows in Figure C-2 a 10 or 11 per cent correction continuing for speeds above 200 cm/sec. The considerable correction at lower speeds is partly due to using 2 arms (in order to compare 2 anemometers without needing to know true airspeed).

The wind tunnel of the University at Berkeley used for calibration at higher speeds has very low turbulence and an exceptionally flat profile in the 32-inch square test section. For low velocity tests, however, it was necessary to mount the anemometers near the outlet face of the 10-foot square plenum chamber ahead of the contraction section. Traverses across this face showed a slight non-uniformity in airspeed so the reductions from speed measurements in the test section to the two test positions ahead of contraction were 13.16 and 12.95 to 1.0 respectively.

Multi-Purpose Pulse Counting System. The development of a multi-purpose pulse counting system stemmed from poor field reliability of the Thornthwaite anemometer counters and inadequate timing of counting periods. A system was designed and built by W. B. Goddard which overcame these difficulties and gave greater flexibility to the anemometer counting and recording system. The new system centers around using a triode tube with the anemometer response causing a drop in grid bias which in turn closes a plate relay. The circuit, see Figure C-3, can be used with the resistance change used in the Thornthwaite or with circuit closure used in the Friez and Casella anemometers.

The Thornthwaite anemometers change their resistance by interrupting a light beam which is incident upon a cadmium sulfide cell. The change ranges from 60,000 ohms lighted to 10 meg ohms dark. Characteristically this high impedance does not work well with transistors and in field operation where heating causes transistors to miss-bias, the original transistorized Thornthwaite counting system did not operate reliably. The new system is not temperature sensitive and has shown good reliability under normal field conditions.

The breaker points of the Friez and Casella anemometers restrict their use to circuits using low current value. The grid bias circuit used in the new system is ideal for this reason having only a few micro amperes flowing across the points which insures long contact life. As a measure of field reliability, Table C-1 shows the range in which normal operation lies.

TABLE C-1

PARAMETER ALLOWABLE DEVIATION WITH NORMAL OPERATION

Plate voltage	150 V ± 50 V
Grid bias	16 V ± 5.0 V
Transducers impedance:	
range closed	0.0 to 150,000 ohms
range open	above 150,000 ohms

The counting system was built with twelve individual channels so that in case of a malfunction extra channels would usually be available. Manual reset electromagnetic A.C. Veeder Root counters capable of 1000 counts per minute were obtained for the integraters. A timing control circuit was built in with time period options of four, eight, twelve, fifteen, sixteen and

twenty minutes. The timing circuit will, upon selection of a time period and pushing the start button, start all twelve integrators counting for exactly the time period selected then stop and ringing a bell to notify personnel to record, turn back counters and start the next sampling period. The fifteen, sixteen and twenty minute timing periods fit in to most averaging periods of other measured field parameters while the four and eight minute time periods have proved very successful in recalibration procedures.

Another useful option was built into the system to continue each circuit closure output while timed integrating periods are being run, stopped, and recorded manually. This output can operate our Esterline Angus 20-pen recorder which will then make a continuous chart record of all anemometers plus a time signal. This option works well in conjunction with shear-stress measurements where the wind velocity must be continuous and accurately timed with the air drag record.

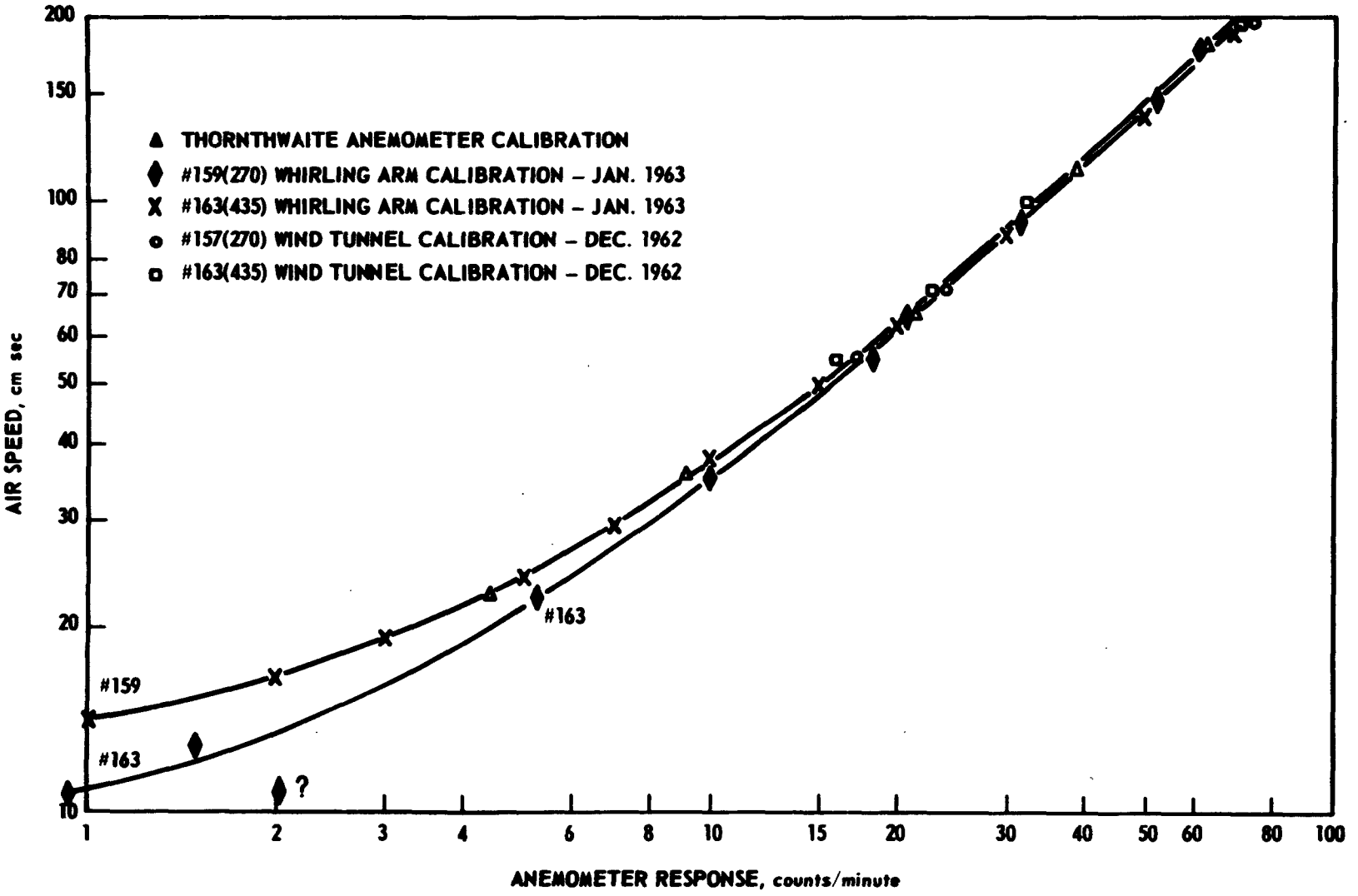

Figure C-1. Two methods of calibration for two Thornthwaite anemometers.

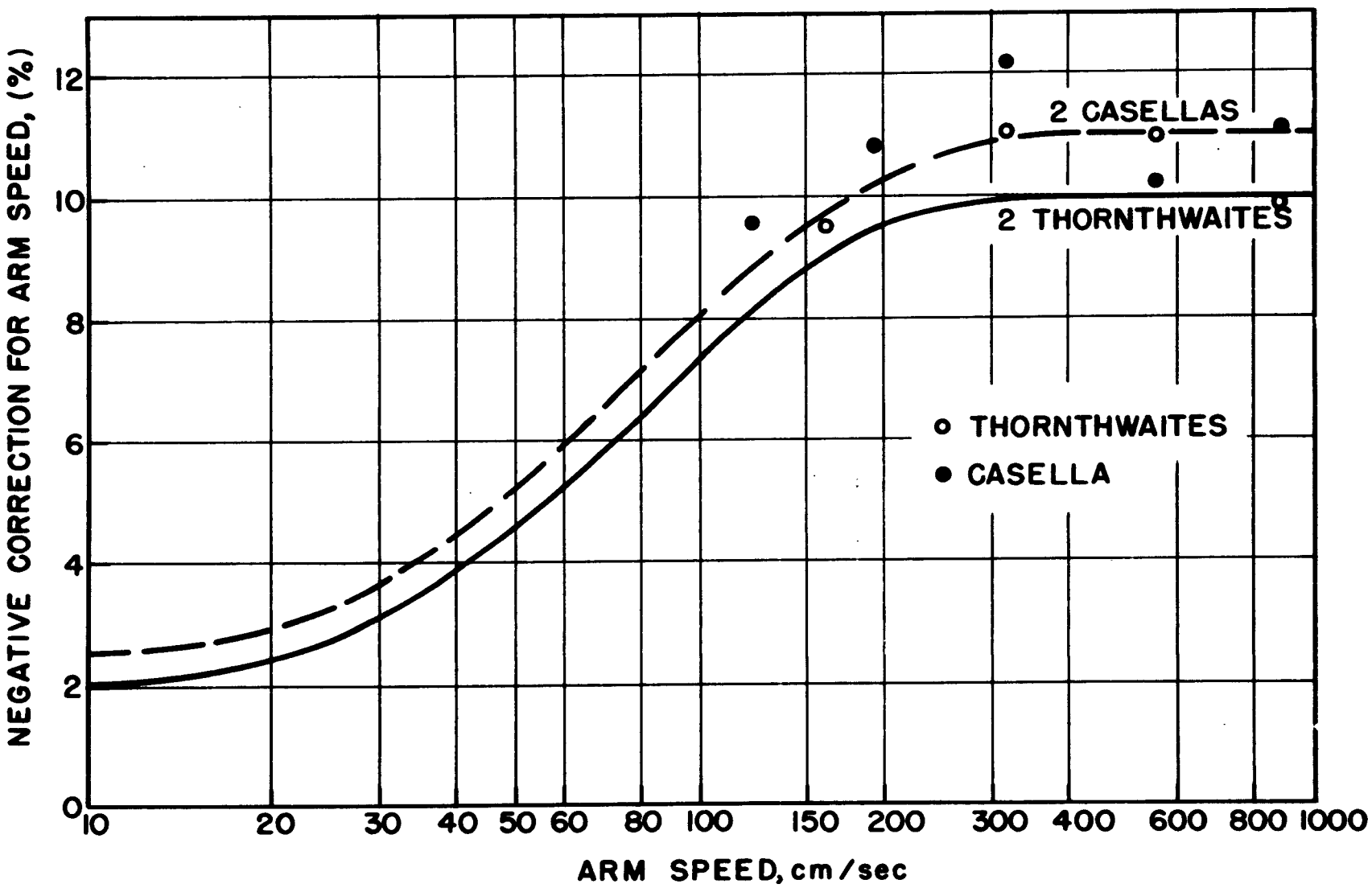

Figure C-2. Whirling-arm correction for circulating air.

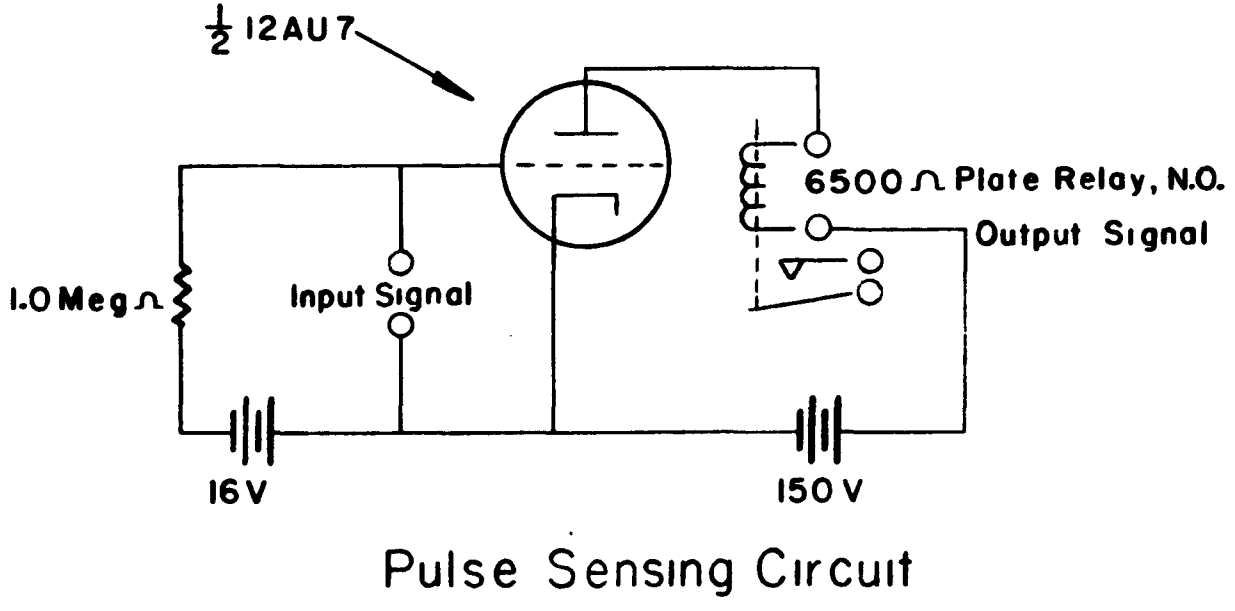

Figure C-3. Pulse sensing circuit.

APPENDIX D

TEMPERATURE PROFILE MASTS

Four identical 6-meter, 9-sampling point, aspirated, thermocouple masts have been constructed and put into operation and used during the December run. Figure D-1 shows the construction details of the masts. A calibration has been made on all of the thermocouples on each of the four masts and all were found to have not more than 4 microvolts difference from one another at any one temperature. Absolute calibration of the thermocouples to .01°C was made using a Leeds and Northrup Standard Platinum Resistance Thermometer which was N.B.S. calibrated. The standard thermometers were read with a 6-decade Kelvin-Varley divider potentiometer circuit which uses N.B.S. certified resistors for its basic resistance calibration.

Aspiration is accomplished by a vacuum pump which draws air past each of the butt welded #24 gage thermocouples located in the center of a 63 mm diameter intake hole in the bottom of plastic pipes extending into the wind 45 cm from the masts. The aspiration velocity is adjusted to standard 100 meters per minute past the thermocouples. At this rate there is little pressure drop in the pipe mast. The time constant of the thermocouples at this particular aspiration rate is approximately 3.5 seconds.

Radiation shades prevent the direct sun from impinging upon the area of the pipes which contains the thermocouple sensing element. The shades are narrow half cylinders 5 cm from the plastic pipes and of elliptical plan so that the direct sun would be shaded while at the same time allowing maximum exposure to the cold sky.

An experimental investigation was made in order to determine what the true physical heights being sampled by the thermocouples are because of the fact that air is being drawn from below at the rate of 52 cm^3/sec into a small hole. A small lighted candle was held near the intake opening and the influence of the air flowing into the intake was observed. No detectable influence was observed on the flame of the candle when it was more than 6 cm from the intake under perfectly calm conditions. At this distance the indraft velocity is 0.5 cm/sec. Thus when there is no wind, the air being sampled by the mast at any particular height is drawn in from a nearly spherical pattern centered around the intake, 1/3 coming within $\pm$ 1 cm in

height. With any wind blowing, the sample passing through the inlet port originates from upwind. If a one-minute sampling period is being considered in a 3 meters second wind, air sample from the masts to as far as 180 meters upwind passes by the thermocouple. At this rate the whole intake of 3120 cm^3/min comes from a ribbon of air only 1/4 mm thick.

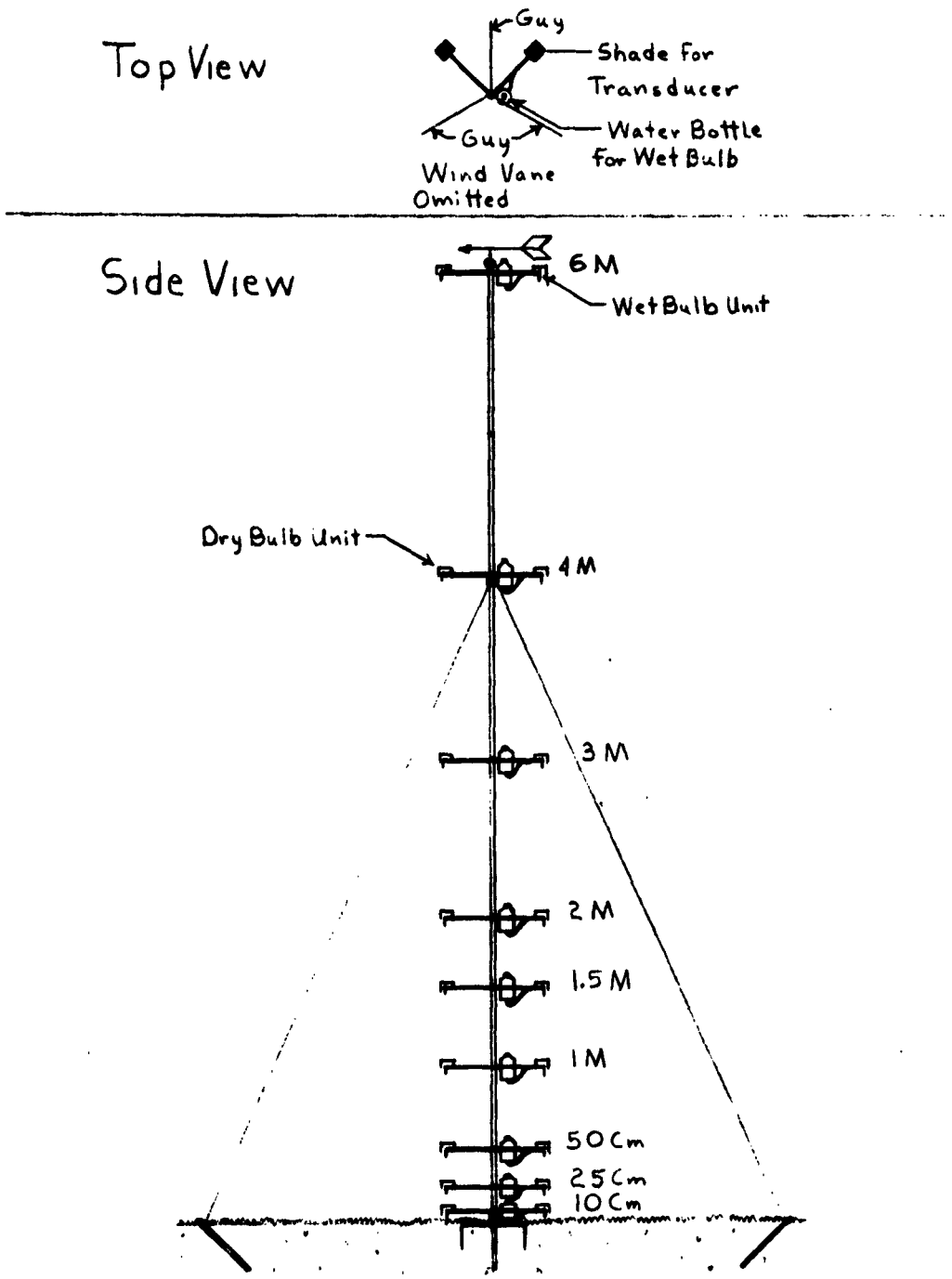

Figure D-1. Temperature, humidity and wind direction mast.

APPENDIX E

HUMIDITY SAMPLING SYSTEM (I.R. HYGROMETER)

An effective water vapor sampling system over the 20-foot weighing lysimeter has been put into operation. The system samples air at 6 different levels up to 4 meters simultaneously and continuously. The water vapor content of the samples of air is then determined by the General Mills Infrared Hygrometer.

Referring to the Figure E-1, the system operates as follows:

1) The air pumps in each line coming from the 6 different sampling points above the 20-foot weighing lysimeter force the air samples through the 3-way solenoid valves into sample-bags 1A, 2A, 3A, 4A, 5A, and 6A.

2) After 15 minutes the 3-way solenoid valves switch, and new air samples are forced into bags 1B, 2B, 3B, 4B, 5B, and 6B.

3) Two minutes after the above switch occurs, shut-off valve 1-a opens and shut-off valve 7 closes. The air sample from bag 1A is then withdrawn into the central manifold system and through the Infrared Hygrometer by a vacuum pump.

4) Before 1.5 minutes have elapsed, the air sample bag has completely emptied. 1.5 minutes after valve 1-a was opened, it closes and valve 1-b opens.

5) This process continues by the same sequence and in 9 minutes the last of the 6 air storage bags is emptied. Valve 7 opens again and remains open until valve 1-b opens.

6) The 3-way valves switch and fill the first set of air storage bags again 15 minutes after their last switch has occurred.

All of the switching is accomplished automatically by means of a Bristol Master Controller Switch. The volume of air samples filling each bag is initially adjusted by individual needle valves so that they will not overfill and the 1.5 minute sampling period will be sufficiently long enough to insure complete evacuation of all the air samples. The storage bags are filled to about 25 liters.

The storage bags are vinyl plastic beach balls, and the air lines are made of clear plastic tubing. Copper tubing is used for the manifolds.

To insure that no condensed moisture exists in the air lines, a vacuum cleaner is used to blow warm dry air through all the lines for about one

hour prior to starting the system. Heating cables which dissipate 25 watts each through the inside of the air lines prevent any condensation from occurring after the system is started. The storage bags are contained in a temperature controlled cabinet and the manifold and valves are enclosed in a heated compartment to prevent any condensation of the air samples within the storage bags and piping.

So far this system has worked out well and has been very dependable. The Infrared Hygrometer output is recorded with a strip chart recorder. There is no problem in identifying which humidity sample level is being measured and recorded on the strip chart recorder because a characteristic dip occurs each time one of the storage bags becomes empty. Calibration by Monteith using saturated air provided a tentative verification of the factory calibration.

The absolute accuracy claimed by the manufacturer for dewpoint determination is $\pm$ 1°C throughout a range from -25°C to +30°C. However, the sensitivity at a dewpoint of around 10°C has been found under actual use on this project to be approximately 0.05°C or less. This is equivalent to 0.0025 g/m^3, thus allowing excellent accuracy in determination of gradients of moisture concentration using the technique described above.

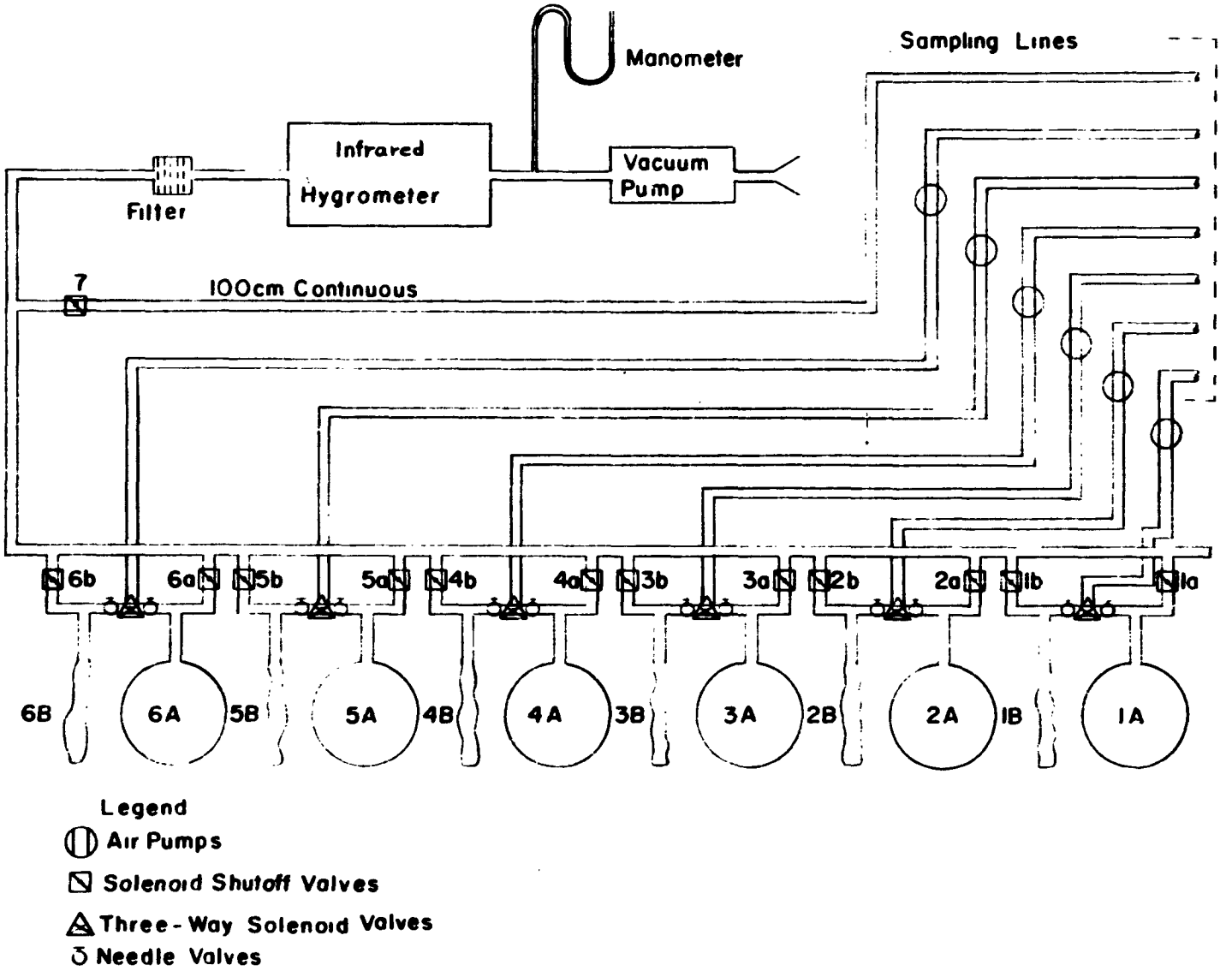

Figure E-1. Infrared hygrometer sampling system.

PROJECT CONCLUSIONS

F.A. Brooks, W.O. Pruitt, and D.R. Nielsen

The primary accomplishment of this 3-year research contract in energy and moisture transfers is the progress made from limited conjectures to well substantiated knowledge of the interaction of the various physical, meteorological and plant factors of most importance in moisture transfers. One conclusion to be drawn from the detail interpretation of flux rates in cloudless weather and in laboratory tests is that some common simplifying assumptions have been used too casually. The physical reasons for several discrepancies, however, have been well demonstrated and even anticipated so it can be concluded that observations which previously were suspected as being merely erroneous can now be studied as real irregularities, each explainable by measurable parameters.

Typical patterns of the various components of the energy balance of a well irrigated grass turf at Davis have been confirmed for clear weather and under various wind, temperature, and humidity conditions. Under calm conditions and to a lesser extent with wind, evaporative cooling of the surface failed to compensate for radiation-heating during morning hours, resulting in establishment of an appreciable lapse rate. It is concluded that convective heating for such a surface is not negligible but is similar in magnitude to evaporative heat flux until mid morning. Under calm conditions the range of stabilities encountered over the grass turf is very large, and we conclude that turbulence due to buoyancy is a major factor in the transfer of moisture away from the surface during morning hours. Flux-gradient studies during 1962 although not conclusive show considerable variation but with $K_H/K_D \geq 1.0$.

Regarding differences in interpretation of field experiments in micrometeorology by various research teams, it can be concluded that most can be ascribed to differences in terrain particularly in the size of the controlled test plot, and in the surrounding area differences in surface moisture and topography. For important cases the effects of these differences might be investigated in the Colorado wind tunnel, but it seems likely that future advection research in Davis with area-distribution of profile masts will provide sufficient explanation, once the accuracy of the various instrumentation systems is established.

Besides the advances made in substantiating physical concepts, the operational difficulties with commercial electronic apparatus and automatic computers leads to the conclusion that occasional faulty operation is to be expected of apparatus especially on continuous day and night runs and that provision must be made both for evading stoppages in the field test and for rejecting false data in computer processing.

PROJECT RECOMMENDATIONS

Now that a specialized electronic capability is in full use by present personnel investigating energy and moisture transfers under the simpler meteorological conditions, usually of clear sky, it is of first importance to continue the comprehensive measurements and several analytical procedures covering full annual cycles and extending them to other weather types. Secondly, the remarkable October 1961 findings on advective effects need to be explored with greater coverage both in area distribution and properties measured so that a useable interpretation of variable terrain can be developed.

Finally, we strongly recommend that some arrangement be made to bring the personnel and the field apparatus of various research teams together to make a joint field run, attended also by Colorado, so that all the outdoor research efforts can be viewed as particular contributions to the whole field of micrometeorology.

MINIMUM DISTRIBUTION LIST FOR SCIENTIFIC TECHNICAL REPORTS
IN METEOROLOGY AND ATMOSPHERIC SCIENCES

	Nr Cys
Hqs, U.S. Army Materiel Command Research Division Attn: AMCRD-RS-ES-A Washington 25, D.C.	1
Hqs, U.S. Army Materiel Command Development Division Attn: AMCRD-DE-MI Washington 25, D.C.	1
Office of Chief of Research & Development Department of the Army Attn: CRD/M Washington 25, D.C.	2
Hqs, U.S. Army Combat Development Command Attn: CDCMR-E Ft. Belvoir, Va.	1
Hqs, U.S. Continental Army Command Attn: ATINT-P&O Ft. Monroe, Va.	1
Office of the Chief Signal Officer Department of the Army Washington 25, D.C.	1
Hqs, U.S. Army Electronics Command Research Division Attn: AMSEL-RE-C Fort Monmouth, New Jersey	2
Hqs, U.S. Army Missile Command Attn: AMSMI-RPA Redstone Arsenal, Alabama	2
Hqs, U.S. Army Munitions Command Attn: AMSMU-RC Dover, New Jersey	2
Hqs, U.S. Army Mobility Command Attn: Research Division Centerline, Michigan	2
Hqs, U.S. Army Test & Evaluation Command Directorate of NBC Testing Aberdeen Proving Ground, Maryland	2
CO, U.S. Army Cold Regions Research & Engineering Laboratory Attn: Environmental Research Branch Hanover, New Hampshire	2
CG, U.S. Army CSR&E Laboratory Attn: Earth Sciences Division Natick, Massachusetts	2
CO, U.S. Army Ballistic Research Laboratories Attn: AMXBR-B Aberdeen Proving Ground, Maryland	2
Director, U.S. Army Engineer Waterways Experiment Station Attn: WESSR Vicksburg, Mississippi	1
CO, U.S. Army Electronics R&D Agency Attn: Meteorology Division, Surveillance Dept. Fort Monmouth, New Jersey	2
CO, U.S. Army Electronics R&D Activity Attn: Meteorological Department Ft. Huachuca, Arizona	50
CO, U.S. Army Electronics R&D Activity Attn: Missile Meteorology Division White Sands Missile Range, New Mexico	2
Commanding Officer U.S Army Biological Laboratories Attn: CB Cloud Research Office Ft. Detrick, Frederick, Maryland	1
CO, U.S. Army Frankford Arsenal Attn: MEIE Division Philadelphia, Pennsylvania	1

	Nr Cys
CO, Picatinny Arsenal Attn: Special Weapons Group Dover, New Jersey	1
CO, U.S. Army Engineering R&D Laboratory Fort Belvoir, Virginia	1
CO, U.S. Army Transportation Research Command Fort Eustis, Virginia	1
CO, U.S. Army Dugway Proving Ground Attn: Meteorological Division Dugway, Utah	1
President U.S. Army Artillery Board Ft. Sill, Oklahoma	1
CO, U.S. Army Artillery Combat Developments Agency Ft. Sill, Oklahoma	1
CO, U.S. Army Communications - Electronics Combat Developments Agency Ft. Huachuca, Arizona	1
Commandant U.S. Army Artillery & Missile School Attn: Target Acquisition Department Ft. Sill, Oklahoma	1
Commander Air Weather Service (MATS) U.S. Air Force, Attn: AWSSS/TIPD Scott Air Force Base, Illinois	1
Commander, Air Force Cambridge Research Laboratories Attn: CRXL, Laurence G. Hanscom Field Bedford, Massachusetts	2
Chief of Naval Research Attn: CODE 427 Department of the Navy Washington 25, D.C.	1
Office of U.S. Naval Weather Service U.S. Naval Air Station Washington 25, D.C.	1
Officer-in-Charge U.S. Naval Weather Research Facility U.S. Naval Air Station, Bldg R 28, Norfolk 11, Va.	1
Director, Atmospheric Sciences Programs National Science Foundation Washington 25, D.C.	1
Director, Bureau of Research & Development Federal Aviation Agency Washington 25, D.C.	1
Director, Bureau of Research & Development Federal Aviation Agency National Aviation Facilities Experimental Center Attn: Technical Library, Bldg 3 Atlantic City, New Jersey	1
Chief, Fallout Studies Branch Division of Biology and Medicine Atomic Energy Commission Washington 25, D.C.	1
Office of the Assistant Secretary of Defense (Research and Engineering), The Pentagon Attn: Technical Library, Room 3E1065 Washington 25, D.C.	1
Director of Meteorological Systems Office of Applications (FM) National Aeronautics & Space Administration Washington 25, D.C.	1
Chief, U.S. Weather Bureau Attn: Librarian Washington 25, D.C.	2

DISTRIBUTION LIST (Continued)

	Nr Cys
Commander Armed Services Technical Information Agency Arlington Hall Station Attn: TIPDR Arlington 12, Virginia	10
Robert A. Taft Sanitary Engineering Center Public Health Service 4676 Columbia Parkway Cincinnati 26, Ohio	1
Commander Air Force Cambridge Research Laboratories Attn: CRZW 1065 Main Street Waltham, Massachusetts	1
Commanding General Deseret Test Center Ft. Douglas, Utah	1
President U.S. Army Arctic Test Board Ft. Greely, Alaska	1
Hqs, U.S. Army Test and Evaluation Command Attn: AMSTE-EL Aberdeen Proving Ground, Maryland	1
Hqs, U.S. Army Test and Evaluation Command Attn: AMSTE-BAF Aberdeen Proving Ground, Maryland	1
Hqs, U.S. Army Missile Command Attn: AMSMI-RB Redstone Arsenal, Alabama	1
Hqs, U.S. Army Missile Command Attn: AMSMI-RR Redstone Arsenal, Alabama	1
Commanding Officer U.S. Army Biological Laboratories Attn: Technical Library, SMUFD-12 TI Ft. Detrick, Frederick, Maryland	1
Commanding Officer U.S. Army CBR Operations Research Group Army Chemical Center, Maryland	1
Commanding Officer U.S. Army Chemical Research & Development Laboratories Attn: Director of Development Support Army Chemical Center, Maryland	1
Office of the Chief Signal Officer Attn: The Technical Director, Command and Control Systems Directorate Department of the Army Washington 25, D.C.	1
Scientific and Technical Information Facility Attn: NASA Representative (S-AK/DL) P.O. Box 5700 Bethesda, Maryland	1
Director, Meteorology Dept. University of Arizona Tucson, Arizona	1
Director, U.S. Water Conservation Lab Agricultural Research Service U.S. Dept. of Agriculture Route 2, Box 816-A Tempe, Arizona	1
Director, Pacific Southwest Forest & Range Experiment Station U.S. Department of Agriculture Forest Service P.O. Box 245 Berkeley 1, California	1
Director, Meteorology Dept. University of California at Los Angeles Los Angeles 24, California	1
Director, U.S. Salinity Lab P.O. Box 672 Attn: Dr. L. A. Richards Riverside, California	1
Department of Irrigation University of California Davis, California	1
Dept. of Agricultural Engineering University of California Attn: Dr. F. A. Brooks Davis, California	1
Meteorology Dept. San Jose State College San Jose, California	1
Chief, Radio Propagation Lab U.S. National Bureau of Standards Boulder, Colorado	1
Librarian, National Center for Atmospheric Research Boulder, Colorado	1
Dept. of Civil Engineering Colorado State University Fort Collins, Colorado	1
Director Attn: M. Martinelli, Jr. Rocky Mountain Forest & Range Experiment Station U.S. Department of Agriculture Forest Service Room 221, Forestry Building Colorado State University Fort Collins, Colorado	1
Director, Meteorology Dept. Florida State University Tallahassee, Florida	1
Director, Southern Piedmont Soil Conservation Field Station U.S. Dept. of Agriculture P.O. Box 33 Watkinsville, Georgia	1
Meteorology Dept. University of Hawaii Honolulu, Hawaii	1
Director, Meteorology Dept. The University of Chicago Chicago 37, Illinois	1
Department of Agronomy Iowa State University Attn: Dr. R. H. Shaw Ames, Iowa	1
Director, Soil & Water Conservation Div. Agricultural Research Svc U.S. Department of Agriculture Beltsville, Maryland	1
Director, Dept. of Civil Engineering Johns Hopkins University Baltimore 18, Maryland	1
Executive Secretary American Meteorological Society 45 Beacon Street Boston 8, Massachusetts	1
Director, Meteorology Dept. Massachusetts Institute of Technology Cambridge 37, Massachusetts	1
Dept. of Meteorology Massachusetts Institute of Technology Round Hill Field Station South Dartmouth, Massachusetts	1
Director, Meteorology Dept. University of Michigan Ann Arbor, Michigan	1

DISTRIBUTION LIST (Continued)

	Nr Cys
University of Minnesota Attn: Dean Spilhouse Minneapolis, Minnesota	1
Director, NSSP Attn: Library Federal Office Building - Rm 806 911 Walnut Street Kansas City, Missouri	1
Director, Meteorology Dept. St. Louis University St. Louis, Missouri	1
Dept. of Geophysics Washington University St. Louis, Missouri	1
Department of Soils University of Missouri Columbia, Missouri	1
Director, Meteorology Dept. New York University University Heights New York 53, New York	1
Soil & Water Conservation Research Division Agricultural Research Service U.S. Dept. of Agriculture Cornell University, Bailey Hall Ithaca, New York	1
Atmospheric Science Branch Scientific Research Institute Oregon State College Corvallis, Oregon	1
Director, Meteorology Dept. Pennsylvania State University University Station, Pennsylvania	1
Dept. of Oceanography and Meteorology The Agricultural and Mechanical College of Texas College Station, Texas	1
Electrical Engineering Research Laboratory The University of Texas Austin, Texas	1
Department of Agronomy Utah State University Attn: Dr. S. A. Taylor Logan, Utah	1
Dept. of Meteorology University of Utah Salt Lake City, Utah	1
Director, National Research Council National Academy of Sciences 2101 Constitution Avenue Washington 25, D.C.	1
Director, Meteorology Dept. University of Washington Seattle, Washington	1
Director, Meteorology Dept. University of Wisconsin Madison, Wisconsin	1
Dept. of Soils University of Wisconsin Attn: Dr. C. B. Tanner Madison, Wisconsin	1
Commander U.S. Navy Electronics Lab Attn: Dr. M. Halstead San Diego 52, California	1
Officer-in-Charge Meteorological Curriculum U.S. Naval Post Graduate School Monterey, California	1

	Nr Cys
Director, Geophysical Research Directorate Attn: CRZHB USAF Cambridge Research Center Hanscom Field Bedford, Massachusetts	2
Commandant Attn: Weather Br, DST U.S. Army Signal School Fort Monmouth, New Jersey	1
Commanding Officer U.S. Army Electronics R&D Laboratory Fort Monmouth, New Jersey	1
Deputy for Defense Research & Engineering Attn: Geophysical Sciences Office of the Secretary of Defense Washington 25, D.C.	1
Climatic Center, USAF Attn: CCCAD Air Weather Service (MATS) Annex 2, 225 D Street, S.E. Washington 25, D.C.	1
Director Department of Transport 315 Bloor Street West Toronto 5, Ontario Canada	1

SPECIAL UCD DISTRIBUTION LIST

Prof. Harold A. Johnson Dept. of Engineering University of California Berkeley, California	1
Mr. Theodor B. Yerke The Library Pac. SW For. and Range Experiment Station Box 245 Berkeley 1, California	2
Library University of California Davis, California	1
Dr. H. F. Poppendiek 8686 Dunnaway Drive La Jolla, California	1
Dean L.M.K. Boelter Dept. of Engineering University of California Los Angeles 24, California	1
Prof. Warren Hall Director, U.C. Water Resources Center University of California Los Angeles 24, California	1
Prof. W. Wurtele Dept. of Meteorology University of California Los Angeles 24, California	1
Stanford Research Institute Weather Dynamics Program Bldg. 404 A Menlo Park, California	1
Department of Water Resources State of California Attn: Mr. John Shannon Attn: Mr. Joe Powers P.O. Box 388 Sacramento 2, California	2
Dr. J. J. Marciano U.S. Naval Electronics Laboratory San Diego 52, California	1
U.S. Flexible Metallic Tubing Co. Attn: Ed. Woodward 63 Main Street San Francisco, California	1

DISTRIBUTION LIST (Continued)

	Nr Cys
Prof. A. L. London Dept. of Mechanical Engineering Stanford University Stanford, California	1
Dr. David M. Gates Consultant for Atmospheric Physics National Bureau of Standards Boulder, Colorado	1
Dr. Walter Orr Roberts Director, National Center Atmospheric Research University of Colorado Boulder, Colorado	1
M. W. Bittinger Civil Engineering Research Sec. Colorado State University Fort Collins, Colorado	1
C. E. Evans Agricultural Research Service U.S.D.A. Fort Collins, Colorado	1
Library Colorado State University Fort Collins, Colorado	1
Dr. William E. Reifsnyder Yale University School of Forestry New Haven 11, Connecticut	1
Mr. D. H. Pack Environmental Meteorological Research Projects, DMR U.S. Weather Bureau Washington 25, D.C.	1
Mr. A. K. Showalter, Chief Observations and Station Facilities Division U.S. Dept. of Commerce Weather Bureau Washington 25, D.C.	1
John F. Gerber, Assistant Climatologist Fruit Crops Dept. Agricultural Experiment Station University of Florida Gainesville, Florida	1
Mr. H. Moses Argonne National Lab. Argonne, Illinois	1
Westinghouse Electric Corp. Friendship International Airport Box 1693 Baltimore 3, Maryland Attn: Mrs. A. E. Battaglia	1
Dr. D. J. Portman Department of Meteorology University of Michigan Ann Arbor, Michigan	1
Dr Ben Davidson Dept of Meteorology New York University University Heights Campus, New York	1
Prof. Hans A. Panofsky Dept. of Meteorology The Pennsylvania State University University Park, Pennsylvania	1
Forestry Library Forestry Department S.F.A. State College Nacogdoches, Texas	1
Dr. A. J. Dyer C.S.I.R.O. Division of Meteorological Physics Aspendale, Victoria Australia	1
Dr. C.H.B. Priestley Dept. of Meteorological Physics C.S.I.R.O. Aspendale, Victoria Australia	1
R. E. Munn Dept. of Transport 315 Bloor Street, W. Toronto 5, Ontario	1
Dr. H. L. Penman Dept. of Physics Rothamsted Experimental Station Harpenden, Herts England	1
Prof. P. A. Sheppard Imperial College London, England	1
Prof. F. Moller Institute of Meteorology University of Munich 52 Amalien Strasse Munchen 13 Germany	1
Dr. W. R. Van Wijk Landbouwhogeschool Laboratorium Voor Natur-En Weerkunde Duwendaal 2, Wageningen, Holland	1
Eiichi Inoue Div. of Meteorology National Institute of Ag. Sciences Nishigahara, Kita-Ku, Japan	1
Prof. J. Neumann University of Jerusalem Jerusalem	1
Project personnel at UCD and reserve copies	20
Extra to meet future requests	17

AD _____ Accession Nr _____

UNCLASSIFIED

University of California, Davis
INVESTIGATION OF ENERGY AND MASS TRANSFERS NEAR THE GROUND, INCLUDING INFLUENCES OF THE SOIL-PLANT-ATMOSPHERE SYSTEM.
by F. A. Brooks, W. O. Pruitt, D. R. Nielsen and others.
Final Report (15 Dec 1961 to 30 June 1963)
Pub. by University of California, Davis, under USAEPG Technical Program, DA Task 3A99-27-005-08. 285 pages - 107 illustrations. Unclassified report.

Results are reported from three years of investigations of energy and moisture transfers near the earth's surface.

Following are the major topics discussed: atmospheric and surface factors affecting evapotranspiration; response of several energy balance and aerodynamic evaporation equations under a wide range of stability; eddy diffusivity as as a function of stability; boundary layer transport under sinusoidal down wind surface fluxes; measurement and description of water infiltration into uniform soils; resistance to water loss from plants; and movement and distribution of THO in tissue, water, and vapor transpired by Helianthus and Nicotiana.

1. Micrometeorology
   Moisture transfer
   Humidity
   Heat transfer
   Instrumentation
   California
2. Evapotranspiration
3. Plants
   Moisture transfer
4. Isotopes (Radioactive)
   (THO) applications
5. Soils
   Moisture transfer

Contract DA-36-039-SC-80334
UNCLASSIFIED

AD _____ Accession Nr _____

UNCLASSIFIED

University of California, Davis
INVESTIGATION OF ENERGY AND MASS TRANSFERS NEAR THE GROUND, INCLUDING INFLUENCES OF THE SOIL-PLANT-ATMOSPHERE SYSTEM.
by F. A. Brooks, W. O. Pruitt, D. R. Nielsen and others.
Final Report (15 Dec 1961 to 30 June 1963)
Pub. by University of California, Davis, under USAEPG Technical Program, DA Task 3A99-27-005-08. 285 pages - 107 illustrations. Unclassified report.

Results are reported from three years of investigations of energy and moisture transfers near the earth's surface.

Following are the major topics discussed: atmospheric and surface factors affecting evapotranspiration; response of several energy balance and aerodynamic evaporation equations under a wide range of stability; eddy diffusivity as as a function of stability; boundary layer transport under sinusoidal down wind surface fluxes; measurement and description of water infiltration into uniform soils; resistance to water loss from plants; and movement and distribution of THO in tissue, water, and vapor transpired by Helianthus and Nicotiana.

1. Micrometeorology
   Moisture transfer
   Humidity
   Heat transfer
   Instrumentation
   California
2. Evapotranspiration
3. Plants
   Moisture transfer
4. Isotopes (Radioactive)
   (THO) applications
5. Soils
   Moisture transfer

Contract DA-36-039-SC-80334
UNCLASSIFIED

AD _____ Accession Nr _____

UNCLASSIFIED

University of California, Davis
INVESTIGATION OF ENERGY AND MASS TRANSFERS NEAR THE GROUND, INCLUDING INFLUENCES OF THE SOIL-PLANT-ATMOSPHERE SYSTEM.
by F. A. Brooks, W. O. Pruitt, D. R. Nielsen and others.
Final Report (15 Dec 1961 to 30 June 1963)
Pub. by University of California, Davis, under USAEPG Technical Program, DA Task 3A99-27-005-08. 285 pages - 107 illustrations. Unclassified report.

Results are reported from three years of investigations of energy and moisture transfers near the earth's surface.

Following are the major topics discussed: atmospheric and surface factors affecting evapotranspiration; response of several energy balance and aerodynamic evaporation equations under a wide range of stability; eddy diffusivity as as a function of stability; boundary layer transport under sinusoidal down wind surface fluxes; measurement and description of water infiltration into uniform soils; resistance to water loss from plants; and movement and distribution of THO in tissue, water, and vapor transpired by Helianthus and Nicotiana.

1. Micrometeorology
   Moisture transfer
   Humidity
   Heat transfer
   Instrumentation
   California
2. Evapotranspiration
3. Plants
   Moisture transfer
4. Isotopes (Radioactive)
   (THO) applications
5. Soils
   Moisture transfer

Contract DA-36-039-SC-80334
UNCLASSIFIED

AD _____ Accession Nr _____

UNCLASSIFIED

University of California, Davis
INVESTIGATION OF ENERGY AND MASS TRANSFERS NEAR THE GROUND, INCLUDING INFLUENCES OF THE SOIL-PLANT-ATMOSPHERE SYSTEM.
by F. A. Brooks, W. O. Pruitt, D. R. Nielsen and others.
Final Report (15 Dec 1961 to 30 June 1963)
Pub. by University of California, Davis, under USAEPG Technical Program, DA Task 3A99-27-005-08. 285 pages - 107 illustrations. Unclassified report.

Results are reported from three years of investigations of energy and moisture transfers near the earth's surface.

Following are the major topics discussed: atmospheric and surface factors affecting evapotranspiration; response of several energy balance and aerodynamic evaporation equations under a wide range of stability; eddy diffusivity as as a function of stability; boundary layer transport under sinusoidal down wind surface fluxes; measurement and description of water infiltration into uniform soils; resistance to water loss from plants; and movement and distribution of THO in tissue, water, and vapor transpired by Helianthus and Nicotiana.

1. Micrometeorology
   Moisture transfer
   Humidity
   Heat transfer
   Instrumentation
   California
2. Evapotranspiration
3. Plants
   Moisture transfer
4. Isotopes (Radioactive)
   (THO) applications
5. Soils
   Moisture transfer

Contract DA-36-039-SC-80334
UNCLASSIFIED